Techniques for Mobile Location Estimation in UMTS

Nicholas James Thomas

A thesis submitted for the degree of Doctor of Philosophy.
The University of Edinburgh.
October 2001

Abstract

The subject area of this thesis is the locating of mobile users using the future 3rd generation spread spectrum communication system UMTS. The motivation behind this work is twofold: firstly the United States Federal Communications Commission (FCC) mandated the provision of user location into services in the United States of America due to the increasing number of emergency calls originating from unknown locations. Secondly the user location can enable a number of other potentially profit–making applications and services. These are generally thought to be the important new applications of the third generation mobile networks.

The UMTS standard has now made provision for a time difference of arrival based mobile user location system in which the mobile measures time differences of arrival of received signals from surrounding base stations (BS's). There are two main problems to such a technique: firstly the problem of detecting enough base stations to make a location fix, the so called 'hearability' problem. In spread spectrum systems all base stations transmit on the same bandwidth thus non–serving BS's may not be detectable in normal operation. The second problem is non–line of sight (NLOS) propagation, in which time difference measurements (or any other measurement types) may be corrupted significantly, thus causing significant location error.

The thesis of this work is that these two problems can be entirely overcome using spatial filtering of measurements and location estimates. Two constraints that are placed on the filtering algorithms are that the operation should be real time and that the precise distribution of NLOS errors is unknown (though certain key characteristics are exploited).

A channel model is first developed, which specifically characterises line of sight and NLOS transitions as well as out of cell radio wave propagation. Several scenarios are then simulated. Slow moving users, low hearability and heavily NLOS conditions pose the biggest challenge. Spatial filtering is achieved by Kalman filters adapted to the problem, as well as simple averaging filters. Results show that improved location accuracy (to within FCC recommendations) is possible in all considered scenarios with spatial filtering as well as improved robustness to low hearability. The detection stage of the receiver is also analysed in detail and methods to improve hearability are presented.

The performance of a hybrid location system using angle of arrival measurements of the mobile at the serving BS is also assessed. A fairly pessimistic model for the spread of NLOS errors is used, however significant location improvement is noted in several scenarios. Worst performance occurs in urban scenarios so finally a novel approach to user location is described which is robust to NLOS propagation conditions and also overcomes the hearability problem since only measurements at the serving BS are required. The technique, termed Scatterer Back Tracing (SBT), uses and requires multipaths to calculate the mobile location. Results suggest this SBT can provide extremely high location accuracy but is very sensitive to measurement noise.

Declaration of Originality

I hereby declare that the research recorded in this thesis and the thesis itself was composed and originated entirely by myself in the Department of Electronics and Electrical Engineering at The University of Edinburgh.

Nicholas Thomas

Acknowledgements

I would like to thank all those who helped contribute to this PhD. Most notably my supervisors David Cruickshank, David Laurenson and Gordon Povey for their support, advice and for reading and checking this thesis; Iain Band for lots of practical advice during the early stages of this work; my father, Giles Thomas for some invaluable contributions; and all my officemates who all at some time helped and encouraged me during the last three years. Finally I'd like to thank EPSRC for providing financial support.

Contents

List of figures

List of tables

Acronyms and Abbreviations

aLS	Adjusted Least Squares
AOA	Angle of Arrival
BS	Base Station
CDF	Cumulative Density Function
CDMA	Code Division Multiple Access
C/I	Carrier to Interference Ratio
CIR	Channel Impulse Response
CLOS	Cellular Line of Sight
CRLB	Cramér–Rao Lower Bound
DAC	Divide and Conquer
E–OTD	Enhanced Observed Time Difference
eSBT	Enhanced Scatterer Back Tracing
ESS	Enhanced Signal Strength
FCC	Federal Communications Commission
fTOA	First Time of Arrival
GCC	Generalised Cross Correlation
GDOP	Geometric Dilution of Precision
GLONASS	Global Navigation Satellite System
GPS	Global Positioning System
GSM	Global System of Mobile Communications
GWSSUS	Gaussian Wide Sense Stationary Uncorrelated Scattering
ieKF	Input Estimation Kalman Filter
IPDL	Idle Period Downlink
KF	Kalman Filter
LLOS	Local Line of Sight
LMU	Location Measurement Unit
LOS	Line of Sight
LS	Least Squares
MF	Matched Filter

ML	Maximum Likelihood
MPR	Multipath Rejection
MS	Mobile Station
NCLOS	Non–Cellular Line of Sight
NLLOS	Non–Local Line of Sight
NLOS	Non–Line of Sight
OLS	Ordinary Least Squares
OTD	Observed Time Difference
PCPICH	Primary Common Pilot Channel
PDF	Probability Density Function
PR–IPDL	Pseudo Random Idle Period Downlink
PSCH	Primary Synchronisation Channel
QoS	Quality of Service
RD	Range Difference
RMS	Root Mean Squared
RTT	Round Trip Time
RV	Random Variable
SA	Smoothed Average
SBT	Scatterer Back Tracing
SS	Signal Strength
SSCH	Secondary Synchronisation Channel
SNR	Signal to Noise Ratio
TA	Timing Advance
TA–IPDL	Time Aligned Idle Period Downlink
TD	Time Difference
TDOA	Time Difference of Arrival
TOA	Time of Arrival
UMTS	Universal Mobile Telecommunications System
VMI	Velocity based Manoeuvre Inhibition
vKF	Kalman Filter using Velocity Estimates
vTA–IPDL	Variant Time Aligned Idle Period Downlink
WA	Weighted Average
WLS	Weighted Least Squares

List of Principal Symbols

$\mathbf{0}$	the zero matrix
a	a signal amplitude
$\mathbf{b}_{WLS}$	WLS solution
$\mathbf{b}_{ML}$	ML solution
c	the speed of light
C_{fTOA}	correction for fTOA filter
C_{LS}	correction for aLS fit
$C_{\Omega-\tau}$	correlation between Ω_{NCLOS} and τ_{NCLOS}
d	MS–BS separation
d_{bp}	breakpoint distance from BS
D_{fu}	the carrier frequency reuse distance in cells
$E[\cdot]$	expectation operator
E_{ce}^{k}	location error at the kth percentile
E_{RMS}	RMS location error
$F_{cluster}$	idle period cluster frequency
f_c	carrier frequency
f_d	Doppler shift
f_{dmax}	maximum Doppler shift
F_{idle}	idle period frequency
$f_X(x)$	the PDF of x
$F_X(x)$	the CDF of x
$\mathbf{G}$	matrix containing partial derivatives in CRLB definition
G_p	processing gain of MF
$h(t,\tau)$	CIR at time t
h_{BS}	BS height
h_{MS}	MS height
$\mathbf{H}_n$	KF Kalman gain
$\mathbf{I}$	the identity matrix
L_{burst}	length of one idle period burst (in idle periods)

L_{CLOS}	CLOS mean obstruction length
L_{dcorr}	shadowing decorrelation length of channel
L_{fTOA}	length of fTOA filter
L_{if}	length of idle frame
L_{ip}	length of idle period
L_{LLOS}	LLOS mean obstruction length
L^0_{LLOS}	mean length in LLOS
L_{LS}	length of LS fit
L^0_{NLLOS}	mean length in NLLOS
L_s	mean scatterer survival distance
L_{SA}	length of SA filter
L_{sep}	separation between idle periods in a cluster
L_{WA}	length of WA filter
m	Nakagami-m distribution value
$n(t)$	noise signal at time t
$N[\mu, \sigma^2]$	a normal (Gaussian) process with specified mean and variance
$N_+[\mu, \sigma^2]$	a positive only normal (Gaussian) process with specified mean and variance
N_{ip}	number of idle periods
N_c	number of idle periods to be combined coherently
N_{LS}	order of LS fit
N_n	number of combined idle periods to be combined non–coherently
N_o	total complex noise power otherwise termed $2\sigma_n^2$
N_p	number of measurement periods in system with no IPDL
N_s	number of combined idle periods over which selection diversity is implemented
O_s	oversampling rate
$P^X_{BSidle}(n, P^X_{idle})$	probability that BS with nth weakest received signal is idle in scheme X
P_{CLOS}	probability of MS being CLOS
P_{det}	detection probability
$P_{det(out)}$	detection probability after non–coherent combining
P_{FA}	false alarm probability
$P_{FA(out)}$	false alarm probability after non–coherent combining
P^X_{idle}	probability of BS being idle during idle period in scheme X
P_{LLOS}	probability of MS being LLOS
P^X_{trans}	probability of BS transmitting during idle period in scheme X

PL_D	Dual slope path loss
PL_S	Simple path loss
$\mathbf{Q}$	covariance matrix of measurements in location estimator
$Q_m(a,b)$	Marcum's Q function of order m
$r(t)$	received signal at time t
r_i	a range to signal source i
$r_{i,j}$	a range difference between signal sources i and j
r_m	MS radius, polar coordinate notation
R_C	cell radius
$\mathbf{R}_n$	covariance matrix of $\mathbf{Y}_n$
$\hat{\mathbf{R}}$	estimated covariance matrix of location estimate
$\tilde{\mathbf{R}}$	estimated covariance matrix of location estimate after final KF
$R_{xx}(\tau)$	the autocorrelation function of $x(t)$
$R_{xy}(\tau)$	the crosscorrelation function of $x(t)$ and $y(t)$
$s(t)$	transmitted signal at time t
s_1, s_2	slope parameters in dual slope path loss model
$\mathbf{S}_n$	KF covariance of $\mathbf{X}_n$
T_c	chip period
T_h	noise threshold
$U[min, max]$	a uniform distribution with specified min and max
$\mathbf{U}_n$	KF dynamic model driving noise vector
v	MS speed
x	x–coordinate of MS position
$\dot{x}$	velocity of x
$\ddot{x}$	acceleration of x
x_i	x–coordinate of BSi position
$\mathbf{X}$	matrix specifying linear relationship between β and μ in location estimator
$\mathbf{X}_n$	KF state vector
y	y–coordinate of MS position
y_i	y–coordinate of BSi position
$\mathbf{Y}$	matrix containing measurements of μ in location estimator
$\mathbf{Y}_n$	KF measurement vector
$\hat{\mathbf{Z}}$	estimated location
$\tilde{\mathbf{Z}}$	estimated location after final KF

α_{BS}	incidence angle at the BS
α_m	MS bearing with respect to origin, polar coordinate notation
α_{MS}	incidence angle at the MS
β	vector containing desired parameters (MS location) in location estimator
γ_1, γ_2	variance correction factors before and after location estimator
Δt	measurement sample period
λ	carrier wavelength
μ	dependent variable vector in location estimator
ξ	minimisation statistic for SBT technique
ξ_e	minimisation statistic for eSBT technique
ρ	correlation value
σ_{err}	residual threshold above which KF is in error
$\sigma_{f_d}^2$	variance of Doppler shift measurement
$2\sigma_n^2$	total complex noise power
σ_{s1}, σ_{s2}	path loss standard deviations in dual slope model
σ_u^2	velocity driving noise power
$\hat{\sigma}_\alpha^2$	estimate AOA variance
$\sigma_{\alpha LOS}^2$	AOA variance in LOS conditions
$\sigma_{\alpha NLOS}^2$	AOA variance in NLOS conditions
$\hat{\sigma}_\tau^2$	estimated TOA variance
$\sigma_{\tau LOS}^2$	TOA variance in LOS conditions
$\sigma_{\tau NLOS}^2$	TOA variance in NLOS conditions
τ	a time delay or pseudo time delay
$\tau_{i,j}$	a time difference between signal sources i and j
τ_{max}	the maximum time delay according to a scatterer model
τ_{min}	the minimum time delay according to a scatterer model
τ_{NCLOS}	NCLOS excess delay
τ_{RMS}	the RMS delay spread
ϕ	phase shift
Φ	KF state transition matrix
ϕ_m	MS direction of travel with respect to LOS to serving BS
Φ^o	CRLB matrix
Φ_{RMS}^o	the trace of Φ^o
ω	weighting matrix for measurements in location estimate
Ω_{NCLOS}	NCLOS power attenutation

Chapter 1
Introduction

1.1 Motivations for Mobile Station Location

In wireless systems the need for accurate mobile station (MS) location estimation has been motivated by the US Federal Communications Commission's (FCC's) E911 mandate for emergency services [1]. The mandate was deemed necessary due to the rising number of emergency calls made from mobile phones by callers reporting accidents who do not know where they are. Vital minutes were being lost to the emergency services at the inevitable cost of lives. The requirements of the accuracy and frequency requirements of the location estimate were initially set to within 125m for 67% of users and within 300m for 95% of users, but were subsequently reduced to within 50m and within 150m at respective percentiles for handset based solutions. Full compliance of new digital handsets to the standards is set for October 2002.

Although the FCC mandate motivated initial plans for MS location access, the potential for introduction of lucrative customer services has further fuelled action. These location services include services which are already available through other technologies, e.g. navigation service, as well as new services including location billing, location advertising and a whole range of location enabled internet based services, from looking up train timetables to ordering food from a local restaurant. Additionally location access may also aid some network functions like traffic/handover management.

There are no doubt numerous benefits available from location enabled services, however there has also been much debate about privacy laws and the sensitivity of such information. For this reason handset based solutions may be favoured by many, for they give the user absolute control over their location information. There have been further complications about whether the network provider has legal ownership of the information and can sell it to interested third parties. Such transactions would have to be authorised by the user in a similar manner to internet based money transactions.

1.2 Challenges to Mobile Station Location

Recent location estimator proposals incorporate either bearing, signal strength, or timing measurements or a combination of the three measured at, or from, several surrounding base stations (BS's) to solve the location function via triangulation or trilateration. Whichever methods are used it is clear that the mobile communication air interface does not provide an ideal environment for making such measurements to provide the required location accuracy.

The main problem is that of non–line of sight (NLOS) scenarios. In these conditions communication is maintained via multipaths. However multipaths will have a different trajectory and path length to the line of sight (LOS) path, which will cause errors in the final location accuracy. These errors will be spatially correlated, potentially over large distances, and often biased in nature and sufficiently large to cause location errors to be worse than accuracy requirements. For future wideband mobile networks like UMTS [2] the main focus of research has been timing measurements since the resolution of such measurements is in the range of 20m. In UMTS time difference of arrival (TDOA) location estimation has been written into the standard. Timing measurements of signals emanating from surrounding BS's are to be made at the MS. Assuming a high signal to noise power, with the timing resolution available, the dominant errors become NLOS errors rather than measurement errors. The propagation environment at the UMTS carrier frequency (1.92GHz) is much more reflective than at the GSM carrier frequency (900MHz), suggesting that the NLOS errors may be worse in UMTS than GSM. Several lines of research have been proposed to mitigate these NLOS errors. Many of these methods require precise *a priori* statistical knowledge of the NLOS conditions and often only work in some special cases. The performance of the mitigation algorithms is directly related to the accuracy of this knowledge.

A further problem is lack of data in systems which require measurements from more than one BS. This is sometimes termed the hearability problem and is especially problematic in CDMA systems in which all BS's transmit on the same carrier frequency. Various techniques to improve hearability in CDMA systems have been proposed.

1.3 Research Area

In this thesis the performance of spatial filtering algorithms on the location accuracy is investigated. It is postulated that using spatial filtering is the most robust way to overcome the NLOS and hearability problems and can provide location accuracy within the FCC regulations. Figure 1.1 shows the generalised receiver architecture to be considered.

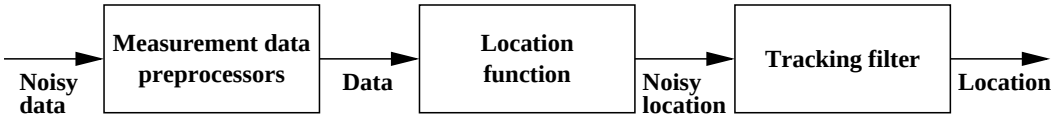

Figure 1.1: Generalised location estimator architecture.

The measured data is fed into a preprocessor which attempts to correct or remove any NLOS errors. Correction can be achieved by supposing that at some point in the past the MS may have been LOS. By utilising known constraints on the manoeuvring capability of the MS, an estimate for the current data can be made even if the MS is NLOS. An important part of the correction procedure is the generation of relative confidence (variance) weightings for each measurement available. The corrected data is then used to calculate the location estimate by the location function. Assuming measurement noise and some residual NLOS noise may still be present in the data, the location estimates will not provide an accurate time continuous motion. Therefore the location estimates are fed into a tracking filter to provide a final location estimate.

Using the spatial filtering techniques, the requirement for *a priori* knowledge is reduced. This is quite important since it necessitates the minimum of calibration of the system. Another advantage is that due to the hearability problem the measurements required to calculate the location are not always available. Using spatial filtering, measurements can be extrapolated in time to provide the maximum information to the location estimator at all times, thus providing good performance when hearability is low. The effect of hearability on the location accuracy of the system and also methods to improve hearability are investigated.

Since TDOA methods have been proposed in UMTS, this is the method of location calculation initially considered. Combining measurement types in the location estimator can improve accuracy and may well provide extra NLOS mitigation capabilities. Therefore an Angle of Arrival (AOA) and TDOA hybrid system, considered the most likely hybrid implementation, is also investigated.

Results show that location accuracy in urban areas for the conventional triangulation techniques is poorest due to a high probability of NLOS errors. A location technique based on backtracing incoming rays is proposed for these situations. This technique can provide perfect location accuracy even in NLOS conditions and also has the added advantage that only measurements at one BS are required to locate the MS.

1.4 Thesis Structure

The next chapter, Chapter 2, contains a summary of background information and the state of current research. In Chapter 3 a channel model suitable for evaluating performance of the location service is presented. This model is used in subsequent chapters to test performance. In Chapter 4 the problem of hearability in the context of UMTS is addressed. The hearability performance of various proposed idle period downlink (IPDL) techniques is assessed, along with several methods to improve this performance. In Chapter 5 the location accuracy performance of a TDOA receiver employing spatial filtering is presented under varying channel scenarios. In Chapter 6 a hybrid AOA/TDOA is considered in a similar fashion. Chapter 7 introduces at a different method to calculate location suitable for urban areas and location accuracy performance is assessed. Chapter 8 contains the final conclusions of the thesis.

Chapter 2
Background

In this chapter the pertinent signal processing theory and current state of the art is summarised. Firstly the mobile communications channel is introduced followed by a summary of channel modelling techniques. Then the various techniques to calculate the mobile location are described. These are standard triangulation/trilateration techniques using range, range difference (RD) or bearing measurements. Following this is a résumé of the various measurement strategies that have been proposed.

At this point the key issues which affect location accuracy in a mobile network, namely the non–line of sight (NLOS) propagation, geometrical dilution of precision (GDOP) and so called hearability problems are introduced. Methods to overcome these problems are explained. The basic operation of the Kalman filter (KF) is also explained since its operation is widely used in tracking applications.

Finally location accuracy results derived from a simple application of theory are presented. These give some impression of the relative merits of the various location calculation techniques under vastly over–simplified assumptions, which form a basis for subsequent chapters.

2.1 Mobile Communications Channel

The radio propagation channel in mobile communications systems is a complicated non–linear function of the environment. Figure 2.1 shows a typical multipath environment, including both reflection and diffraction, and its associated channel impulse response (CIR). Each multipath can be characterised by its amplitude, a_l; phase shift, ϕ_l; time delay, τ_l; AOA, α_l; and Doppler shift, f_{dl}. Typically the characteristics of the channel that are critical to algorithm performance are fast fading of the received power caused by superposition of rays from a diffuse scatterer(s), superposition of multipaths with differing absolute delays and power levels, and long term power fading caused by shadowing.

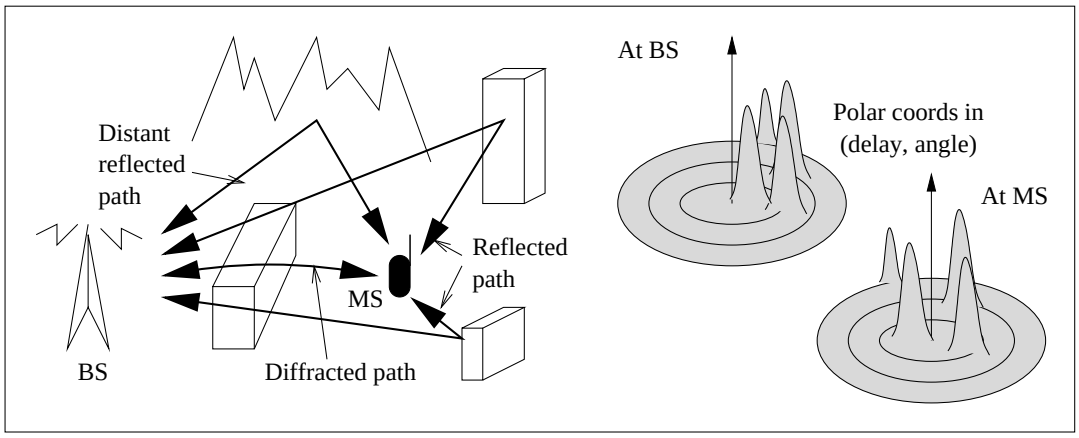

Figure 2.1: A typical urban multipath environment and angular/delay CIR at MS and BS

Classically the CIR at any point in space for an omnidirectional antenna, $h(t,\tau)$, has been represented as a time varying function of the form [3]

$$h(t,\tau) = \sum_{l=0}^{L(t)-1} a_l(t) e^{j\phi_l(t)} \delta\left(t - \tau_l(t)\right) \tag{2.1}$$

where L is the number of multipath components. The received signal, $r(t)$, is found from the convolution of the transmitted signal, $s(t)$, with the CIR [4].

$$r(t) = \int_{-\infty}^{+\infty} h(t,\tau) s(t-\tau) d\tau + n(t) \tag{2.2}$$

where $n(t)$ is a complex Gaussian noise process. It should be noted that in reality the integration takes place over a finite range, defined by the delay spread of the channel.

Since the introduction of mobile networks several methods have been used to model the propagation channel, the choice of which depends on the application being studied. These are discussed in Sections 2.1.1 to Section 2.1.3.

2.1.1 Stored and Deterministic Models

A stored model is simply an actual measured CIR. Note that the CIR is a continuous function in delay.

An extension of this idea is to use deterministic modelling. Ray tracing techniques [5], [6], [7]

can be used. These apply the geometrical theory of diffraction and reflection to the geographical, topographical and morphographical structure of the region of interest. Naturally these methods are extremely computationally intensive, but can give extremely accurate representations of the complex field and thus the CIR at each point in space.

2.1.2 Path Loss and Shadowing Models

Simpler field strength prediction models have been developed based on empirical formulae derived from experimental data. Okumura [8] and Hata [9] developed path loss formulae from test measurements in urban areas which showed that path loss is generally greater than free space path loss predictions (the exception can be when wave guiding down urban canyons occurs e.g. [10]). MS–BS separation, MS and BS height are the main parameters, however a number of correction factors were found to be required to account for general geographical, topographical and morphographical features as well as the LOS state.

The COST 231–Walfisch–Ikegami model was developed to account more accurately for the conceptual notion of multiple rooftop diffraction and rooftop to street level diffraction. More recently dual slope models, (e.g. Min *et al* [11]) have been developed to account for the flat earth propagation model which predicts a breakpoint after which the path loss exponent increases.

Actual measured path loss tends to be distributed around the path loss predictions of the above models. For this reason a shadowing term is usually included to model this uncertainty. The uncertainty stems from a series of multiplicative attenuations of the wave power by the surroundings. Using the central limit theorem the uncertainty will be approximately lognormal distributed. Standard deviations of 8-12dB's are typically used, however this can be reduced if the MS is constrained to be LOS [11]. Gudmundson [12] found the shadowing term to be spatially correlated over 5–20m with a decaying exponential autocorrelation function. Much longer decorrelation lengths, L_{dcorr}, of 100m for rural scenarios have also been reported [13].

The single slope path loss model in the UMTS testbed [2] is

$$PL_S = 128.1 + 37.6 \log_{10}\left(\frac{d}{1000}\right) \tag{2.3}$$

where PL_S is the path loss in dB and d is the MS to BS separation. Lognormal shadowing with 8dB standard deviation is assumed unless otherwise stated. Spatial autocorrelation of the

shadowing term is modelled by a decreasing exponential autocorrelation function defined by:

$$\rho(\Delta d) = \exp\left(-\frac{|\Delta d|}{L_{dcorr}} \ln 2\right) \tag{2.4}$$

where Δd is the spatial separation of two samples and $\rho(L_{dcorr}) = 0.5$. The method for generating this form of correlated Gaussian random variables is well known and defined by a 1st order IIR filter as

$$y[i] = y[i-1]\rho + x[i]\sqrt{1-\rho^2} \tag{2.5}$$

where $x[i]$ is a Gaussian distributed random variable, $y[i]$ is the autocorrelated output fed back into the filter, and ρ is the correlation factor obtained from the previous equation.

2.1.3 Stochastic Model

Stochastic models have been developed from observations of typical channel characteristics over the last few decades. In this way the models encompass a wide range of scenarios. There are many different models currently used. Generally there are distinctions between macrocell, microcell (both outdoor) and picocell (indoor) models. The carrier frequency and bandwidth also affect the model characteristics. Both the Turin–Suzuki–Hashemi [14] outdoor model and the Saleh–Valenzuela indoor model [15] define multipath delays with Poisson point processes. The distributions can be modified to give realistic clustering of paths. The COST 207 model [16] was created as a standard testbench for GSM. In this model typical, non–time varying channel delay profiles are defined, each with a Doppler spectrum to define the fading characteristics. Several scenarios exist to model dense scatterers and distant scatterers with both Gaussian and Clarke's (Classical) Doppler spectra. In [17] a computationally efficient implementation of the model is reported. A modification to the Saleh–Valenzuela model was proposed by Spencer *et al* [18] to introduce an AOA distribution.

2.1.3.1 Geometrical scatterer model

Driven by the need to model AOA information in order to simulate antenna array performance, geometrically based single bounce scatterer models have been proposed.

Figures 2.2(a), (b) show a circular model and elliptical model respectively. The circular model,

first proposed by Jakes [19], assumes a macrocellular environment, in that the BS antenna height is large and therefore above the rooftop height. In such cases the majority of scatterers will be located around the MS. These scatterers are defined as being uniformly distributed in space within a circle of radius R_m around the MS. Ertel *et al* [3] and Piechocki *et al* [20] characterise the delay–angular distributions at the MS and BS.

In the elliptical model the BS antenna height is assumed to be at or below rooftop. In such cases the scattering will occur around both the MS and BS [21]. The MS and BS are placed at the foci of an ellipse, within which scatterers are located. The dimensions of the ellipse, a, b, are defined by the maximum delay, $\tau_{max} = 2\,R_m$ and the MS–BS separation, d.

$$a = \tfrac{d+c\tau_{max}}{2}, \quad b = \tfrac{1}{2}\sqrt{(c\tau_{max})^2 + 2c\tau_{max}d} \tag{2.6}$$

where c is the speed of light. Liberti *et al* [21] calculate the delay–angular distributions at the MS and BS assuming a uniform scatterer distribution within the ellipse. These show a much larger angular spread at the BS than those in the circular model.

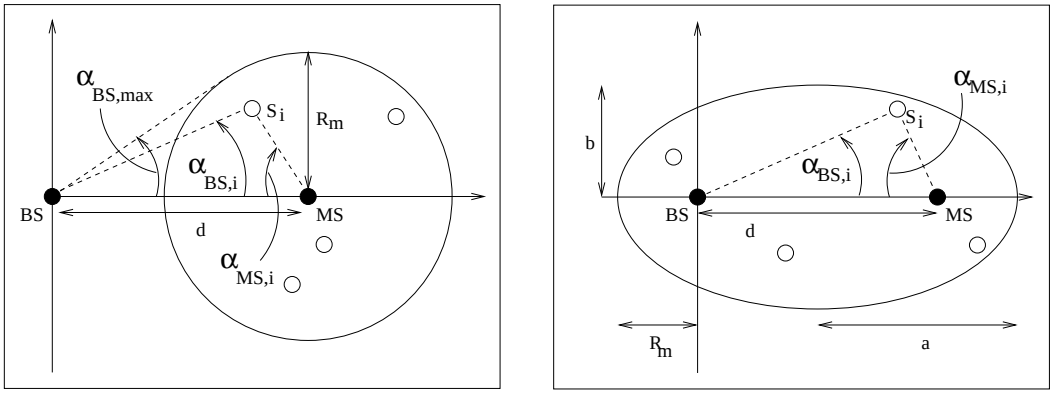

(a) (b)

Figure 2.2: Geometrically based (a) circular, (b) elliptical scatterer models

Gaussian Wide Sense Stationary Uncorrelated Scattering (GWSSUS) models have been proposed to model realistic frequency selective fading channels. In geometrical scatterer models individual scatterers can be broken down into clusters of scatterers, assumed to have identical delay, but time varying phase differences. In this case (2.1) becomes

$$h(t,\tau) = \sum_{i=0}^{L(t)-1} \sum_{k=0}^{N_i} a_{i,k}(t) e^{j\alpha_{i,k}(t)} \delta\left(t - \tau_i(t)\right) \tag{2.7}$$

where N_i is a sufficiently large number so that the central limit theorem can be applied.

The CoDiT model [22] developed as a testbed for 3rd generation systems is an amalgamation of these ideas. An elliptical model is employed however the scatterer distribution is not uniform in space. A Gaussian angle of arrival model is used to generate GWSSUS.

2.2 Measures of Location Accuracy

Location accuracy can be measured in terms of the Euclidean distance between the estimate, (x_e, y_e), and the true location, (x, y). This is often termed the circular error.

$$E_{ce} = \sqrt{(x_e - x)^2 + (y_e - y)^2} \tag{2.8}$$

For any set of location estimates the cumulative density function (CDF) of location errors can then be determined. The error at a certain percentile k is the value of location error, E_{ce}^k that satisfies $F_{E_{ce}}(E_{ce}) = k/100$. The 67%ile, E_{ce}^{67}, and 95%ile errors, E_{ce}^{95}, are of specific interest since the FCC regulations use these performance measures.

The root mean square (RMS) error is also used. For N location estimates (x_i, y_i) for $i = 1..N$ of the true location (x, y) it is defined

$$E_{RMS} = \sqrt{\frac{1}{N}\sum_{i=1}^{N}[(x_i - x)^2 + (y_i - y)^2]} \tag{2.9}$$

If the location estimates have a 2D Gaussian distribution around the true location with equal variances in each dimension then E_{ce} has a Rayleigh distribution. The percentile errors can therefore be related directly to the RMS error by suitable evaluation of the Rayleigh CDF, giving $E_{ce}^{67} = 1.05E_{RMS}$ and $E_{ce}^{95} = 1.73E_{RMS}$.

2.3 Location Estimators

The Weighted Least Squares (WLS) estimator is a popular method to solve for the MS location when range and/or bearing measurements are available. The estimator aims to minimise the

weighted mean squared error sum given by [23]

$$S_{WLS} = (\mathbf{Y} - \mathbf{X}\beta)^T \omega (\mathbf{Y} - \mathbf{X}\beta) \tag{2.10}$$

where $\mathbf{Y}$ is an $[n \times 1]$ matrix containing the measured dependent variable, β is a $[p \times 1]$ matrix containing the parameters to be estimated, ω is an $[n \times n]$ weighting matrix which can be used to weight measurements which are more accurate, and $\mathbf{X}$ is an $[n \times p]$ matrix which specifies the linear relationship between β and the dependent variable, μ. The weighting matrix ω is the only *a priori* information required and if it is not known then replacing it with the identity matrix reduces the estimator to Ordinary Least Squares (OLS).

The estimator that minimises S_{WLS} is then given by

$$\mathbf{b}_{WLS} = (\mathbf{X}^T \omega \mathbf{X})^{-1} \mathbf{X}^T \omega \mathbf{Y} \tag{2.11}$$

which minimises S_{WLS} with respect to β as long as $n \geq p$. Note that if $n = p$ the solution fits all measured data.

Assuming that ω is the inverse of the true error covariance matrix, $\mathbf{Q}^{-1}$ and the errors are zero mean, then by the Gauss–Markov theorem $\mathbf{b}_{WLS}$ is the minimum variance estimate with covariance matrix given by

$$\begin{aligned} cov(\mathbf{b}_{WLS}) = \mathbf{R}_{WLS} &= (\mathbf{X}^T \omega \mathbf{X})^{-1} \\ &= (\mathbf{X}^T \mathbf{Q}^{-1} \mathbf{X})^{-1} \end{aligned} \tag{2.12}$$

Additionally if the errors have a Gaussian distribution the WLS estimator is also the Maximum Likelihood (ML) estimator. The ML estimator maximises the probability $f(\mathbf{Y}|\beta)$. If through *a priori* knowledge the errors are known to be non–Gaussian, e.g. as in the case of NLOS errors, then the ML estimator must be solved numerically. Iterative methods for minimisation (or maximisation) of functions are well established [24], but add significantly to the burden of calculation and may be prone to finding local minima if the starting estimate of β is not well chosen.

The goodness of an estimator is determined by how accurate the location errors are compared to the theoretical lower bound on estimation accuracy determined by the measurement noise

power and noise sensitivity of the equations to be solved around the true solution. This lower bound is discussed in more detail in Section 2.3.4. The closer an estimator performance comes to this lower bound the more efficient it is said to be.

2.3.1 Estimators for Bearings

Figure 2.3 shows the intersection of bearings from several BS's. In the case of two bearings the solution is trivial, the intersection of two lines. Note that with three or more bearings in the presence of measurement noise the bearings may not all intersect at the same point. The equation for each of n bearings, α_i, is given by

$$\begin{aligned} \tan\alpha_i &= \frac{x - x_i}{y - y_i} \\ x - y\tan\alpha_i &= x_i - y_i\tan\alpha_i \end{aligned} \tag{2.13}$$

where $\beta = [\ x \quad y\ ]^T)$ is unknown location to be solved and (x_i, y_i) is the location of sensor (BS) i.

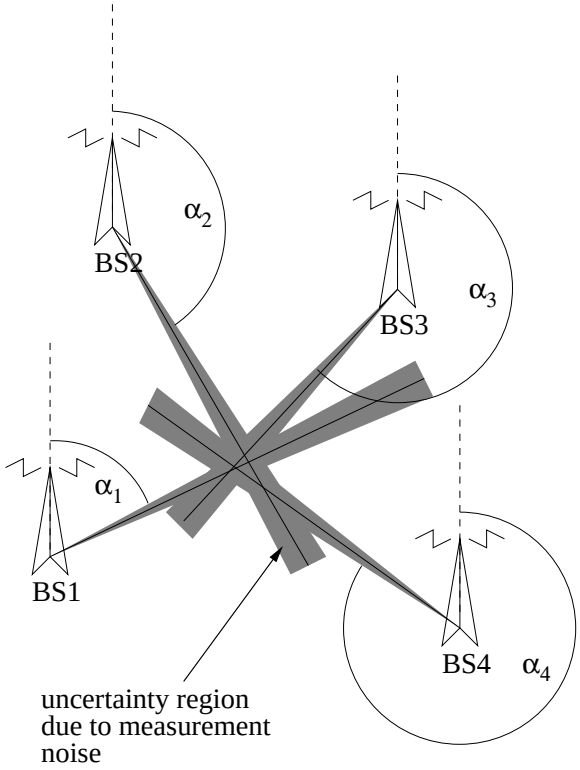

Figure 2.3: Location by bearings

Thus to form the WLS estimator

$$\mathbf{Y} = \begin{bmatrix} x_1 - y_1 \tan\alpha_1 \\ .. \\ x_n - y_n \tan\alpha_n \end{bmatrix} \tag{2.14}$$

$$\mathbf{X} = \begin{bmatrix} 1 & \tan\alpha_1 \\ .. & .. \\ 1 & \tan\alpha_n \end{bmatrix} \tag{2.15}$$

Since the WLS estimator is straightforward there is no need to consider other estimators unless the measurement noise is known to be non–Gaussian in which case an ML estimator should be considered.

2.3.2 Estimators for Ranges

Figure 2.4 shows the intersection of range circles from several BS's. Again the range circles need not intersect at one point in the presence of measurement noise. In fact the range circles need not intersect at all if the errors are large and negative. The equation for each of n range circles is

$$(x - x_i)^2 + (y - y_i)^2 - r_i^2 = 0 \tag{2.16}$$

where r_i represents the measured range to sensor i. For 3 ranges a unique minimum mean square error solution exists which may not be the intersection of the circles since they do not necessarily cross. Song [25] developed an empirical method which works in all cases in which square terms are cancelled to produce three straight lines. The intersection points of these lines are averaged to produce the final location estimate.

In the presence of an overdetermined system ($>$3 ranges) a WLS estimator can be used. Unfortunately (2.16) is non–linear in x and y and matrices $\mathbf{X}$ and β cannot be isolated. In this case either the function S_{WLS} can be minimised numerically or (2.16) can be linearised using a Taylor series expansion. The Taylor series for a function of two independent variables states

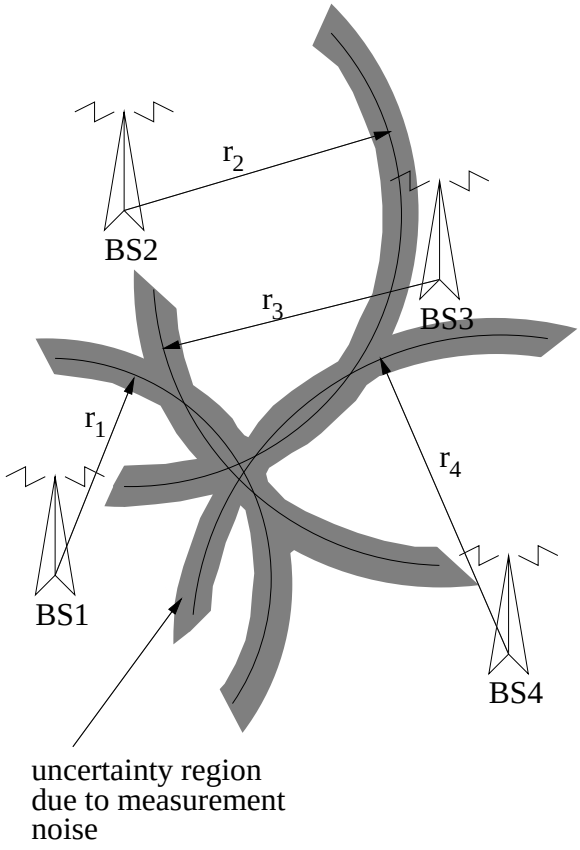

Figure 2.4: Location by ranges

[26]

$$f(x+h, y+k) = f(x,y) + \{h f_x^{'}(x,y) + k f_y^{'}(x,y)\} + \frac{1}{2!}\{h^2 f_{xx}^{''}(x,y) + 2hk f_{yx}^{''}(x,y) + k^2 f_{yy}^{''}(x,y)\} + .. \quad (2.17)$$

Since h and k are small steps the higher power terms are usually discarded. The Taylor series method uses an initial guess for (x, y) then iteratively determines the local linear WLS solution. Thus

$$\begin{bmatrix} \Delta x \\ \Delta y \end{bmatrix} = (\Delta \mathbf{X}^T \omega \Delta \mathbf{X})^{-1} \Delta \mathbf{X}^T \omega \Delta \mathbf{Y} \quad (2.18)$$

Where for range location

$$\Delta \mathbf{X} = \begin{bmatrix} \frac{\delta \mu_1}{\delta x} & \frac{\delta \mu_1}{\delta y} \\ .. & .. \\ \frac{\delta \mu_1}{\delta n} & \frac{\delta \mu_n}{\delta y} \end{bmatrix} = \begin{bmatrix} \frac{x-x_1}{r_1} & \frac{y-y_1}{r_1} \\ .. & .. \\ \frac{x-x_n}{r_n} & \frac{y-y_n}{r_n} \end{bmatrix} \tag{2.19}$$

and

$$\Delta \mathbf{Y} = \begin{bmatrix} \sqrt{(x-x_1)^2 + (y-y_1)^2} - r_1 \\ .. \\ \sqrt{(x-x_n)^2 + (y-y_n)^2} - r_n \end{bmatrix} \tag{2.20}$$

The derivation of the derivative terms is shown in Section A.1.1. After each iteration the estimate for (x, y) is updated to $(x + \Delta x, y + \Delta y)$ and applied to the next iteration until Δx and Δy converge to zero. This method is known to be efficient if the initial guess is sufficiently accurate.

Another method to solve the overdetermined case is the Divide and Conquer (DAC) approach [27] in which measurements subsets containing all possible combinations of 3 range estimates are used to calculate possible locations. All locations are then combined using a weighted average.

2.3.3 Estimators for Range Differences

Figure 2.5 shows the intersection of range difference (RD) hyperbolae between several pairs of BS's. Again if the solution is overdetermined ($>$2 RD's) in the presence of measurement noise the hyperbolae may not intersect at one point. Note that each pair of hyperbolae intersect twice. The second solution is not shown and is generally sufficiently far from the region of interest that it can be ignored. The equation of each of the $n-1$ hyperbolae is given by

$$\sqrt{(x-x_i)^2 + (y-y_i)^2} - \sqrt{(x-x_1)^2 + (y-y_1)^2} - r_{i,1} = 0 \tag{2.21}$$

where $r_{i,1}$ represents the measured RD between sensor i and sensor 1.

The solution of these equations even in the case where they are precisely determined is not straightforward since the equations are non–linear. Fang [28] and Chan [29] have derived closed form solutions which are mathematically identical. Chan's method is shown below. Firstly

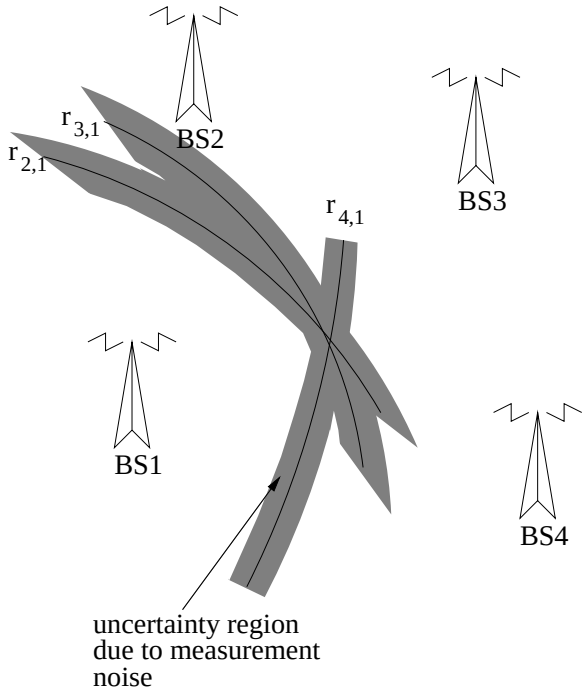

Figure 2.5: Location by RD's

(2.21) can be rearranged then squared to give

$$r_{i,1}^2 + 2r_{i,1}r_1 + r_1^2 = K_i - 2x_i x - 2y_i y + x^2 + y^2 \tag{2.22}$$

where $K_i = x_i^2 + y_i^2$ and r_i is as defined in (2.16). Subtracting (2.16) at $i = 1$ from (2.22) gives

$$r_{i,1}^2 + 2r_{i,1}r_1 = -2x_{i,1}x - 2y_i, 1y + K_i - K_1 \tag{2.23}$$

where $x_{i,1} = x_i - x_1$ and similarly for $y_{i,1}$.

With $n = 3$ sensors and thus two RD's (x, y) can be solved from (2.23) in terms of r_1. i.e.

$$\begin{bmatrix} x \\ y \end{bmatrix} = -\begin{bmatrix} x_{2,1} & y_{2,1} \\ x_{3,1} & y_{3,1} \end{bmatrix}^{-1} \left(\begin{bmatrix} r_{2,1} \\ r_{3,1} \end{bmatrix} r_1 + \frac{1}{2} \begin{bmatrix} r_{2,1}^2 - K_2 + K_1 \\ r_{3,1}^2 - K_3 + K_1 \end{bmatrix} \right) \tag{2.24}$$

Substituting the intermediate solution into (2.16) at $i = 1$ gives a quadratic in r_1. The positive solution is then substituted back into (2.24) and resolved.

In the case where $n > 3$, i.e. the solution is overdetermined, there are several methods. The Taylor–series expansion can again be used. This leads to an identical iterative WLS estimator

as in (2.18) with

$$\Delta \mathbf{X} = \begin{bmatrix} \frac{\delta \mu_1}{\delta x} & \frac{\delta \mu_1}{\delta y} \\ .. & .. \\ \frac{\delta \mu_1}{\delta n} & \frac{\delta \mu_n}{\delta y} \end{bmatrix} = \begin{bmatrix} \frac{x-x_2}{r_2} - \frac{x-x_1}{r_1} & \frac{y-y_2}{r_2} - \frac{y-y_1}{r_1} \\ .. & .. \\ \frac{x-x_n}{r_n} - \frac{x-x_1}{r_1} & \frac{y-y_n}{r_n} - \frac{y-y_1}{r_1} \end{bmatrix} \tag{2.25}$$

and

$$\Delta \mathbf{Y} = \begin{bmatrix} r_{2,1} - (r_2 - r_1) \\ .. \\ r_{n,1} - (r_n - r_1) \end{bmatrix} \tag{2.26}$$

The derivation of derivatives is shown in Section A.1.2. The DAC method is also applicable.

Chan [29] developed a closed form solution. This is achieved by solving in terms of variables $\beta = [\ x \quad y \quad r_1\ ]^T$ which are initially assumed independent using the WLS method. From (2.23) it is straightforward to generate

$$\mathbf{X} = - \begin{bmatrix} x_{2,1} & y_{2,1} & r_{2,1} \\ .. & .. & .. \\ x_{n,1} & y_{n,1} & r_{n,1} \end{bmatrix} \tag{2.27}$$

and

$$\mathbf{Y} = \frac{1}{2} \begin{bmatrix} r_{2,1}^2 - K_2 + K_1 \\ .. \\ r_{n,1}^2 - K_n + K_1 \end{bmatrix} \tag{2.28}$$

The true covariance matrix $\mathbf{Q}$ is a function of the actual values of r_i. Assuming the weighting matrix, ω, accurately represents the inverse of the covariance matrix of the RD's then $\mathbf{Q}$ is given by

$$\mathbf{Q} = \mathbf{B}\omega^{-1}\mathbf{B} \tag{2.29}$$

where

$$\mathbf{B} = diag\{r_2, .., r_n\} \tag{2.30}$$

Since r_i are not known initially the estimator can first be solved with $\mathbf{Q} = \omega^{-1}$ then the solution used to calculate r_i and recalculate $\mathbf{b}_{WLS}$ (one iteration is sufficient). As mentioned this solution assumes the elements of β are independent. However they are related by (2.16) at $i = 1$. Without expanding the details of the paper the ML estimate (assuming Gaussian noise still) of $[\ (x - x_1)^2 \quad (y - y_1)^2\ ]^T$ may be obtained by a further step

$$\mathbf{b}_{ML} = (\mathbf{X}'^T\mathbf{Q}'^{-1}\mathbf{X}')^{-1}\mathbf{X}'^T\mathbf{Q}'^{-1}\mathbf{Y}' \tag{2.31}$$

where

$$\mathbf{X}' = \begin{bmatrix} 1 & 0 \\ 0 & 1 \\ 1 & 1 \end{bmatrix} \tag{2.32}$$

and

$$\mathbf{Y}' = \begin{bmatrix} (b_{WLS1/1} - x_1)^2 \\ (b_{WLS2/1} - y_1)^2 \\ b^2_{WLS3/1} \end{bmatrix} \tag{2.33}$$

and

$$\mathbf{Q}' = 4\mathbf{B}'\mathbf{R}_{WLS}\mathbf{B}' \tag{2.34}$$

where

$$\mathbf{B}' = diag\{b_{WLS1/1} - x_1, b_{WLS2/1} - y_1, b_{WLS3/1}\} \tag{2.35}$$

The final solution is then given by

$$\mathbf{Z} = \pm\sqrt{\mathbf{b}_{ML}} + \begin{bmatrix} x_1 \\ y_1 \end{bmatrix} \tag{2.36}$$

with covariance matrix

$$\mathbf{R} = (\mathbf{B}''\mathbf{X}'^T\mathbf{B}'^{-1}\mathbf{X}^T\mathbf{B}^{-1}\omega\mathbf{B}^{-1}\mathbf{X}\mathbf{B}'^{-1}\mathbf{X}'\mathbf{B}'')^{-1} \tag{2.37}$$

where

$$\mathbf{B}^{''} = diag\{b_{ML1/1} - x_1, b_{ML2/1} - y_1\} \tag{2.38}$$

The analysis in [29] shows that Chan's method performs as well as the Taylor–series method without the problems of requiring a good initial guess and that it is better then the DAC method in the high noise region. In future chapters to provide consistency only Chan's method is used in RD calculations.

Finally in [30] a technique called RD averaging is introduced. This involves fixing all RD's in a loop to sum to zero (e.g. $r_{2,1} + r_{3,2} + r_{1,3} = 0$) thus ensuring a real solution (or real solution plane in 3D location) exists. This method is applicable when all components of the loop could be measured independently, for instance via the generalised cross correlation (GCC) method. For a known signal when a MF is used this method is not required since all loops will sum to zero.

2.3.4 Cramér–Rao Lower Bound

The Cramér–Rao Lower Bound (CRLB) is the theoretical best performance of an estimator given input measurements corrupted with Gaussian distributed noise [23] and is given by

$$\Phi^o = \left(\mathbf{G}^T \mathbf{Q}^{-1} \mathbf{G}\right)^{-1} \tag{2.39}$$

where $\mathbf{G}$ is a matrix containing the partial derivatives of the measured variables (e.g. RD's, ranges, angles) with respect to the unknown parameters (e.g. MS location). The derivation is given in Appendix A.

The best RMS error for a location system is therefore defined $\Phi^o_{RMS} = \sqrt{trace\{\Phi^o\}}$.

2.4 Measurement Techniques

In this section current methods used to obtain the measurements required for location calculation are summarised. Rappaport *et al* [31] and Caffrey *et al* [32] also provide a comprehensive reference.

2.4.1 Signal Strength

Received signal strengths vary with MS–BS separation. Thus a measured signal strength can be converted to a range. Measurement of three such ranges from the MS to three different BS's can allow a position estimate. Unfortunately the dependence between range and signal strength is a complex one. In Section 2.1.2 standard path loss models are presented which have been based on large sets of measured data. Path loss typically attenuates 20–60dB per decade (range multiplied by ten times). However in reality every scenario has slightly different path loss characteristics due to features and obstructions in the environment. To allow for these variations shadowing models are introduced which usually allow for a lognormal distribution around the median path loss with 8-12dB log standard deviation. On a shorter scale fast fading in signal strength also occurs which can have a Rayleigh probability density function (PDF). These fluctuations can be as much as 30dB with MS movements of a fraction of a wavelength.

Clearly long term averaging is required to remove the effect of Rayleigh fading. Unfortunately shadow fading cannot be averaged since such averaging would have to take place over large distances across which the true range would also have changed significantly. In the first paper to deal with MS location Figel [33] proposes a median average technique to calculate range estimates from signal strength measures. Results show smaller cell radii allow better location accuracy. For a cell radius of 2.4km location accuracy of $E_{ce}^{67} = 350$m may be possible. Song [25] also presents similar accuracy results, using a geometrical solution to the circles of range. Hata *et al* [34] explores the relationship between detection time and standard deviation of median signal strength error in more detail. Theoretical results show that even with slow Rayleigh fading rates the median can be estimated with standard deviation less than 1dB with detection time less than 10 seconds.

Hellebrandt *et al* [35] show results in a GSM environment, the standard of which specifies signal strengths for surrounding BS's are measured, quantised into 64 levels, and returned to the network at all times in case a handover is required. They propose a LS estimator to solve for location and also suggest precise knowledge via a database of past measurements could be used to further enhance location accuracy. This technique is sometimes referred to as enhanced signal strength (ESS) location. In [36] further use of a Kalman filter (KF) (see Section 2.10) to track successive location estimates is proposed, giving RMS location accuracy to 70m. Salcic *et al* [37] propose a similar method with a a neural network employed to learn the semi–random relationship between position and actual signal strengths (caused by shadowing) from

test measurements. They give location errors within 270m for real tests.

2.4.2 Time of Arrival (TOA)

Since the advent of high bit rate digital communication timing measurements can be used to locate the MS. If the transmit time of a signal is known then the receive time (with reference to the transmit time), τ_i, can be used to calculate a range as $r_i = c\tau_i$ where c is the speed of light. Three ranges provide a unique location estimate. Measurement of TOA's implies both transmitter and receiver are tightly synchronised which is not the case in mobile networks. Therefore the method generally used is to calculate the Round Trip Time (RTT) of a signal transmitted and then sent back. The TOA is simply half the RTT (adjusted for processing time at the relay point). This system has been proposed in GSM networks where the timing advance (TA) is already required to maintain frame synchronisation of received signals at the BS from multiple MS's. TA's are required from non–serving BS's which can be achieved without modification to the GSM terminals by a forced handover request to the BS's of interest (chosen from the signal strength data). The correlation method is generally used to calculate the TOA with a matched filter (MF) (see Section 2.6) to the known transmitted signal. The major problem with GSM is that the bit rate is still fairly low. Timing resolution is only required in the GSM standard to a quarter of the bit interval corresponding to a distance of 277m [38]. Silventoinen *et al* [39], [40] and Fischer *et al* [41] give basic location accuracy evaluation of TOA location in GSM with variable accuracy expectations ranging from 100 to 1000m. Pent *et al* [42] examines the performance with additional tracking via a KF. Dumont *et al* [43] apply the MUSIC super–resolution algorithm [44] to improve the correlation resolution. Multipaths arriving within the bit period cannot be individually resolved by correlation alone and this superposition can cause a large timing error. An improvement ratio of over 40% in RMS TOA error over correlation methods is achieved in a test scenario. Such methods may be unnecessary in higher bit rate systems (e.g. UMTS) when the resolution is sufficient to give the accuracy required and other errors (such as NLOS and z direction differences) start to dominate.

Chen [45] looks at a method for solving the ambiguity of having (possibly) two location estimates when only 2 TOA's are available by use of sector knowledge in tri–sectored BS's. Morley *et al* [46] propose an ML type estimator (as opposed to LS) since NLOS errors have a positive only distribution. The premise for this is that the estimate must be within all range estimates (plus Gaussian measurement noise). Improvement of around 20% is noted with this more

efficient estimator. On the down side this sort of ML estimator must be solved numerically.

2.4.3 Time Difference of Arrival (TDOA)

The drawback of TOA systems is the tight synchronisation required or in RTT mode the need for additional communication overhead (since a message must be sent both ways) and processing delays at the mid point of the round trip as the message is returned which cause further timing uncertainty. For this reason TDOA methods have been proposed for future systems. The difference in arrival time of signals from several BS's at one MS can be measured by MF(s) if the signal is known or by the GCC method [47] if it is not (see Section 2.5). Assuming the transmit time of all signals is the same the time differences (TD's) can be converted to RD's by multiplying by c. Two RD's are required to calculate a location. If the transmitters are not synchronised the difference in transmit time must be independently measured by a fixed node in the network (these have been termed Location Measurement Units, LMU's). Alternatively a signal from the MS may be received at several BS's or LMU's and the TD's measured. In this case the GCC method may be most suitable to calculate the TD from the received signals since the actual transmitted signal may not be known. Again relative synchronisation of the receiving stations must be known. The latter method is often termed Observed Time Difference (OTD).

A whole family of alternatives to GCC have been developed which exploit the cyclic stationarity of signals [48], [49] to reduce the effect of interferers. However these cyclic methods are not applicable in many mobile communications systems since all the interferers (other users) have the same cyclic frequency. Also in CDMA systems since all users transmit on the same bandwidth multiple cross correlation peaks will occur for each user which is problematic. Aatique [50] notes that the bit decisions of the unscrambled and despread signal at the serving BS can be used to reconstruct the transmitted signal. The reconstructed signal can then be used as a MF on the received signal from other BS's. As long as the bit error rate is low performance is near the single user case.

An OTD system has already been developed for GSM by Cambridge Positioning Systems (CPS) [51]. This system also uses super–resolution techniques to overcome the lack of time resolution available in GSM thus is termed enhanced OTD (E–OTD). CPS claim accuracy of up to 50m (though it is unclear which measure of accuracy this refers to). Clearly at higher bit rates one might expect accuracy to increase, though with higher carrier frequencies the propagation environment becomes more reflective (higher diffraction losses) and thus prone to larger

NLOS errors. Silventoinen *et al* [40] show simulation errors of 100-200m for the OTD system.

Porcini *et al* [52] presents results for the proposed IPDL location method (see Section 2.8) for UMTS. The simulation results using standard 3rd generation channel models show location errors between $E_{ce}^{67} = 50\text{–}100$m. Similar results are presented in the author's own paper [53] and by Ludden *et al* [54]. In [55] a rather constrained urban grid like scenario, with a delay locked loop that can synchronise tightly to the incoming rays, is examined. In such scenarios constraining the MS to lie on the road connecting LOS BS's is better than using the information from other NLOS BS's.

2.4.4 Angle of Arrival (AOA)

Resolving AOA's is not as straightforward as resolving TOA's or signal strengths especially in highly multipath environments. An antenna array is required (currently this is not practical at the MS). By comparing the received signal at each element of the array the AOA can be estimated. Phase interferometry and beamforming are well known techniques. In phase interferometry the phase differences of signals across the array are measured. In beamforming a power distribution is generated by applying complex steering weights to each elements of the array. Neither of these methods work well in multipath. Tyler *et al* [56] propose using TD's in a widely spaced antenna array to calculate the incident AOA('s) rather than phase differences. For realistic antenna geometries this implies super high resolution of TD's. More complicated algorithms exist such as MUSIC [44], ESPRIT [57] and ML [58] techniques, the latter of which is very complicated since all combinations of possible incident paths are searched. Usually the number of antenna elements in the antenna array must be equal to or greater than the number of incoming paths (per frequency channel). In CDMA type systems this adds further problems since all users are interfering on the same frequency channel with differing AOA profile. If the signal is despread first (each user with different spreading code) a reconstructed single user signal can be used in the AOA search algorithms [31].

A further drawback of AOA systems is that the antenna array elements must use tightly matched components to ensure all filtering and amplification across the array is linear and equal. Further to this the antenna orientation must be precisely measured since if the array moves even slightly (e.g. by high winds) the AOA's measured would no longer be accurate. This implies regular servicing of the antennae would be required.

Telesentinel [59] and Swales *et al* [60] use AOA technology and claim location accuracy within FCC requirements at test sites for low carrier frequency systems. Thompson *et al* [61] report much larger location errors in a real experiment ($E_{ce}^{67} >> 50$m).

2.4.5 Hybrid Techniques

Combinations of the previously described techniques are possible and may be more robust to measurement noise. Combining measurement types is usually a straightforward adaption of the location estimator. Spirito [62] describes a multilateration technique using TDOA and TOA and simulation results show this performs significantly better than a TDOA only location estimator in a GSM system. The simulations assume that the large measurement noise in GSM is the dominant error mechanism so the improvement may not be realistic when NLOS errors dominate the measurements. Korthris *et al* [63] report actual location accuracy results for combinations of TOA and AOA measurements. It is shown that location accuracy varies considerably from location to location. Increasing the number of AOA's and TOA's used in the location calculation increases the accuracy considerably. Cong *et al* [64] consider a TDOA technique augmented with one AOA from the serving BS. Results show that if the serving BS is considered LOS using the AOA can improve location accuracy of the standard TDOA only system by 70%. This hybrid technique is also analysed in the author's own paper [65].

2.4.6 Satellite Methods

The use of a Global Positioning System (GPS) receiver built into the MS has been suggested. GPS, owned by the US government, calculates a 3D location by the measurement of TDOA's from 4 or more satellites. Much is already known about the location accuracy of such a system. In stand alone mode location accuracy of 10m is now possible since the deliberate degradation of the GPS signals to civilian users was switched off. This can be countered by using reference receivers at fixed locations which transmit the continuously varying location corrections to surrounding users. This differential GPS can achieve location accuracy to within 10m [66]. The Global Navigation Satellite System (GLONASS) is the Russian equivalent to GPS. Location accuracy of 20m is possible since no deliberate errors are introduced.

The major problem with GPS type systems is the time taken to acquire the signals. In normal operating conditions the receiver may take up to 16 minutes to locate the user dependent on the

position of satellites in the sky. Each signal must be acquired by a lengthy 2D search in delay and Doppler shift since the pseudo noise codes used are long and the satellites have variable Doppler shift dependent on where they are located in the sky. The user also must have a clear line of sight to each horizon. To overcome this Soliman *et al* [67] propose use of a hybrid GPS receiver called 'gpsOne^{TM}' which utilises TOA measures from the BS network. If one TOA is known the precise GPS clock time can be known at the MS. This knowledge reduces the number of satellites that need be detected to 3 since only 3 TOA's are required to determine a location in 3D space. NLOS errors to the BS do not effect this location estimate since the TOA is only used to reference the GPS clock. The one TOA can also be used in the location estimate which reduces the number of satellites required to 2. This method introduces errors cause by NLOS. Since fewer satellites are needed acquisition time can be reduced to several seconds. Location accuracy of $E_{ce}^{67} = 19$m and $E_{ce}^{67} = 88$m is observed with 3 satellite and 2 satellite location respectively.

2.4.7 Multipath Fingerprinting

Fingerprinting methods involve building up a comprehensive database of complex multipath delay profiles at locations throughout the cell. At any time the MS can report its multipath delay to the BS and via a one to one mapping between delay profile and location the location can be estimated. This technique is only useful for urban locations when other methods may fail due to NLOS conditions. Naturally errors might occur when two disjoint areas of the cell have similar multipath profiles. Other problems include creating the database which must also be updated each time the cell environment changes, and non–stationary scatterers (e.g. vehicles) which could never be built into the model. If the fingerprinting is done at the BS the system might be more robust since a unique profile in delay and AOA could be measured.

2.4.8 Scatterer Tracing

It is possible to use the multipath make up of the channel to locate the mobile. Thompson [68] locates the source of a signal by using the TD between the arrival of the LOS signal and the signal reflected off a scatterer of known location. It is noted that location in this manner is possible however very sensitive to measurement noise. In the author's own paper [69] a more complicated algorithm is proposed that does not rely on knowledge of scatterer locations. The location accuracy again is very sensitive to measurement noise.

2.5 Generalised Cross Correlation

The generalised cross correlation (GCC) method provides a way to estimate TD between signals arriving at different sensors from one source. Knapp *et al* [47] provide a comprehensive reference.

Consider a signal, $s(t)$, transmitted from a remote source through a single path channel with noise and received at two separate BS's. The two received signals, $r_1(t)$ and $r_2(t)$ may be modelled

$$\begin{aligned} r_1(t) &= s(t) + n_1(t) \\ r_2(t) &= As(t - \tau_{2,1}) + n_2(t) \end{aligned} \tag{2.40}$$

where A is the relative attenuation difference between $r_1(t)$ and $r_2(t)$, $n_1(t)$, $n_2(t)$ are noise components and $\tau_{2,1}$ is the signal delay difference. $s(t)$, $n_1(t)$ and $n_2(t)$ are assumed to be real, joint stationary, zero mean random processes, with $n_1(t)$ and $n_2(t)$ uncorrelated to $s(t)$.

The crosscorrelation of r_1 and r_2 is described mathematically as

$$\begin{aligned} R_{r_1 r_2}(\tau) &= \int_{-\infty}^{\infty} r_1(t) r_2(t - \tau) dt \\ &= AR_{ss}(\tau - \tau_{2,1}) + R_{n_1 n_2}(\tau) \end{aligned} \tag{2.41}$$

If $n_1(t)$ and $n_2(t)$ are uncorrelated then $R_{n_1 n_2}(\tau) = 0$. This equation can be rewritten

$$R_{r_1 r_2}(\tau) = AR_{ss}(\tau) \otimes \delta(\tau - \tau_{2,1}) \tag{2.42}$$

where $\otimes$ represents convolution. The signal autocorrelation, $R_{ss}(\tau)$ peaks at $\tau = 0$ (though in cyclic signals there may be equal peaks present), thus estimation of delay difference $\tau_{2,1}$ is simply a matter of finding the delay value at which $R_{r_1 r_2}(\tau)$ peaks. In practice the integration period must be finite especially since $s(t)$, $\tau_{2,1}$ and A in practice are non stationary, thus

$$\hat{R}_{r_1 r_2}(\tau) = \frac{1}{T - \tau} \int_{\tau}^{T} r_1(t) r_2(t - \tau) dt \tag{2.43}$$

where T is a practical integration time. $\hat{R}_{r_1 r_2}(\tau)$ may also be represented as a digital sampled

signal as

$$\hat{R}_{r_1 r_2}(m) = \frac{1}{N-m} \sum_{n=m}^{N-1} r_1(n) r_2(n-m) \tag{2.44}$$

where $m = \tau$ in samples to the nearest sample.

Practical implementations of (2.43) and (2.44) are integrate and dump circuits or the sliding correlator followed by peak detection.

In (2.42) a single delay is assumed. However in many situations multipaths and thus multiple delays will exist. Therefore

$$R_{r_1 r_2}(\tau) = R_{ss}(\tau) \otimes \sum_i A_i \delta(\tau - \tau_{2,1i}) \tag{2.45}$$

The sum of δ functions is the CIR. The convolution operation can smear one δ function into another, making it impossible to distinguish peaks or delay times. For such cases there have been several prefiltering processes operating in the frequency domain that aim to accentuate the received signals at those frequencies with the highest signal to noise ratio (SNR) [47].

2.6 Matched Filter

If $s(t)$ is known the GCC methods can be greatly simplified. In such cases use of a filter matched to $s(t)$ is the optimal filter to maximise the SNR of a received signals $r_1(t)$ and $r_2(t)$ [4] in a single path channel. The response to such a Matched Filter (MF) is defined by

$$\begin{aligned} f_1(t) &= \int_0^t r_1(\tau) s(T - t + \tau) d\tau \\ f_2(t) &= \int_0^t r_2(\tau) s(T - t + \tau) d\tau \end{aligned} \tag{2.46}$$

This $f_1(t)$ and $f_2(t)$ are the time autocorrelation function of $s(t)$ convolved with each CIR. The time delay difference, $\tau_{2,1}$, can then be evaluated by comparing the relative difference in peaks in $f_1(t)$ and $f_2(t)$. Multipath conditions may cause several peaks in both $f_1(t)$ and $f_2(t)$. In such case it is desirable to select the earliest peak in terms of t since multipaths have an additional delay component over the LOS path caused by a longer signal path. This is termed Multipath Rejection (MPR).

2.7 Non–Line of Sight Problem

The Non–Line of Sight (NLOS) problem has often been termed the killer issue in MS location. In NLOS propagation the signal paths between MS and BS are all either reflected or diffracted. These paths are generally termed multipaths. Figure 2.1 shows an example of these multipaths. If the line of sight (LOS) path is not present then the first arriving path will have an additional time delay, termed excess delay, and possibly an angular difference at both MS and BS from the hypothetical LOS path. The signal will also be attenuated due to the reflection/diffraction coefficients and also the increased path length. This leads to the shadowing model previously described.

Caffrey *et al* [70] note the excess delay distance can average 400–700m in a GSM system, however little is known about the true distribution since excess delay is not critical to the communication performance of the system and these factors have not been reliably measured. More is known about the multipath delay power profile which through numerous measurements has been shown to be well approximated by an impulse plus decreasing exponential distribution [71]. The impulse part is caused by the higher power LOS component. It is reasonable to assume that in NLOS propagation the spike component is not present, thus the delay power profile is exponentially distributed. It seems reasonable to assume that the excess delay PDF is also exponentially distributed with mean inversely proportional to the number of multipaths detected. Maxwell's distribution and a non–zero mean Gaussian distribution have also been observed [72], [40] . Whichever case is true it should be noted that the excess delay distribution has a positive mean which causes significant biases in range or RD measurements.

The angular distribution at the BS is generally thought to be Gaussian like in nature, with mean the true LOS AOA. The angular spread defines the angle that encompasses directions over which significant energy is received. Paulraj *et al* [73] report typical angular spreads of 360^o in indoor scenarios, 20^o in urban scenarios, and 1^o in flat rural scenarios. Piechocki *et al* [20] present general formula for the PDF of AOA's based on the circular scatterer model. The angular distribution is

$$f_\alpha(\alpha) = \begin{cases} \frac{2d^2}{\pi r^2}\cos\alpha\sqrt{\cos^2\alpha + (r/d)^2 - 1} & -\sin^{-1}(r/d) \leq \alpha \leq \sin^{-1}(r/d) \\ 0 & otherwise \end{cases} \tag{2.47}$$

where d is the MS–BS separation, r is the radius of the circular scatterer area. The equation is

only valid for $d \geq r$. The equation shows the intuitive assumption that angular spread increases as the MS–BS separation decreases. The delay angular spread is also significant since the earlier arriving multipaths tend to have a reduced angular spread. A reasonable estimate for the LOS AOA could therefore be the mean AOA of all multipaths, the AOA of the first arriving multipath or a composite mean with higher weightings to the earliest arriving multipaths.

Several strategies have been suggested to overcome NLOS errors in timing measurements. Range residual tests have been proposed in [74], [45], [64]. Wylie *et al* [74] show that the range residual between the measured range and the estimated location using all range estimates tend to be higher for the NLOS range estimates than the LOS range estimates. For the scenario with one NLOS BS out of three they estimate correctly the NLOS BS 60% of the time. Chen [45] and Cong *et al* [64] generate subsets of measurements to generate possible location estimates. Chen [45] produces a weighted average of all possible locations using the squared range residual sum as a weighting for each location. Cong *et al* [64] propose simply using the summed squared RD residuals from each location to detect any NLOS BS. This algorithm only performs well with one NLOS BS among many LOS BS's.

Borras *et al* [75] propose a decision theoretic framework to detect NLOS BS's via a time series of estimates based on the fact that in NLOS the delay will have a higher variance than under LOS conditions. This is a reasonable assumption if the NLOS errors are larger than the measurement noise variance and the excess delay changes in a random manner due to the changing multipath profile which could not caused by erratic movement of the MS. Actually measuring NLOS delay variance is somewhat problematic since a high degree of spatial correlation occurs. Rhe CoDiT report [22] proposes modelling multipath survival lengths to be of the order of 1000 wavelengths. To detect the increased variance the MS has to move to experience spatial diversity. Since the mean true LOS delay may also change as the MS moves tracking is required to estimate the instantaneous delay mean. Wylie *et al* [74] propose using a LS fit to model the mean and calculate the variance.

Once an NLOS BS is recognised it can be removed from the location calculation. However the measurement can still improve the location estimation accuracy. Morley *et al* [46] and Cong *et al* [64] propose using ML estimators matched to the NLOS delay error distribution of range and RD's. Location accuracy can improve significantly with such implementations since the location uncertainty can effectively be limited to the positive side of the delay distribution.

NLOS delay correction methods have also been proposed. Wylie *et al* [74] propose an adjusted LS technique. A LS fit to the TOA measurement series is adjusted to pass through the earliest TOA measurements. The assumption is that at some point in the past the MS might have been LOS and this TOA can be extrapolated into the future. This method is described in more detail in Section 5.2. Jeong *et al* [76] propose exploiting an apparent relationship between mean multipath delay, τ_m and multipath delay spread τ_{RMS}. Ratios of $k = \tau_{RMS} : \tau_m = 1$ to 2 for urban areas have been reported and $\tau_{RMS} : \tau_m = 2$ in rural areas. Utilising a predetermined k the estimated $\hat{\tau}_{LOS}$ can be calculated as $\hat{\tau}_{LOS} = \tau_m - k\tau_{RMS}$. Improvement of around 40% in E_{ce}^{67} is observed using this method.

The drawbacks of many of the methods proposed to overcome NLOS errors is that they rely heavily on *a priori* knowledge of the NLOS error distributions. If these assumptions are found to be in error then the location accuracy improvement may well be diminished or even reversed.

Detection and correction of AOA NLOS errors may be possible by similar methods. Publications in this area are somewhat limited. NLOS detection may also be possible by analysing the power ratio between impulse and exponential in the power delay profile.

2.8 Hearability Problem

Hearability is a term dubbed to mean the measure of the ability of the MS to detect surrounding BS's (or vice versa). Hearability is usually expressed in terms of the number of BS's detectable in a given time interval. In most location techniques measurements from at least 3 BS's are required to make a location estimate. Using hybrid systems, e.g. TDOA/AOA or TOA/AOA, this requirement can be reduced, potentially to only 1 BS. However these systems tend to be more complicated to implement, e.g. requiring accurately calibrated antenna arrays at the BS, and lack the LOS state diversity afforded by taking measurements from several BS's. In UMTS a TDOA technique has been proposed as part of the standard [77], thus non–serving BS hearability will be an issue as TD measurements involving at least 3 BS's are required for a location estimate.

Electromagnetic radiation attenuation in mobile systems has been found to increase in proportion to anywhere between the 2nd and 6th power of the transmitter to receiver separation, R_{MS}, dependent on the terrain. This factor alone implies that a distant BS will be undetectable as the signal power will fall well below the thermal noise level. However in practical systems

(with more than one BS) carrier frequencies must be reused. In systems with several available frequencies, e.g. GSM, there will be many carrier frequencies available. Each BS is assigned a different subset of these carriers deliberately so adjacent BS's do not produce co–channel interference. The frequency reuse distance, D_{fu}, measured in cell diameters, is defined as the minimum separation between BS's using the same frequencies. Large D_{fu} implies reduced co–channel interference, however to support the same number of users per cell more carrier frequency spectrum would be required.

The hearability of distant BS's will clearly be dependent on the co–channel interference from the serving BS and thus on D_{fu}. In a system with several available frequencies this will not be a major concern as the co–channel interference levels on frequencies used by adjacent BS's should be low, even if $D_{fu} = 2$ cell diameters, the minimum for a working system. This means that, assuming the transmit power is well above the thermal noise level, several adjacent BS's can be detected and a location estimate can be made. However in CDMA systems $D_{fu} = 1$ as all BS's share the same wideband frequency. As complete code orthogonality is not practical co–channel interference will limit hearability. Clearly when an MS is close to the serving BS there is little chance of detecting other BS's due to the large difference in received power levels. This effect is often termed the 'near–far effect'. At current signal bandwidths power differences of greater than 30–40dB are probably impossible to overcome. Figure 2.6(a) shows the PDF of signal powers received by MS's placed randomly in the centre cell of a hexagonal cell arrangement (cell radius $R_C = 500$m). The simple path loss model (2.3) with 8dB lognormal shadowing was used. Figure 2.6(b) shows the same distribution with a dual slope model (3.11).

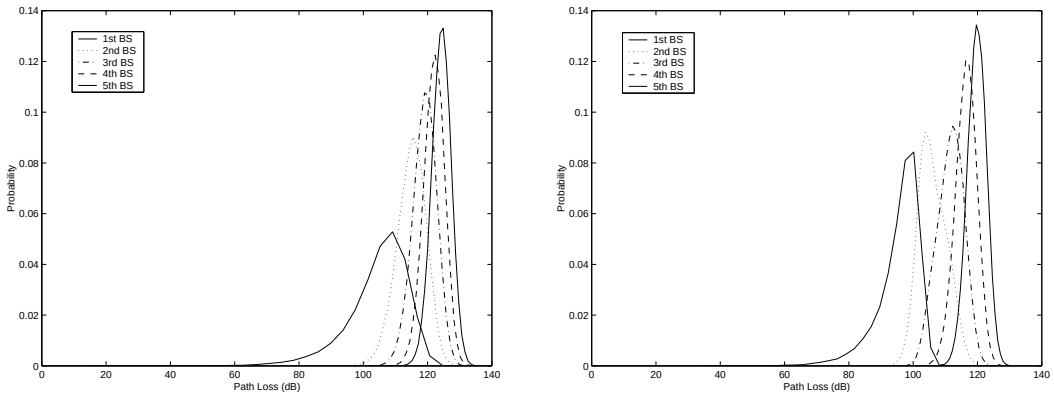

(a) (b)

Figure 2.6: Path loss distribution for BS's with 1st–5th highest received power for (a) simple, (b) dual slope path loss models

From Figure 2.6 it is possible to see that power differences between the 1st BS and all other BS's are above 30–40dB for much of the time (though it is worth noting that the correlation between power levels is not shown in the figure). Similarly the 2nd BS can also overpower the lower power BS's. The power levels of subsequent BS's tend to be similar. The dual slope model marginally increases the power of the 1st and 2nd closest BS's relative to more distant BS's and thus heightens the near–far problem.

To overcome this near–far problem various techniques have been proposed among which IPDL has been favoured. Recently IPDL has been added to UMTS. These techniques are discussed in more detail in Chapter 4.

[78] consider the hearability statistics for a UMTS system. In the former this is expressed as a hearability histogram. This is the hearability statistic that is used in this thesis. Silventoinen *et al* [40] present a similar statistic for a GSM system. Nortel Networks [79] and Ludden *et al* [54] consider the CDF of the received C/I ratio for the BS's with the 1st, 2nd and 3rd strongest received C/I. After processing and taking into account a suitable noise threshold, it is then possible to calculate hearability probabilities. Chen [45] considers the probability of detecting a BS and shows this has a significant impact on performance. The hearability distribution could be extrapolated as a simple function of the number of BS's in the simulation. The drawback of this work is that this probability is considered constant for all BS's, however realistically this will be a function of the relative separations between all BS's and the mutual interference levels. In Chapter 4 the relationship between mean hearability and location error is explored in a more realistic manner.

2.9 Geometric Dilution of Precision Problem

Geometric Dilution of Precision (GDOP) occurs when MS to be located is far away from the BS's, or when the location equations intersect nearly parallel to each other. A numerical value for GDOP [80] can be defined as

$$\begin{aligned} GDOP &= \frac{\sqrt{\sigma_x^2 + \sigma_y^2}}{\sigma_r} \\ &= \frac{\Phi^o_{RMS}}{\sigma_r} \end{aligned} \tag{2.48}$$

where σ_x^2 and σ_y^2 represent the mean square location errors in the x and y directions and σ_r^2 the measurement noise variance. Clearly high GDOP situations have to be avoided in the location calculation by suitable selection of measurements based on a current estimate of the MS location. As noted in (2.48) the GDOP value is related to the CRLB.

2.10 Kalman Filter

The Kalman Filter (KF) has wide spread use in prediction and tracking of moving targets or parameters. A KF is a tracking filter that allows for an uncertainty in the target motion by adding a random acceleration component, $\mathbf{u}_n$, between measurement samples [81]. In matrix notation the target dynamics are described

$$\mathbf{X}_n = \Phi \mathbf{X}_{n-1} + \mathbf{U}_n \tag{2.49}$$

where

$$\mathbf{X}_n = \begin{bmatrix} \mathbf{x}_n \\ \dot{\mathbf{x}}_n \end{bmatrix} \tag{2.50}$$

is the state vector and

$$\Phi = \begin{bmatrix} \mathbf{I} & \Delta t \mathbf{I} \\ \mathbf{0} & \mathbf{I} \end{bmatrix} \tag{2.51}$$

is the state transition matrix, where Δt is the sample time, and

$$\mathbf{U}_n = \begin{bmatrix} \mathbf{0} \\ \mathbf{u}_n \end{bmatrix} \tag{2.52}$$

is the dynamic model driving noise vector. $\mathbf{I}$ and $\mathbf{0}$ are the identity matrix and zero matrix respectively with the same size as the tracked dimensions in $\mathbf{X}_n$. The target state vector components can be described in as many dimensions as required though usually one (parameter tracking) or two (target tracking) dimensions are all that is required. The state vector can be extended to higher order derivatives of x_n.

Kalman [82] first derived the optimum filter which minimises the mean square error between

filter prediction, $\hat{\mathbf{X}}_{n+1,n}$, and true target value, $\mathbf{X}_{n+1}$. Equations (2.53–2.57) define the recursive operation of the filter.

$$\hat{\mathbf{X}}_{n,n-1} = \Phi\hat{\mathbf{X}}_{n-1,n-1} \tag{2.53}$$

$$\hat{\mathbf{S}}_{n,n-1} = \Phi\hat{\mathbf{S}}_{n-1,n-1}\Phi^T + \mathbf{Q}_u \tag{2.54}$$

$$\mathbf{H}_n = \hat{\mathbf{S}}_{n,n-1}\mathbf{K}^T[\mathbf{R}_n + \mathbf{K}\hat{\mathbf{S}}_{n,n-1}\mathbf{K}^T]^{-1} \tag{2.55}$$

$$\hat{\mathbf{X}}_{n,n} = \hat{\mathbf{X}}_{n,n-1} + \mathbf{H}_n[\mathbf{Y}_n - \mathbf{K}\hat{\mathbf{X}}_{n,n-1}] \tag{2.56}$$

$$\hat{\mathbf{S}}_{n,n} = \hat{\mathbf{S}}_{n,n-1} - \mathbf{H}_n\mathbf{K}\hat{\mathbf{S}}_{n,n-1} \tag{2.57}$$

where $\mathbf{Y}_n$ is the measured data vector, $\hat{\mathbf{S}}_{n,n}$ is the covariance matrix of $\hat{\mathbf{X}}_{n,n}$,

$$\mathbf{K} = \frac{\delta\mathbf{X}_{n,n-1}}{\delta\mathbf{X}_n} = \begin{bmatrix} \mathbf{I} & \mathbf{0} \end{bmatrix} \tag{2.58}$$

is the Kalman gain matrix, $\mathbf{R}_n$, is the covariance matrix of the measurement noise vector corrupting $\mathbf{Y}_n$ and $\mathbf{Q}_u$ is the covariance matrix of $\mathbf{U}_n$.

The output state vector, $\hat{\mathbf{X}}_{n,n}$, is calculated from a variance weighted sum, set by the Kalman gain, $\mathbf{H}_n$, of the filter prediction, $\hat{\mathbf{X}}_{n,n-1}$, based on the previous state vector output and the current measured data, $\mathbf{Y}_n$.

In practice the covariance matrices $\mathbf{R}_n$ and $\mathbf{Q}_u$ may not be known and so should be estimated. Usually covariance terms are zero thus for tracking to $\dot{x}$

$$\mathbf{R}_u = \begin{bmatrix}\sigma_y^2\mathbf{I}\end{bmatrix} \tag{2.59}$$

$$\mathbf{Q}_u = \begin{bmatrix} \mathbf{0} & \mathbf{0} \\ \mathbf{0} & \sigma_u^2\mathbf{I} \end{bmatrix} \tag{2.60}$$

σ_y^2 could be estimated from the variance of measured data in a test environment. A reasonable

approximation for σ_u^2, termed the velocity driving noise or sometimes the plant noise, can be calculated from the maximum acceleration of the target $\ddot{x}_{max}$ as

$$\sigma_u = \frac{\Delta t \ddot{x}_{max}}{B} \tag{2.61}$$

where $1 \geq B \geq 3$ depending on target type and the manoeuvre independence between samples.

2.10.1 KF with Manned Manoeuvring Targets

Manned manoeuvring targets have different characteristics to non–manned targets. The principal difference is that manned targets, such as vehicles, tend to manoeuvre in short bursts, maintaining constant velocity for other periods. Singer [83] proposes a manned manoeuvring target model. The target acceleration is supposed to have an exponential correlation function of the form

$$R_{\ddot{x}\ddot{x}}(\tau) = \sigma_u^2 \exp[-\alpha|\tau|] \tag{2.62}$$

where α represents the reciprocal of the manoeuvre time constant. $\alpha = 1/60$ might represent a slow turn. The KF is implemented to track derivatives of x to $\ddot{x}$ giving state transition matrix

$$\Phi = \begin{bmatrix} \mathbf{I} & \Delta t\mathbf{I} & \frac{\Delta t^2}{2}\mathbf{I} \\ \mathbf{0} & \mathbf{I} & \Delta t\mathbf{I} \\ \mathbf{0} & \mathbf{0} & \mathbf{I} \end{bmatrix} \tag{2.63}$$

if $\alpha\Delta t$ is small. The correlation model $R_{\ddot{x}\ddot{x}}(\tau)$ is introduced into $\mathbf{Q}_u$ giving

$$\mathbf{Q}_u = 2\alpha\sigma_u^2 \begin{bmatrix} \Delta t^5/20 & \Delta t^4/8 & \Delta t^3/6 \\ \Delta t^4/8 & \Delta t^3/3 & \Delta t^2/2 \\ \Delta t^3/6 & \Delta t^2/2 & \Delta t \end{bmatrix} \tag{2.64}$$

if $\alpha\Delta t << 0.5$. The performance of the Singer filter is shown to improve tracking performance during a manoeuvre.

Since the target is not manoeuvring for much of the track several manoeuvre detection methods have been proposed, the idea being that when the target is not manoeuvring the velocity driving noise power, σ_u^2, can be reduced to zero (or close to zero), a constant velocity KF. When a

manoeuvre is detected σ_u^2 can increased. McAuley *et al* [84] suppose that if a manoeuvre occurs the residual sequence between the filter prediction and the measured parameters will contain a bias. This bias can be detected recursively using an exponential detector of the form

$$\Lambda_n = \exp[-\Delta t/k]\Lambda_{n-1} + (x_n - y_n) \tag{2.65}$$

where k is a constant matched to the manoeuvre time constant. If Λ_n exceeds a threshold a manoeuvre is detected. Chan *et al* [85] propose a least squares (LS) fit to the residuals to solve for the unknown forcing velocity $\mathbf{u}_n$. The covariance matrix of the fit is used to determine whether the manoeuvre has occurred and if so $\mathbf{u}_n$ is applied to the state transition. This is advantageous in that no *a priori* knowledge of the target is required to set the threshold. Kawase *et al* [86] propose an identical method, except that rather than using LS fitting to solve for the unknown $\mathbf{u}_n$, they use previous filter predictions $\mathbf{X}_{n,n}$, $\mathbf{X}_{n-1,n-1}$, $\mathbf{X}_{n-2,n-2}$ to compute $\mathbf{u}_n$ geometrically.

Gholson *et al* [87] model $\mathbf{u}_n$ as a semi–Markov process. The probability of each discrete magnitude of $\mathbf{u}_n$ being the true forcing velocity given $\mathbf{X}_{n,n-1}$ and Y_n is calculated. These probabilities are used in a weighted sum which also includes the transition probabilities between each discrete $\mathbf{u}_n$ and the last selected $\mathbf{u}_{n-1}$. Thus during periods of constant velocity $\mathbf{u}_n$ will tend towards the lowest forcing velocity (zero), while during manoeuvres $\mathbf{u}_n$ will build up successively. Ricker *et al* [88] use a similar method in which a bank of KF's representing each forcing velocity combination is used. The outputs of these are combined in a weighted sum.

2.10.2 Extended Kalman Filter

If the location estimation uses non–linear equations then non–linear target dynamics can be specified in the KF model. This type of KF is often termed the extended KF (EKF). In the EKF, $\mathbf{K}$ can be modified to take into account the non–linearities in the equations by adjusting the Kalman gain matrix accoriding to

$$\mathbf{K} = \frac{\delta \mathbf{X}_{n,n-1}}{\delta \mathbf{X}_n} \tag{2.66}$$

The modified gain extended Kalman filter (MGEKF) has also been suggested to overcome track biasing that can occur in non–linear problems [89], [90]. In this case a further gain modification is applied to $\hat{\mathbf{S}}_{n,n}$ which equalises the difference between filter prediction and the true data

before and after the gain stage of the EKF.

For the purposes of this thesis a linear model is assumed (though in practice the problems are non–linear) and these more complicated implementations are not considered further. The reasons for this is that the equations are linearised in the location estimator, thus causing the location errors to behave in a more linear manner, and that other errors (e.g. NLOS errors) outweigh the errors caused by non–linearity.

2.11 Performance Comparison of Location Techniques

In this section the performance of several triangulation based location techniques is compared by evaluating the CRLB statistic, Φ^{o}_{RMS}. Since several different schemes with different measurement types (and some hybrid schemes) are examined the GDOP statistic is not used. This also allows direct comparison between location errors produced by different measurement types.

Various cell geometries are considered. A 2 BS geometry with BS's at (0,0)m and (1000,0)m, a 3 BS geometry with an additional BS at (500,865)m and finally a 3 BS linear geometry where the additional BS is at (2000,0)m. The noise power is arbitrarily fixed to correspond to some reasonable lower bound on the measurement noise that might be expected in a real system. Such a lower bound will only occur in LOS conditions. Noise power of 100m^2 for range measurements and 10^{-5}rad^2 for angular measurements are used. In NLOS conditions the expected noise power would be much larger and would no longer be reasonably approximated by the Gaussian distribution, thus the CRLB performance is less relevant. However the analysis does show trends in performance and highlights poor location performance. Note that the performance of the systems only utilising timing measurements remains scalable with respect to cell radius. However the precision of angular based systems is reduced with increased cell radius. Signal strength measurement based location performance is more difficult to assess as measurement noise (or noise caused by shadowing) does not transform linearly to range. In this case a Gaussian noise PDF assumption is no longer adequate.

Derivations of the gradient terms for range, RD and bearing measurements required to construct $\mathbf{G}$ are shown Appendix A. Each row in $\mathbf{G}$ represents one measurement type thus for an M

TOA/N TDOA location estimator $\mathbf{G}$ is constructed as follows

$$\mathbf{G} = \begin{bmatrix} \frac{x-x_1}{r_1} & \frac{y-y_1}{r_1} \\ .. & .. \\ \frac{x-x_M}{r_M} & \frac{y-y_M}{r_M} \\ \frac{x-x_2}{r_2} - \frac{x-x_1}{r_1} & \frac{y-y_2}{r_2} - \frac{y-y_1}{r_1} \\ .. & .. \\ \frac{x-x_N}{r_N} - \frac{x-x_1}{r_1} & \frac{y-y_N}{r_N} - \frac{y-y_1}{r_1} \end{bmatrix} \tag{2.67}$$

Figures 2.7, 2.8 and 2.9 show the performance of various schemes employing one measurement technique. Location error defined by the red colour is well outwith FCC regulations, whereas green and blue colours would be within the regulations. Figures 2.7(a), (b), (c) show the location accuracy for AOA schemes with 2 BS's, 3 BS's and 3 BS's in a linear arrangement respectively. Note that the 2 BS location fails when the MS is directly between the 2 BS's but in other regions is reasonable. The 3 BS location has reduced accuracy as the MS moves outside the region of the BS's. The linear arrangement has similar problems to the 2 BS scenario. Figures 2.8(a), (b), (c) show the location accuracy for TOA schemes with 2 BS's, 3 BS's and 3 BS's in a linear arrangement respectively. The 2 BS location scheme again suffers from poor performance when the MS is directly between BS's. Note also that two solutions may exist in this scenario in which case *a priori* knowledge would have to be used to ascertain which location is correct. The 3 BS location performs well in all regions but the linear arrangement location accuracy is little better than the 2 BS scenario. Figures 2.9(a), (b) show the location accuracy for TDOA schemes with 3 BS's and 3 BS's in a linear arrangement respectively. The 3 BS location performs the best for the region between all BS's, however performs poorly outwith this triangle. There are regions linear to the orientation of each pair of BS's in which location accuracy is very poor. In the linear arrangement location accuracy is again poor in line with the BS's and distinctly worse than the TOA method outside the area enclosed by the BS's. Both TDOA methods provide two solutions. In the linear arrangement these may be especially difficult to distinguish.

Figures 2.10 and 2.11 show the performance of various hybrid schemes. Figure 2.10(a) shows the location accuracy for an AOA, TOA scheme with 1 BS. Location accuracy diminishes with distance. Although the performance looks good the 1 BS scheme is especially vulnerable to NLOS errors which are correlated in AOA and TOA. Figure 2.10(b) shows the location accuracy

for an AOA (BS at (0,0) only), TDOA scheme with 2 BS's. The location is poor in places which are not between the two BS's. As a method for locating the MS when 2 TDOA's are not available this seems quite promising. Figure 2.10(c) shows the location accuracy for a similar scheme where both BS's supply AOA's. There are no poor areas between the 2 BS's. Figure 2.11(a) shows the location accuracy for an AOA (BS at (0,0) only), TDOA scheme with 3 BS's. Here the location is overdetermined in that there is more information than required to calculate the location. The extra information removes several of the areas with poor location accuracy, seen in the 2 TDOA case in Figure 2.9(a) and further improves location accuracy between the 3 BS's. Figure 2.11(b) shows the same set up but for a linear arrangement. The location accuracy is much improved over the 2 TDOA linear case in Figure 2.9(b) and a unique solution exists. The performance is also a considerable improvement over the one TD case in Figure 2.10(b) since the areas where location accuracy is poor between the BS's are removed. Finally Figure 2.11(c) shows the location accuracy for a TOA (BS at (0,0) only), TDOA scheme with 2 BS's. This has similar performance to the 2 TOA scheme in Figure 2.8(a).

To conclude even in good (LOS) conditions the location accuracy can vary a lot depending on the location of the MS with respect to the BS's. Generally speaking increasing the number of measurements available increases the location accuracy. Using hybrid schemes can also remove areas of poor location accuracy which are characteristic of using one measurement type only.

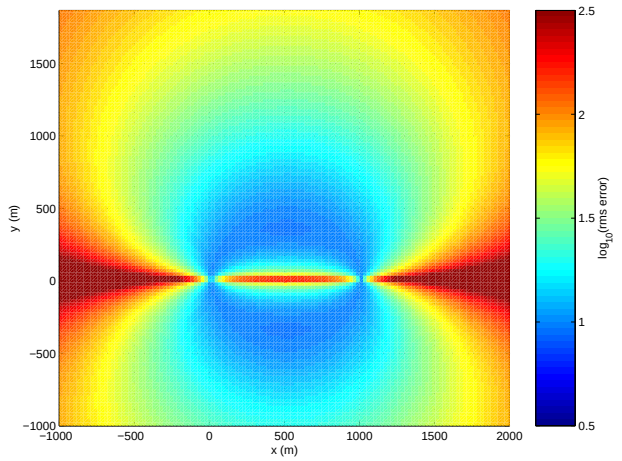

(a)

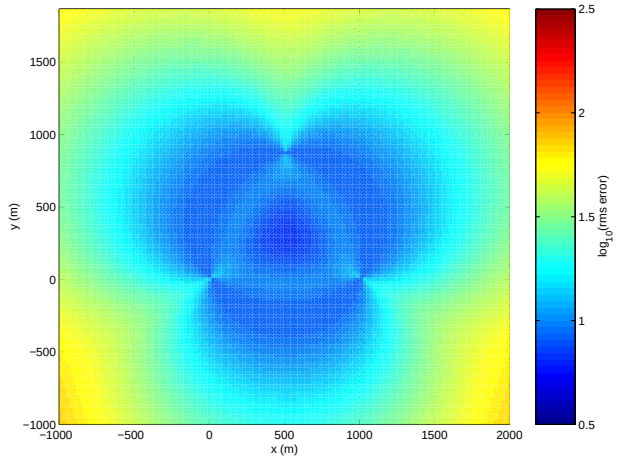

(b)

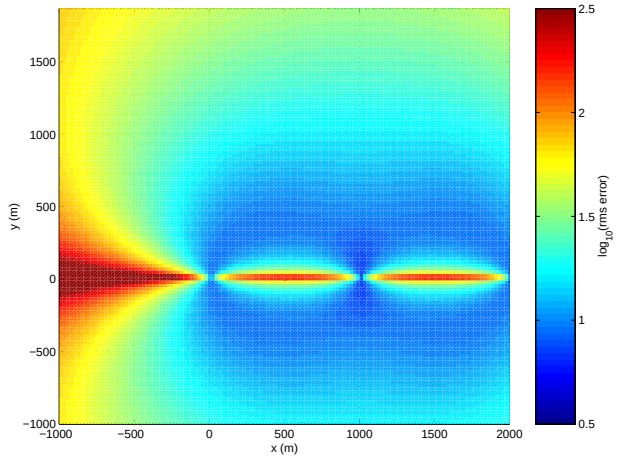

(c)

Figure 2.7: Location accuracy lower bound for (a) 2AOA – 2BS's, (b) 3AOA – 3BS's, (c) 3AOA – 3BS's linear array

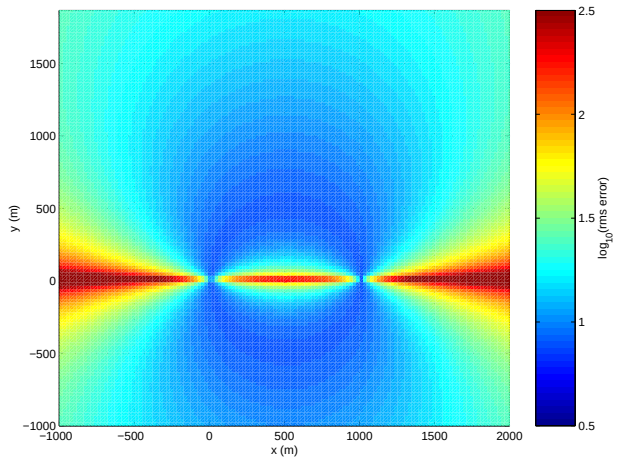

(a)

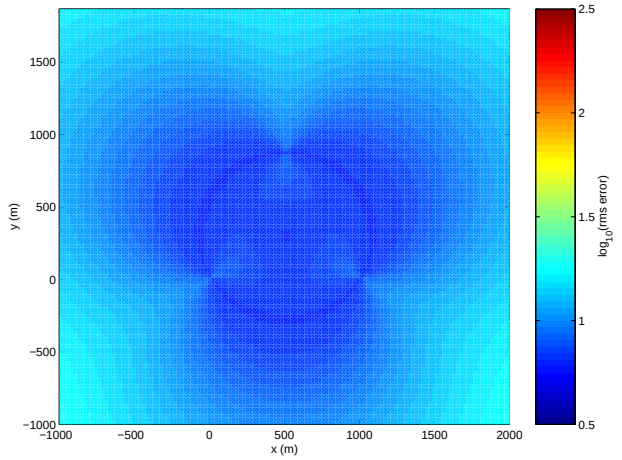

(b)

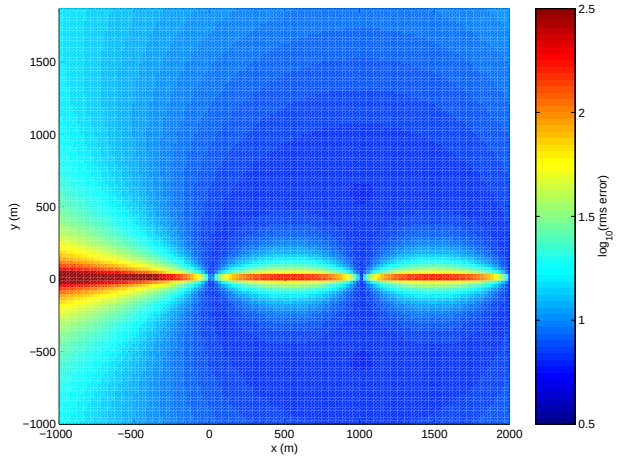

(c)

Figure 2.8: Location accuracy lower bound for (a) 2TOA – 2BS's, (b) 3TOA – 3BS's, (c) 3TOA – 3BS's linear array

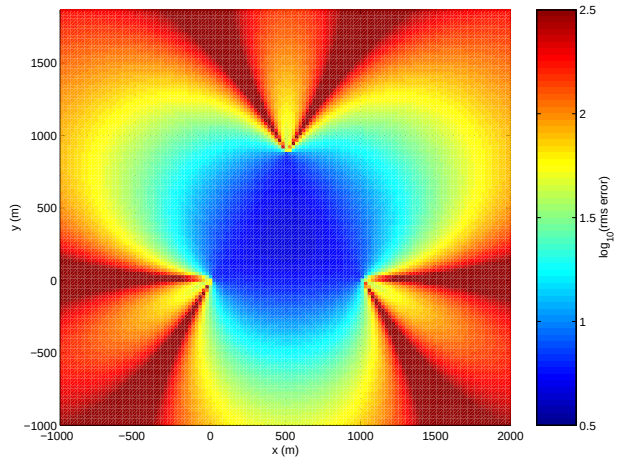

(a)

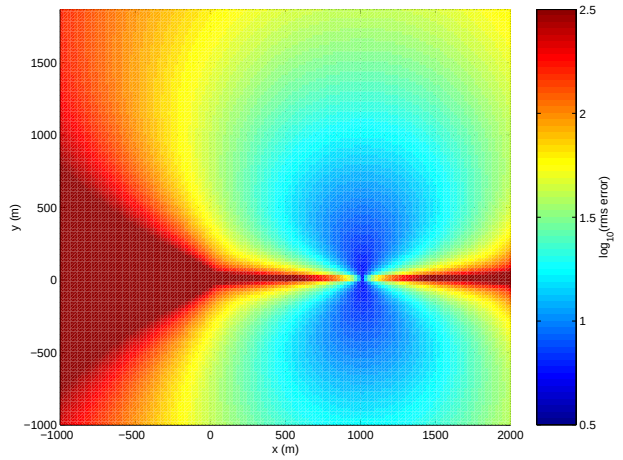

(b)

Figure 2.9: Location accuracy lower bound for (a) 2TDOA – 3BS's, (b) 2TDOA – 3BS's linear array

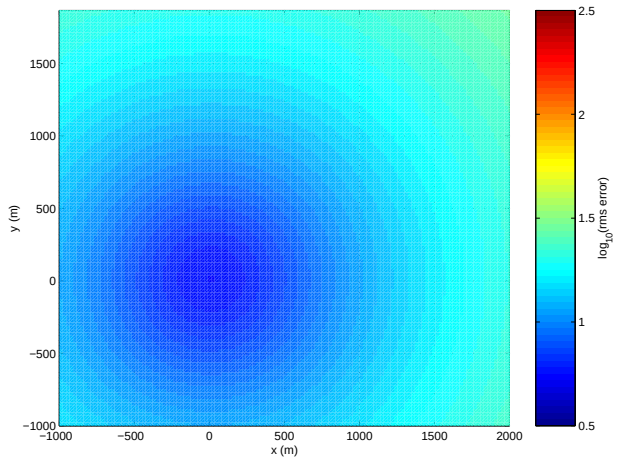

(a)

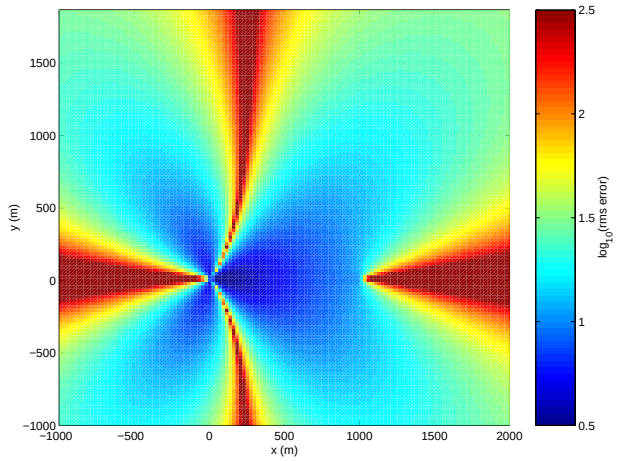

(b)

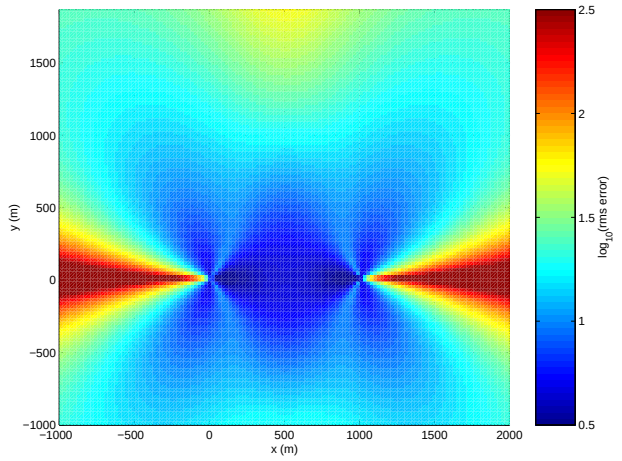

(c)

Figure 2.10: Location accuracy lower bound for some hybrid schemes (a) 1AOA, 1TOA – 1BS, (b) 1AOA, 1TDOA – 2BS's, (c) 2AOA, 1TDOA – 2BS's

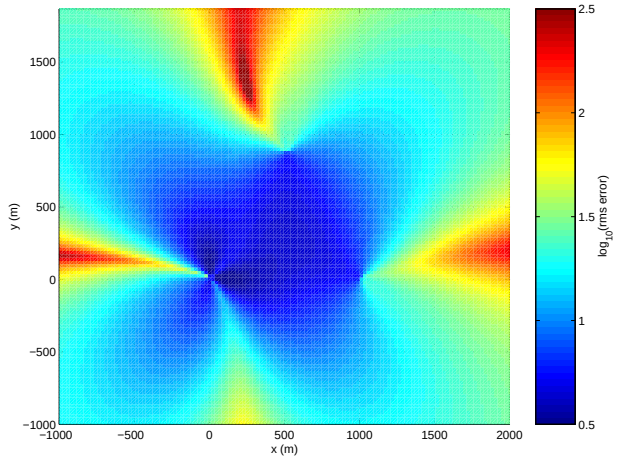

(a)

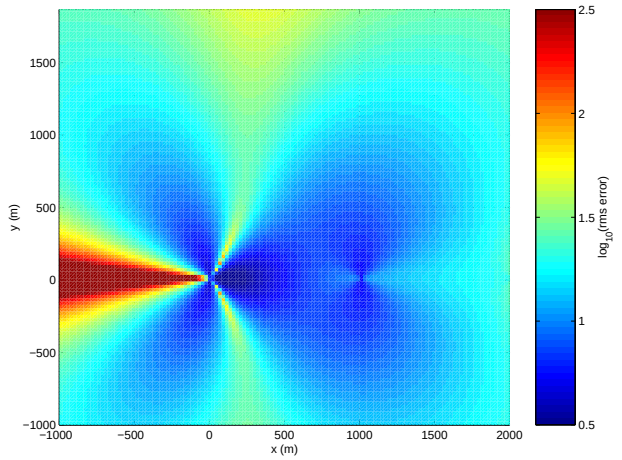

(b)

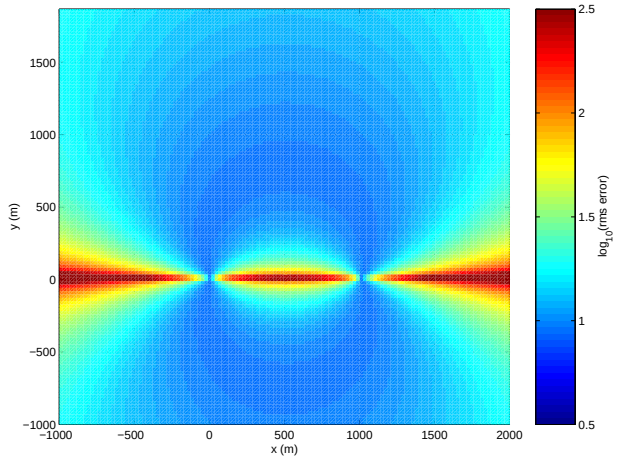

(c)

Figure 2.11: Location accuracy lower bound for some hybrid schemes (a) 1AOA, 2TDOA – 3BS's, (b) 1AOA, 2TDOA – 3BS's linear array, (c) 1TOA, 1TDOA – 2BS's

Chapter 3
Channel Model for Location Performance Evaluation

Conventional channel models are of limited suitability for realistic simulation of mobile location services, as they tend not to distinguish between LOS and NLOS situations. In this chapter a simple model is developed which explicitly includes LOS/NLOS conditions as part of a geometrical scatterer model.

In the next section the requirements of a suitable model are introduced. The CoDiT model, used as a framework for the developed model, is then discussed in more detail. In the last section the LOS/NLOS model is described and characterised with respect to excess delay and AOA PDF's.

3.1 Requirements of Channel Model for Simulation of MS Location Accuracy

In order to model the channel realistically for simulation of location estimation performance, the model must include space/time varying power levels, absolute delays and AOA's. Critical areas to consider are the:

- LOS path and corresponding statistics. NLOS conditions will seriously degrade the performance of all types of location techniques (e.g. TDOA, TOA, AOA systems) as the received signal will tend to be of lower power, be delayed and impinging at a different angle at both MS and BS in comparison to a LOS path.
- Time of arrival of multipaths with reference to a true LOS path. NLOS timing offsets will cause errors in location estimation using time based systems (e.g. TDOA, TOA systems).
- Dynamic delay and angular profile. Multipath delay and incident angle will not be constant due to the dynamic propagation environment.

- Realistic out of cell path loss model and shadowing. Transmission from several sources must be compared at one receiver (or vice versa).
- Spatial correlation factors. Delay and angular CIR's are correlated over distance.

As summarised in Section 2.1.1 through to Section 2.1.3 there are several methods generally used to model the channel. However most of these are not suitable for the simulation of MS location accuracy.

Stored models Although the model is, by definition, realistic, to rely solely on one CIR for testing location algorithms would not be a sensible idea. A large number of such CIR's would be required to test a number of possible scenarios. There are several additional drawbacks to this method of modelling for location services. Firstly, accurate MS locations would be required (probably using GPS) during the track as well as a precise timing reference between the transmitter and receiver. Additionally, the CIR's from several BS's are required simultaneously to estimate location accuracy in most schemes. These sorts of measurements are not available to the author at the time of writing.

Deterministic models These methods are extremely computationally intensive and, similarly to stored models, a large number of different locations would need to be tested.

Path loss and shadowing models Both path loss and shadowing models are required since signals from multiple sources are compared, but these should be adapted to model LOS and NLOS situations. In Section 3.3.3 a path loss model is developed which predicts LOS path loss with a small shadowing term and models LOS obstructions with additional shadowing factors.

Stochastic models The discussed models (without scatterer modelling) do not provide all the required statistical variability. Specifically the angular distribution of multipaths are not developed other than by Doppler PDF's in the COST 207 model (e.g. the classical Doppler spectrum suggests rays impinging from all AOA's). The COST 207 model also provides no variability in delay profile. The geometrical scatterer models match certain requirements. For instance absolute delay and AOA (single bounce assumption) spreads can be generated. The CoDiT model, discussed in more detail in Section 3.2, has been used as the basis for the channel model developed as it contains definitions for a number of useful scenarios and also is a standard ratified by numerous field measurements.

However none of the standard models discuss the LOS/NLOS state statistics, for which a separate model has been developed in Section 3.3.

3.2 CoDiT Model

In this section the pertinent features of the CoDiT model [22] are reproduced. The CoDiT model is an elliptical scatterer model (See Section 2.1.3.1) with several scenarios defined, e.g. urban, suburban, rural. Each scenario contains a scatterer makeup with individual scatterers characterised by mean power (Ω_i), coherence (Nakagami distribution, m_i), mean incidence angle at the MS with respect to LOS direction (α_{MSi}) and mean time delay (τ_i). The model differs from the previously described model in that α_{MS} and τ are defined as uniformly distributed and independent RV's, as opposed to the typical spatially uniform definition.

α_{MS} is uniform in the range $[0..2\pi]$ and τ is uniform in range $[\tau_{min}..\tau_{max}]$. Note that in subsequent analysis $c\tau$ is used to denote the delay distance. It is interesting to compare the joint PDF $f_{x,y}(x,y)$ (x and y are coordinates in 2D) with the spatially uniform scatterer distribution of other models. The derivation of $f_{x,y}(x,y)$ is given in Appendix B.1.

$$f_{x,y}(x,y) = \frac{1}{2\pi c(\tau_{max}-\tau_{min})}\left|\frac{y^2-(d-x)x}{(y^2+(d-x)^2)\sqrt{x^2+y^2}}+\frac{1}{\sqrt{(d-x)^2+y^2}}\right| \tag{3.1}$$

Figure 3.1 shows $f_{x,y}(x,y)$ plotted with $d = 500$m, $c\tau_{min} = 0m$ and $c\tau_{max} = 450$m. The BS is at x–y coordinate (0, 0) and the MS at (500,0). Clearly the spatial distribution of scatterers is greatest around the MS, though there is a slight increase around the BS. Directly between MS and BS there is a reduced scatterer probability. The overall effect is a composite between the circular and elliptical models with uniform spatial distribution.

Similarly $f_{\alpha_{BS},\tau}(\alpha_{BS},c\tau)$ is of interest as this will in some way reflect the performance of an AOA based location system in NLOS conditions. The derivation of $f_{\alpha_{BS},\tau}(\alpha_{BS},c\tau)$ is given in Section B.2. Equation (B.14) is not repeated here due to its length. Figure 3.2 shows $f_{\alpha_{BS},\tau}(\alpha_{BS},c\tau)$ plotted with $d = 500$m, $c\tau_{min} = 0$m and $c\tau_{max} = 450$m. The figure shows that with the model scatterers tend to lie in the true direction of the MS. Even with a large delay the distribution favours the true direction (but naturally less so than with small delay).

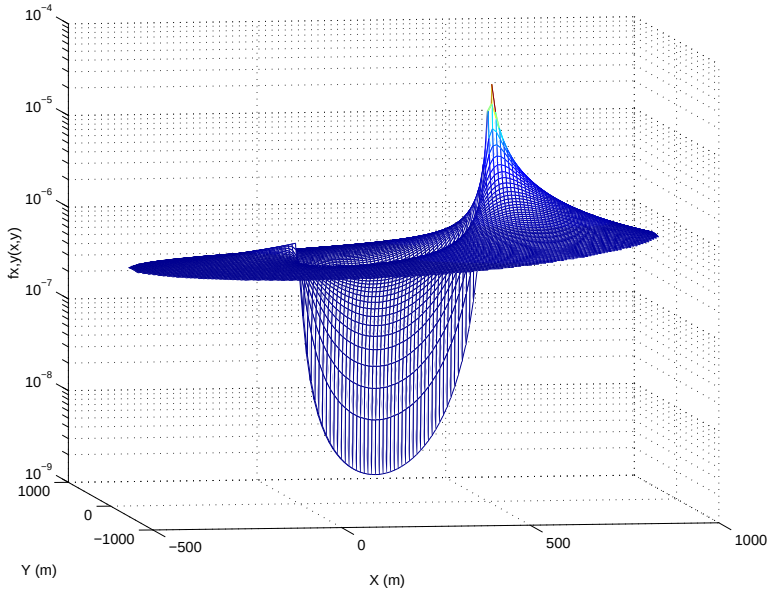

Figure 3.1: $f_{x,y}(x,y)$ plotted with $d = 500m$, $c\tau_{min} = 0m$ and $c\tau_{max} = 450m$

The channel is defined as a sum of contributions from several scatterers as in (2.7). This equation is modified slightly to give

$$h(t,\tau) = \sum_{i=0}^{L(t)-1} a_i(t)\, E_{si}(t)\, \delta\left(t - \tau_i(t)\right) \tag{3.2}$$

where $a_i(t)$ is a long term sinusoidal variation in power, $\tau_i(t)$ is a sinusoidally varying time delay, and

$$E_{si}(t) = \left[a_{i0} e^{j\left(\phi_{i0} + \frac{2pi}{\lambda} vt \cos \alpha_{MSi0}\right)} + \sum_{k=1}^{N_{waves}} a_{ik} e^{j\left(\phi_{ik} + \frac{2pi}{\lambda} vt \cos \alpha_{MSik}\right)} \right]$$

$E_{si}(t)$ is a short term field contribution from scatterer l. a_{ik} are field amplitude terms, ϕ_{ik} are random phase offsets that are uniformly distributed in the range $[0..2\pi]$, λ is the carrier wavelength, v the MS velocity, and α_{MSik} the MS incident angle of the kth component of the ith scatterer. The contribution is split into two parts, the coherent part which will typically be strong in a LOS 'scatterer', and the diffuse parts which are of equal amplitude with incident angle α_{MSik} normally distributed about the central angle α_{MSi0}. The distribution variance is

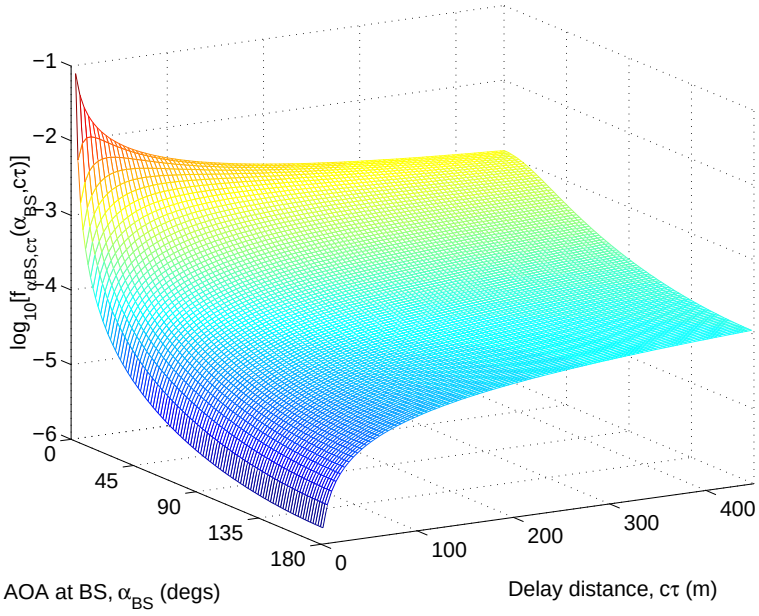

Figure 3.2: $f_{\alpha_{BS},\tau}(\alpha_{BS}, c\tau)$ plotted with $d = 500$m, $c\tau_{min} = 0$m and $c\tau_{max} = 450$m

set to 0.15 rads^2. Amplitude terms for a_{ik} are defined from the Nakagami-m distribution as

$$a_{i0} = \sqrt{\Omega_i \sqrt{1 - m_i^{-1}}}$$

$$a_{ik} = N\left[0, \frac{\Omega_i}{N_{waves}}\left(1 - \sqrt{1 - m_i^{-1}}\right)\right]$$

where N[mean, variance] represents a normal distribution. $m_i = 1$ implies all components have equal power, thus corresponds to Rayleigh fading. $m_i > 1$ implies a strong contribution from the central component, and thus could resemble Rician scattering if a classical Doppler spectrum is present. In this case the number of scatterers are limited so a spiky Doppler spectrum is obtained. $N_{waves} = 100$ is chosen to ensure the correct fading statistics are obtained. Using smaller values for N_{waves} is possible if α_{MSik} and a_{ik} are not chosen randomly but evenly spaced across their respective distributions [19].

The scatterer definitions for the scenarios which will be used in this thesis are supplied in Appendix B (Section B.4). Note that these definitions have been adjusted slightly as will be discussed in Section 3.3.1. In each scenario the number of scatterers, $L(t)$, is fixed. However, to reflect a time changing environment, individual scatterers are allowed to appear and disappear.

Each NLOS scatterer therefore has a survival length which is chosen from a positive only normal process $N_+[L_s, L_s^2/9]$. Suitable values for the mean scatterer length, L_s, of 5m and 20m for urban and suburban environments respectively have been suggested in the CoDiT model [22]. The LOS scatterer has different statistics and this is addressed in the next section.

3.3 LOS Model

For the purpose of evaluating the performance of location services whether the MS is LOS or NLOS is very important to the accuracy of the results. For instance if all BS are considered LOS the location accuracy will be very good even in the presence of many multipaths since measured propagation delay and angles of arrival of the first arriving path will reflect the true geometrical separation of BS and MS. In real scenarios the MS will not always be LOS thus conventional channel models which model typical scenarios are not always very useful, e.g. the CoDiT rural and suburban model are always LOS and the urban model is always NLOS.

In NLOS cases there are many different types of objects that can be obstructing the LOS path, e.g. buildings, vehicles, hills, and foliage. For the purpose of this work these are divided into two categories – those close or local to the MS, and distant large obstructions which might cause severe shadowing thus would be located between cells. The local obstructions occur between the MS and all BS's whereas the cellular obstructions would generally not occur between MS and its serving BS. Figure 3.3 shows the two different types of LOS obstructions in a typical scenario.

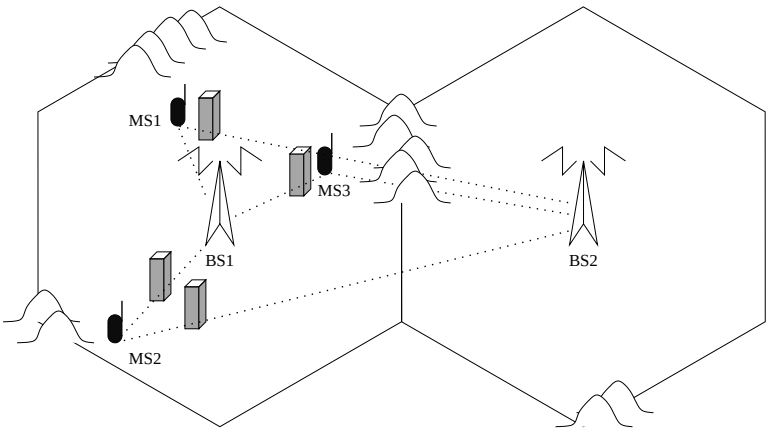

	BS1		BS2	
	LLOS	CLOS	LLOS	CLOS
MS1	✓	✓	✗	✗
MS2	✗	✓	✗	✓
MS3	✗	✓	✓	✗

Figure 3.3: LLOS and CLOS obstructions in a typical cellular environment

In the next sections the local LOS (LLOS) and cellular LOS (CLOS) models are described, with particular attention to the LOS probabilities and spatial characteristics of the LOS/NLOS transitions. For simplicity the two models are considered to be statistically independent. Following this a path loss/shadowing model is proposed which accounts for the fact that LOS states are already modelled. Finally the statistical properties of excess delay (the TOA of the first arriving path with respect to a LOS path) and AOA of first arriving path (with respect to a LOS path) are analysed and compared to theory.

3.3.1 Local LOS (LLOS)

The shortest signal path around an obstruction is always a diffractional path. However diffraction around obstructions situated close to the MS will tend to be heavily attenuated. Figure 3.4 shows the diffracted path and generalised geometry. The diffraction parameter, v_d, is defined by [91]

$$v_d = -h\sqrt{\frac{2(d_1+d_2)}{\lambda d_1 d_2}} \tag{3.3}$$

The diffraction loss may be calculated from the uniform theory of diffraction [92]. Figure 3.5 [91] shows this loss as a function of v_d. Figure 3.6 shows v_d as a function of $d_1/(d_1+d_2)$ for various obstruction heights and source separations with $\lambda = 0.15625$m. Clearly as the geometry size is reduced and the obstruction is moved closer to either transceiver the diffraction parameter becomes very negative, thus huge attenuation is experienced.

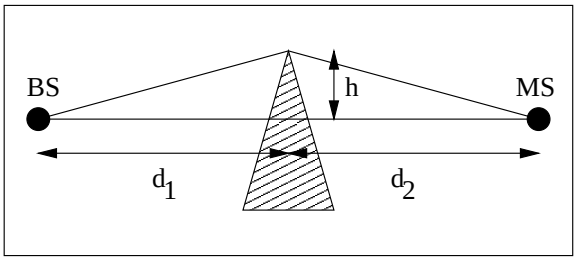

Figure 3.4: Generalised diffraction geometry

Communication with the MS is then primarily by multipaths generally by reflection off nearby objects which are outwith the heavy shadow region of the LLOS obstruction. In this model the LLOS or non–LLOS (NLLOS) state is considered a binary decision. In the NLLOS state the LLOS path is simply removed from the CoDiT channel definition by means of the disap-

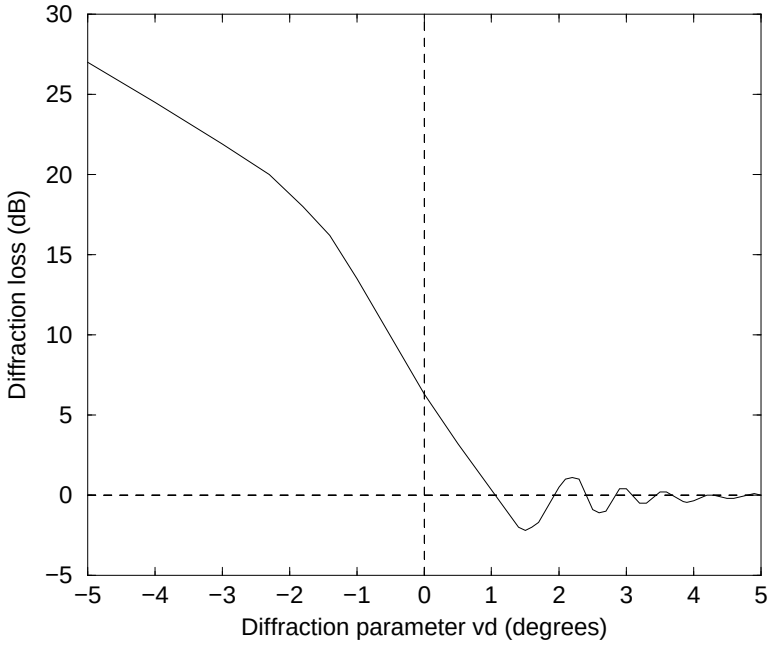

Figure 3.5: Diffraction loss against v_d

pearance function (defined in [22]). Note for the CoDiT channel definitions where no LLOS scatterer (a scatterer at zero delay) is defined, the definition has been adjusted to include an LLOS scatterer (see Section B.4).

Figure 3.7 shows a conceptual street model for LLOS analysis, where d is the MS–BS separation, θ the angle of the BS from the MS w.r.t. street orientation, h_{BS} is the BS height, h_{MS} is the MS height, h_b is the building height, w_{st} is the street width. θ_b is the critical value of θ at which the building top edge is in a perfect line with the BS. d_b is the distance from the MS to the building at this point.

By similar triangles

$$d_b = \frac{d(h_b - h_{MS})}{h_{BS} - h_{MS}} \tag{3.4}$$

Also, neglecting the effect of side streets,

$$\theta_{b-,+} = -\sin^{-1}\left(\frac{w_{MS}}{d_b}\right), \sin^{-1}\left(\frac{w_{st} - w_{MS}}{d_b}\right) \tag{3.5}$$

A conceptual value for the LLOS probability, P_{LLOS}, can be calculated. Assuming θ to be

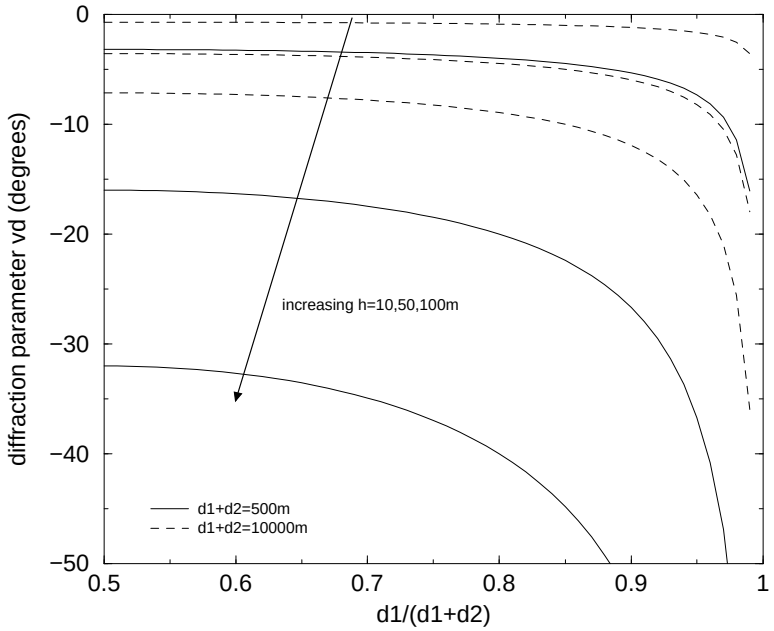

Figure 3.6: v_d for different diffraction geometries

uniformly distributed in 2π and noting that if the MS is located at an intersection P_{LLOS} is approximately doubled the following expression can be derived

$$\begin{aligned} P_{LLOS} &= \left(\frac{2w_{st}+l_{st}}{w_{st}+l_{st}}\right)\left(\frac{\theta_{b+}-\theta_{b-}}{\pi}\right) \\ &= \left(\frac{2w_{st}+l_{st}}{w_{st}+l_{st}}\right)\frac{\sin^{-1}\left(\frac{(w_{st}-w_{MS})(h_{BS}-h_{MS})}{d(h_b-h_{MS})}\right)+\sin^{-1}\left(\frac{w_{MS}(h_{BS}-h_{MS})}{d(h_b-h_{MS})}\right)}{\pi} \end{aligned} \tag{3.6}$$

Figure 3.8 shows the function plotted as a function of d and w_{MS} with $h_{BS} = 50$, $h_{MS} = 2$, $h_b = 15$, $w_{st} = 20$, $l_{st} = 100$. d has a major effect on P_{LLOS}, however it is probable that the model is unrealistic for $d > 500m$ as changing street structure and altitude differences are not considered. Location across the street, w_{MS} makes little difference to P_{LLOS} so can be neglected from simulation. The assumption that θ is uniformly distributed in 2π may be unrealistic as BS's will tend to be located in orientation with the street layout.

Although P_{LLOS} does vary with MS–BS separation, for simplicity in the model a fixed probability is used for to generate LLOS sequences between the MS and all surrounding BS's. In reality when an obstruction only just breaks the LOS path between MS and BS the near LLOS path will have no appreciable effect on location accuracy as the delay is almost the same as a genuine LLOS path. For this reason the P_{LLOS} values chosen for simulation are higher than

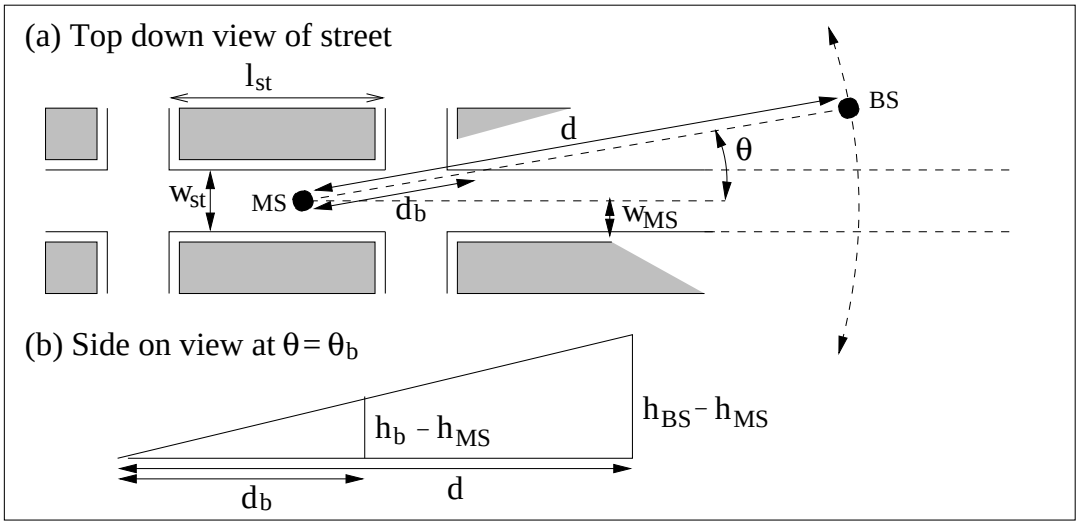

Figure 3.7: Street model for LLOS analysis, (a) top down view, (b) side on view at $\theta = \theta_b$

those shown in Figure 3.8. In the urban scenario $P_{LLOS} = 0.2$ is used; in the suburban scenario $P_{LLOS} = 0.8$ is used; and in the rural scenario $P_{LLOS} = 1.0$ is used. The higher value in the suburban scenario reflects the fact that typically the suburban area is less built up than the urban scenario, i.e. the MS is not surrounded by buildings on all sides, and that the buildings will be lower, thus the MS will typically be in a near LLOS state. In the rural scenario the MS is always LLOS or near LLOS.

As the MS moves around in the environment the LLOS state will change from LLOS to NLLOS and vice versa. The length of time spent in each state is very critical to the performance of any location estimator that uses tracking techniques to improve the location accuracy. The method chosen to construct sequences was to choose a LLOS state survival length at every state decision. The next state decision is carried out once the MS has travelled this distance. The LLOS state survival length has a positive only normal process $N_+[L_{LLOS}, L_{LLOS}^2/9]$ where L_{LLOS} is the mean LLOS state survival length in metres. L_{LLOS} is chosen to reflect the typical dimension of streets and buildings in the scenario. The mean distance in LLOS and NLLOS states, L_{LLOS}^0 and L_{NLLOS}^0 respectively, may then be calculated as

$$\begin{aligned} L_{LLOS}^0 &= L_{LLOS}(1 + P_{LLOS} + P_{LLOS}^2 + P_{LLOS}^3 + ...) \\ &= \frac{L_{LLOS}}{1 - P_{LLOS}} \end{aligned} \tag{3.7}$$

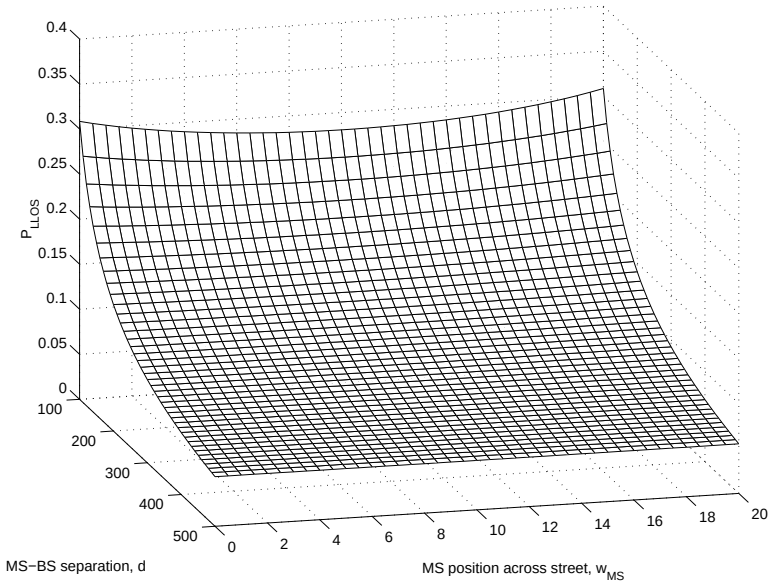

Figure 3.8: P_{LLOS} plotted as a function of d and w_{MS}

Similarly

$$L^0_{NLLOS} = \frac{L_{LLOS}}{P_{LLOS}} \tag{3.8}$$

Another method to generate the state sequences would be to use a Markov model. This is discussed in Section 3.4.

Table 3.2 summarises the parameter values selected for the created scenarios.

3.3.2 Cellular LOS (CLOS)

In a typical cell geometry, cell coverage areas are not circular in shape due to different terrain features. Large features that cause heavy attenuation to signals passing over or through will therefore tend to form the natural boundaries between cells as this is the most efficient way to plan a cell network. Generally speaking these features will be hills or possibly large buildings (taller than the BS). Diffraction is the dominant mechanism for propagation over or around these obstructions.

In these non–CLOS (NCLOS) conditions the signal is additionally attenuated, fractionally delayed and possibly subject to a small shift in incident angle at the receiver. Due to the un-

evenness of the diffraction edge over the obstruction it might also be expected that the fading becomes more severe (tending towards a Rayleigh distribution). These changes will affect all (or nearly all) paths to the MS, thus the effective signal source of the LLOS model is the diffraction edge of the CLOS obstruction.

In subsequent simulations three models are used to define the probability of being CLOS, P_{CLOS}.

Unobstructed – no obstructions between cells. $P_{CLOS} = 1$ for all BS's.

Partially obstructed – flat terrain with some large features. P_{CLOS} is defined by (3.9), used in the absence of any real measurement data, for non–serving BS, while $P_{CLOS} = 1$ for serving BS.

$$P_{CLOS}(d) = \begin{array}{ll} 1 & d < 1; \\ 1 - \frac{(d-1)}{4} & 1 \leq d \leq 5; \\ 0 & d > 5; \end{array} \tag{3.9}$$

where d is the MS–BS separation in cell radii. Figure 3.9 shows this equation.

Obstructed – all surrounding BS's are obstructed (e.g. by hills). $P_{CLOS} = 0$ for all but serving BS except $P_{CLOS} = 1$ for serving BS.

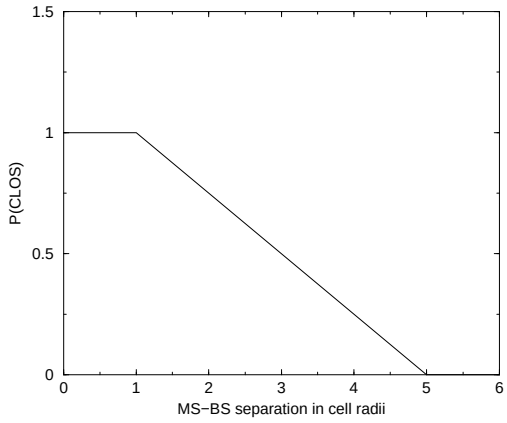

Figure 3.9: P_{CLOS} plotted against MS–BS separation for partially obstructed scenario

The mechanism for generating the CLOS state is identical to that of the LLOS state. In this case the mean CLOS state survival length, L_{CLOS}, is defined by the typical width of the shadow

region of large buildings or hills. Perahia *et al* [13] note that the shadowing autocorrelation in rural environments can be much longer than urban environments, typically > 100m, due to the presence of much larger obstructions. Table 3.2 summarises the values chosen.

As previously mentioned the shadow regions caused by NCLOS conditions have four effects on the channel (all local scatterers) experienced by the MS.

Loss of coherence (m_{NCLOS}) The diffracted path can be assumed to contain a summation of diffuse parts caused by the irregularity of the diffraction edge. This has an effect of decreasing the coherence of the path. Within the CoDiT model this can be modelled by decreasing the Nakagami–m value of the paths in the CoDiT model (towards Rayleigh fading, $m = 1$). The m distribution defined for other scatterers in each scenario is used to select the NCLOS m value for the LLOS path.

Power attenuation (Ω_{NCLOS}) All paths to the MS will be attenuated. From Figures 3.5, 3.6 it can be seen that for $d_1/(d_1 + d_2) \sim 0.5$, v_d varies from -1 to 8 depending on h. This corresponds to a diffraction loss in the region of 10 to 30dB. In the following simulations a uniform distribution across subsections of this range is used. Table 3.1 summarises the parameter ranges chosen for each CLOS scenario.

Time delay (τ_{NCLOS}) The additional distance travelled round the obstruction causes a delay in the signal arriving at the MS. Typically this will be a small delay (0–1μs). In the following simulations a uniform distribution across subsections of this range is used as shown in Table 3.1.

Angular deflection (α_{NCLOS}) There is a possibility of a small angular deflection caused by the obstruction which can be modelled by a Gaussian distribution with a mean of zero degrees. This was not implemented in the model.

Parameter	Unobst.	Partial	Obstructed
P_{CLOS} (serving BS)	1	1	1
P_{CLOS} (other BS's)	1	see (3.9)	0
Ω_{NCLOS} (dB)	NA	U[0,10]	U[10,20]
$\tau_{NCLOS})$ (μs)	NA	U[0.0,0.4]	U[0.2,0.6]

Table 3.1: Scenario specific parameters

Ω_{NCLOS} and τ_{NCLOS} will clearly be correlated with each other across their specified ranges. A correlation factor, $C_{\Omega-\tau}$, is used in the following simulations. Correlation is achieved by the following

$$y = (1 - C_{\Omega-\tau})y + C_{\Omega-\tau}x \tag{3.10}$$

where y and x represent the two random uniform variables used. Each time the MS enters an NCLOS region the four parameters are generated as defined by their PDF's. During transition from CLOS to NCLOS regions parameter values are smoothed over the first tenth of the actual CLOS state survival length using a simple function for greater realism.

3.3.3 Path Loss and Shadowing Model

Since the LOS model already incorporates heavy shadowing due to NLOS conditions, the path loss and shadowing model required need only model the LOS path loss expected. A dual slope path loss model is used which is matched to the single slope model at a distance $d = 100$m.

$$\begin{aligned} PL_D &= 30.5 + 10s_1 \log(d) && d \leq d_{bp} \\ &= 30.5 + 10s_1 \log(d_{bp}) + 10s_2 \log(d/d_{bp}) && d > d_{bp} \end{aligned} \tag{3.11}$$

The breakpoint, d_{bp}, the point at which the slope changes, can be calculated from [93]

$$d_{bp} = \min\left(\frac{4h_{BS}h_{MS}}{\lambda}, R_C\right) \tag{3.12}$$

where R_C is the cell radius, h_{BS} is the BS height, h_{MS} is the MS height and λ is the carrier wavelength. The breakpoint maximum is set to the cell radius so that out of cell radiation is reduced, which is desirable to the network operator for system performance (though in CDMA type systems partial overlapping of cells for soft handover is possible). The slope parameters used, $s_1 = 3.0$, $s_2 = 6.0$ were derived from LOS measurements by Min *et al* [11], who found that the dual slope model fits LOS measurements much better than the standard single slope model. This is due to the flat earth effect, wherein a different phase component reflected off the ground interferes with the LOS component. After the breakpoint this interference is always destructive. The dual slope model therefore has the effect of attenuating the signal more severely at greater distance, which in terms of location services requiring to detect several BS's is the worst case scenario.

The long term sinusoidal variation of scatterer received power, $a_i(t)$, already within the CoDiT model (see (3.2)) is probably only suitable for short simulation lengths, less than the period of the sinusoid. More realistic and more frequently used is the lognormal distributed exponential autocorrelation model as discussed in Section 2.1.2. Lognormal shadowing is therefore added to the path loss model with standard deviations $\sigma_{s1} = 2.6dB$ and $\sigma_{s2} = 5.8dB$ for before and after the breakpoint, again derived from measured data by Min *et al* [11]. This shadowing can be thought of as modelling the uncertainty in received LLOS power, due to flat earth effects. The sinusoidal variation in the CoDiT model is kept to allow variation in shadowing between scatterers. In this way each scatterer has partially correlated long term fading.

The shadowing decorrelation lengths, L_{dcorr}, used for for each CoDiT scenario are summarised in Table 3.2. Note that low values are used even for the rural scenario since the CLOS model accounts for shadows caused by large obstructions.

Parameter	Rural	Suburban	Urban
CoDiT model	rural	suburban	urban
R_C (km)	10.0	2.0	0.5
h_{BS} (m)	50.0	30.0	30.0
L_s (m)	NA	20	5
L_{dcorr} (m)	20	20	5
P_{LLOS}	1.0	0.8	0.2
L_{LLOS} (m)	NA	30	15
L^0_{LLOS} (m)	NA	150	18.75
L^0_{NLLOS} (m)	NA	37.5	75
L_{CLOS} (m)	1000	200	50

Table 3.2: Terrain specific parameters

3.3.4 Statistical Analysis of NLOS Errors in Time and Angle

The PDF of the channel model excess delay can be derived under some simplifications. Firstly the PDF for the LLOS excess delay is considered.

In each scenario there are N arriving rays. The first arrives at zero time delay with probability P_{LLOS} (otherwise it is undetectable) and detection probability P_{det1}. The subsequent $N-1$ rays arrive uniformly distributed in the interval (τ_{min}, τ_{max}) with, for simplicity, equal detection

probability P_{detn}. The probability of detecting $W = x$ multipath rays is a binomial distribution.

$$P(W = x) = \begin{pmatrix} N-1 \\ x \end{pmatrix} P_{detn}^{x}(1 - P_{detn})^{N-1-x} \tag{3.13}$$

From this the cumulative probability of the excess delay, τ_{ed} given that the MS is NLLOS, can be derived.

$$\begin{aligned} F_{\tau_{ed}}(\tau) &= \sum_{x=0}^{N-1} P(W = x) \prod_{n=1}^{x} P(\tau_n > \tau) \\ &= \sum_{x=0}^{N-1} \begin{pmatrix} N-1 \\ x \end{pmatrix} P_{detn}^{x}(1 - P_{detn})^{N-1-x} \left(1 - \left(\frac{\tau_{max} - \tau}{\tau_{max} - \tau_{min}}\right)^{x}\right) \end{aligned} \tag{3.14}$$

where $\tau_{min} \leq \tau \leq \tau_{max}$. Using the binomial sums theorem

$$(a + b)^n = \sum_{j=0}^{n} \begin{pmatrix} n \\ j \end{pmatrix} a^j b^{n-j} \tag{3.15}$$

(3.14) simplifies to

$$\begin{aligned} F_{\tau_{ed}}(\tau) &= 1 - \left(1 - P_{detn}\left(1 - \frac{\tau_{max} - \tau}{\tau_{max} - \tau_{min}}\right)\right)^{N-1} \\ &= 1 - \left(1 - P_{detn}\frac{\tau - \tau_{min}}{\tau_{max} - \tau_{min}}\right)^{N-1} \end{aligned} \tag{3.16}$$

Differentiating gives the PDF

$$\begin{aligned} f_{\tau_{ed}}(\tau) &= \frac{d}{d\tau} F_{\tau_{ed}}(\tau) \\ &= \frac{P_{detn}(N-1)}{\tau_{max} - \tau_{min}} \left(1 - P_{detn}\frac{\tau - \tau_{min}}{\tau_{max} - \tau_{min}}\right)^{N-2} \end{aligned} \tag{3.17}$$

The excess delay in the CLOS model is simply a uniform distribution in the range $(\tau_{cmin}, \tau_{cmax})$. Thus in CLOS conditions the excess delay PDF of (3.17) can be convolved with the uniform CLOS distribution to give the final distribution.

Figure 3.10 shows the excess delay PDF for the CoDiT urban model ($N = 20, \tau_{min} = 0\mu s, \tau_{max} = 2\mu s$) and suburban model ($N = 6, \tau_{min} = 0.1\mu s, \tau_{max} = 15\mu s$) with $P_{detn} = 0.1, 1.0$. The excess delay is normalised to its standard deviation, the evaluation of which is not

concise and therefore not given.

Lee [72] gives two PDF's generally used to represent the time delay distribution of a mobile channel. These are the Maxwell distribution

$$f_{ed}(\tau) = \frac{\sqrt{2/\pi}(3-8/\pi)^{3/2}}{\Delta^3}\tau^2 \exp\left[-\frac{(3-8/\pi)\tau^2}{2\Delta^2}\right] \tag{3.18}$$

and the exponential distribution

$$f_{ed}(\tau) = \frac{1}{\Delta}\exp\left[-\frac{\tau}{\Delta}\right] \tag{3.19}$$

where Δ is the standard deviation of τ. These are also shown in Figure 3.10 for comparison purposes. It can be seen that the CoDiT model is similar to the exponential distribution.

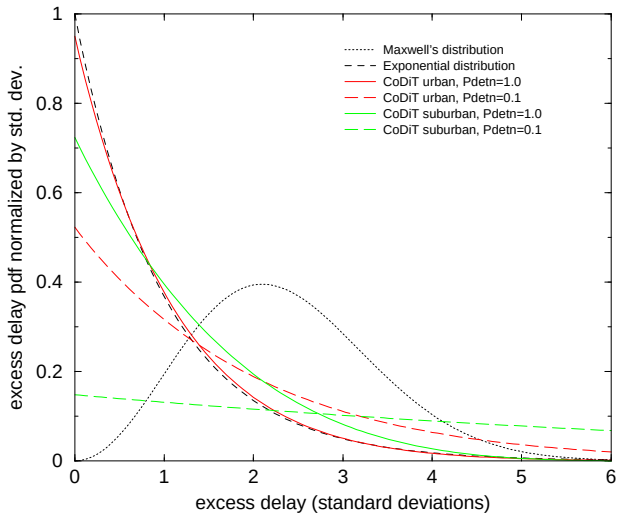

Figure 3.10: Probability density functions for excess delay model

The PDF of α_{BS} for the first arriving NLLOS path can be calculated with knowledge of $f_{ed}(\tau)$ in a similar fashion to the previous calculation of $f_{\alpha_{BS},c\tau}$. The derivation is shown in Appendix B.3, however a closed form solution does not exist. Figure 3.11 shows this PDF and the PDF for all paths for comparison for the CoDiT model with MS–BS separation, $d = 500$m. It can be seen that the first arriving path has a more compact PDF, thus according to the model, detecting the AOA of the first arriving path will give more accurate location estimates than choosing a path at random or the strongest powered path. The angular spread for the AOA is similar to models proposed by Piechocki *et al* [20], though their elliptical model assumes scattering

around the MS only. Owen *et al* [94] measure an angular spread with standard deviation 17.6 degrees in an urban environment, which again is similar to the model prediction.

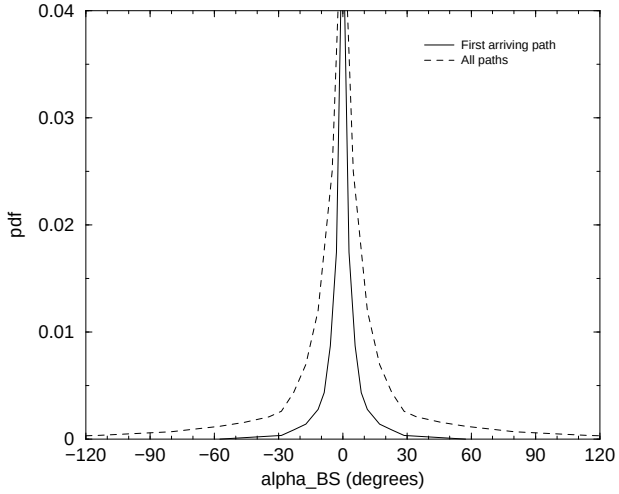

Figure 3.11: α_{BS} probability density function for first arriving path and all paths

3.4 Improvements to Model

The LLOS model would probably be more realistic if treated in a similar fashion to the CLOS model, i.e. rather than simply removing the first arriving path from the multipath profile, the first path would be subject to an attenuation, additional delay, angular deflection and fading type change. The LLOS model would be characterised by significantly larger attenuation than the CLOS model, e.g. uniform distribution from 0 to 60dB, and a larger angular deflection variance. The delay model and fading model would be similar to the CLOS model. In this way near LLOS states would be modelled more realistically.

A different way to model the LLOS and CLOS states is to use a Markov model. Markov models have been used previously in communications to model burst transmission errors [91] for example. Figure 3.12(a) shows a simple state diagram for the LLOS or CLOS state model.

Taking the LLOS model as an example, the state transition probabilities, q_1 and q_2, can be defined by

$$q_1 = \frac{D_S}{L^0_{LLOS}} \tag{3.20}$$

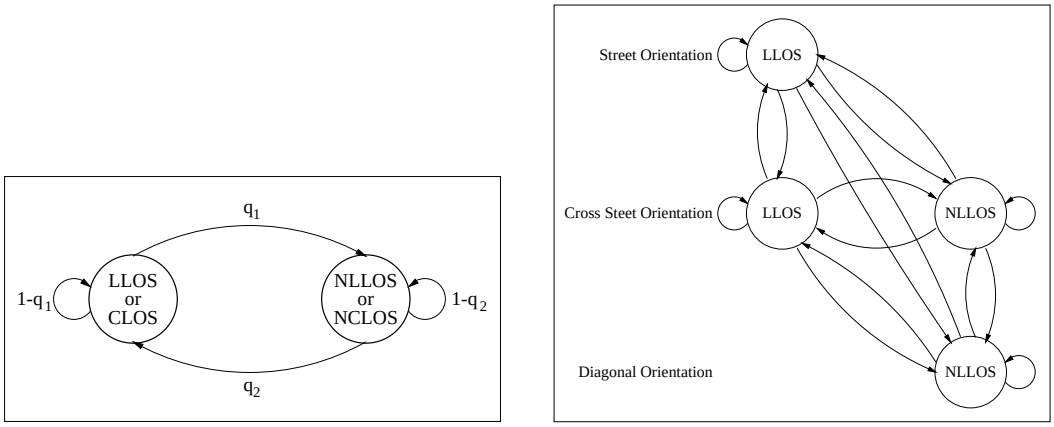

(a) (b)

Figure 3.12: Markov state diagrams for (a) simple LLOS, CLOS model, (b) LLOS model with street orientation

and

$$q_2 = \frac{D_S}{L^0_{NLLOS}} \tag{3.21}$$

where D_S is the sampling distance. Here the mean time spent in LLOS and NLLOS states, L^0_{LLOS} and L^0_{NLLOS} respectively, are defined individually. P_{LLOS} can be derived as

$$P_{LLOS} = \frac{L^0_{LLOS}}{L^0_{LLOS} + L^0_{NLLOS}} \tag{3.22}$$

Thus the LLOS model can be defined similarly to the model in Section 3.3.1 by two parameters P_{LLOS} and L^0_{LLOS}.

Figure 3.12(b) shows a more complicated implementation for the LLOS model, in which street orientation is considered. The justification for using such a model is that typically in an urban area the BS might be located pointing down a street or streets. Therefore the MS might be expected to experience long LLOS sequences as it travels down a street with a BS. If it is travelling perpendicular to streets with BS's then LLOS will occur at junctions only. Finally if the street orientation is at some other angle to the street the BS is on, LLOS would be infrequent.

A possible improvement to the model would be to include angular crosscorrelation in the shadowing, LLOS and CLOS generation between signals arriving at the MS from different BS's. Shadowing measurements by Graziano *et al* [95], Mawira *et al* [96] and Sorenson *et al* [97] show that in certain scenarios large correlations appear to exist across AOA differences of up

to 60^o. Figure 3.13 shows the azimuth location of surrounding BS's against path loss (using (2.3)), for a MS circling its serving BS in the centre of a hexagonal array with 19 BS's.

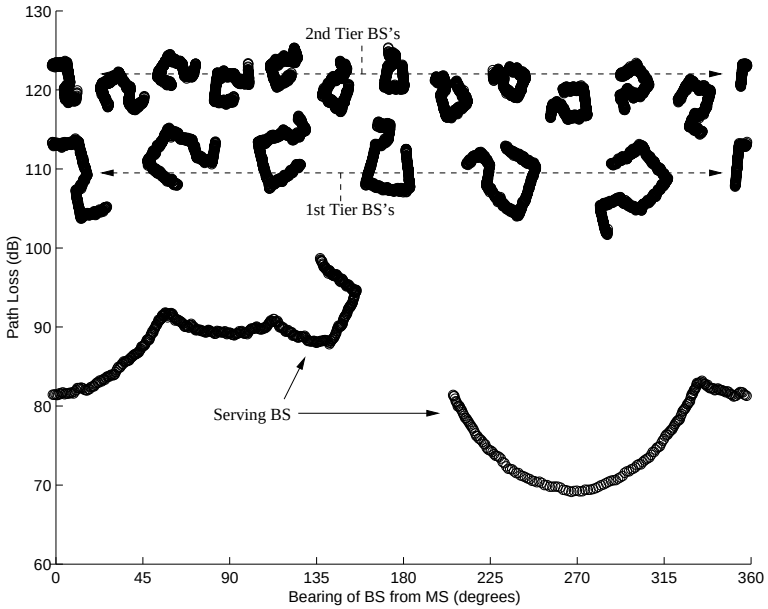

Figure 3.13: BS azimuth locations against MS–BS path loss for an MS in the urban tracking environment

From the figure it can be seen that the location in azimuth and path loss for each BS remain quite separated. Thus it is reasonable to suggest that angular shadowing variation will have very little effect on the performance of the location estimator. It should be noted that for this example the MS path was not near the cell boundary. However even in this case, when the path loss to the serving and 2nd closest BS's might be expected to be similar, the AOA's will be nearly opposite each other. Klingenbrunn *et al* [98] presents an angular correlation model for shadowing and show the method for the derivation of multiply correlated Gaussian random variables by means of a Cholesky factorisation.

In terms of the timing and angular errors generated by NLLOS and NCLOS conditions then angular correlation becomes much more important. Clearly signals impinging at the MS from a similar angle will have similar multipath profiles and LLOS states. Thus the NLLOS errors would be expected to be highly correlated. Similarly the first and second tier of BS's would be expected to have highly correlated CLOS states and NCLOS errors. The correlations would reduce the measurement diversity available and thus would be expected to reduce location accuracy. The effect might be similar to reducing the number of BS's detectable, which in

subsequent chapters is shown to reduce location accuracy but not greatly if parameter tracking is used.

Trying to incorporate such correlations into the geometrical model is impractically complex. A practical way to do it might be to use a ray tracing model, at least for the area close to the MS, which is an area to consider for future work.

3.5 Conclusions

In this chapter a channel model suitable for evaluation of location services has been developed with some modification to the CoDiT model which addresses the critical factors of spatial correlation and LOS modelling.

The mechanism for modelling spatial and LOS characteristics has been based on observed data from other sources as far as possible, however there were a number of parameters for which intuitive values were chosen. In subsequent chapters sensitivity to these parameters is determined.

The critical statistics of excess delay and AOA of the first arriving path were evaluated and shown to be similar to theoretical models. However the geometrical scatterer model used allows more realistic simulation of spatial correlation than the theoretical models alone.

In the final section several methods to improve the model were proposed, these include angular correlation of shadowing and the LOS model as well as utilising a more complicated Markov model to address typical street layout to BS alignment in the LOS model.

Chapter 4
Hearability and Idle Period Downlink Techniques

In many location techniques non–serving BS hearability is required. In CDMA systems this becomes a critical limiting factor due to the frequency reuse between BS's. Several methods have been proposed to increase BS hearability and thereby overcome this limitation. In this chapter these methods, including the author's own method, are compared in terms of hearability.

In the last section simple techniques to improve hearability by coherent and non coherent summation of measurement samples are introduced. A theoretical framework is devised under some simplifying assumptions. Integrating these into simulations leads to an evaluation of the optimum measurement sample spacing.

4.1 Hearability Assessment in UMTS

Following on from Section 2.8 it is of interest to evaluate the hearability distribution that might be expected in a CDMA system (e.g. UMTS) if no method to lower the mutual interference between BS's is implemented. Figure 4.1 shows typical pilot signal hearability figures for a CDMA system with no method to overcome the near–far effect. Table 4.1 shows the key system parameters (in the 'No IPDL' column – see Section 4.2 for a description of IPDL). The hearability for different receiver processing gains is shown. Detection of each BS is evaluated by calculating the received pilot SNR, then evaluating the detection probability, P_{det}, according to an acceptable false alarm probability, P_{FA}. An independent decision is then made as to the hearability of each BS according to P_{det}. Without loss of generality the pilot C/I ratio for BS i can be expressed as

$$\left(\frac{E_c}{I}\right)_i = \frac{sP_i}{N_o + (1-s)P_i + \sum_{k=1,k\neq i}^{N_{BS}} P_k} \tag{4.1}$$

where P_i is the path loss between BS i and the MS, s is the pilot transmit power fraction, N_o is the noise power, N_{BS} is the number of BS's in the system and all BS's are assumed to be transmitting at equal power with identical s.

	No IPDL	PR–IPDL	TA–IPDL	vTA–IPDL
P_{FA}	2.60e-5			
Path loss model	Simple path loss (2.3)			
Thermal noise power	Path loss evaluated at R_C			
N_{ip}	8			
R_C	500m			
Shadowing std dev.	8dB			
P_{idle}	0	$\frac{1}{16}$	NA	NA
P_{trans}	NA	NA	0.3	1.0
Pilot fraction	0.05	0.05	1.00	1.00

Table 4.1: Hearability simulation system parameters

For a low processing gain (24dB for one UMTS pilot symbol) only the serving BS can be detected (note that $P_{FA} = 2.6 \cdot 10^{-5}$ is much smaller than might normally be accepted for synchronisation purposes thus it is possible to not detect any BS. This high value is used since the MPR techniques discussed in Section 5.1.2 make the location receiver very sensitive to noise). Even at large processing gains (37dB for a two UMTS slot integration length), although there are often many BS's detected, about 40% of the time only two or less BS's can be detected, not enough to make a TDOA location estimate.

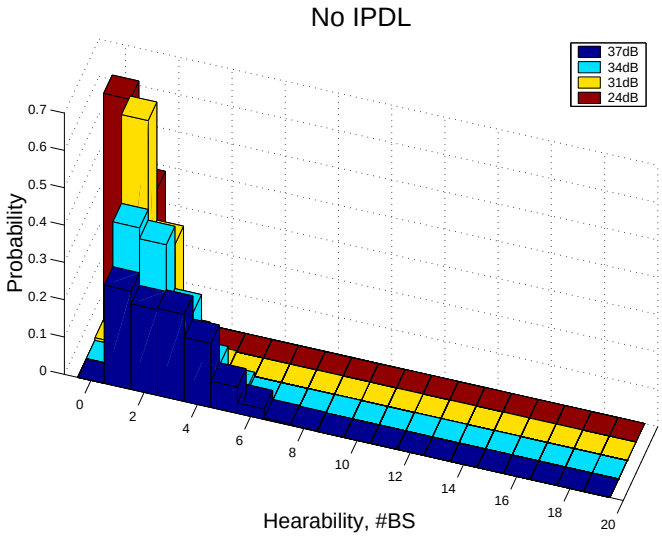

Figure 4.1: Hearability of simple system with different processing gains

The previous results apply for a single signal search. However it is possible to carry out many searches in a time interval over which the MS is approximately stationary. By simply increasing the number of measurements periods, N_p, a selection diversity scheme is obtained whereby the largest C/I ratio received will define the hearability. The measurement periods are separated in time so time diversity is obtained. The performance of such a scheme in uncorrelated Rayleigh fading is well known if the interference is assumed constant power and Gaussian distributed [91]. In Rayleigh fading the PDF of the C/I ratio during one measurement period is given by the chi–squared distribution

$$p(\gamma) = \frac{1}{\gamma_0} \exp\left(-\frac{\gamma}{\gamma_0}\right) \tag{4.2}$$

where γ_0 is the mean C/I ratio. The CDF is given by

$$F(\gamma) = \int_0^{\gamma} p(\gamma) d\gamma = 1 - \exp\left(-\frac{\gamma}{\gamma_0}\right) \tag{4.3}$$

If now N_p samples are considered, the probability that the individual C/I ratios, γ_i, are all less than or equal to a specific C/I ratio, γ, is simply

$$F(\gamma, N_p) = Pr[\gamma_1, \gamma_2, ..., \gamma_{N_p} \leq \gamma] = (F(\gamma))^{N_p} = \left(1 - \exp\left(-\frac{\gamma}{\gamma_0}\right)\right)^{N_p} \tag{4.4}$$

The mean C/I ratio can then be evaluated as

$$\begin{aligned} E[\gamma] &= \int_0^{\infty} \gamma p(\gamma, N_p) d\gamma \\ &= \int_0^{\infty} \gamma \frac{dF(\gamma, N_p)}{d\gamma} d\gamma \\ &= \int_0^{\infty} \gamma \frac{N_p}{\gamma_0} \exp\left(-\frac{\gamma}{\gamma_0}\right) \left(1 - \exp\left(-\frac{\gamma}{\gamma_0}\right)\right)^{N_p} d\gamma \\ &= \gamma_0 \sum_{k=1}^{N_p} \frac{1}{k} \end{aligned} \tag{4.5}$$

Figure 4.2 show the effect on pilot hearability of different N_p with selection diversity. Between each of N_p measurements there is uncorrelated Rayleigh fading, while lognormal shadowing is stationary. $N_p = 16$ improves performance considerably over $N_p = 8$, however even with high processing gain there is still a residual 10–20% of MS's that only detect one or two BS's.

In this analysis only uncorrelated Rayleigh fading and selection diversity has been considered.

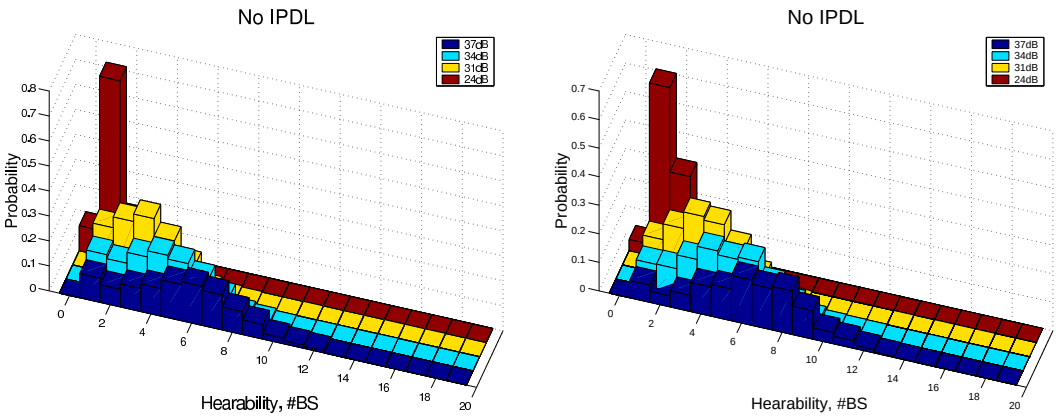

(a) (b)

Figure 4.2: Hearability of simple system with selection diversity of (a) 8, (b) 16 measurements

In Section 4.3 performance under correlated fading, shadowing and with coherent and non–coherent integration of measurements is considered.

Norrel Networks [79] proposed that a system with a processing gain of 30dB or more would be able to locate the MS in the majority of cases. Their results show (similarly to Figure 4.8(a1–3)) that 90% of MS's will be able to detect 3 BS's, suitable for a TDOA location estimate, and 94% 2 BS's. In the latter case they propose a TDOA–RTT hybrid location estimate. However there are two fundamental flaws to such a proposition. Firstly 6% of all MS's can only be located by cell ID. Assuming this 6% is a circular area around the BS, this corresponds to all MS's within $\sqrt{0.06}R_C = 0.245R_C$ of the serving BS. Consider this for a rural scenario where $R_C = 10km$. Any MS within 2.5km of the BS cannot be located to any degree of accuracy. Secondly the TDOA–RTT estimator is very unstable as the equations tend to be close to parallel at the point of intersection. In Section 2.11 the CRLB for such a system is derived and the sensitivity demonstrated. It is also possible to have two realistic solutions to the equations leading to further ambiguity.

4.2 Techniques to Improve Hearability in CDMA systems

Methods have been proposed to improve hearability in CDMA systems at the expensive of capacity. One proposal was to deploy a so called power up function (PUF) (Bruckert *et al* [99]) which would, when required on an ad hoc basis, boost the transmitted signal power of the

MS so the signal could be detected at neighbouring BS's. This proposal works in the opposite direction to the previously discussed system in that the signal from the MS is detected by several BS's rather than vice versa. The hearability figures previously discussed would directly relate to the number of BS's able to detect the MS since the downlink and uplink path losses will be statistically identical. The proposal was rejected on the grounds that the transmit power would adversely affect surrounding users, including those in other cells, by increasing the interference noise floor in an uncontrolled manner. Other considerations were possible lowering of battery life and the requirement to reduce the transmit power at the MS due to possible health risks associated with exposure to electromagnetic radiation.

The other proposals are based on idle period downlink (IPDL) structures. In IPDL each BS stops transmitting for a period. In this time interval the MS can detect surrounding BS's. Inherently the system introduces a capacity loss due to the idle times, however this does not adversely effect users in other cells and fractionally reduces the overall interference level. In the next subsections two variation of the IPDL technique are described.

4.2.1 Pseudo Random IPDL (PR–IPDL)

In PR–IPDL the idle periods at each BS occur once within each designated idle frame with a pseudo random position within the frame, Ericsson [78], (see Figure 4.3). During the idle period the MS can then hopefully detect other BS's around which are transmitting as normal. The idle period length, L_{ip}, along with the length of the idle frame, L_{if}, define the probability of each BS being idle at any time in the idle frame, P_{idle}^{PR}, as

$$P_{idle}^{PR} = \frac{L_{ip}}{L_{if}} \tag{4.6}$$

L_{if} matches the UMTS frame length and idle period lengths of $L_{ip} = 0.5$ or 1.0 UMTS slot length have been proposed as standard [100], thus $P_{idle}^{PR} = \frac{1}{16}, \frac{1}{32}$. The UMTS slot length has been chosen to assure channel stationarity over the entire slot thus increasing L_{ip} beyond this value may cause a loss of channel coherence across the MF at high Doppler frequencies. Idle period frequencies $F_{idle} = 1, 2, 5, 10$Hz have been proposed. Naturally increasing the frequency reduces the data capacity of the system. As the idle frames become more closely spaced the quality of service (QoS) for real time data transmission may be reduced. Support of two modes of operation, continuous and burst mode have been proposed [101]. In burst mode the idle periods occur in bursts at F_{idle}Hz. Between bursts no idle periods occur, thus saving

capacity at the expensive of measurement frequency and possibly location accuracy as less multipath/LOS diversity will be available. The effect of measurement frequency on location accuracy is explored in Section 5.3.6.

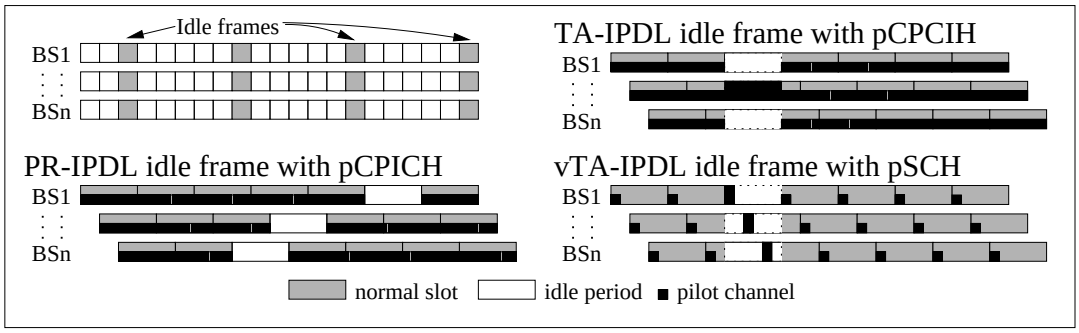

Figure 4.3: IPDL idle frame structures

The timing measurements can be taken from any physical channel, however the Primary Common Pilot Channel (PCPICH) has been proposed. This is a scrambling code one UMTS frame in length, unique to each BS. Thus the receiver will be complex as a number of codes must be integrated and the precise chip position at the start of the idle period for each BS is unknown. The processing gain available for such codes will be 31dB or 34dB for the two proposed values of L_{ip} (with 2560 chips per slot).

The purpose of using idle periods is to remove the interference from the dominant BS. However there may still be a near–far problem associated with the second highest powered signal. Similarly if that signal is idle there may be a near–far problem with the next signal and so on. Naturally as propagation distances increase the near–far effect tends to fade away. An intuitive measure of how well the technique might perform is to consider the probability that the n most high powered signals are idle and the $(n+1)$th signal is not. This probability, $P^{PR}_{BSidle}(n, P^{PR}_{idle})$, shows the probability of receiving the signal from BS_{n+1} with no higher powered interference present, in which case, assuming the signal can be brought out from the thermal noise, a measurement can be taken. Noting that the serving BS will always be idle at the measurement time it is straightforward to evaluate an expression for $P^{PR}_{BSidle}(n, P^{PR}_{idle})$ as

$$P^{PR}_{BSidle}(n, P^{PR}_{idle}) = (P^{PR}_{idle})^{n-1} - (P^{PR}_{idle})^{n} \tag{4.7}$$

Note that for simplicity the case of partially overlapping idle periods is ignored.

If there are N_{ip} idle periods then the probability of the idle event defined by $P^{PR}_{BSidle}(n, P^{PR}_{idle})$ occurring at least once is given by

$$\begin{aligned} P^{PR}_{BSidle}(n, P^{PR}_{idle}, N_{ip}) &= \sum_{i=1}^{N_{ip}} \begin{pmatrix} N_{ip} \\ i \end{pmatrix} (P^{PR}_{BSidle}(n))^i (1 - P^{PR}_{BSidle}(n))^{N_{ip}-i} \\ &= 1 - \begin{pmatrix} N_{ip} \\ 0 \end{pmatrix} (P^{PR}_{BSidle}(n))^0 (1 - P^{PR}_{BSidle}(n))^{N_{ip}} \\ &= 1 - \left[1 - (P^{PR}_{idle})^{n-1} + (P^{PR}_{idle})^n\right]^{N_{ip}} \end{aligned} \quad (4.8)$$

This probability only takes into account whether the idle states occur at least once. Naturally if they occur more often then this allows greater selection diversity in the presence of signal power level variation. The conditional expectation of the maximum signal power from N_{ip} measurements with Rayleigh fading can thus be calculated by including (4.5) in (4.8) to give

$$E\left[\frac{\gamma}{\gamma_0}|n, P^{PR}_{idle}, N_{ip}\right] = \frac{\sum_{i=1}^{N_{ip}} \sum_{k=1}^{i} \frac{1}{k} \begin{pmatrix} N_{ip} \\ i \end{pmatrix} (P^{PR}_{BSidle}(n))^i (1 - P^{PR}_{BSidle}(n))^{N_{ip}-i}}{P^{PR}_{BSidle}(n, P^{PR}_{idle}, N_{ip})} \quad (4.9)$$

A useful performance measure of the expected signal power gain for any n, P^{PR}_{BSidle} and N_{ip} can then be derived by multiplying (4.8) and (4.9) to give

$$\begin{aligned} \xi^{PR}(n, P^{PR}_{idle}, N_{ip}) &= E\left[\frac{\gamma}{\gamma_0}|n, P^{PR}_{idle}, N_{ip}\right] \cdot P^{PR}_{BSidle}(n, P^{PR}_{idle}, N_{ip}) \\ &= \sum_{i=1}^{N_{ip}} \sum_{k=1}^{i} \frac{1}{k} \begin{pmatrix} N_{ip} \\ i \end{pmatrix} (P^{PR}_{BSidle}(n))^i (1 - P^{PR}_{BSidle}(n))^{N_{ip}-i} \end{aligned} \quad (4.10)$$

As previously mentioned the hearability of the 3rd highest to weakest powered BS's is decided entirely by the presence of the dominant 2 BS's. As hearability of the 3rd BS is required for a TDOA estimate a reasonable performance criterion is to decide on suitable values for P^{PR}_{idle} and N_{ip} that maximise $\xi^{PR}(1, P^{PR}_{idle}, N_{ip})$ and $\xi^{PR}(2, P^{PR}_{idle}, N_{ip})$. Figure 4.4(a) shows the function plotted at the two values of n. Figure 4.4(b) shows the equally weighted sum of the two lines. Note that $P^{PR}_{idle} = 0$ is a limit that cannot be attained as the previous equations only hold during the serving BS idle period.

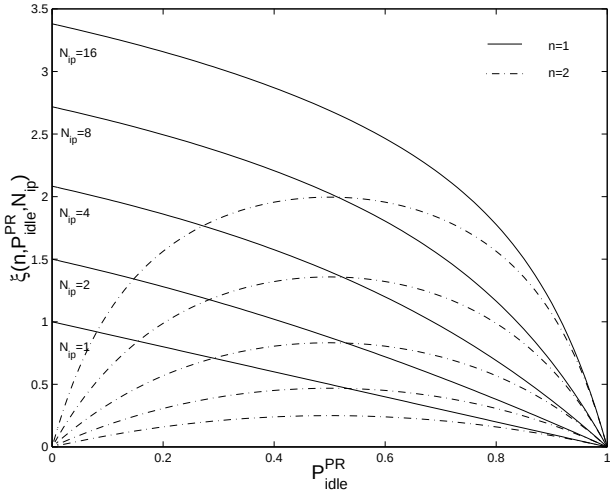

(a)

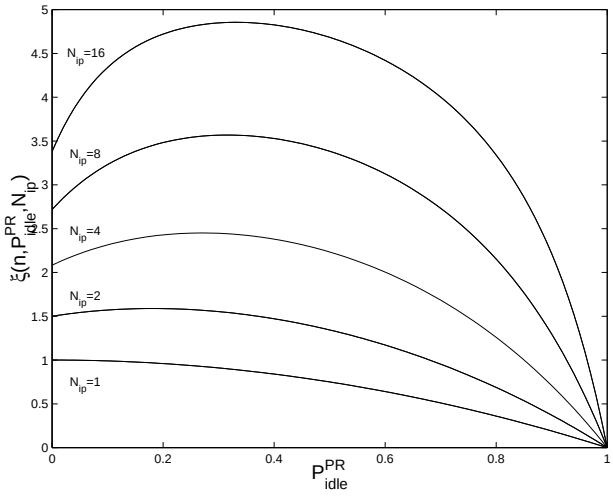

(b)

Figure 4.4: $(a)\xi^{PR}(n, P^{PR}_{idle}, N_{ip})$ plotted for n=1 and n=2, (b) the equally weighted sum

From these results it is clear that the optimum P^{PR}_{idle} is in the range $[0.2, 0.4]$. Thus the proposed value for $P^{PR}_{idle} = \frac{1}{16}$ (proposed in [101]) performs about 1dB worse for large N_{ip}. P^{PR}_{idle} could be increased by for instance reducing L_{if}, however there are other considerations to consider. One key advantage of the PR–IPDL system is that tight synchronisation between BS's is not required. As long as the idle frames from different BS's mostly overlap at the reception point the performance should stay fairly constant. Reducing L_{if} will therefore tighten the synchronisation requirements which is not desirable.

4.2.2 Time Aligned IPDL (TA–IPDL)

In TA–IPDL the idle periods are synchronised so that each BS goes idle at the same time in the idle frame, Motorola [102], see Figure 4.3. During the idle period the pilot channel only is transmitted with probability P_{trans}^{TA}. $P_{trans}^{TA} = 0.3$ has been proposed [101]. In such a scheme it is sensible to boost the pilot transmit fraction, i.e. the fraction of the total transmit power that is used for the pilot, to 1 during the idle period [103]. This could potentially gain 7–13dB in transmit power, thus increasing the pilot range by 1 to 2 octaves depending on the path loss exponent. Naturally at the reception point fractional misalignment will occur so L_{ip} should be significantly greater than the maximum channel delay, or idle guard periods should be utilised.

Again the PCPICH is proposed to be utilised for measurement purposes with similar problems as described in the PR–IPDL case.

TA–IPDL can substantially improve the hearability of the system compared with PR–IPDL as will be demonstrated in the next section. The main disadvantage is that tight synchronisation between BS's is required to give this improvement. However to calculate the location using TDOA the relative desynchronisation times are required no matter the technique. It is proposed that these are supplied by LMU's which are fixed receivers at precisely known locations (probably located at most BS's). These LMU's will measure the desynchronisation so it is reasonable to suppose they could be used to provide timing adjustments to ensure tight synchronisation.

Similarly to the PR–IPDL case the equivalent probability $P_{BSidle}^{TA}(n, P_{idle}^{TA})$ can be derived as

$$P_{BSidle}^{TA}(n, P_{idle}^{TA}) = (P_{idle}^{TA})^n - (P_{idle}^{TA})^{n+1} \tag{4.11}$$

where $P_{idle}^{TA} = 1 - P_{trans}^{TA}$. For this scheme it should be noted that the serving BS may transmit during the idle period. Considering N_{ip} idle periods then, similarly to (4.8),

$$P_{BSidle}^{TA}(n, P_{idle}^{TA}, N_{ip}) = 1 - \left[1 - (P_{idle}^{TA})^n - (P_{idle}^{TA})^{n+1}\right]^{N_{ip}} \tag{4.12}$$

Similarly to the PR–IPDL case a performance measure, $\xi^{TA}(n, P_{idle}^{TA}, N_{ip})$, is formed,

$$\xi^{TA}(n, P_{idle}^{TA}, N_{ip}) = \sum_{i=1}^{N_{ip}} \sum_{k=1}^{i} \frac{1}{k} \begin{pmatrix} N_{ip} \\ i \end{pmatrix} (P_{TAidle}^{PR}(n))^i (1 - P_{TAidle}^{TA}(n))^{N_{ip}-i} \tag{4.13}$$

Again it is desired to maximise $\xi^{TA}(n, P_{idle}^{TA}, N_{ip})$ for $n = 1, 2$. Figure 4.5(a) shows the func-

tion plotted at the two values of n. Figure 4.5(b) shows the equally weighted sum of the two lines.

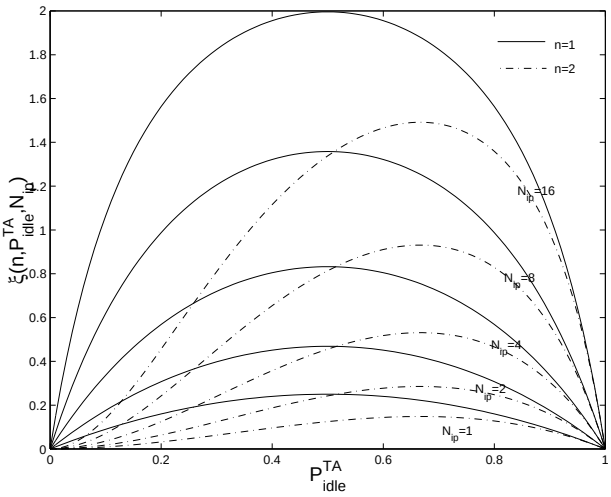

(a)

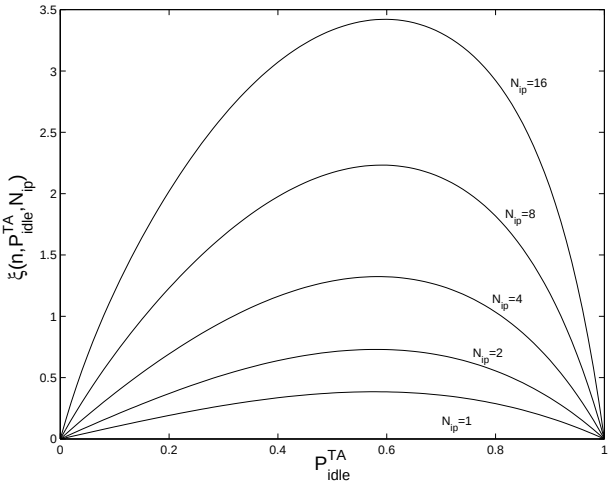

(b)

Figure 4.5: $(a)\xi^{TA}(n, P^{TA}_{idle}, N_{ip})$ plotted for n=1 and n=2, (b) the equally weighted sum

From these results the proposed value of $P^{TA}_{trans} = 0.3$ (corresponding to $P^{TA}_{idle} = 0.7$) seems to be a reasonable choice.

4.2.3 Variant of TA–IPDL using the PSCH (vTA–IPDL)

One disadvantage in using a TA–IPDL system is that it only works well with low P^{TA}_{trans}. This implies that timing measurements can be made much less frequently than the idle period fre-

quency, thus losing fading and potential multipath diversity (though the time between measurements should still be smaller than the rate of change of the multipath profile of the channel). A disadvantage of both TA–IPDL and PR–IPDL is the receiver complexity, in that the MS will have to integrate over different long scrambling codes to detect each BS.

To improve matters somewhat a variant of TA–IPDL has been proposed by the author which uses time allocated slots within the idle period to transmit a pulsed pilot channel with $P_{trans}^{vTA} = 1$. A suitable pilot channel already present in the system is the primary synchronisation channel (PSCH), see Figure 4.3, which is the same for all BS. In this way the receiver can be greatly simplified as only integration of one short code is required. Note again the pilot fraction can be increased to 1. The PSCH is a pulsed $L_c = 256$ chip code once per UMTS slot (2560 chips). Thus if L_{ip} is 1 UMTS slot the processing gain is 10dB down from the other IPDL schemes, however there are other benefits to compensate for this. Figure 4.6 shows the make up of an idle frame at transmission and reception.

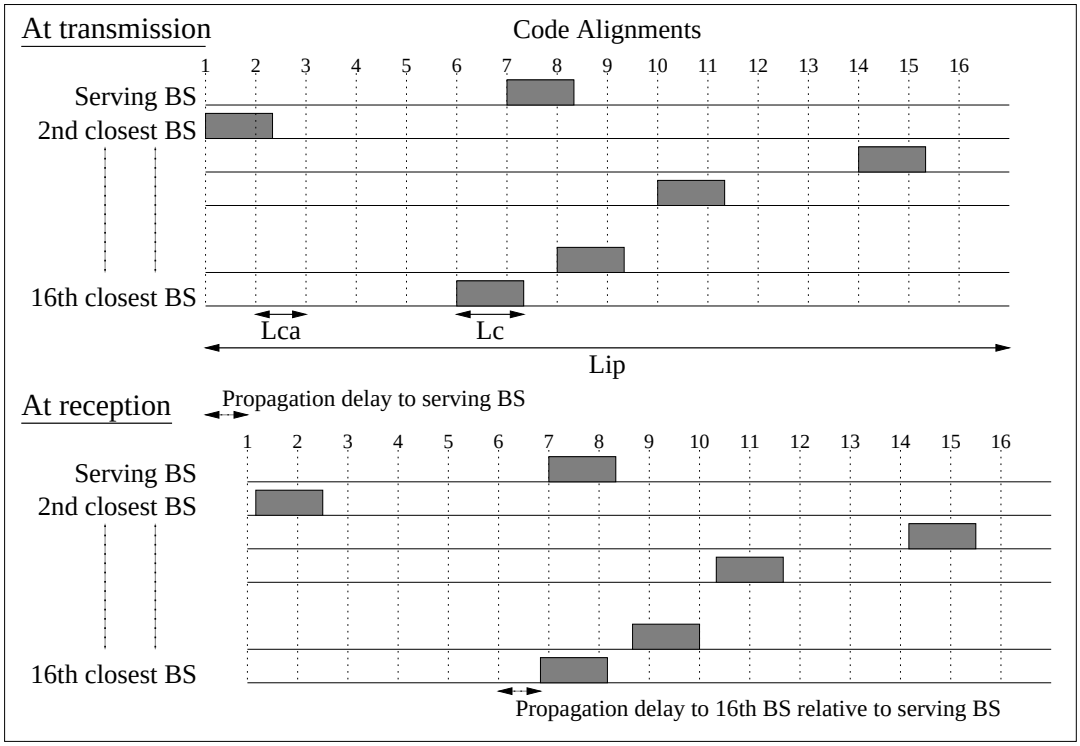

Figure 4.6: vTA-IPDL idle period structures

Although identical codes are used by each BS, BS identification can be achieved by identifying the relative code alignment with respect to the serving BS and reporting this back to the serving

BS. 16 PSCH code alignments have been specified in [2] (the code alignment slot length $L_{ca} = 160$ chips), leading to marginal overlapping of codes in time. Due to different propagation delays to the MS further overlapping can occur. Since the codes are quite short, thus limiting processing gain, this effect must be carefully considered. It is possible to arrange the 16 codes in a hexagonal cell tessellation so that adjacent BS's do not use adjacent code alignments, see Figure 4.7(a), thus the serving BS near–far effect will be confined to more distant BS's. For large cells the propagation delays become such that at reception the codes may have shifted past the next code alignment relative to the serving BS. Note for the signal from one of the BS's in the second tier surrounding the serving BS travels between $2R_C$ to $4R_C$ more than than signal from the serving BS. Therefore to facilitate code identification

$$4R_C \leq cT_cL_{ca} \tag{4.14}$$

where T_c is the chip duration in seconds and c is the speed of light (ms^{-1}). For UMTS parameters therefore $R_C \leq 3$km. In larger cells only every second alignment can be used otherwise BS identification becomes more difficult (though signal strength measurements could be used to assist the process) and hence a shorter alignment reuse distance is required, see Figure 4.7(b).

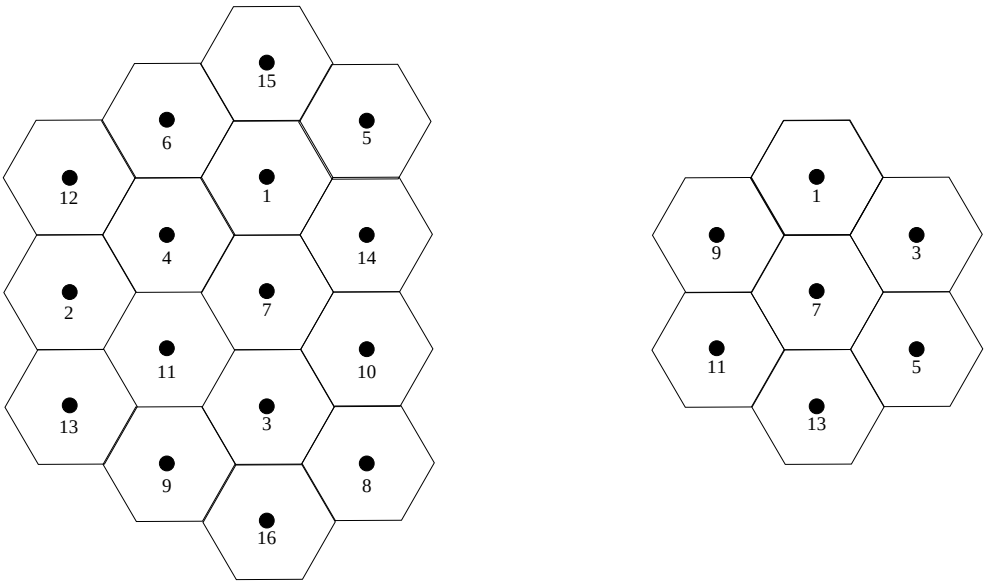

(a) (b)

Figure 4.7: Possible code alignment reuse plans in a vTA–IPDL system for (a) small cells, $R_C \leq 3$km (b) large cells

The processing loss previously mentioned can be partially offset by the increase in selection diversity gain (the code is always present within the idle period). Therefore as $P_{BSidle}^{vTA}(n, P_{idle}^{vTA} = 1, N_{ip}) = 1$ the performance measure $\xi^{vTA}(N_{ip})$ is simply, from (4.5),

$$\xi^{vTA}(N_{ip}) = \sum_{k=1}^{N_{ip}} \frac{1}{k} \tag{4.15}$$

Summing $\xi^{vTA}(N_{ip})$ for 2 BS's gives an expected gain improvement of 2–3dB's over TA–IPDL and PR–IPDL for $N_{ip} = 8, 16$. There will also be (ignoring misalignment and code overlap) no other BS's transmitting anything during each BS's PSCH which again should improve hearability.

4.3 Hearability Performance Comparison Between Systems

The hearability is assessed for a set of 19 BS's in a hexagonal arrangement. 1000 MS's are randomly placed in the middle cell. Each MS takes N_{ip} measurements with uncorrelated Rayleigh fading and stationary lognormal shadow fading. The pilot channel C/I ratio during each measurement, derived from (4.1), is given by

$$\left(\frac{E_c}{I}\right)_i = \frac{sP_iT_p(i)}{N_o + (1-s)P_iT_p(i) + \sum_{k=1,k\neq i}^{N_{BS}} P_kT_p(k)} \tag{4.16}$$

where $T_p(k)$ is 1 if the kth BS is transmitting and 0 otherwise. Note for vTA–IPDL $T_p(k) = 1$ for $k = i$ and 0 otherwise (thus code overlaps are neglected). Hearability is assessed with a variable processing gain $G_p = 24, 31, 34, 37$dB corresponding to $L_{ip} = 0.1, 0.5, 1.0, 2T_{slot}$. For vTA–IPDL $G_p = 24$dB is the proposed gain whereas PR–IPDL and TA–IPDL both have had $G_p = 31$ and 34dB proposed. The detection probability P_{det} can then be evaluated based on the post processing C/I ratio and the false alarm probability P_{FA}. A detection decision is then made based on P_{det}. Table 4.1 shows the system parameters used. A system without IPDL is used as a performance benchmark.

In Figure 4.8 the effect of increasing N_{ip} (N_p for no IPDL) is shown. The hearability of all schemes increases dramatically as N_{ip} increases and at $N_{ip} = 8$ all schemes provide hearability ≥ 3 BS's at the higher processing gains. The vTA–IPDL and TA–IPDL show significantly better hearability. Figure 4.9 shows the effect of adjusting the pilot fraction for no IPDL and

PR–IPDL schemes with $N_{ip} = 8$ ($N_p = 8$). With a pilot fraction of 0.02 PR–IPDL no longer provides acceptable hearability at $G_p = 34dB$. Increasing the pilot fraction in the no IPDL scheme does increase the hearability, however a residual 10% of MS's still detect only 1 or 2 BS's at $G_p = 34dB$. Figure 4.10 shows the effect of adjusting P_{idle}^{PR} in the PR–IPDL scheme. There is very little difference in performance for the values chosen, thus a lower value should be favoured as this implies the lowest capacity loss. Figure 4.11 shows the effect of adjusting P_{trans}^{TA} in the TA–IPDL scheme. $P_{trans}^{TA} = 0.1$ performs poorly compared to the other values as might be expected from Figure 4.5, however is still much better than the PR–IPDL and no IPDL schemes. In Figure 4.12 the effect of varying the standard deviation of lognormal shadow fading is shown. Large log standard deviations decrease hearability marginally. In Figure 4.13(1) results for the dual slope path loss model (equation 3.11) are shown. Comparing these to Figure 4.8(2), they show a marked decrease in performance with the dual slope path model as opposed to the simple path loss model. The dual path loss model is used in simulations in subsequent chapters as it is the worst case performance model. Further to this, results with the partially obstructed CLOS and fully obstructed CLOS model are shown in Figures 4.13(2–3). The partially obstructed model has little effect on the hearability, however the fully obstructed model reduces hearability significantly so that none of the schemes work adequately.

Overall the results show that hearability is best with the TA–IPDL scheme which provides adequate hearability ($\geq$3BS's) with $G_p \geq 31$dB for all but the no CLOS scenario. The vTA–IPDL scheme with $G_p = 24$dB performs slightly worse than TA–IPDL with $G_p = 34$dB, and in practice would be further limited (at high hearability) by code overlapping. PR–IPDL performs worse but is still viable in most scenarios with $G_p = 34$dB. The advantages and disadvantages of each scheme are summarised in the Table 4.2.

	Synch.	Min L_{ip}	Receiver	Remarks
PR–IPDL	loose	1 UMTS slot	Many codes	Synchronisation less of an issue
TA–IPDL	tight	0.5 UMTS slot	Many codes	Lowest capacity loss
vTA–IPDL	tight	1 UMTS slot	One code	Simplest receiver, cell planning

Table 4.2: Advantages and disadvantages of IPDL schemes

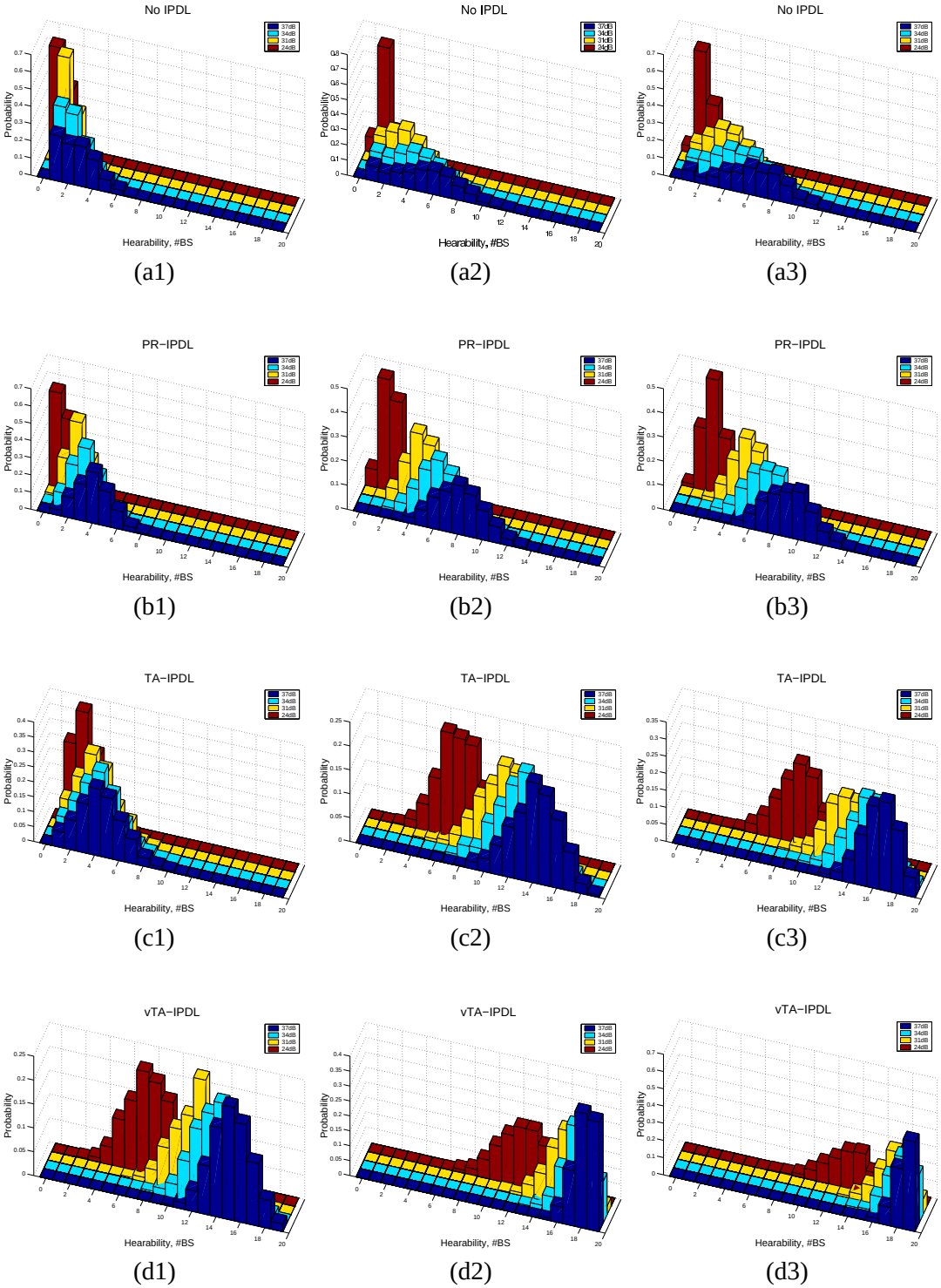

Figure 4.8: Hearability against number of idle periods with uncorrelated Rayleigh fading: (a) no IPDL, (b) PR–IPDL, (c) TA–IPDL, (d) vTA–IPDL; (1) 1, (2) 8, (3) 16 periods

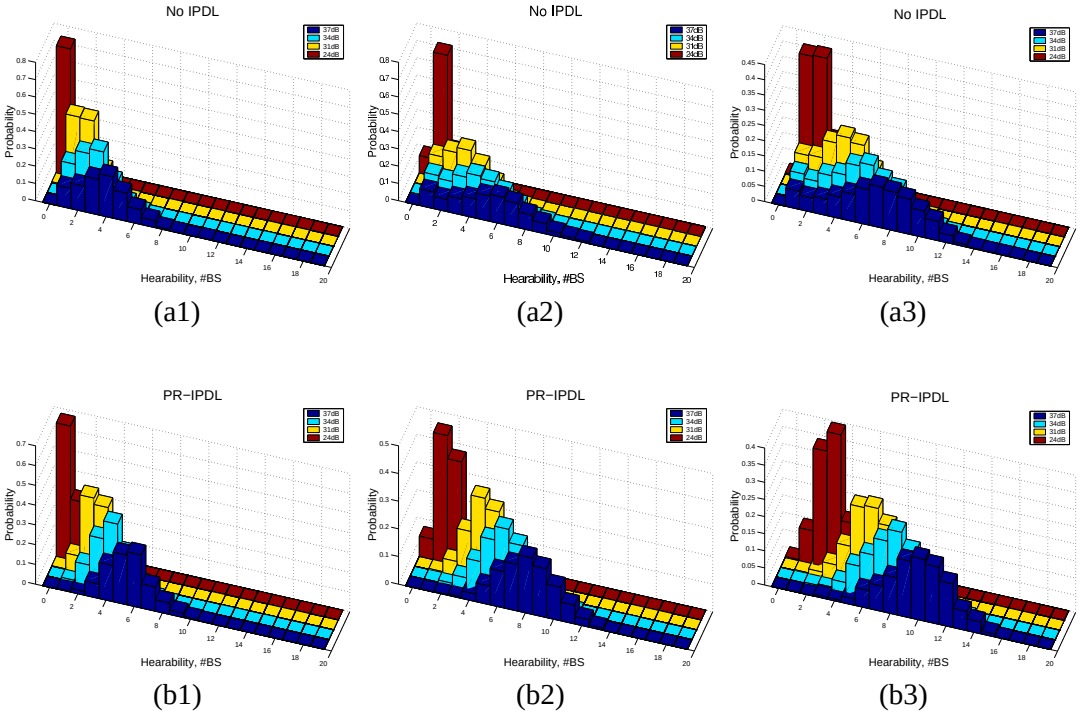

Figure 4.9: Hearability against pilot transmit power fraction: (a) no IPDL, (b) PR–IPDL; (1) 0.02, (2) 0.05, (3) 0.10 pilot fraction

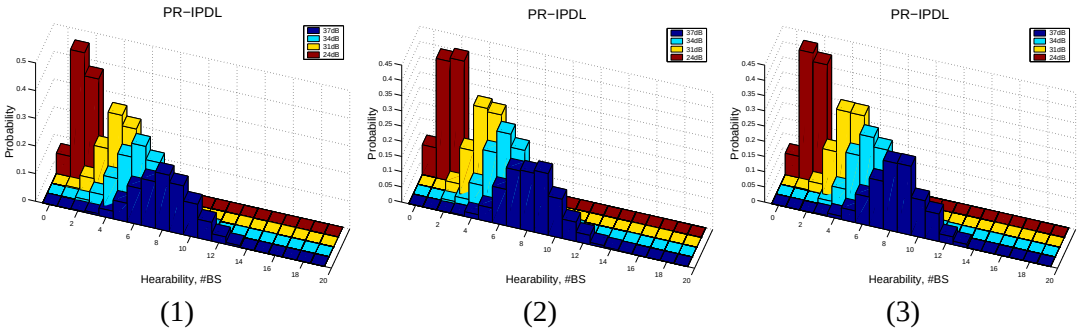

Figure 4.10: Hearability against P_{idle} for PR–IPDL with P_{idle} of (a) $\frac{1}{16}$, (b) $\frac{1}{4}$, (c) $\frac{1}{2}$

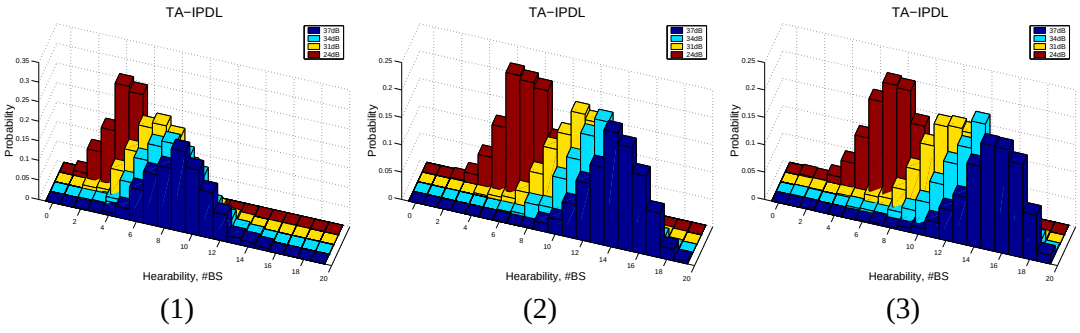

Figure 4.11: Hearability against P_{trans} for TA–IPDL with P_{trans} of (a) 0.1, (b) 0.3, (c) 0.5

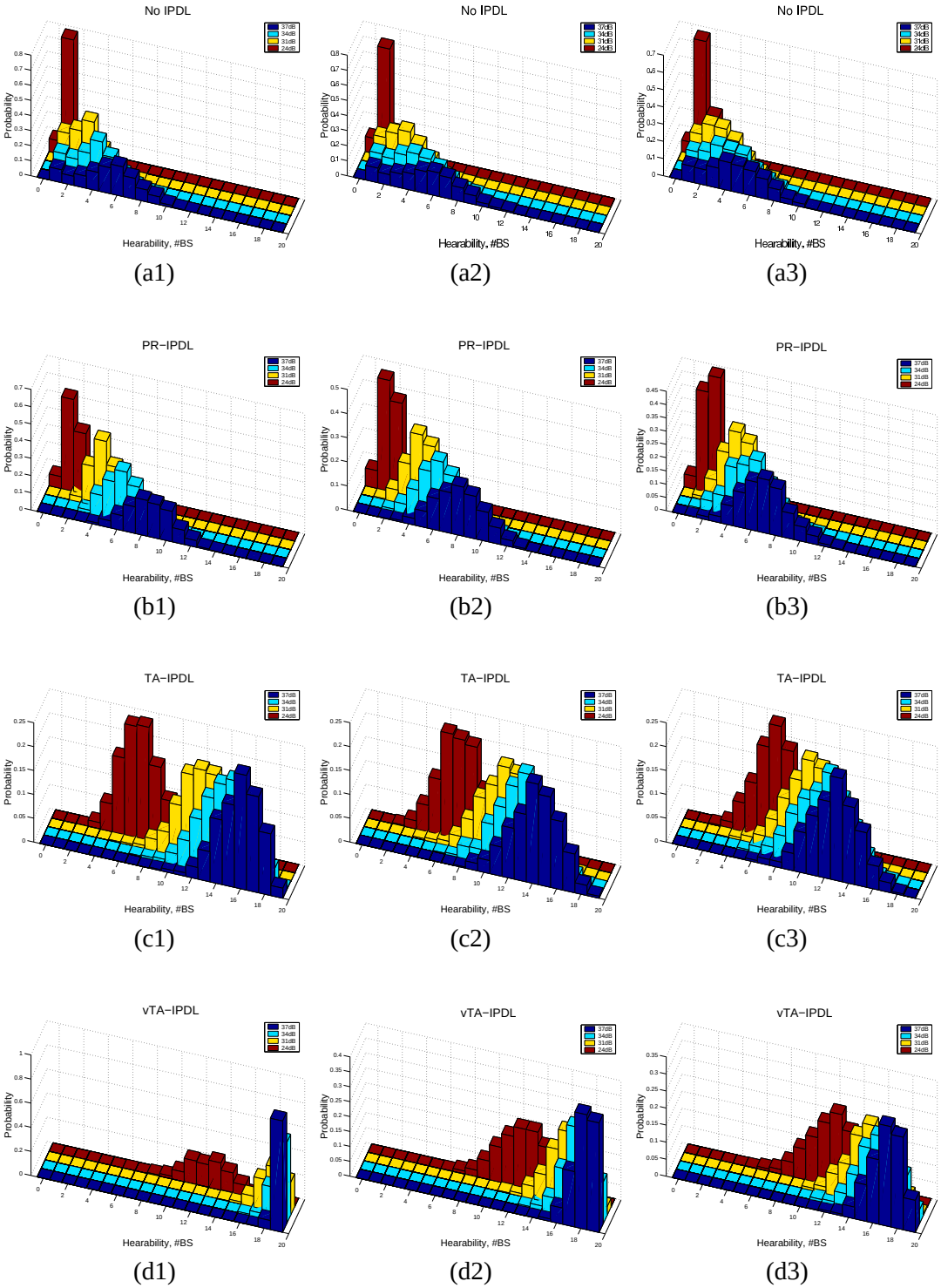

Figure 4.12: Hearability against lognormal shadowing: (a) no IPDL, (b) PR–IPDL, (c) TA–IPDL, (d) vTA–IPDL; (1) 4dB, (2) 8dB, (3) 12dB standard deviation

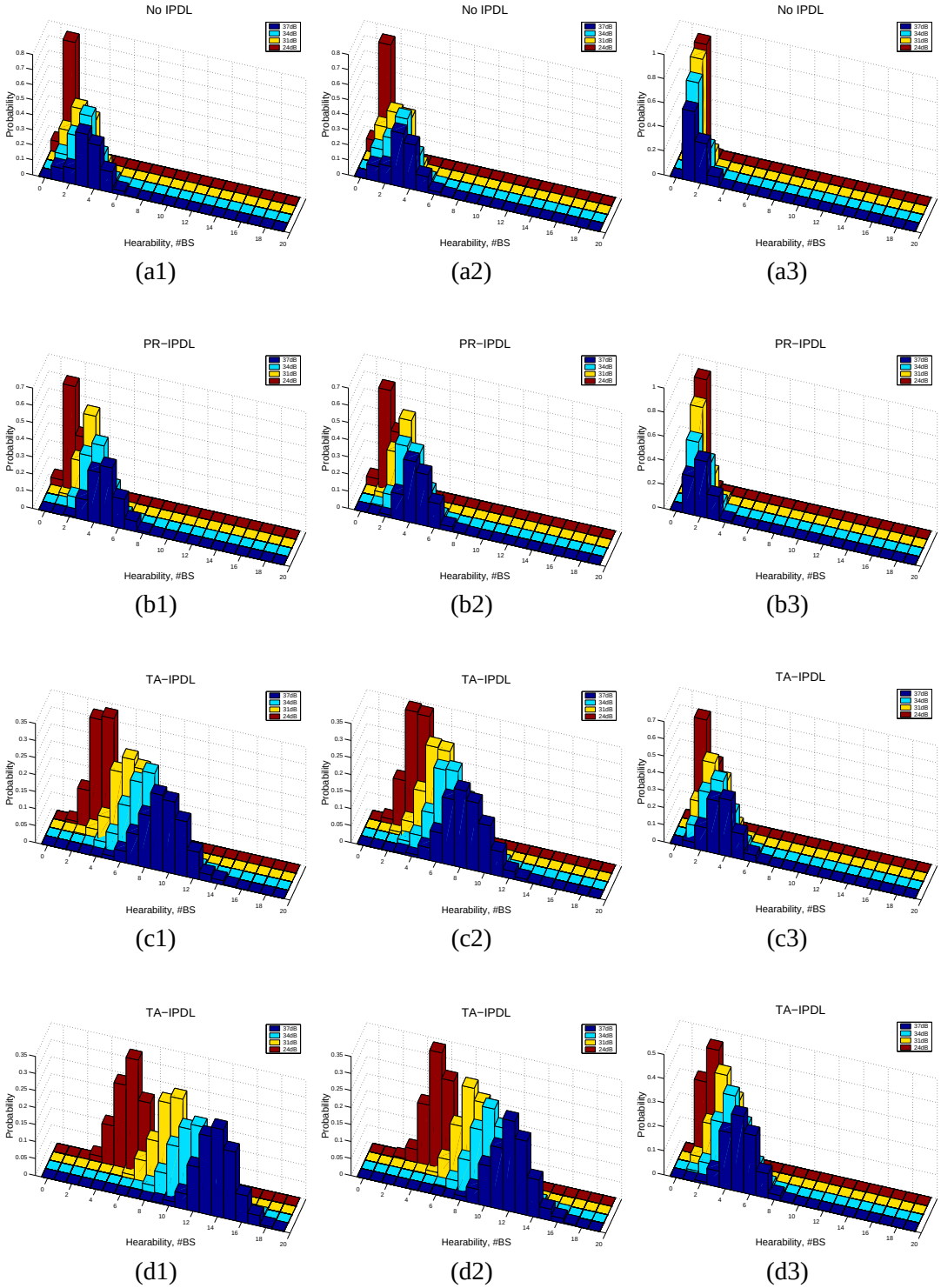

Figure 4.13: Hearability for dual slope path loss and CLOS models: (a) no IPDL, (b) PR–IPDL, (c) TA–IPDL, (d) vTA–IPDL; (1) all CLOS, (2) partial CLOS, (3) no CLOS

4.4 Performance of an Adaptive Receiver

In the previous section it was shown that in extreme conditions the IPDL schemes do not guarantee the required hearability. In such conditions more C/I ratio gain can be found by using coherent and non–coherent integration of the N_{ip} measurements as well as the selection diversity schemes previously considered.

The receiver architecture (R1) (see Figure 4.4) is based on a conventional MF synchronisation circuit. N_{ip} is divided down into N_c and N_n, the number of idle periods to be combined coherently and non–coherently respectively, where $N_c N_n \leq N_{ip}$. If $N_c N_n < N_{ip}$ selection diversity between $N_s = N_{ip}/N_c N_n$ integrals is also used. To limit the possible combinations of N_c and N_n, only values that are powers of 2 are used. It is supposed that the receiver can perfectly adapt the coherent and non–coherent integration, and selection diversity components to maximise the power of the output signal, $I(i)$. In a practical system a serial search of possible values can be performed aided by past measurements, terminating when or if the threshold is exceeded. Note that this search method should not affect the false alarm probability as the noise component is fixed.

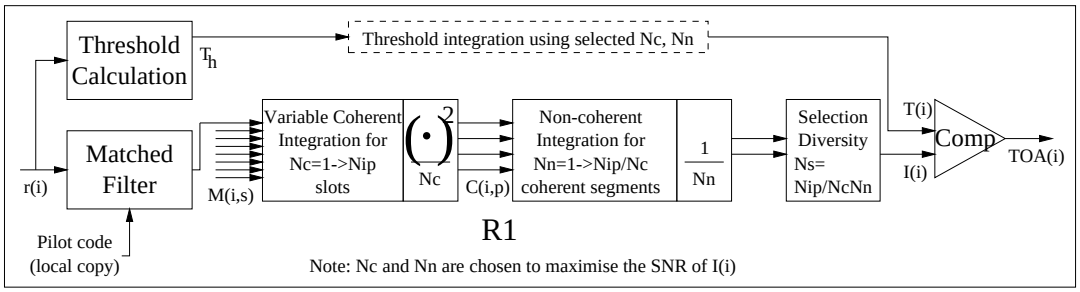

Figure 4.14: Adaptive receiver architecture, R1

4.4.1 Practical Limit to Number of Idle Periods

N_{ip} is in practical cases limited by the maximum possible F_{idle} due to QoS considerations and thus the maximum time over which the MS can be considered stationary (in the location sense), itself a function of the MS speed and how accurately the MS is to be located. A reasonable location stationary distance might be about 20m, in which case the maximum time over which measurements are not out of date would be between 1 and 10 seconds between vehicular and walking speeds.

In integration schemes (as opposed to selection diversity) a further consideration is the stationarity of the multipath channel in NLOS conditions. Typical survival lengths for multipaths in urban environments tend to be around 5–10m [22], thus further reducing the integration time possible. The pulse shaping should also be considered since the pulse shapes will become fractionally misaligned with each other at the MS as the MS travels radially (w.r.t. the scatterer location). Since the chip time in UMTS corresponds to a propagation distance of 77m, above the desired location accuracy, the pulse shaping misalignment (or slippage) loss will be small if N_{ip} has already been chosen to ensure approximate MS location stationarity. Figure 4.4.1 shows the slippage loss for several values of N_n.

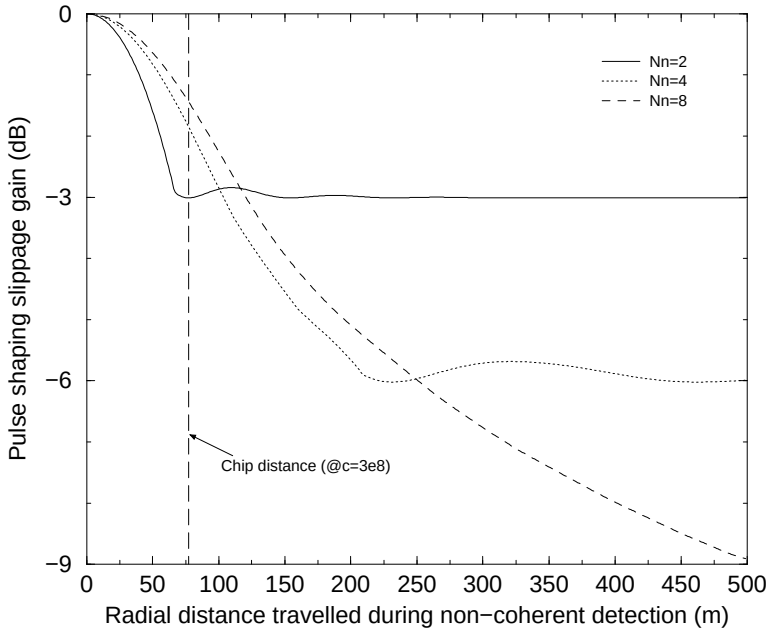

Figure 4.15: Pulse slippage loss for several N_n values

4.4.2 Optimum Idle Period Spacing and Clustering

Since the receiver is capable of exploiting channel coherence between successive idle periods, a reasonable strategy is to reduce the separation of the idle periods in time, L_{sep}, in order to increase the probability of coherence occurring. As previously mentioned, due to QoS considerations, there is a practical minimum limit to this separation.

If the Doppler shift experienced by the MS is high then the channel coherence between idle periods even with low L_{sep} becomes low. In this case ideally L_{sep} would be large to exploit the

fading diversity inherent in the channel.

Clearly there is a trade off between taking measurements closely together in time thus maintaining a coherent channel for MS's with low Doppler shift and taking measurements far apart in time to exploit fading diversity for those MS's with high Doppler shift. In subsequent sections it is shown that coherent gain is greater than fading gain. For this reason clustering of idle periods together in groups is proposed within one burst of idle periods. A burst of idle periods contains N_{ip} of length $L_{burst} = N_{ip}/F_{idle}$ for one location estimate. Figure 4.4.2 shows this clustering method. $F_{cluster} > 1/L_{burst}$ implies that more than one cluster will be in a burst. In this case fading diversity can be achieved. In subsequent simulations the optimum L_{sep} and $F_{cluster}$ combinations are evaluated.

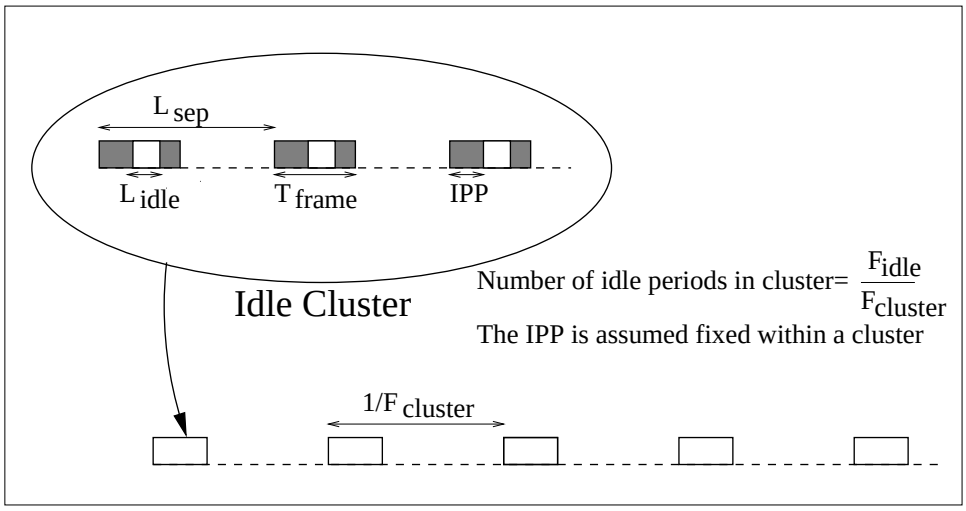

Figure 4.16: IPDL clustering within a burst

4.4.3 Coherent Integration

The MF output is stored slotwise as $M(i,s)$ (i is the sample in slot index and s is the idle slot index) and integrated over N_c idle slots. In receiver R1 it should be noted that due to the variable gain factor, N_c, the MF output power must be normalised by a factor $1/N_c$ to provide the same noise power in each signal and thus allow power levels to be compared. The output of the coherent integration stage, $C(i,p)$ (p is the coherent segment index), is the signal power envelope.

The normalised power gain of the MF depends on the Doppler shift of the channel and, for a

simple single phasor channel, can be expressed as [104]

$$G_{fgMF} = \frac{1}{L_{code}^2} \frac{\sin^2(\pi f_d T_c L_{code})}{\sin^2(\pi f_d T_c)} \tag{4.17}$$

where T_c is the chip duration and f_d is the Doppler shift. For variable coherent integration length with a pulsed pilot code the gain is defined with $N_c \epsilon \{2^K, K = 0..\log_2(N_{ip})\}$ to maximise

$$G_{vgMF} = \frac{N_c \sin^2(\pi f_d T_c (L_{code} + L_{sep}(N_c - 1)))}{(L_{code} + L_{sep}(N_c - 1))^2 \sin^2(\pi f_d T_c)} \tag{4.18}$$

where L_{sep} is measured in chips. For computational simplicity only $N_c = 2^K$, $K \in I$ (all integers) values are used. Figure 4.17 visualises (4.18) with $L_{code} = 256$ chips, $L_{sep} = 2560$ chips and $T_c = 0.26\mu s$. At zero Doppler shift the gain is 3dB/octave.

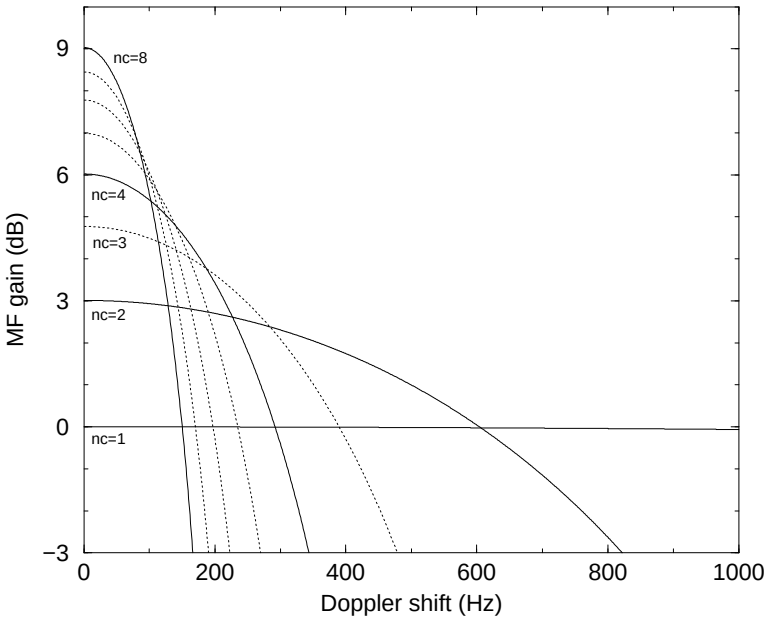

Figure 4.17: MF coherent gain for $N_c = 1 \rightarrow 8$

It can be seen that using only powers of two as N_c values (solid lines in the figure) does not decrease performance significantly.

Since the coherent integration occurs before squaring the integration stage output noise has a complex Gaussian distribution. Thus $C(i, p)$ (after the squarer) with no signal and complex Gaussian noise present has a chi squared PDF with 2 degrees of freedom of the form

$$f_{Cns}(y) = \frac{1}{2\sigma_n^2} e^{-\frac{y}{2\sigma_n^2}} \tag{4.19}$$

where $2\sigma_n^2$ is the total noise power (identical in $M(i,s)$ and $C(i,p)$), which must first be estimated. There are several strategies for noise power estimation which are outside the scope of this work. $C(i,p)$ with signal present has a non–central chi squared PDF with 2 degrees of freedom of the form

$$f_{Cs}(y) = \frac{1}{2\sigma_n^2} e^{\frac{(S^2+y)}{2\sigma_n^2}} I_0\left(\sqrt{y}\frac{S}{2\sigma_n^2}\right) \tag{4.20}$$

where $I_\alpha(x)$ is the αth order modified Bessel function of the first kind, and S^2 is the signal power in $C(i,p)$, assumed constant over N_c idle periods, and N_c times the signal power in $M(i,s)$. In Rayleigh fading S^2 has a chi squared distribution about the short term mean signal power $\bar{S}^2$. In Rician fading a non–central chi squared distribution applies.

4.4.3.1 Threshold calculation

A Neyman–Pearson decision threshold, T_h, can be calculated based on an acceptable false alarm probability, P_{FA}, caused by the noise process. T_h (expressed as a power) can be calculated from (4.19) as

$$T_h = 2\sigma_n^2 \ln\left(\frac{1}{P_{FA}}\right) \tag{4.21}$$

In practice the autocorrelation sidelobes of the pilot code may be greater than T_h in high SNR conditions. So a further additive threshold is required to ensure that the autocorrelation sidelobes do not exceed the threshold. In this thesis low SNR's are assumed so the effect of the autocorrelation threshold is not considered.

The probability of detecting a signal, P_{det}, can be calculated from (4.20) as

$$P_{det} = Q_1\left(\frac{\sqrt{C(i,p)}}{\sigma_n}, \frac{\sqrt{T_h}}{\sigma_n}\right) \tag{4.22}$$

where $Q_m(a,b)$ is Marcum's Q function of order m.

4.4.3.2 Coherent Integration versus Selection Diversity

It is interesting to calculate the point at which selection diversity becomes advantageous to coherent integration. This will be the case if there is a wide discrepancy between the SNR levels in samples. Coherent integration will be favourable if the SNR after coherent integration is greater than the largest SNR (chosen from all samples) before coherent integration. For 2 samples, one with power $\frac{p^2}{N_o}$ and the other with power $k^2\frac{p^2}{N_o}$ where $k \leq 1$ then

$$\begin{aligned} CI\left(\frac{p^2}{N_o}, k^2\frac{p^2}{N_o}\right) &> \frac{p^2}{N_o} \\ \frac{(p+kp)^2}{2N_o} &> \frac{p^2}{N_o} \\ k &> \sqrt{2}-1 \\ k^2 &> -7.66dB \end{aligned} \tag{4.23}$$

where $CI(.)$ represents the coherent integration process.

4.4.4 Non–coherent Integration

$C(i,p)$ for the last N_n idle periods are summed non–coherently to give $I(i)$. Values of $I(i)$ larger than $T(i)$ are selected as arrival peaks. Again a normalisation factor, $1/N_n$, is applied to allow power levels to be compared when selecting an optimum N_n value. Assuming $2\sigma_n^2$ is constant over N_n idle periods $T(i) = T_h$, $I(i)$ with no signal present has a chi squared PDF with $2N_n$ degrees of freedom of the form

$$f_{Ins}(y) = \frac{N_n}{\sigma_n^{2N_n} 2^{N_n}\Gamma(N_n)}(N_n y)^{N_n-1}e^{-\frac{N_n y}{2\sigma_n^2}} \tag{4.24}$$

With signal present $I(i)$ has a non–central chi squared PDF with $2N_n$ degrees of freedom of the form

$$f_{Is}(y) = N_n\left(\frac{N_n y}{P^2}\right)^{\frac{N_n-1}{2}} \frac{e^{\frac{(P^2+N_n y)}{2\sigma_n^2}}}{2\sigma_n^2} I_{N_n-1}\left(\sqrt{N_n y}\frac{P}{2\sigma_n^2}\right) \tag{4.25}$$

where P^2 is the mean of N_n S^2 values.

The false alarm probability after the non-coherent detection stage, $P_{FA(out)}$, assuming constant

noise power, can be evaluated as

$$P_{FA(out)} = e^{-\frac{N_n T_h}{2\sigma_n^2}} \sum_{k=0}^{N_n-1} \frac{1}{k!} \left(\frac{N_n T_h}{2\sigma_n^2} \right)^k \tag{4.26}$$

Figure 4.18(a) shows $P_{FA(out)}$ against P_{FA} for various values of N_n. Clearly the effect of increasing N_n is to reduce $P_{FA(out)}$ for the same P_{FA}.

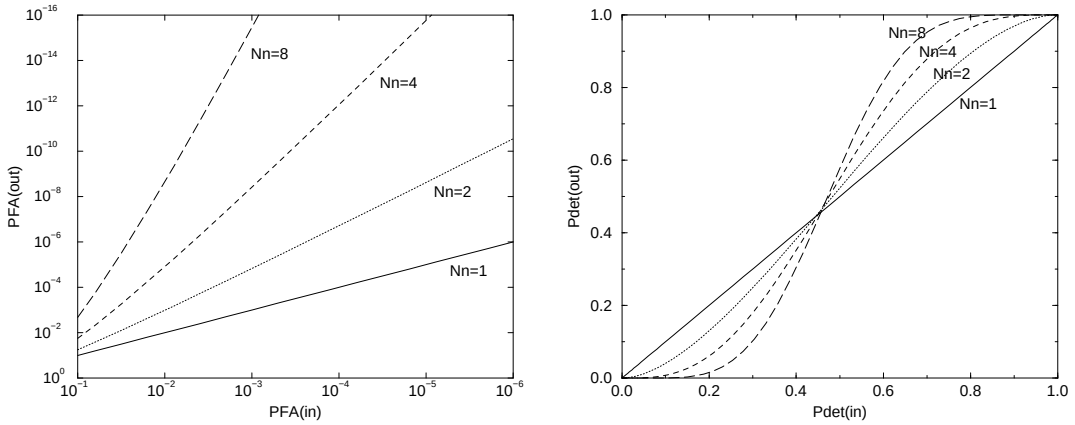

(a) (b)

Figure 4.18: (a) $P_{FA(out)}$ against P_{FA}, (b) $P_{det(out)}$ against P_{det}, for various N_n values

Similarly $I(i)$ with signal present has a non–central chi squared distribution with $2N_n$ degrees of freedom. The detection probability after the non-coherent detection stage, $P_{det(out)}$ can be evaluated as

$$P_{det(out)} = Q_{N_n} \left(\frac{\sqrt{P}}{\sigma_n}, \frac{\sqrt{N_n T_h}}{\sigma_n} \right) \tag{4.27}$$

Figure 4.18(b) shows $P_{det(out)}$ against P_{det} for various values of N_n. For $P_{det} > 0.45$ $P_{det(out)}$ is increased and for $P_{det} < 0.45$ $P_{det(out)}$ is decreased.

If $P_{FA(out)}$ is fixed then (from Figure 4.18) as N_n is increased P_{FA} can be increased and subsequently T_h lowered. This allows signals at lower SNR's to have increased $P_{det(out)}$ values. Figure 4.19 shows the SNR gain achieved by non–coherent integration, against N_n for various values of $P_{det(out)}$ and $P_{FA(out)}$. The SNR gain is the difference in SNR of signals with the same P_{det} before and after non–coherent integration. For small $P_{FA(out)}$ values the gain available is close to 3dB/octave. For more useful values of $P_{FA(out)}$ the gain is close to 2dB/octave. As the P_{det} value drops the SNR gain possible from non–coherent integration decreases. For signals well below the noise power non–coherent integration can produce little gain.

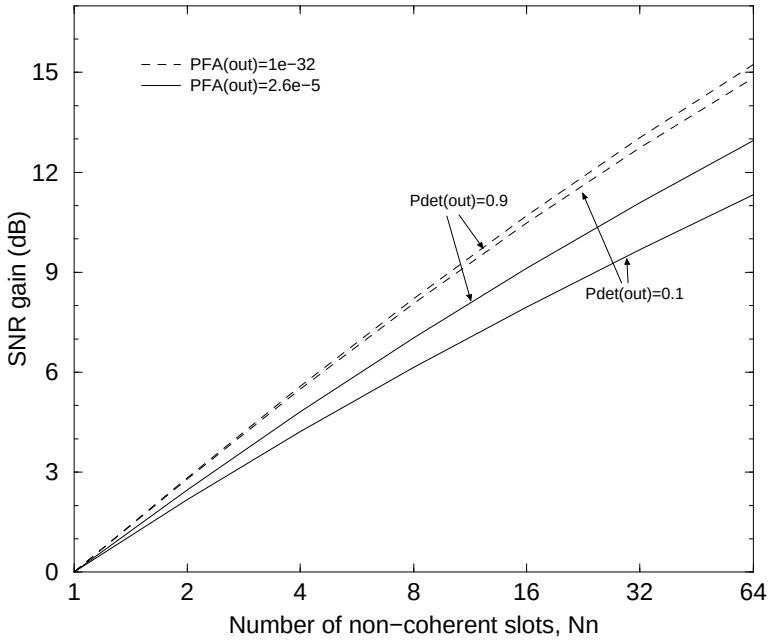

Figure 4.19: SNR gain against N_n for fixed $P_{FA(\,out)}$

4.4.4.1 Non–coherent Integration versus Selection Diversity

Similarly to the coherent integration case the point at which selection diversity becomes favourable to non–coherent integration can be calculated. For 2 samples, one with power $\frac{p^2}{N_o}$ and the other with power $k^2\frac{p^2}{N_o}$ where $k \leq 1$ then

$$\begin{aligned} NC\left(\frac{p^2}{N_o}, k^2\frac{p^2}{N_o}\right) &> \frac{p^2}{N_o} \\ T_R\frac{(p^2+k^2p^2)}{2N_o} &> \frac{p^2}{N_o} \\ k^2 &> \frac{2}{T_R} - 1 \end{aligned} \tag{4.28}$$

where $NC(.)$ represents the non–coherent integration process and T_R is the threshold reduction obtainable from Figure 4.19. For $T_R = 2$dB then

$$k^2 > -5.82dB \tag{4.29}$$

4.4.5 Effects of Fading Correlation

In previous hearability results only uncorrelated (in time) Rayleigh and stationary (completely correlated) shadow fading were considered. However if L_{sep} is to be varied it is important to quantify the effect of correlation. In the following subsection the performance difference across possible correlation values for different fading types is evaluated with respect to the different time diversity schemes.

4.4.5.1 Uncorrelated Rayleigh Fading with Selection Diversity

This has been dealt with in Section 2.8. The expectation of the maximum power in N_{ip} uncorrelated chi squared random variables (RV's), $Z_1..Z_{N_{ip}}$, has been shown to be, from (4.5),

$$E[\max_{n=1..N_{ip}}\{Z_n\}] = \sum_{k=1}^{N_ip}\frac{1}{k} \tag{4.30}$$

Figure 4.20(a) shows this function plotted as a function of N_{ip}. Note the gain increment per octave reduces as N_{ip} increases, and is never more than 2dB per octave.

4.4.5.2 Correlated Rayleigh Fading with Selection Diversity

Dealing with correlated RV's is somewhat more complicated than independent RV's and it is well known that for $N_{ip} > 2$ it is not possible to calculate the required expectations in the general case [19]. In this thesis, under correlated fading, only the case with $N_{ip} = 2$ is considered.

In terms of the fading power the correlation leads to two correlated chi squared RV's, Z_1, Z_2 with normalised power composed from identical normal RV's $X_1..X_4$ as

$$Z_1 = \frac{1}{2}(X_1^2 + X_2^2) \quad , \quad Z_2 = \frac{1}{2}(X_3^2 + X_4^2) \tag{4.31}$$

A standard correlation term, ρ, exists between jointly normal pairs (X_1, X_3) and (X_2, X_4) as described in [105]

$$f_{X,Y}(x,y) = \frac{1}{2\pi\sigma^2\sqrt{1-\rho^2}}\exp\left[-\frac{1}{2(1-\rho^2)}\left(\frac{x^2 - 2\rho xy + y^2}{\sigma^2}\right)\right] \tag{4.32}$$

The joint PDF of Z_1 and Z_2, known as Moran's distribution [106], is then given by

$$f_{Z_1,Z_2}(z_1,z_2) = \sum_{j=0}^{\infty} \rho^{2j} \left[\prod_{k=1}^{2} \left(\sum_{g=0}^{j} (-1)^g \begin{pmatrix} j \\ g \end{pmatrix} (g!)^{-1} z_k^g e^{-z_k} \right) \right] \tag{4.33}$$

In selection diversity the expectation of the maximum power of the two chi squared RV's, $E[\max\{Z_1, Z_2\}]$ is of interest. This can be calculated by first considering the conditional expectation as follows

$$E[\max\{Z_1, Z_2\}|Z_1 = z_1] = \int_0^{z_1} z_1 f_Z(z_2|z_1) dz_2 + \int_{z_1}^{\infty} z_2 f_Z(z_2|z_1) dz_2 \tag{4.34}$$

Integrating over all values of Z_1 then gives

$$\begin{aligned} E[\max\{Z_1, Z_2\}] &= \int_0^{\infty} f_Z(z_1) E[\max\{Z_1, Z_2\}|Z_1 = z_1] dz_1 \\ &= \int_0^{\infty} \int_0^{z_1} z_1 f_Z(z_1) f_Z(z_2|z_1) dz_2 dz_1 + \int_0^{\infty} \int_{z_1}^{\infty} z_2 f_Z(z_1) f_Z(z_2|z_1) dz_2 dz_1 \\ &= \int_0^{\infty} \int_0^{z_1} z_1 f_{Z_1,Z_2}(z_2,z_1) dz_2 dz_1 + \int_0^{\infty} \int_{z_1}^{\infty} z_2 f_{Z_1,Z_2}(z_2,z_1) dz_2 dz_1 \end{aligned} \tag{4.35}$$

Noting the area of integration of both double integrals is the same, it is apparent that the double integrals are identical leaving

$$E[\max\{Z_1, Z_2\}] = 2 \int_0^{\infty} \int_0^{z_1} z_1 f_{Z_1,Z_2}(z_2,z_1) dz_2 dz_1 \tag{4.36}$$

Figure 4.20(b) shows this function plotted as a function of ρ^2. Note that the correlation causes minimal effect until ρ^2 is quite large.

Figure 4.21(a) shows a typical power profile with Rayleigh fading. The MS is moving at 5kmph giving a maximum Doppler shift of 8.9Hz with a 1.92GHz carrier frequency. Figure 4.21(b) shows the corresponding autocorrelation functions of the actual power and real voltage. It can be seen that the power autocorrelation drops to about 0.4 and stays fairly constant. Due to the regular fading properties the real voltage autocorrelation drops rapidly then oscillates between -0.2 and 0.2 corresponding to $\rho^2 < 0.05$. In practice the correlation factor ρ will have negligible impact on the selection diversity except if measurements occur within the same fade.

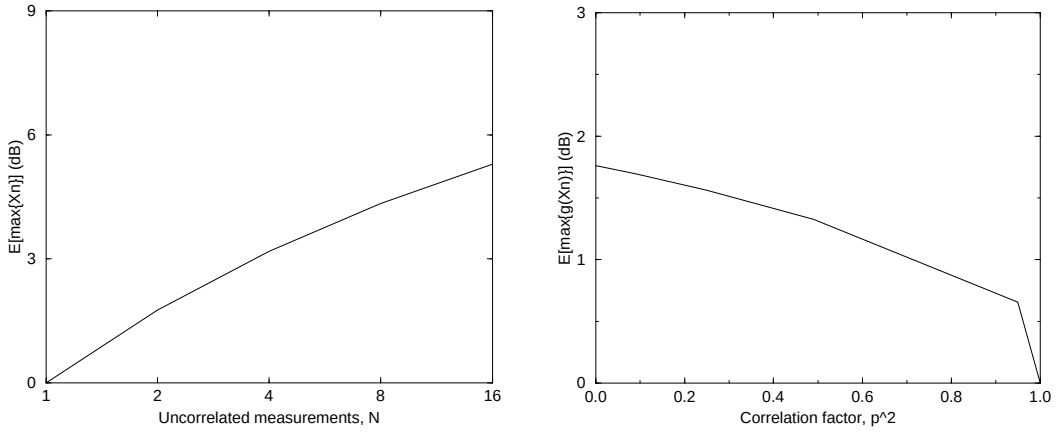

(a) (b)

Figure 4.20: $E[\max\{Z_n\}]$ plotted against (a) N_{ip} for uncorrelated Rayleigh fading, (b) ρ^2 for correlated case, $N_{ip} = 2$

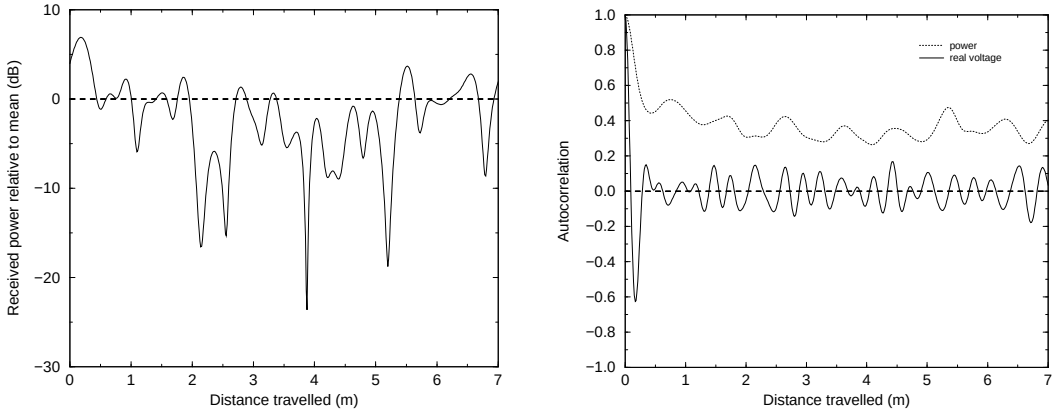

(a) (b)

Figure 4.21: (a) Typical received power profile with Rayleigh fading and (b) its auto-correlation function

4.4.5.3 Uncorrelated Shadow Fading with Selection Diversity

Supposing that the shadowing is uncorrelated between N_{ip} measurements then the expectation of the maximum of N_{ip} lognormal RV's is required. If $X_1..X_{N_{ip}}$ are independent normally distributed RV's then

$$f_X(x) = \frac{1}{\sigma\sqrt{2\pi}} \exp\left[-\frac{x^2}{2\sigma^2}\right] \tag{4.37}$$

$$g(x) = 10^{x/10} \tag{4.38}$$

Thus $g(X)$ is a lognormally distributed RV on a dB scale. The CDF of the maximum in N_{ip} RV's, x_{max}, is derived as

$$\begin{aligned} F_{X_{max}}(x_{max}) &= Pr[x_1..x_n \leq x_{max}] \\ &= [F_X(x_{max})]^{N_{ip}} \end{aligned} \tag{4.39}$$

where $F_X(x)$ is the CDF of the normal density function. Therefore the PDF of x_{max} is

$$\begin{aligned} f_{X_{max}}(x_{max}) &= \frac{d}{dx_{max}} F_{X_{max}}(x_{max}) \\ &= N_{ip}\left[F_X(x_{max})\right]^{N_{ip}-1} f_X(x_{max}) \end{aligned} \tag{4.40}$$

The expectation of $g(x_{max})$, i.e. the maximum power in N_{ip} lognormal RV's is by definition

$$E[g(X_{max})] = \int_{-\infty}^{\infty} g(x) f_{X_{max}}(x) dx \tag{4.41}$$

Noting the moment generating function identity [105]

$$E[e^{tx}] = \exp\left[\mu t + \frac{1}{2}\sigma^2 t^2\right] \tag{4.42}$$

where t is a constant and x is a normally distributed RV with mean μ and variance σ^2, for $N_{ip} = 1$ the integral in (4.41) can be evaluated, since in this case (4.41) simplifies significantly, to

$$\begin{aligned} E[g(X_1)] &= \int_{-\infty}^{\infty} g(x) f_X(x) dx \\ &= E[10^{x/10}] \end{aligned} \tag{4.43}$$

where x is a normally distributed RV, thus

$$E[g(X_1)] = \exp\left[\frac{\sigma^2 \ln(10)^2}{200}\right] \tag{4.44}$$

Figure 4.22(a) shows (4.41) plotted as a function of N_{ip} for $\sigma = 4$dB and $\sigma = 8$dB. Note that the lognormal distribution provides a mean power bias with $N_{ip} = 1$ (the median power

is at 0dB). In subsequent simulation results this bias is removed. The gain increment for 8dB shadowing decreases with increasing N_{ip}, with a maximum of about 2.5dB per octave. Note that this is greater than that provided by Rayleigh fading, and is similar to non–coherent gain, but less than the coherent gain performance.

4.4.5.4 Correlated Shadow Fading with Selection Diversity

Again, in the case of correlated fading, only $N_{ip} = 2$ is considered. In this case X_1, X_2 are identical jointly normal RV's as in (4.32). In this case the conditional PDF is [105]

$$f_X(x_2|x_1) = \frac{1}{\sigma\sqrt{2\pi(1-\rho^2)}} \exp\left[-\frac{(x_2-\rho x_1)^2}{2\sigma^2(1-\rho^2)}\right] \tag{4.45}$$

where ρ represents the correlation factor between the normal RV's X_1 and X_2. It should be noted that the conditional density of x_2 is simply a normal density with mean ρx_1 and variance $2\sigma^2(1-\rho^2)$. Similarly to (4.36) the expectation of the maximum can be derived as

$$\begin{aligned} E[\max\{X_1, X_2\}] &= 2\int_{-\infty}^{\infty}\int_{-\infty}^{x_1} g(x_1) f_{X_1,X_2}(x_2, x_1)\, dx_2 dx_1 \\ &= 2\int_{-\infty}^{\infty} g(x) f_X(x) F_X\left(\frac{x(1-\rho)}{\sqrt{1-\rho^2}}\right) dx \\ &= 2\int_{-\infty}^{\infty} g(x) f_X(x) F_X\left(x\sqrt{\frac{1-\rho}{1+\rho}}\right) dx \end{aligned} \tag{4.46}$$

When $\rho = 1$ (4.46) simplifies to (4.41) with $N_{ip} = 1$. When $\rho = 0$ (4.46) simplifies to (4.41) with $N_{ip} = 2$. When $\rho = -1$ (4.46) simplifies to twice (4.41) with $N_{ip} = 2$. The later point means that negative correlation will improve the selection diversity performance, however it is noted that shadow fading is usually modelled with decaying exponential autocorrelation function [12], thus implying positive ρ values.

Figure 4.22(b) shows (4.46) plotted as a function of ρ for $\sigma = 4$dB and $\sigma = 8$dB. Small values of ρ cause little degradation in expected power.

Gudmundson's [12] experimental results show that a decreasing exponential autocorrelation function accurately models the behaviour of lognormal shadow fading. The decorrelation length of lognormal shadow fading, L_{dcorr}, is defined as the distance at which the autocorrelation function has value 0.5. Typical values for L_{dcorr} have been suggested as 5m for urban scenarios and 20–100m for suburban/rural scenarios [77], [22]. The required correlation value

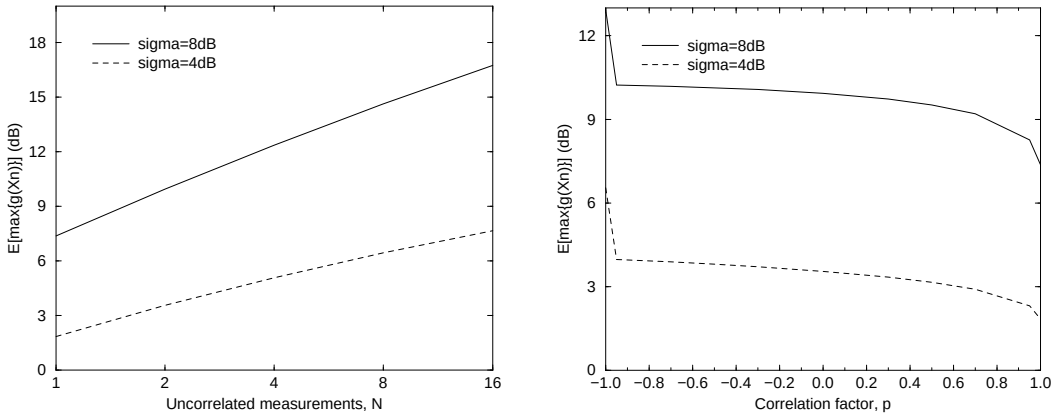

(a) (b)

Figure 4.22: $E[\max\{Z_n\}]$ plotted against (a) N_{ip} for uncorrelated shadow fading, (b) ρ for correlated case, $N_{ip} = 2$

for ρ can be calculated from

$$\rho = 0.5^{\frac{v L_{sep}}{L_{dcorr}}} \tag{4.47}$$

With typical values of $v = 5$kmph (pedestrian), $L_{dcorr} = 5$m in an urban environment and $L_{sep} = 0.125$secs this gives $\rho = 0.976$; at $v = 50$kmph (vehicular) gives $\rho = 0.786$. These correlation factors are quite high thus shadow fading correlation will be quite important to the performance of the receiver.

4.4.5.5 Fading with Coherent Integration

Coherent integration in the receiver will usually occur over a period when the channel is approximately stationary. Thus correlation in fading is of no interest.

4.4.5.6 Fading with Non–coherent Integration

For fixed shadowing, non–coherent integration is the sum of N_n 2nd order chi squared RV's, thus giving the post integration signal power distribution, $f(P^2)$, as a chi squared distribution of order $2N_n$. It is easy to see $E[P^2] = E[S^2]$ and thus correlation in fading will have no effect on the mean value of fading gain.

4.4.6 Simulation Results and Discussion

An IPDL scheme with $N_{ip} = 8$, $L_{burst} = 1$ second and $F_{idle} = 8$Hz was simulated. The performance of a selection diversity receiver, fixed ($N_n = 8$) non–coherent integration receiver, and adaptive receiver, R1, were compared with respect to the mean SNR gain achieved over the mean SNR for signals from the 2nd and 3rd closest BS's (BS's A, B) in a hexagonal cell array. Figure 4.23 shows the location of the BS's and the area over which MS were dropped with uniform distribution and uniform direction of travel over 2π. Results are shown for the MS travelling at 5kmph and 50kmph, corresponding to typical pedestrian and vehicular motion (max Doppler shifts of 8.9Hz and 89.0Hz respectively for 1.92GHz carrier frequency).

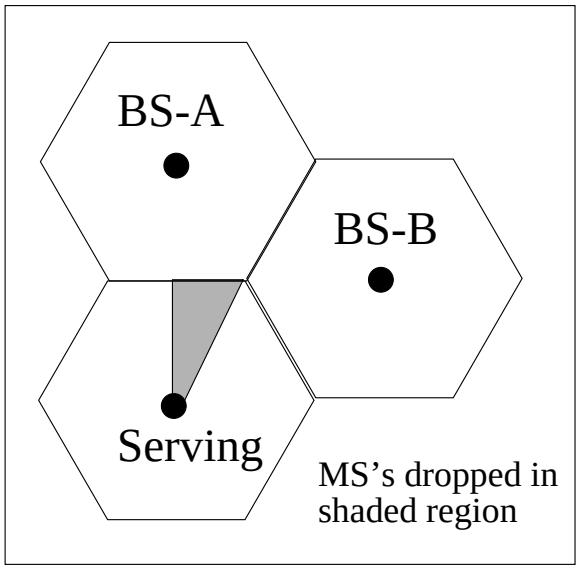

Figure 4.23: BS arrangement and MS drop zone

LOS and NLOS scenarios were simulated. In the LOS scenario Nakagami-m ($m = 15$) short term fading, and lognormal shadowing with 4dB log standard deviation were simulated. In NLOS Nakagami-m ($m = 1$), i.e. Rayleigh fading, and lognormal shadowing with 8dB log standard deviation were simulated. In both cases the decorrelation length of lognormal shadowing was 20m. Change in path loss from movement during the measurement period was not modelled thus cell radius was not a factor. In the LOS scenario the Doppler shifts for each BS are correlated to each other as shown in Figure 4.24. Typically this correlation means that if there is a higher Doppler shift from one BS, the other BS will tend to have a low Doppler shift. In NLOS a uniform angular distribution is assumed for the arrival angle at the MS, therefore

leading to uncorrelated Doppler shifts as described by the following PDF,

$$f_{F_1,F_2}(f_1,f_2) = \frac{1}{\sqrt{1-f_1/f_{max}}\sqrt{1-f_2/f_{max}}}, \qquad -f_{max} \leq f_1, f_2 \leq f_{max} \quad (4.48)$$

where f_{max} is the maximum Doppler shift calculated as $f_{max} = v/c\lambda$, where v is the MS speed, and λ is the carried wavelength. The mean SNR gain across the two BS's remains unaffected by the Doppler shift correlation, so differences in results are due only to the fading types simulated.

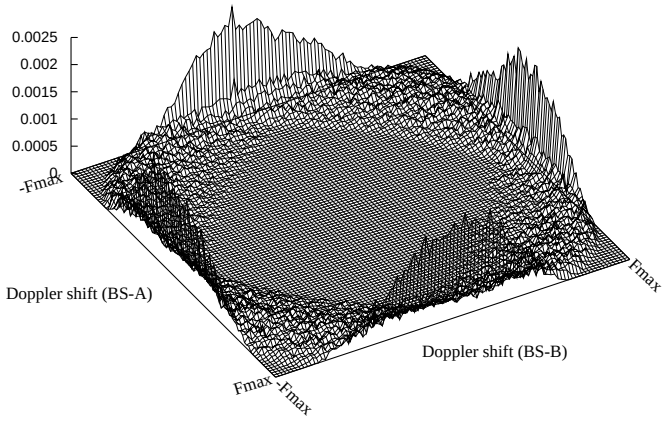

Figure 4.24: Joint Doppler PDF for 2nd and 3rd closest BS in LOS hexagonal cell scenario

To compute the non–coherent integration gain $P_{det} = 0.1$ and $P_{FA} = 2.6 \cdot 10^{-5}$ are used. The analysis assumes that in each idle period the BS pilot channel is present and a measurement can be taken. This is not the case where $P_{trans} < 1$ as in PR–IPDL and TA–IPDL. This factor is further considered in Section 4.4.6.1.

The parameters L_{sep} and $F_{cluster}$ are varied. L_{sep} is varied from 1 UMTS slot, the minimum separation if $L_{idle} = 1$ slot, to $1/F_{idle}$, the maximum separation with $L_{burst} = 1$ second. $F_{cluster}$ is varied from 1Hz to 4Hz, where clusters are spaced $1/F_{cluster}$ seconds apart.

Figures 4.25(a), (b) show the results for the LOS and NLOS scenarios respectively. The mean maximum SNR gain is mean with respect to 10000 random MS drops and the SNR gain from both non–serving BS's and the maximum SNR gain possible for each receiver since the receiver

R1 parameters can adapt ideally. The performance of the selection diversity only receiver in all cases is improves with increased L_{sep} simply because the fading diversity increases. With higher $F_{cluster}$ the idle periods are further spread apart thus the improvement at low L_{sep}. At higher speeds the performance is better as more spatial diversity thus fading diversity is obtained. In the LOS scenario 1–2dB of improvement (still well below the uncorrelated fading expectation) at the largest L_{sep} is achieved, in the NLOS scenario 3.5–5dB gain is possible.

The performance of the fixed ($N_n = 8$) non–coherent integration receiver is dependent on only the expectation of the fading which is constant with regard to L_{sep} and MS speed. Varying the parameters makes no difference therefore for clarity only one line is shown. An SNR gain of 6.2dB is achieved (due to threshold reduction as shown in Figure 4.19). The fixed non–coherent integration receiver always performs better than the selection diversity receiver.

The performance of the adaptive receiver improves with decreased L_{sep} due to the increased coherency in the channel. At higher speeds the performance is worse and deteriorates more quickly with increasing L_{sep}. At maximum L_{sep} the performance is slightly better than the fixed non–coherent integration receiver. This can be attributed to selection diversity gain. Low $F_{cluster}$ performs better in the LOS scenario however in the NLOS scenario where there is more fading diversity, $F_{cluster} = 2$ can outperform $F_{cluster} = 1$ (by 0.3–0.5dB).

Low L_{sep} values may be undesirable due to QoS considerations for real time services, or unworkable, e.g. in PR–IPDL an idle frame is required in which only one frame is idle (the idle period length to idle frame length ration defines P_{idle}^{PR}). A reasonable minimum $L_{sep} = 1$ UMTS frame would provide an SNR gain of about 1.5dB for the adaptive receiver R1 over the non–coherent integration receiver at low speeds and 0.5dB at higher speeds. In the NLOS case $F_{cluster} = 2$Hz would be beneficial to increase fading diversity at high speeds. The gain over the selection diversity only receiver is larger still. In LOS this gain is about 4.5dB at high speed, 6.5dB at low speed; in NLOS 1.5dB at high speed, 4dB at low speed.

Clearly only one possible configuration of F_{idle} and L_{burst} has been considered here. The results show that some gain is possible with a slight increase in receiver complexity. Specifically in an emergency scenario where the MS is near stationary with poor hearability the adaptive receiver could provide a critical hearability improvement. In practice it may be feasible to use a variable length L_{burst} and even L_{sep} if an emergency request is made by a MS with low hearability or integrate across bursts for very slow moving MS's.

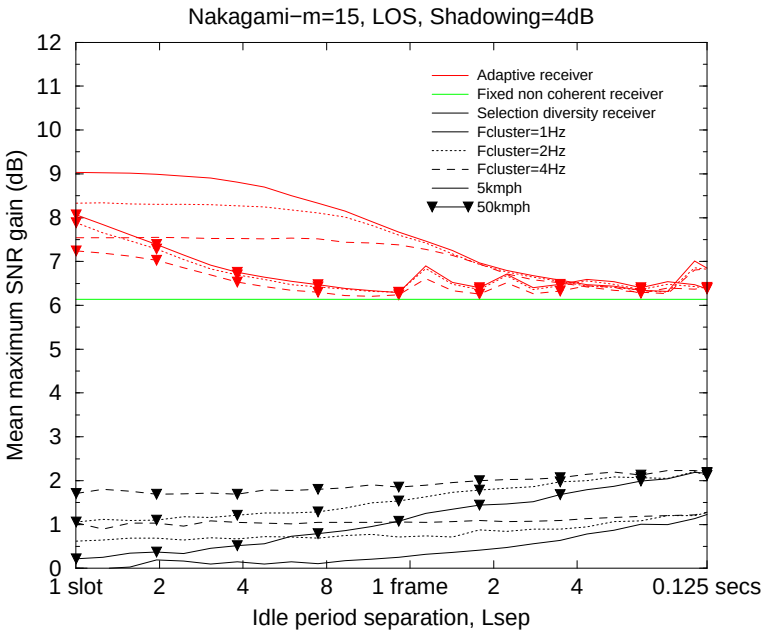

(a)

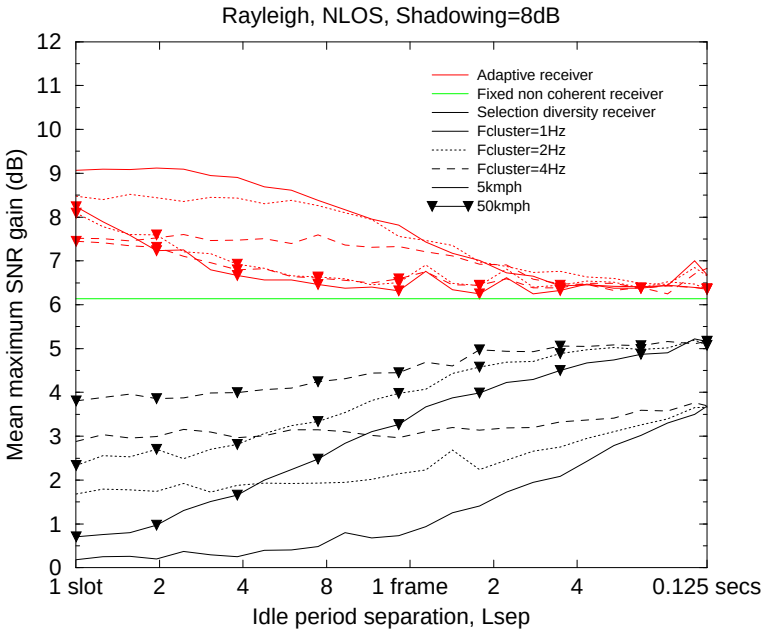

(b)

Figure 4.25: Mean maximum SNR gain against L_{sep} and $F_{cluster}$ for (a) LOS, (b) NLOS scenarios

4.4.6.1 Effect of P_{trans} on receiver performance

In the previous analysis $P_{trans} = 1$ was assumed. In practice this is not the case for PR–IPDL with proposed $P_{trans}^{PR} = \frac{15}{16}$ and TA–IPDL with $P_{trans}^{TA} = 0.3$. The vTA–IPDL scheme does however have $P_{trans}^{vTA} = 1$. The transmit probability can be included into the simulation model, or alternatively effective F_{idle}^{eff} and N_{ip}^{eff} can replace F_{idle} and N_{ip} in the previous simulations to give an approximate performance, where

$$F_{idle}^{eff} = F_{idle} P_{trans}, \qquad N_{ip}^{eff} = N_{ip} P_{trans} \tag{4.49}$$

From these equations it is easy to see TA–IPDL performance will be affected greatly by such a consideration, in which case potential gains are reduced. For this reason a slightly higher $P_{trans}^{TA} = 0.4 - 0.5$ is proposed by the author.

4.5 Conclusions

In this section the concept of hearability has been examined. It has been shown that in a CDMA system (with frequency reuse distance of 1 cell) the hearability performance will limit the performance of conventional triangulation based location estimation techniques, e.g. TDOA. Simulation results show that for the simple path loss model with a reasonable transmit power upwards of 20% of MS's would not be able to detect the required 3 BS's even exploiting Rayleigh fading diversity. For this reason IPDL techniques have been include in the UMTS specifications. A comparison of several such techniques has shown merits for each method. Based purely on hearability TA–IPDL is the best choice, however PR–IPDL requires less synchronisation constraints and has been accepted as the standard [101]. The author's own vTA–IPDL proposal also performs well and requires only one code in the MF.

When slightly more challenging channel conditions are simulated, e.g. a dual path slope model with cellular obstructions, the performance of all techniques, and especially PR–IPDL, becomes poor with a simple MF. For this reason the possibility of coherently and non–coherently integrating idle periods, as opposed to simple selection diversity, is investigated. To provide coherent gain the separation of idle periods has to be reduced, however for fast moving scenarios, where little coherency is available even for low L_{sep}, widely spaced idle periods are required to benefit from shadowing diversity. For this reason clustered idle periods are proposed, which

improve performance in the NLOS scenario. For the particular configuration simulated the adaptive receiver had performance gains of 1.5dB over the non–coherent integration receiver and upwards of 4dB gain over the selection diversity receiver at low speeds.

Chapter 5
Performance of a TDOA Location Estimator

In this chapter the performance of location estimators utilising TDOA measurements taken at the MS, as proposed for UMTS, under several different scenarios are presented.

Initially a simple receiver architecture which does not exploit spatial diversity is described. Location accuracy results for this simple receiver are presented under a number of scenarios. Sensitivity of location accuracy to several key channel parameters is also examined. Subsequently performance of a receiver architecture which allows the estimator to exploit spatial diversity in propagation conditions is presented. The performance of this location estimator is shown to be a great improvement over the simple receiver architecture.

5.1 Simple TDOA Location Estimator Architecture

Figure 5.1 shows the proposed receiver architecture, R2. The adaptive coherent and non–coherent integration stages of the previously proposed adaptive receiver, R1, (see Figure 4.4) are not implemented since the performance of that receiver can be gauged by considering the performance of the receiver R2 with higher transmit power.

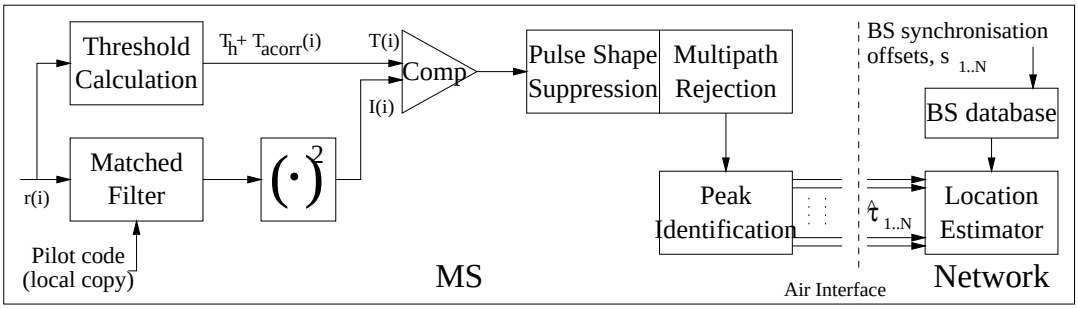

Figure 5.1: TDOA location estimator receiver architecture, R2

Since a short pilot code is used in vTA–IPDL the MF is of length $L_{MF} = L_{code} \cdot O_s$ where O_s is the oversampling rate. In TA–IPDL or PR–IPDL the length of the MF would be $L_{MF} = L_{idle} \cdot$

O_s. Such a long MF is currently impractical, thus an integrate and dump architecture might be preferred. Figure 5.1 shows an example of the output of the MF stage, $I(i)$ (i represents the sample index in the idle period), during a vTA–IPDL idle period having $L_{idle} = 1$ UMTS slot (10240 samples with $O_s = 4$), with a single path channel between the MS and all surrounding BS. The threshold, $T(i)$, is also shown.

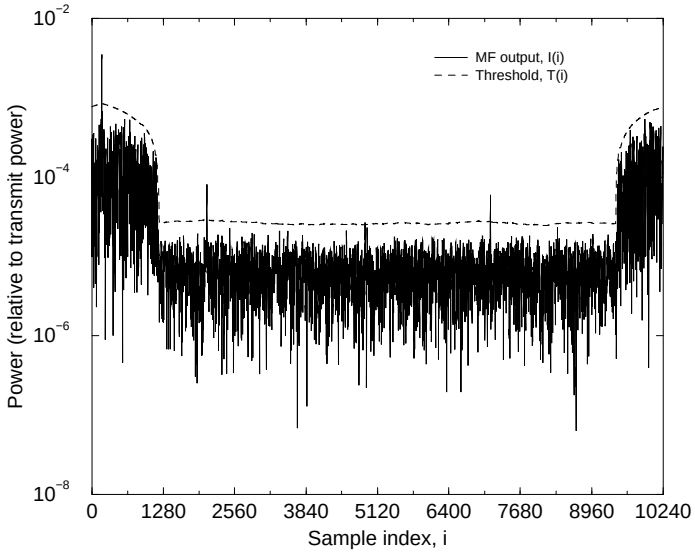

Figure 5.2: MF output and threshold example

The serving BS has a much stronger signal since it is closer and the autocorrelation sidelobes can be seen clearly above the noise floor centred at $i = 200$. Several more distant BS's can still be detected above the threshold. The threshold is not constant since the autocorrelation sidelobes must not trigger the threshold. The method used to control the threshold is discussed in the following subsections.

5.1.1 Autocorrelation Suppression

Since as many TD's as possible are required it is necessary to suppress the pilot code autocorrelation function so that peaks in the autocorrelation sidelobes are not falsely identified.

Initial attempts were made to implement an iterative subtraction technique. In this technique, starting with the largest peak, the estimated complex autocorrelation functions associated with each peak are subtracted (prior to the complex envelope detector). This subtraction process allows signals from BS's with lower power to show through the autocorrelation noise of another

higher powered signal. Unfortunately the technique proved to be too sensitive to noise, since any noise component on the highest peaks propagates through the iterative subtraction. In these cases the technique produced many more false peaks above the threshold.

A simpler method was finally used. The signal plus noise power going in to the MF is estimated from

$$P_{in} = \frac{1}{L_{MF}} \sum_{j=1}^{L_{MF}-1} |r(j)|^2 \tag{5.1}$$

The maximum signal output power assuming the signal is an autocorrelation sidelobe is then

$$P_{acorr}(i) = A_{max}^2 L_{MF}^2 (P_{in}(i) - N_o) \tag{5.2}$$

where A_{max}^2 is the power ratio of the maximum autocorrelation sidelobe to the main lobe and $N_o = 2\sigma_n^2$ is the noise power estimate. In the following simulations N_o is estimated as P_{in} during a completely idle guard band prior to the idle period. The code assigned to the PSCH in the UMTS specifications has $A_{max}^2 = -10.1$dB [2], however better codes exist in the group assigned to the secondary synchronisation channel (SSCH) channel. For the following simulations a code with $A_{max}^2 = -17.0$dB is used.

A power threshold is then generated as

$$T_{acorr}(i) = P_{adj} P_{acorr}(i) \tag{5.3}$$

where by simulation $P_{adj} = 1.35$ was found to be necessary to account for inaccuracies in the power estimates P_{in} and N_o.

The final threshold is then the sum of the independent noise and autocorrelation thresholds, i.e.

$$T(i) = T_h + T_{acorr}(i) \tag{5.4}$$

The probability of a MF output above this new threshold remains approximately P_{FA}. Uncertainty exists since various power estimates have been used.

5.1.2 Multipath Rejection and Pulse Shape Suppression

The output after the threshold comparator stage gives a fairly accurate representation of the CIR. To generate the RD's for the location estimator only the earliest arriving path arrival time is required. Therefore multipath rejection (MPR) is required. The function of the rejection stage is not only to pick out the first path in the channel impulse response but to ensure that as accurately as possible a consistent point on the pulse shaping main lobe is chosen as the output peak, ideally the central peak of the main lobe.

Three simple algorithms are proposed:

Highest Peak – the highest peak above the false alarm threshold on the channel impulse response is taken. This is a typical strategy in initial signal acquisition and synchronisation.

First Response – the first occurrence of the CIR above the threshold is taken.

First Peak – the first peak of the CIR above the threshold is taken. The strategy for selecting the peak is to first find the first occurrence as in the first response technique then to search within one chip for a higher peak. The highest peak within one chip is chosen.

Before the latter two strategies can be implemented it is very important to remove the pulse shape sidelobes which may be above the threshold if the SNR is high and thus could cause a false peak to be detected. Raised cosine pulse shaping, $p(t)$, is used with $\alpha = 0.22$ defined by

$$p(t) = \frac{\sin \pi t \cos \alpha \pi t}{\pi t(1 - 4\alpha^2 t^2)} \tag{5.5}$$

where t represents time measured in chips. Figure 5.1.2 shows the power of the pulse shaping waveform as a function of distance in chips from the main lobe. The sidelobe power is within 14dB's of the peak. Again it may be possible to iteratively subtract the pulse shaping waveform before the signal envelope detector, however for similar reasons to the autocorrelation suppression a simple power threshold is used. This need only be applied to the negative side of the waveform. A threshold of 7dB/chip was used as shown in Figure 5.1.2. This will limit the ability to resolve temporally close multipaths but since in true LLOS the first arriving wave will generally be of higher power to subsequent waves it should not have a great bearing on location accuracy performance.

The performance of the MPR techniques were assessed by simulation. The relative position of

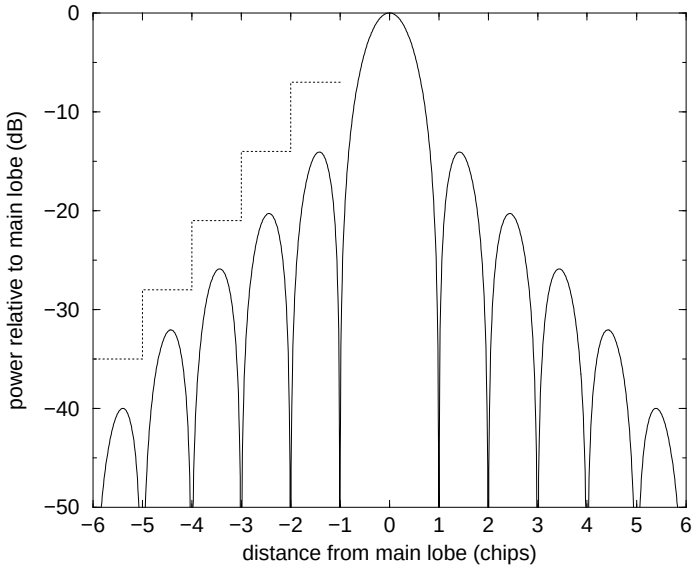

Figure 5.3: The pulse shaping waveform and threshold

the output peak was measured with reference to the true arrival time of the centre of the pulse shape using the highest peak, first response and first peak algorithms. UMTS system parameters were used with only the pilot channel simulated. The CoDiT rural (single path) and CoDiT urban (multipath) channels were simulated and the LOS state of the channels fixed to LLOS and CLOS. The received SNR (before the MF) was varied from -30dB to 0dB and the code used in the MF had length 256 chips thus giving a processing gain of 24dB. An oversampling rate of $O_s = 4$ was used. In each simulation the results were collected for 1000 different but statistically identical channels. For each channel the sampling instance was varied randomly with uniform distribution of $\pm 1/2$ sample to ensure the receiver did not always sample precisely on the pulse shape peak.

Figures 5.4(a)-(c) show the PDF's of the output peak compared to the true position of the pulse shape peak for all three techniques with the rural (single path) channel. It can be seen that the first response algorithm (Figure 5.4(b)) at high SNR's tends to pick the leading edge of the pulse which occurs 4 samples before. However as the SNR decreases the detection rate falls and the detected peak shifts closer to the centre of the true peak. This shift is undesirable since it introduces a bias when comparing detected peaks between signals from several BS's at different SNR's. For the one path channel the first peak and highest peak detectors (Figures 5.4(a), (c)) perform similarly with both giving timing within one sample of the true peak with highest frequency, though the first peak strategy tends to pick the leading side of the peak.

Decreasing the SNR does not significantly affect the mean peak position, but does reduce the detection probability.

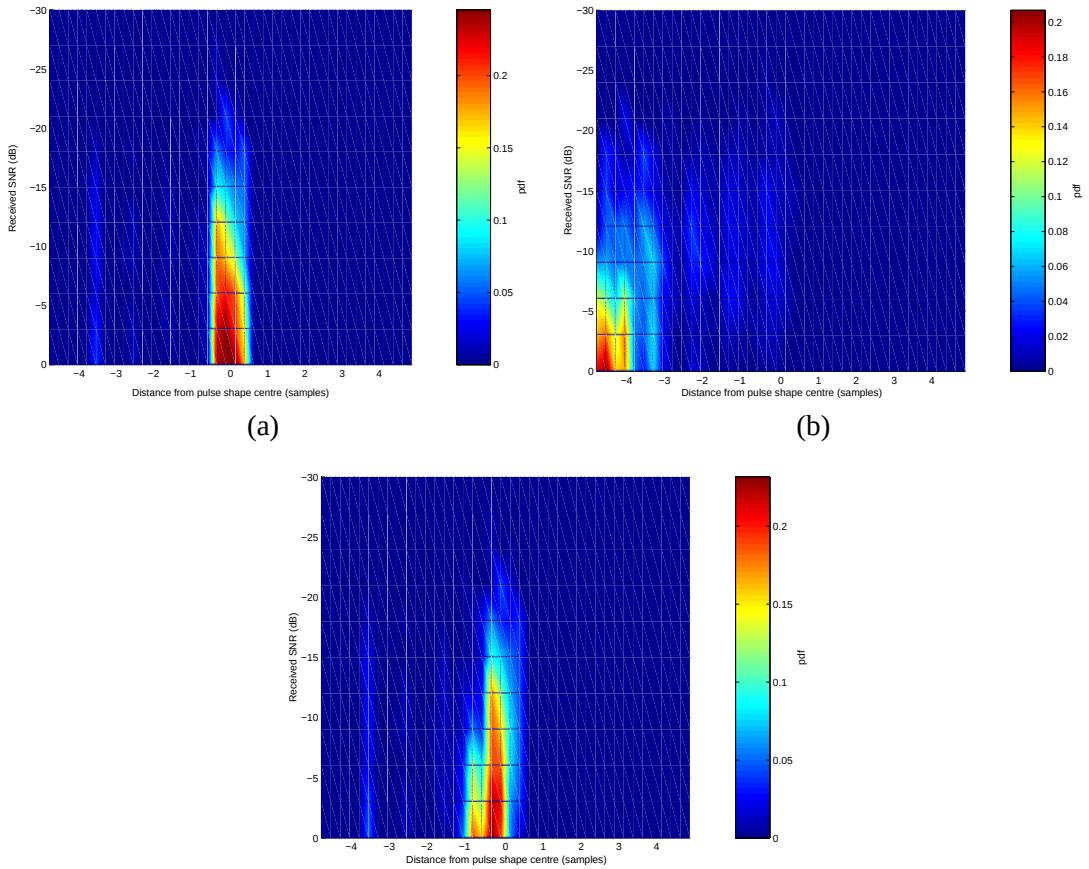

Figure 5.4: Output peak relative position PDF's in single path channel for (a) highest peak, (b) first response, (c) first peak strategies

Figures 5.5(a)-(c) show the same PDF's for the urban (multipath) channel. This time the output peaks are detected over a significant delay spread even thought the channel is LOS. In this case since multipaths can combine coherently to give higher power than the LOS path (especially if the LOS path is in a fast fade) the first peak performs better than the highest peak algorithm.

The conclusions to be drawn from these simulations are that the first peak algorithm, while being fairly simple, works adequately at detecting the peak to the nearest sample time consistently over all SNR's and for multipath channels. In UMTS the chip rate is high, corresponding to 78.3m propagation distance per chip. Since oversampling is employed to further increase the time resolution at the receiver, super resolution techniques are unnecessary. Since a constant false alarm threshold is employed reducing the SNR does not increase the measurement

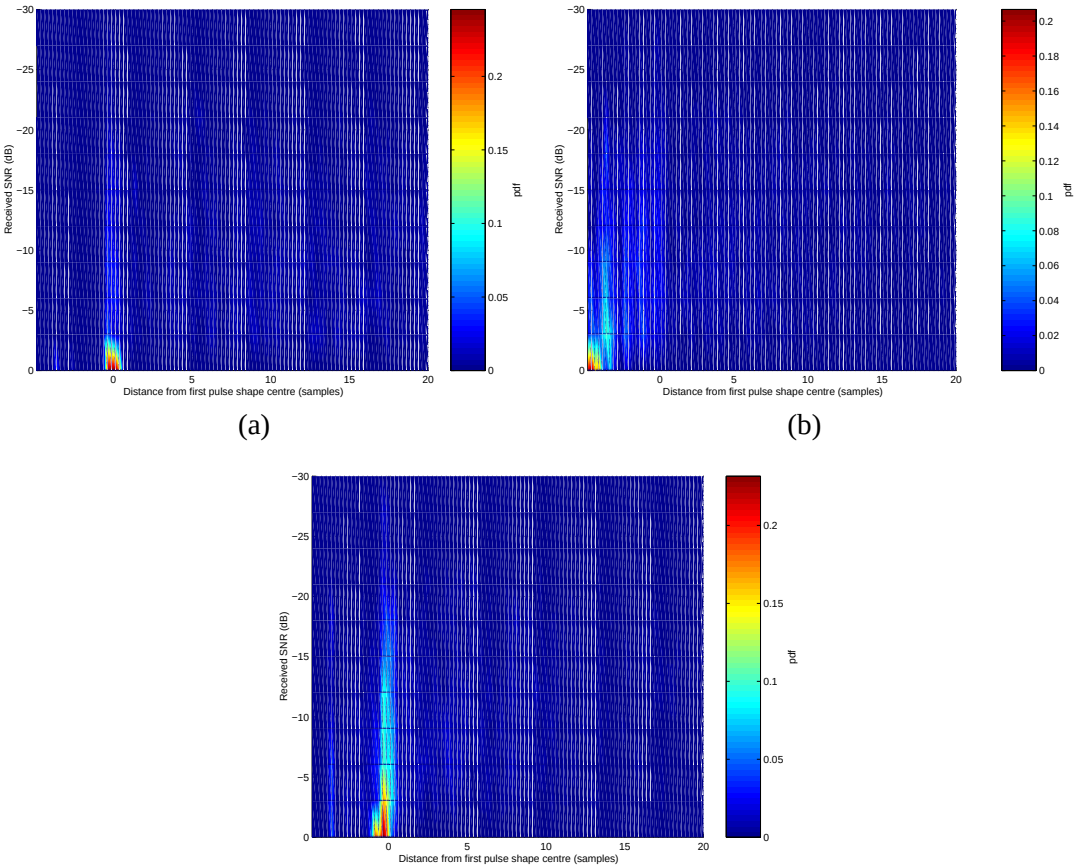

Figure 5.5: Output peak relative position PDF's in multipath channel for (a) highest peak, (b) first response, (c) first peak strategies

noise (in fact it may marginally reduce the noise) thus SNR itself is not a necessary or indeed useful measure for measurement confidence as has been proposed in [100]. In all subsequent simulations the first peak algorithm is used.

5.1.3 Peak Identification

The transmitting BS for each peak must be identified. If the PCPICH channel were being used this would be straightforward since each BS would be transmitting a different code. In the case of vTA–IPDL the PSCH is used which is identical for each BS. Since the serving BS is known and each BS has a unique code alignment relative to the serving BS (see Figure 4.6), peak identification is still straightforward.

5.1.4 BS Synchronisation Offsets

Typically in a mobile network all the BS's are not tightly synchronised. In order to calculate the MS location the BS's must either be tightly synchronised or their synchronisation offset known. Since for other applications of the mobile network tight synchronisation is not required the latter strategy has been proposed as part of the UMTS standard [2]. So called LMU's need to be located in known fixed positions throughout the network to measure the synchronisation offsets of surrounding BS's through pilot channel measurements. Naturally LMU's should be placed to be LOS to all the surrounding BS's.

5.1.5 Location Estimator

A TD vector, $\Delta\hat{\tau}(n)$, can be formed from $\hat{\tau}(n)$ defined as

$$\Delta\hat{\tau}(n) = \begin{bmatrix} \hat{\tau}_1(n) - \hat{\tau}_2(n) - s_{1,2} \\ .. \\ \hat{\tau}_1(n) - \hat{\tau}_N(n) - s_{1,N} \end{bmatrix} \tag{5.6}$$

where $s_{i,j}$ represents the measured synchronisation offset between BS$_i$ at location (x_i, y_i) and BS$_j$ and n is the measurement index.

Since the receiver R2 is not utilising spatial or temporal variation the relative variances of $\tau_{1..N}$ are unknown. Therefore the weighting matrix, ω_τ, is constructed with equal weights, the absolute magnitude being of no significance.

$$\omega_\tau^{-1} = \begin{cases} 2 & i = j, \\ 1 & i = 1 || j = 1, \\ 0 & \text{otherwise} \end{cases} \tag{5.7}$$

ω_τ^{-1} is an N by N matrix with terms as defined. Note $||$ represents the exclusive–or operation.

Where 3 or more TD's are available Chan's TDOA location estimator is used (see Section 2.3.3). If 2 TD's are available the intersection point(s) of the TD's are used (see Section 2.3.3). There are two solutions to the equations, so the solution that minimises the total summed distance between the MS and the 3 BS's is used. If only one TD is available then the intersection point of that TD with the line connecting the two detected BS's is used in which case

$\hat{\mathbf{Z}} = [\ x \quad y\ ]^T$ is given by

$$\hat{\mathbf{Z}} = \begin{bmatrix} x_1 \\ y_1 \end{bmatrix} + \frac{\begin{bmatrix} x_2 \\ y_2 \end{bmatrix} - \begin{bmatrix} x_1 \\ y_1 \end{bmatrix}}{2} - \begin{bmatrix} \cos\theta \\ \sin\theta \end{bmatrix} \frac{c(\hat{\tau}_1(n) - \hat{\tau}_2(n) - s_{1,2})}{2} \tag{5.8}$$

where

$$\theta = \tan^{-1}\left(\frac{y_2 - y_1}{x_2 - x_1}\right)$$

Finally if no TD's are available the serving BS location, $\begin{bmatrix} x_1 & y_1 \end{bmatrix}^T$ is used as the MS location estimate.

5.1.6 Location Estimation Accuracy Performance

A vTA–IPDL UMTS system is simulated. 1000 MS's are placed randomly in the central cell of a hexagonal array with uniform spatial distribution. Rural, suburban and urban scenarios are simulated with varying cell radius, R_C, and channel model parameters. The MS's travel with random bearing uniformly distributed across 2π at speeds of 150kmph, 50kmph, and 5kmph in rural, suburban and urban scenarios respectively. Tables 5.1, 3.1 and 3.2 show the simulation, channel, LLOS, CLOS and IPDL parameters. The dual slope path loss model, (3.11), is used. For the rural scenario a 7 BS array is used while for the other scenarios a 16 BS array is used (see Figure 4.7).

Timing difference measurements are taken at the MS during eight consecutive idle periods ($N_{ip} = 8$) over 1 second ($f_{idle} = 8$Hz) from the PSCH (with processing gain 24dB) and are used to calculate a location estimate. In this time the MS will experience little or no spatial diversity of LOS/NLOS or shadowing conditions, but will benefit from Rayleigh (fast) fading diversity. For each BS the earliest TOA is used in the location calculation, but only those BS's that are detected in at least half the idle measurements are used.

Initially a suitable false alarm probability, P_{FA}, needs to be found to give optimum performance. Setting P_{FA} too high results in too many false peaks being used in the location estimator. If P_{FA} is too low then the hearability of BS's will drop so that insufficient timing measurements

Parameter	Value
Carrier frequency	1.92GHz
Chip rate	3.86Mchips/s
Over sampling rate O_s	4
Modulation scheme	QPSK
Slot frequency	1600Hz
Time resolution	1/64 chip
Max. frame desynchronisation, $s_{1..N}$	0 chips
Pulse shaping roll off rate (α)	0.22
h_{MS}	2m
IPDL scheme	vTA–IPDL
Idle period frequency	8Hz
Idle period length	2560 chips
Pilot length	256 chips
Pilot transmit power (% of total)	100%
Pilot SNR	0dB
Path loss model	Dual slope (3.11)
s_1,σ_1	3.0, 2.6
s_2,σ_2	6.0, 5.8
$C_{\Omega-\tau}$	0.8
m_{NCLOS}	5

Table 5.1: System parameters

are available to calculate a location. Figure 5.6 shows the effect of varying P_{FA} in the rural (one LLOS path) scenario. The value of the location error CDF at 50m is plotted against P_{FA}. The peak performance occurs at $P_{FA} = 2.65 \cdot 10^{-5}$. In all subsequent simulations this value is used. With $L_{idle} = 2560$ chips and noting the noise is bandlimited, the optimum P_{FA} corresponds to one false peak every 15 idle periods regardless of O_s, though due to incorrect noise power estimation these errors tend to be bursty in nature.

Figure 5.7(a) shows the cumulative probability function for circular location error in the rural scenario with varying pilot powers. The transmit power is varied such that the received pilot SNR from the serving BS at the serving BS cell boundary varies from -12dB to 12dB. Figure 5.7(b) shows the corresponding hearability results. It can be seen that for high hearability location accuracy well within the FCC regulations is obtained. At the 67th percentile accuracy of within 30m is observed. There is a residual 10% of MS's which are unable to be located to within 250m due to using the wrong solution in the 2 TD case (which has two solutions) or having hearability less than 3 BS's. As hearability drops, the percentage of wayward location estimates increases, which can be directly related to the fraction of MS's with below 3 BS

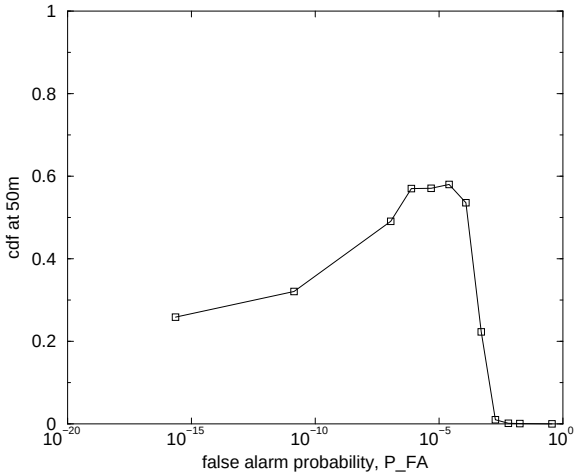

Figure 5.6: Location error CDF at 50m against P_{FA} in the rural scenario

hearability. Since the cell radius is large the back up strategies for calculating the location with hearability less than 3 BS's still give large errors, which is the reason for the characteristic flattening of the CDF's.

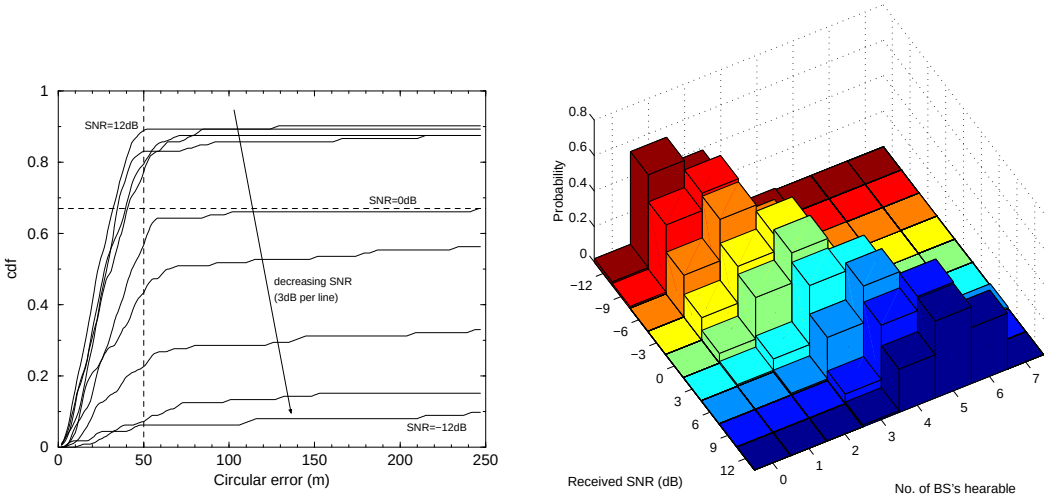

(a) (b)

Figure 5.7: (a) CDF of circular location error and (b) hearability histograms with varying received pilot SNR in the rural scenario

Figure 5.8(a) shows the effect of different CLOS scenarios on the location performance. Notably the difference between the unobstructed scenario and the partially obstructed scenario is slight, the partially obstructed scenario having slightly worse location accuracy. The implication of this is that there would be no real need to perform calibration to take into account the

NCLOS propagation delays for this scenario. The obstructed scenario performs much worse. Of most interest is the fact that its CDF only begins to rise at 50m. Thus, even assuming the pilot power could be boosted to overcome the hearability problem, location accuracy would not be good enough to meet FCC regulations. This implies some sort of calibration of NCLOS delays would be required. Figure 5.8(b) show the effect on hearability for the CLOS scenarios. Clearly in the obstructed scenario a much greater pilot power would be required. In all future simulations only the partially obstructed CLOS scenario is used.

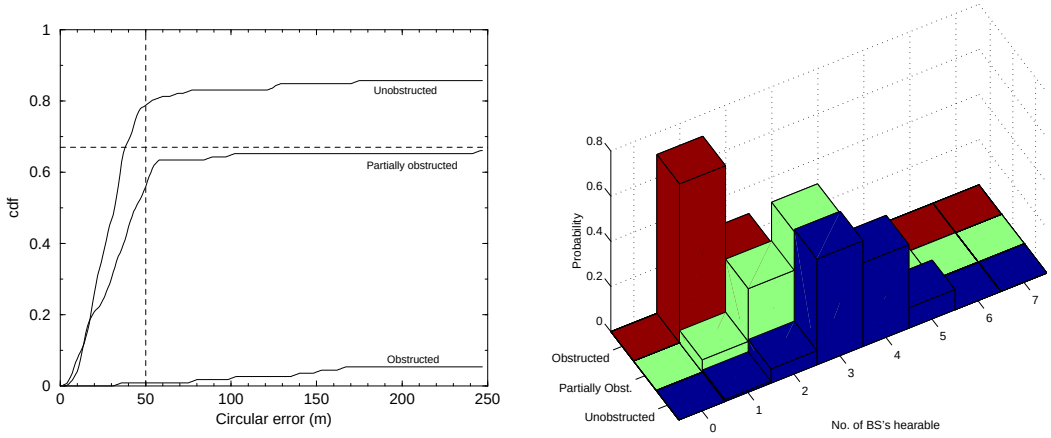

(a) (b)

Figure 5.8: (a) CDF of circular location error and (b) hearability histograms with varying CLOS model in the rural scenario

Figure 5.9 shows the effect of varying the oversampling rate O_s. Somewhat surprisingly the sampling rate had little effect on the accuracy of location estimates over the range tested. $O_s = 1$ corresponds to a distance resolution of 77.3m, whereas $O_s = 16$ corresponds to a distance resolution of $4.9m$.

Figure 5.10 shows the effect of varying the synchronisation offsets, $s_{1..N}$ (measured in μs. The synchronisation offsets for each BS are uniformly distributed within the ranges specified. In the calculation of location it is assumed that the offsets are known to the nearest sample. Since the IPDL scheme used requires time alignment of the idle periods the degree of desynchronisation has a slight impact on performance. This can be attributed to the increased tendency for pilot pulses from different BS's to overlap and thus mask each other or be falsely recognised. In TA–IPDL and PR–IPDL the performance would not deteriorate since pilot codes are already overlapping and each BS uses its own code and would not be falsely recognised.

Figure 5.11(a) shows the results of varying the pilot SNR for the suburban scenario. Figure

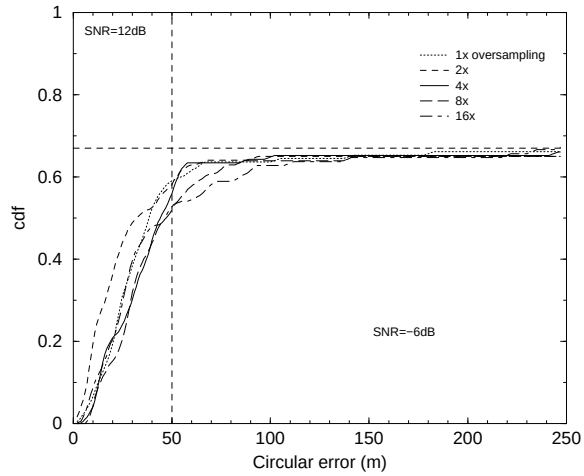

Figure 5.9: CDF of circular location error with varying O_s in the rural scenario

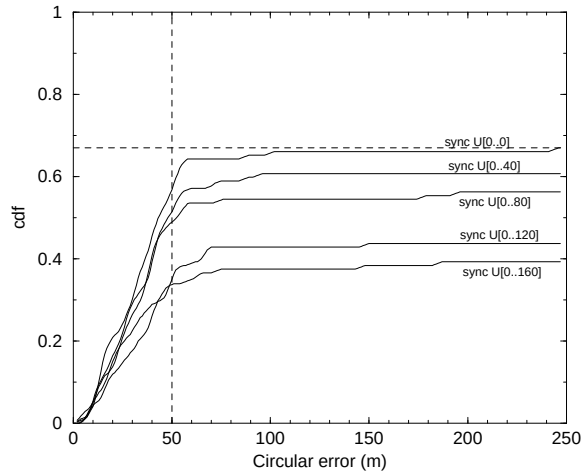

Figure 5.10: CDF of circular location error with varying synchronisation offset range in the rural scenario

5.11(b) shows the corresponding hearability results. At low SNR the location accuracy performance is poor since the hearability is generally below 3 BS's. As the SNR increases the performance increases but reaches an SNR level above which accuracy fails to increase. This is because of NLLOS errors entering the location estimator. Even one NLLOS measurement can cause large errors in the location estimate, especially since the delay spread of the suburban model is large.

Figure 5.12(a) shows the effect of varying P_{LLOS} in the suburban scenario. Figure 5.12(b) shows the corresponding hearability results. With $P_{LLOS} = 1.0$ the location accuracy ap-

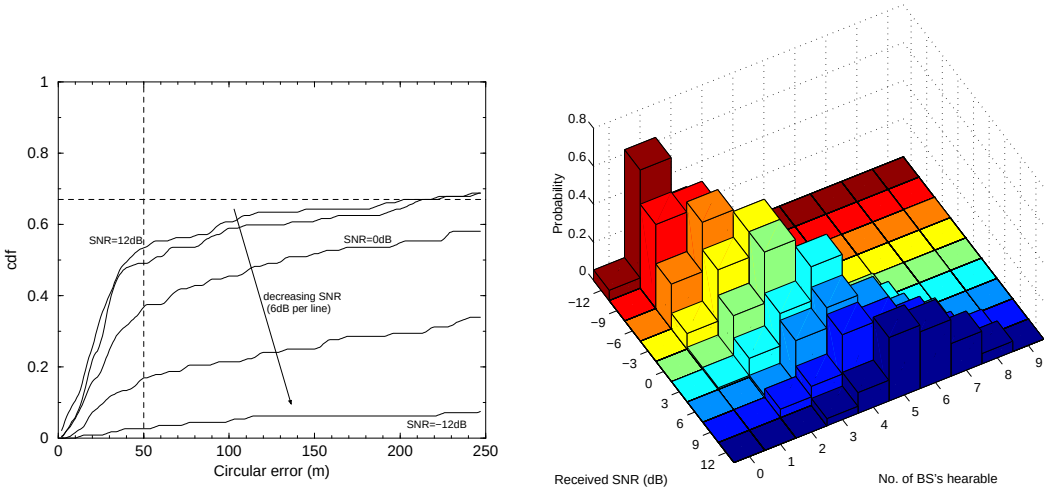

(a) (b)

Figure 5.11: (a) CDF of circular location error and (b) hearability histograms with varying pilot SNR in the suburban scenario

proaches that of the rural scenario and exceeds the FCC requirements at 67%. Performance can not be as good as the rural scenario since the multipaths cause added interference and could still be detected if the LLOS path was in a fast fade. As P_{LLOS} decreases location accuracy deteriorates rapidly. Hearability drops slightly with decreasing P_{LLOS}.

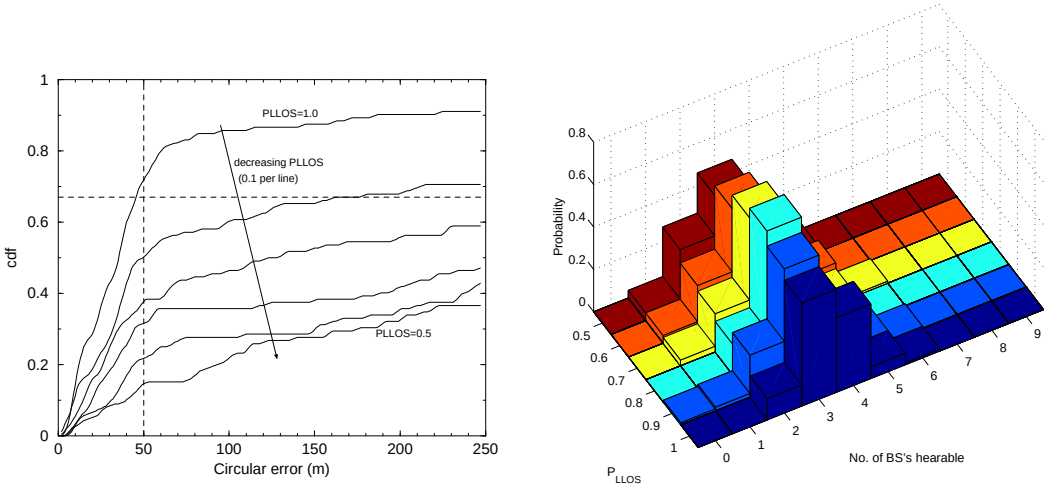

(a) (b)

Figure 5.12: (a) CDF of circular location error and (b) hearability histograms with varying P_{LLOS} in the suburban scenario

Figure 5.13(a) shows the results of varying the pilot SNR for the urban scenario. Figure 5.13(b) shows the corresponding hearability results. In this case the location accuracy at low SNR is

not as poor as the other scenarios. This is because the cell radius, $R_C = 500$m, is an order of magnitude smaller thus the strategies for locating the MS with only one or two BS's become more accurate. In general hearability is higher at the same SNR levels compared to the rural and suburban scenario. Again this gain can be attributed to the lower R_C value. As the SNR is increased the location accuracy improves, again reaching a limit, which notably fails the FCC regulations. This limit is again a function of P_{LLOS} though in the urban model the delay spread is not so large, thus utilising NLLOS measurements is not as detrimental as in the suburban scenario.

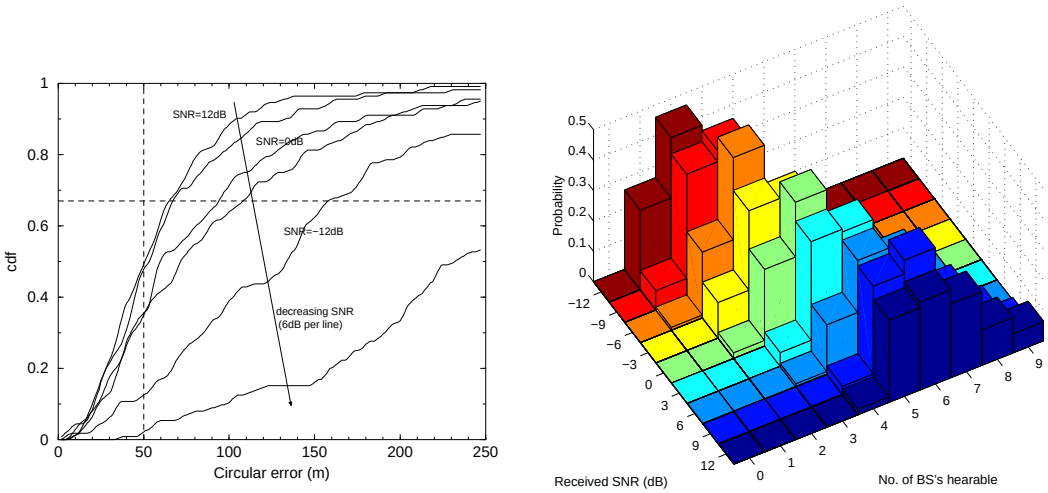

(a) (b)

Figure 5.13: (a) CDF of circular location error and (b) hearability histograms with varying pilot SNR in the urban scenario

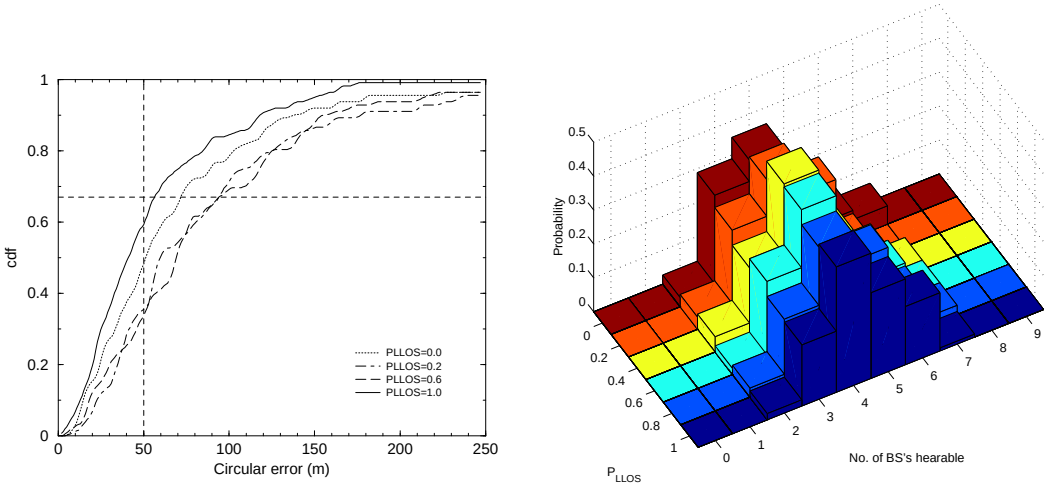

(a) (b)

Figure 5.14: (a) CDF of circular location error and (b) hearability histograms with varying P_{LLOS} in the urban scenario

Figure 5.14(a) shows the effect of varying P_{LLOS} in the urban scenario. Figure 5.14(b) shows the corresponding hearability results. The effect of varying P_{LLOS} does not produce a linear relationship as might be expected. $P_{LLOS} = 1.0$ naturally performs the best though not as well as the suburban or rural scenarios since the multipath component of the channel has a large power, thus is more likely to overpower the LLOS component than in the other scenarios during a fast fade on the LLOS component. At $P_{LLOS} = 0.0$ the performance is better than $P_{LLOS} = 0.2$ or $P_{LLOS} = 0.6$. This can be explained by the fact that since all BS's have identical NLLOS delay statistics the delays tend to cancel each other out. In a scenario with both NLLOS and LLOS BS's this does not occur so the full NLLOS delay errors propagate into the estimator. Variation in P_{LLOS} has little or no effect on hearability since the multipath power is the majority of the channel power.

To conclude the results show that two factors, hearability and P_{LLOS} will affect the location accuracy considerably. Notably in the suburban scenario if $P_{LLOS} < 1$, regardless of the hearability level, the FCC guidelines cannot be reached. In the urban scenario the same applies for all values of P_{LLOS}. For this reason methods to improve location accuracy in NLLOS conditions are required. One such method is to exploit spatial diversity of measurements as is investigated in the remainder of this chapter.

5.2 Filtering of TOA Measurements to Exploit Spatial Diversity

The distribution of NLOS errors in TOA measurements was described in Section 2.7. Figure 3.10 shows the distribution developed from the LLOS model, which is similar to the exponential model. Measurement noise is also present on the TOA as shown in Figures 5.4 and 5.5. The overall distribution of TOA's in NLOS conditions is therefore the convolution of these two noise processes, see Figure 5.15.

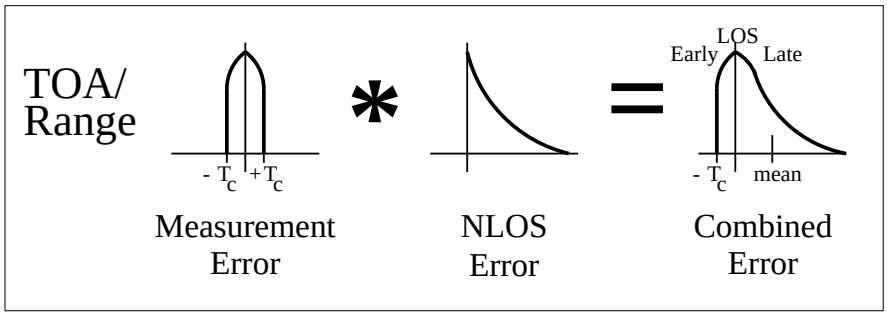

Figure 5.15: PDF of TOA/Range in NLOS with measurement noise

The value T_c represents the chip period/distance. The measurement noise does not fall outside of this distance except due to false alarms. The key point to notice from the TOA distribution is that the mean is not equivalent to the true LOS TOA, which complicates the filtering process. The earliest arriving TOA's are closest to the true LOS TOA. Furthermore the spread of the distribution is large enough that corrupted data can cause large location errors. This has been demonstrated through simulation in Section 5.1.6. A final problem is the large spatial correlation between NLOS errors.

Ideally the filter would discard all NLOS data. However the environment may be such that no good data is available for considerable periods of time, so the function of the prefilter stage should be to make the best use of the available data by generating variance estimates for each measurement stream. In tracking the measured parameters, the manoeuvring capability of the MS may be taken into account. The aim here is a real time estimate, thus any significant delay would render a final location estimate out of date.

Kalman filters are often used in such real time tracking applications. In the next subsections this and other ways to prefilter the TOA data are presented and their performance on simulated data compared.

5.2.1 Input Estimation Kalman Filter Implementation

The KF (see Section 2.10) is optimal for tracking a parameter in time with unbiased Gaussian distributed noise. However the TOA distribution in NLOS is not Gaussian distributed and the true LOS TOA is not equal to the mean of the distribution. Furthermore as the MS moves from LOS to NLOS conditions the variance of measurements will change significantly. If the measurement variance is set to be the estimated LOS variance, $\sigma^2_{\tau LOS}$, then the KF will add too much significance to NLOS data and perform poorly. If the measurement variance is set to be the estimated NLOS variance, $\sigma^2_{\tau NLOS}$, the KF will converge slowly during transition to LOS regions. For this reason an input estimation stage is added to the KF to estimate the measurement variance real time. This is termed an input estimation KF (ieKF). The justification for this input estimation stage is described below.

If the true TOA value is known the PDF of the TOA's new value after a time interval can be predicted. For example if the MS has manoeuvred and its velocity is considered uniform in

speed (to a maximum speed) and direction, a PDF of the new TOA, $f_\tau(\tau)$ can be derived as

$$\begin{aligned} f_\tau(\tau) &= \int_0^{\cos^{-1}(\tau/\tau_{max})} \frac{1}{\pi\tau_{max}\cos\phi} d\phi \\ &= \frac{\ln\left[\left(\tau_{max}+\tau_{max}\sqrt{1-\frac{\tau^2}{\tau_{max}^2}}\right)/|\tau|\right]}{\pi\tau_{max}} \end{aligned} \tag{5.9}$$

where τ_{max} is the maximum change in TOA in the time interval.

Figure 5.16 shows this equation. (5.9) is of similar shape to the Gaussian PDF with equal variance; the major difference being that the Gaussian PDF is over an infinite range whereas (5.9) is limited to 2.5σ.

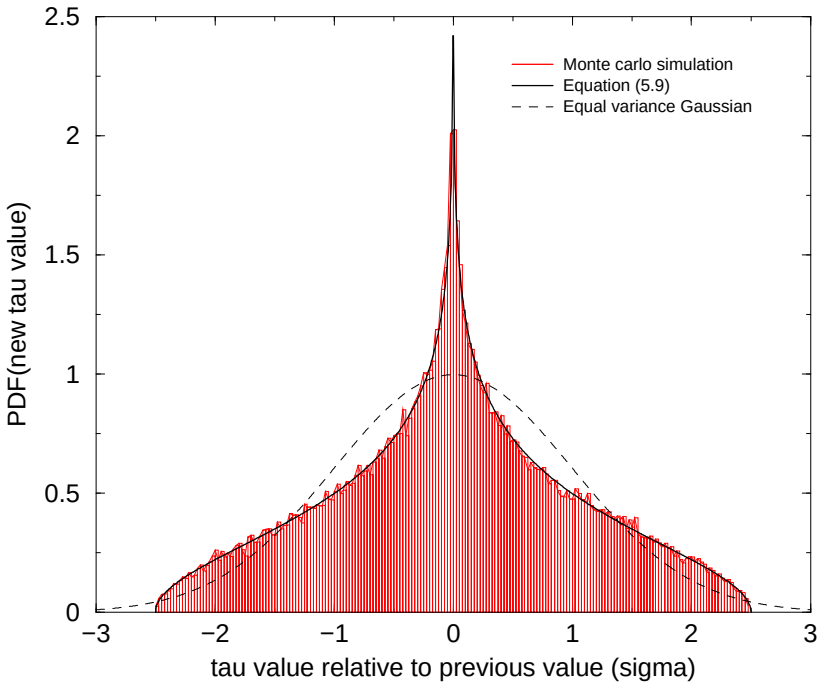

Figure 5.16: TOA uncertainty after a time interval.

This PDF leads to a simple input estimator which discards data that is definitely NLOS and cannot be due to a manoeuvre. A weighting is applied to the measurement noise variance estimate, σ_Y^2, (contained in $\mathbf{R}_n$) as follows

$$\hat{\sigma}_Y^2 = \max\left(\sigma_{\tau LOS}^2, \frac{s_{1/1}}{W(r)}\right) \tag{5.10}$$

where $s_{1/1}$ is the TOA variance predicted by the KF (first term in $\hat{\mathbf{S}}_{n,n-1}$), and $W(r)$ is a weighting function, a function of the residual r between the measured TOA and the KF predic-

tion. In the following the weighting function is defined as a Gaussian curve normalised to one at its maximum,

$$W(r) = e^{-\frac{r^2}{2s1/1}}$$

though in practice any function could be used.

In TOA filtering, the NLOS error PDF is not symmetric about the true LOS TOA. A KF will track to the mean and not the true LOS TOA. Therefore if a TOA is measured that is more than T_c earlier than the predicted TOA the filter outputs are forced to take the measured value on the assumption that a manoeuvre has occurred. This is done by setting $\hat{\sigma}_Y^2 = \sigma_{\tau LOS}^2$. Furthermore if this difference is larger than a threshold, σ_{err}, the filter prediction must be so badly wrong that estimates of $\dot{x}_{n,n}$ and its variance will also be inaccurate so should be reinitialised. In this way the filter attempts to track to the LOS edge of the data.

It should be noted that due to this favouring of early TOA, the filter is extremely sensitive to noise generated by false alarms in the TOA measurement device. TOA values falling below σ_{err} were only used if the previous measured TOA also occurred within one chip of it.

The MS manoeuvring capability can be controlled by the velocity driving noise power parameter, σ_u^2. This value must be carefully chosen, since if σ_u^2 is too small the KF will loose track with the MS path, and if σ_u^2 is too large the KF will follow the measured data and offer no filtering benefit at all.

The output variance estimate, $\hat{\mathbf{S}}_{n,n}$, can reflect three modes of operation. If the MS is LOS, $\hat{\mathbf{S}}_{n,n}$ will reflect the LOS measurement variance. In the absence of new measurements or if new measurements must be NLOS according to the filter prediction, $\hat{\mathbf{S}}_{n,n}$ reflects uncertainty caused by manoeuvring capability of the MS. Finally if the MS is NLOS and the NLOS measurements could be true according to the filter predictions, $\hat{\mathbf{S}}_{n,n}$ will reflect the NLOS measurement variance (assuming little spatial correlation in measurements). Since the ieKF is biased to the early end of the NLOS PDF and the PDF is exponential–like the variance estimated in this fashion will be similar to $\mu_{\tau NLOS}^2$. The distribution of the uncertainty in the former two cases is approximately Gaussian, the latter case is a mixture of exponential–like and Gaussian since there is also so manoeuvring uncertainty present.

The variance estimation process is not perfect all the time, since sometimes NLOS measure-

ments fit the filter prediction, but the method is robust in most cases.

5.2.2 Adjusted LS Filter Implementation

Wylie *et al* [74] describe an adjusted least squares (aLS) implementation to remove NLOS errors from corrupted data. This is described in more detail in Section 2.7. The technique does not use information about the MS manoeuvring capability.

This filter length, L_{LS}, in seconds and filter order N_{LS} are parameters in this technique, the effect of which is to be investigated. The implementation in [74] assumes post processing of data, i.e. a delay is acceptable. For this implementation the performance is examined with delay of half L_{LS} and no delay, the latter being more appropriate to the real time approach studied in this thesis.

The correction factor, C_{LS}, applied to the aLS fit will tend towards T_c as the length of the filter in measurement samples increases. Figure 5.17 shows an example of the LS fit with $L_{LS} = 90$ seconds and $N_{LS} = 2$.

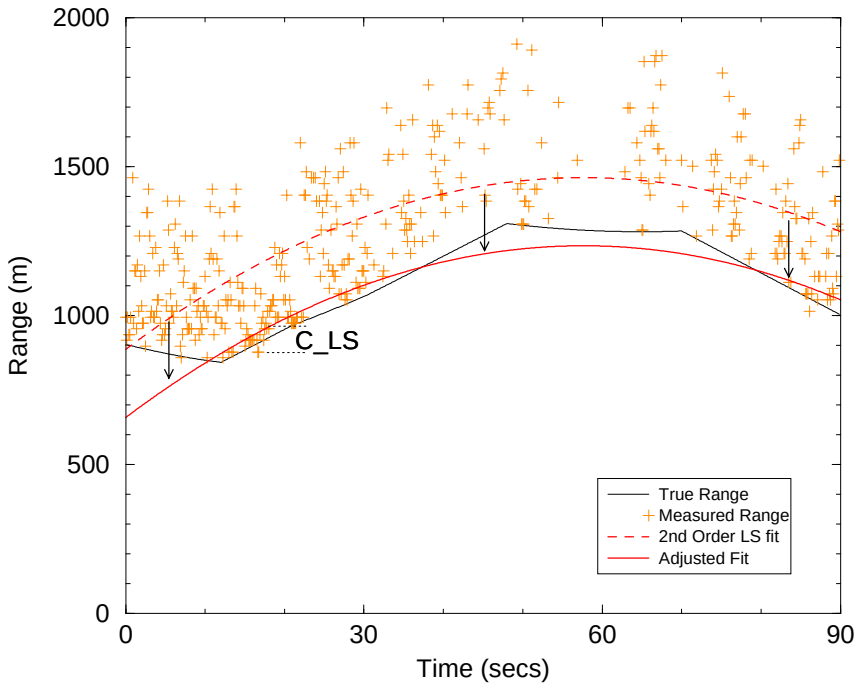

Figure 5.17: Example of aLS fit.

The measurement variance estimate from the aLS technique can be obtained from the fit residual.

5.2.3 First TOA (fTOA) Filter Implementation

In this filter the first TOA is selected from the last L_{fTOA} seconds worth of data. The assumption is that the MS is stationary or near stationary. Similarly to the LS filter a correction factor C_{fTOA} is required since the first TOA will tend towards T_c as the length of the filter in measurement samples increases.

It is also important to note that since early TOA's are selected the technique is susceptible to errors caused by false alarm detection. To overcome this only data within 10 chips of the mean TOA value are accepted as good data.

An approximation of the measurement variance can be calculated by

$$\hat{\sigma}^2 = E[\tau^2] - \hat{\tau}^2 \tag{5.11}$$

where expectations are calculated over the filter length L_{fTOA} and $\hat{\tau}^2$ has replaced $E[\tau]^2$ in the standard definition of variance.

5.2.4 Performance Comparison of Prefiltering Techniques

The performance of the KF, ieKF, aLS and fTOA algorithms are compared for simulated TOA data in an urban environment at 50kmph and at 5kmph with measurement frequency $f_{idle} = 8$Hz over 90 seconds. In Section 5.3.6 the MS course is described in more detail. Tables 5.1, 3.2 show the parameter settings. 10 statistically identical datasets are tested for several different average received pilot SNR levels. Note the pilot SNR changes throughout the track since the MS–BS separation distance varies. The performance of each technique is assessed in terms of RMS range error of the filtered TOA to the true TOA (timing errors are converted to range errors) for the middle 30 seconds of the track. The fractional hearability of the BS (i.e. the fraction of measurements periods which yield a TOA measurement) varies as the SNR is changed and is the x–axis of the results graphs.

For the KF and ieKF implementations Φ, $\mathbf{K}$ and an initial value of $\mathbf{S}_{0,0}$ are

$$\Phi = \begin{bmatrix} 1 & \Delta t \\ 0 & 1 \end{bmatrix}, \mathbf{K} = \begin{bmatrix} 1 & 0 \end{bmatrix},$$

$$\mathbf{S}_{0,0} = \begin{bmatrix} 10000 & 0 \\ 0 & 1.00 \end{bmatrix}$$

where the variances (measured in terms of the sampling rate) in $\mathbf{S}_{0,0}$ are initially set high so the measurement data is initially favoured. σ_u^2 is set to $1.5^2(\text{ms}^{-2})^2$, or equivalently $0.035(\text{m samp}_{\Delta t}^{-2})^2$ where the sample period $\Delta t = 0.125s$. This relatively large acceleration capability is required since several instantaneous manoeuvres of the MS occur. $\sigma_{err} = 3$ standard deviations are used. The KF is implemented with both $\sigma_Y^2 = \sigma_{\tau LOS}^2$ and with $\sigma_Y^2 = \sigma_{\tau NLOS}^2$. These KF's are termed LOS–KF and NLOS–KF respectively. The noise power values are estimated to be $\sigma_{\tau LOS}^2 = 1/12$ chip^2 and $\sigma_{\tau NLOS}^2 = 6.25$ chip^2.

For the aLS filter $L_{LS} = 10, 30$ seconds and $N_{LS} = 1, 2$ are tested. $C_{LS} = 0.75$ chips was found to give the best performance.

Similarly for the fTOA filter $L_{fTOA} = 10, 30$ seconds and $C_{fTOA} = 0.75$ chips are used.

For all simulations it is assumed that the arbitrary time reference for TOA's stays constant, thus ignoring MS clock instability. However if the MS clock instability changes slowly with respect to the idle period frequency the KF or LS filter could effectively track the instability. In the case of the fTOA filter this is more problematic. Once the TDOA's are formed the clock stability is not an issue, however as is discussed in the next subsection it is advantageous to filter the two TOA streams separately first.

Figures 5.18(a), (b) show example tracks for the 50kmph and 5kmph scenarios respectively. At 50kmph the measurements display far less temporal correlation than at 5kmph. It is clear from these examples that the non–delayed aLS and fTOA filters perform worse than the same filter with delay. The LOS-KF and NLOS–KF track to the mean of the data which is not very useful, while the ieKF tracks the lower edge of the data, most successfully at higher speeds when the acceleration constraint allows it to discard NLOS data.

Figures 5.19(a), (b) show the RMS error between the true range and the filtered range for the 50kmph scenario. The raw data RMS error does not stay constant over the range of hearability

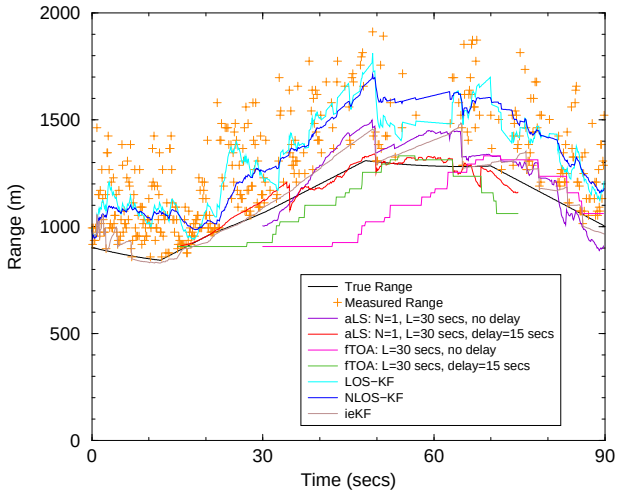

(a)

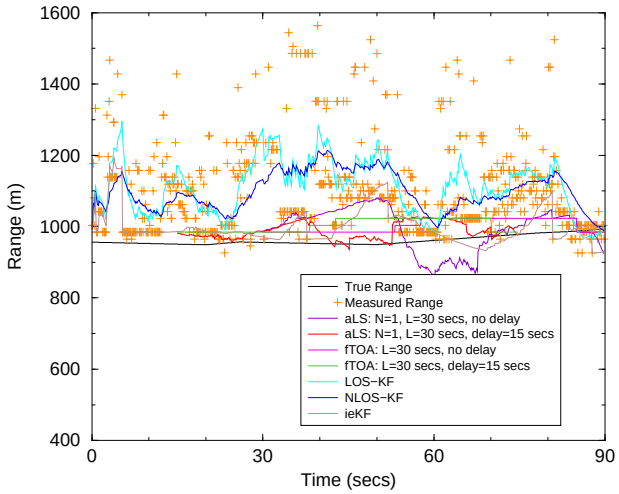

(b)

Figure 5.18: Example prefilter tracks for (a) urban 50kmph, (b) urban 5kmph scenarios

since at lower hearability false alarms add considerably to the range error. The aLS filter works best with $N_{LS} = 1$ and $L_{LS} = 30$ seconds. The RMS range error can be reduced from 180m to 40m. The lower order fit works better since the MS trajectory is fairly linear, and even when this maps to the range parameter it remains fairly linear. Increasing the order simply allows a better fit to the errors thus increasing the range error at the edge of the fit. The aLS filter with no delay performs significantly worse than that with a delay. Somewhat surprisingly the fTOA filter with $L_{fTOA} = 10$ seconds performs well at high fractional hearability with or without delay. The ieKF performed well over the hearability range though not as well as the fTOA. The ieKF was generally better than the aLS without delay.

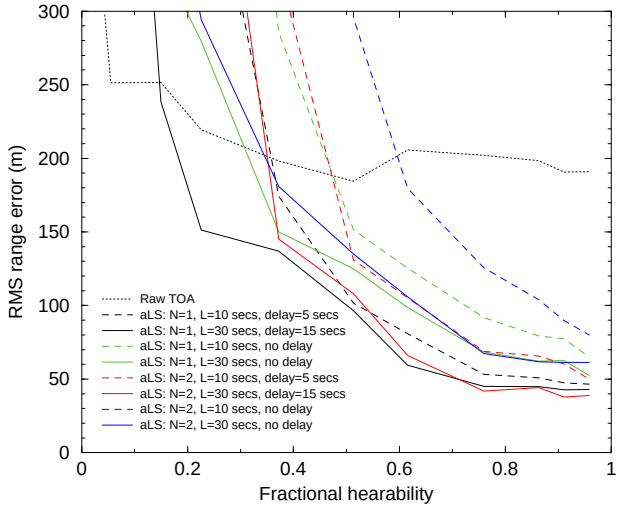

(a)

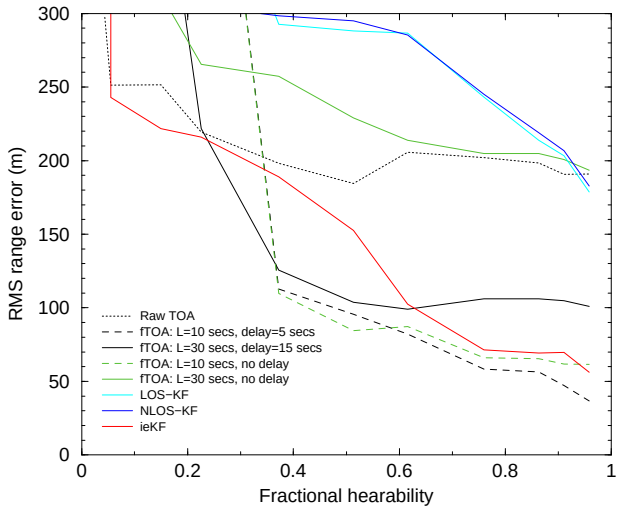

(b)

Figure 5.19: RMS range errors with (a) aLS, (b) fTOA, ieKF, LOS–KF, NLOS–KF filters in the urban 50kmph scenario

Figures 5.20(a), (b) show the results for the 5kmph scenario. This time the fTOA performs the best across a wide range of fractional hearability. The fTOA without delay performs a little worse than the fTOA with delay. The RMS range error can be reduced from 180m to 60m.

To conclude, for the fast moving scenario the aLS fit with delay gives the best error performance. However the ieKF is marginally better than the aLS fit without delay. It should also be noted that the ieKF performance is pessimistic since the velocity driving noise was set deliberately high so the ieKF would not lose track at the instantaneous manoeuvre points. At lower

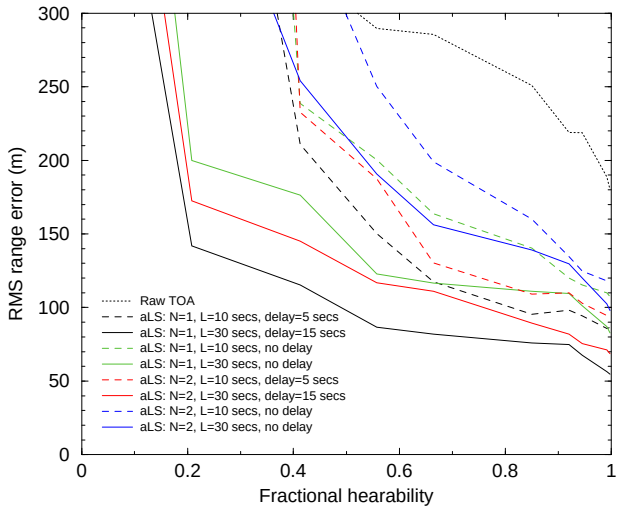

(a)

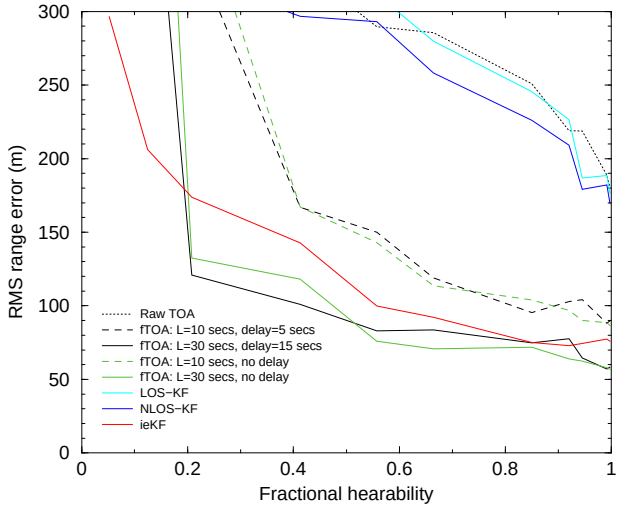

(b)

Figure 5.20: RMS range errors with (a) aLS, (b) fTOA, ieKF, LOS–KF, NLOS–KF filters in the urban 5kmph scenario

speeds the fTOA filter with $L_{fTOA} = 30$ seconds performs the best. Generally speaking the RMS range error of real time range estimates can be reduced by about 67%. In the following work the real time location accuracy improvement possible by utilising the ieKF and fTOA filter is assessed.

5.3 Location Estimator Architecture Utilising Spatial Diversity

In Section 5.1 the location estimate was based on measurements over a very short period of time. In this case there was no spatial diversity experienced (since the MS was approximately stationary) and it is impossible to estimate whether measured data is good data or heavily corrupted by NLOS errors. In Figure 1.1 a generalised architecture was introduced and in Section 5.2 suitable preprocessors to exploit spatial diversity in TOA measurements have been examined.

Figure 5.21 shows the proposed location estimator architecture. The measured TOA data streams, $\tau_{1..N}$, for each of N BS's, including corrupting noise, are each fed into a KF which estimates the true uncorrupted TOA, $\hat{\tau}_{1..N}$, and provides the estimated variance of $\hat{\tau}_{1..N}$, $\hat{\sigma}^2_{\tau 1..N}$. Note that $\hat{\tau}_{1..N}$ are relative to an arbitrary time (possibly the start of the idle period) and do not reflect the true MS–BS separation.

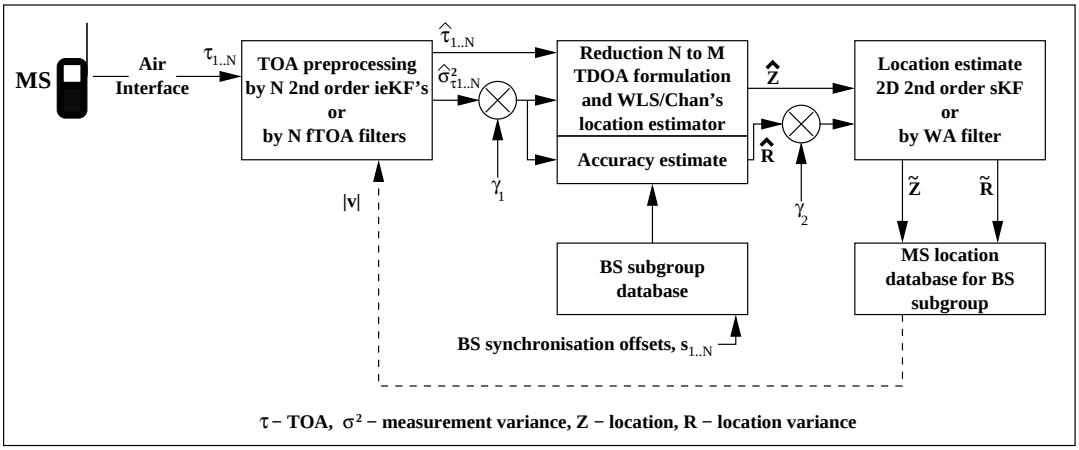

Figure 5.21: TDOA location estimator receiver architecture with spatial filtering, R3

The set of N TOA estimates is reduced to M by considering the variance estimates. The reduced data set is then converted to TDOA's (incorporating any measured synchronisation offsets between BS's) and fed into the location estimator. The location estimator determines the covariance matrix, $\hat{\mathbf{R}}$, for the location estimate, $\hat{\mathbf{Z}}$, which is the estimated accuracy of $\hat{\mathbf{Z}}$ with the given input variances $\hat{\sigma}^2_{\tau 1..M}$. The outputs $\hat{\mathbf{Z}}$ and $\hat{\mathbf{R}}$ are fed into one last KF to give the final time continuous location estimate, $\tilde{\mathbf{Z}}$, and estimated RMS error, $\tilde{R}_{RMS}$. γ_1 and γ_2 are multiplicative terms applied to the variance estimates. Feedback of the smoothed velocity estimator is required to optimally set some of the parameters.

The KF implementation is good at picking up the dynamics of a moving MS. However if the

MS is moving slowly in an NLLOS environment the KF implementation fails to pick up the MS motion. In this case the preferred approach is to use long term smoothing which is achieved by the fTOA prefiltering algorithm and a weighted average (WA) location smoothing algorithm instead of the KF stages. In the following subsections the implementation is discussed in more detail.

In the following the ieKF–KF implementation of receiver R3 is called receiver R3A and the fTOA–WA filter implementation is called receiver R3B.

5.3.1 Preprocessor Stage

The ieKF (tracking to first derivative) with early biasing is used except for the low speed NLLOS scenario in which case the fTOA filter is used. The output variance estimates are, for the case of the KF implementation, taken from $\mathbf{S}_{n,n}$. Studying the deviation of estimates $\hat{\tau}_{1..N}$ from the true LOS $\tau_{1..N}$ revealed that the estimated $\hat{\sigma}^2_{\tau 1..N}$ is lower than the true variance. Thus a multiplicative term, γ_1 is applied. Since it is a multiplicative term it does not affect the location estimator so could be combined with γ_2 (discussed later).

5.3.2 Dataset Reduction

Ideally only LOS data would be used in the estimator. Thus a LOS state estimator was initially proposed. Borras *et al* [75] present several LOS state estimators based on timing measurement. However, where no *a priori* knowledge of the LOS and NLOS processes is available, the optimum detector is simply a LOS variance decision threshold. According to the LOS/NLOS model the CLOS/NCLOS state will be undetectable to the LOS state estimator since the CLOS/NCLOS state is a slowly varying effect. Thus the LOS estimation techniques in [75] could only be expected to detect the LLOS/NLLOS state. From the PDF's in Figures 5.4(c), 5.5(c) the LLOS variance could be calculated and a suitable threshold determined. This threshold could be applied to the preprocessor TOA variance estimates $\hat{\sigma}^2_{\tau 1..N}$ and NLLOS measurements could then be discarded.

The problem with such a method is simply that sufficient LLOS measurements may not be available. By test simulations the most reliable method was to pass all measurements whose variances fell within 100 times the lowest variance estimate since the variances can be accounted for in the location estimator as weightings. When less than 3 such measurements exist the

measurements with the lowest three variances are passed on. This upper threshold on variances is required since all the variances are estimates which tend to become less accurate with increasing variance.

5.3.3 Location and Location Variance Estimator

A variance estimate for the input TDOA streams now exists (from the preprocessing stage). The variance estimates for each TD are composed of the measurement and NLOS noise processes for both BS's as well as the manoeuvring uncertainty noise. These may not be Gaussian in distribution, but since the true distribution are not known it is reasonable to make the Gaussian assumption without much loss in performance. This also makes the ML estimator solvable by algebraic methods whereas a ML estimator fitted to a non–Gaussian distribution perhaps may only be solved numerically. Chan's estimator [29] can now be used with a weighting matrix ω_τ. ω_τ^{-1} can be created as

$$\omega_\tau^{-1} = \begin{cases} c^2(\hat{\sigma}_{\tau 1}^2(n) + \hat{\sigma}_{\tau j}^2(n)) & i = j, \\ c^2\hat{\sigma}_{\tau 1}^2(n) & i = 1 || j = 1, \\ 0 & \text{otherwise} \end{cases} \tag{5.12}$$

Note that $\hat{\mathbf{Q}}_\tau = \omega_\tau^{-1}$.

The estimated accuracy of the location estimate $\hat{\mathbf{Z}}$ is determined by evaluating its covariance matrix, $\hat{\mathbf{R}}$, which for Chan's estimator is given by (2.37)

In the case where the solution is precisely determined, i.e. two TD's, the Cramér Rao lower bound (CRLB) is used as an estimate of $\hat{\mathbf{R}}$. The CRLB, Φ^0, for the TDOA estimator can be derived as

$$\Phi^o = (\mathbf{G}^T\hat{\mathbf{Q}}_\tau^{-1}\mathbf{G})^{-1} \tag{5.13}$$

where

$$\mathbf{G} = \begin{bmatrix} \frac{(x_1-x)}{r_1} - \frac{(x_2-x)}{r_2} & \frac{(y_1-y)}{r_1} - \frac{(y_2-x)}{y_2} \\ .. & .. \\ \frac{(x_1-x)}{r_1} - \frac{(x_N-x)}{r_N} & \frac{(y_1-y)}{r_1} - \frac{(y_N-x)}{y_N} \end{bmatrix}$$

The derivation is shown in Appendix A.

Simulation shows that trace$\{\hat{\mathbf{R}}\}$ is often smaller than the true mean squared error. The variance calculation assumes no bias in the measured TD's. Clearly the prefilters can never correct perfectly the NLOS bias, thus a multiplicative factor, γ_2, is applied to $\hat{\mathbf{R}}$ before the final KF tracking stage to give a more realistic error measure.

The variance estimate for a location generated by one TD is set to $(R_C/4)^2$. Where no TD's are used and the serving BS location is used for the location estimate the variance estimate is set to $(R_C/2)^2$. These estimates are deliberately high so locations generated by 2 or more TD's are favoured.

5.3.4 Location Kalman Filter

An orthodox 2D 2nd order KF is used to track the location estimates. Successful use of such a filter specifically for the purpose of locating mobile phones has been reported in [36].

The observation inputs, $\mathbf{Y}$ and $\hat{\mathbf{R}}$, are equated to $\hat{\mathbf{Z}}$ and $\hat{\mathbf{R}}$ (the outputs of the location and variance estimator) respectively. The output $\tilde{\mathbf{Z}}$ is the final location and velocity estimate which could then be stored in an MS location database. The final RMS error confidence, $\tilde{R}_{RMS}$, is given by the square root of the sum of the first two diagonal terms of $\tilde{\mathbf{R}}$ (though in practice this might also be stored as separate x and y direction confidences).

5.3.5 Weighted Average (WA) Location Filter

At low speeds it is impossible to capture the true dynamics of the MS movement. In this case a WA over the last L_{WA} seconds worth of location data is proposed. The WA operation performed can be describe in matrix form

$$\tilde{\mathbf{Z}}(n) = \sum_{j=0}^{L_{WA}I_{freq}-1} \hat{\mathbf{Z}}(n-j)^T \hat{\mathbf{R}}(n-j)^{-1} \sum_{j=0}^{L_{WA}I_{freq}-1} \hat{\mathbf{R}}(n-j)^{-1} \tag{5.14}$$

where n represents the current idle period index.

5.3.6 Location Estimation Accuracy Performance

In this section the location accuracy of the receivers utilising spatial diversity, R3A and R3B, are presented. A UMTS system incorporating vTA-IPDL with $F_{idle} = 8$Hz is simulated (see

Section 4.2.3). Table 5.1 shows the system parameters. The LOS/NLOS model of Section 3.3 is implemented. All simulations use the partial CLOS model (see Table 3.1) and the dual slope path loss model of (3.11).

Four scenarios were simulated: fast car in rural terrain (150kmph, curve, 90 seconds), car travelling in suburban terrain (50kmph, zig–zag, 90 seconds), car travelling in urban terrain (50kmph, zig–zag, 90 seconds), and pedestrian walking in urban terrain (5kmph, zig–zag, 90 seconds). Table 3.2 shows the scenario dependent parameters. All the scenarios assume a constant speed, however in each scenario instantaneous direction changes occur. These were provided to prevent the KF from correctly predicting the true path in the case when the MS is initially detected but then lost entirely, which would lead to an underestimate of location errors. However the instantaneous manoeuvres cause all results to be pessimistic since the KF cannot adapt to the manoeuvre with the velocity driving noise limited to a realistic value. The tracks are shown in Figure 5.22. A hexagonal array of 16 BS's for urban and suburban and 7 BS's for rural scenarios is simulated (see Figure 4.7). Ten statistically identical runs at each scenario and each transmit power were made. To allow time for convergence of the filtered track to the true track the location accuracy results are calculated from the last 45 seconds of the filtered track.

The ieKF's bank have identical parameter settings as described in Section 5.2.4. A no delay fTOA filter bank is used with parameters $L_{fTOA} = 30$ seconds and $C_{fTOA} = 0.75$ chips.

For the 2D location KF

$$\Phi = \begin{bmatrix} 1 & 0 & \Delta t & 0 \\ 0 & 1 & 0 & \Delta t \\ 0 & 0 & 1 & 0 \\ 0 & 0 & 0 & 1 \end{bmatrix}, \mathbf{K} = \begin{bmatrix} 1 & 0 & 0 & 0 \\ 0 & 1 & 0 & 0 \end{bmatrix},$$

$$\mathbf{S}_{0,0} = \begin{bmatrix} \hat{\mathbf{R}} & \mathbf{0} \\ \mathbf{0} & 15^2\mathbf{I} \end{bmatrix}$$

For the WA location filter $L_{WA} = 30$ seconds.

Optimum values for γ_1 and γ_2 were determined by simulation to match the variance estimates to the true RMS errors observed at the filter and location estimator output. Table 5.2 shows the parameter values used. In the rural scenario choice of γ_2 is not critical.

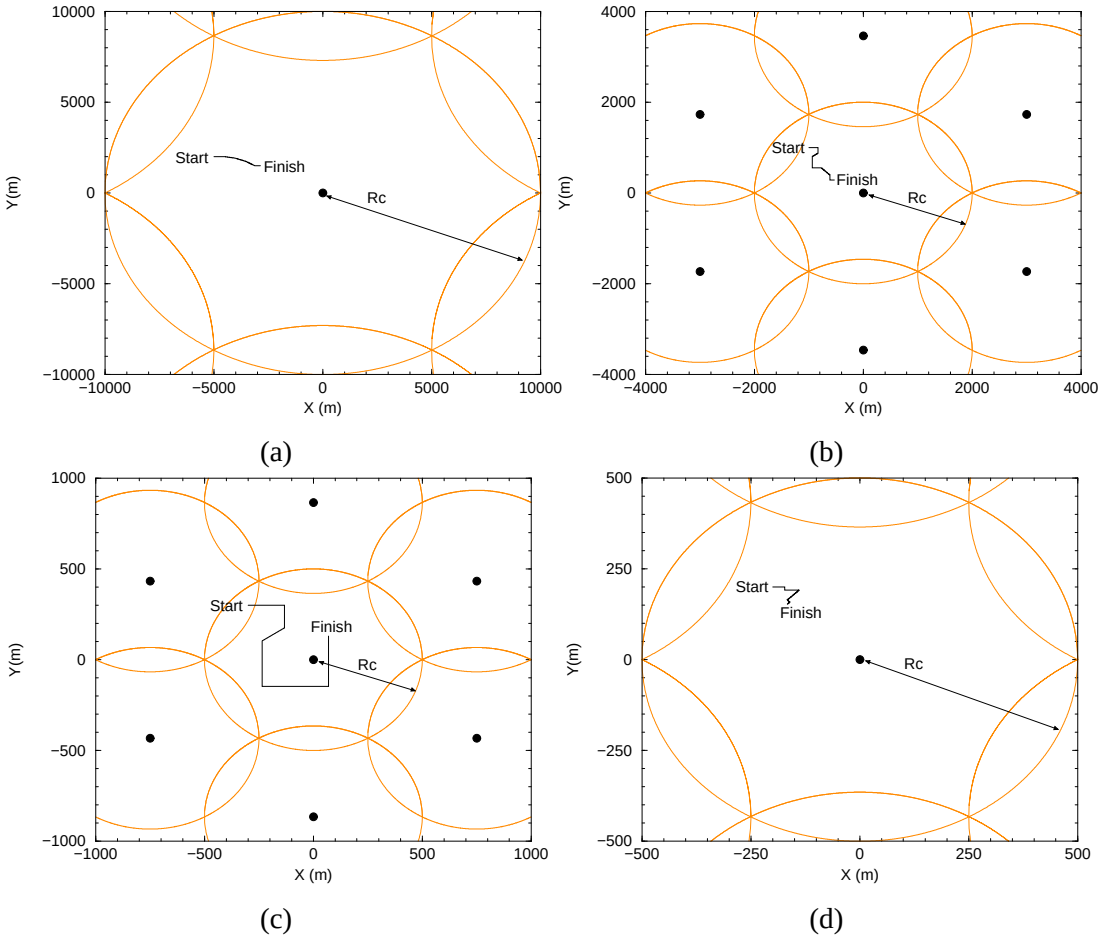

Figure 5.22: MS paths in simulation for (a) rural, (b) suburban, (c) urban car, (d) urban pedestrian scenarios

Scenario	γ_1	γ_2
Rural	1	1–16
Suburban	1	16
Urban car	4	25
Urban ped	4	40

Table 5.2: Values for variance correction factors

Figures 5.23(a), (b), (c), (d) show example tracks for the rural, suburban, urban car and urban pedestrian scenarios respectively for receiver R3A. Although the time scale is not discernible the figures demonstrate the improvement possible utilising the ieKF for prefiltering. In the Figures 5.23(a), (b), (c) the effect of the instantaneous manoeuvres can be seen on the final KF output. The KF output tends to overshoot the corners and for this reason the location accuracy results may be pessimistic. Note also the initial acquisition of the path can take several seconds. In the urban pedestrian track (Figure 5.23(d)) the track filtering process is not able to pick

out the true MS path. Furthermore since the KF allows rather large acceleration capabilities to accommodate the acceleration of a car the KF output oscillates as the individual location estimates jump around due to NLOS errors. In Figure 5.24 the response of the fTOA prefilter and WA location filter is shown. Again the track fails to pick out the true motion of the MS but does give a more reasonable estimate of it compared to the KF implementation.

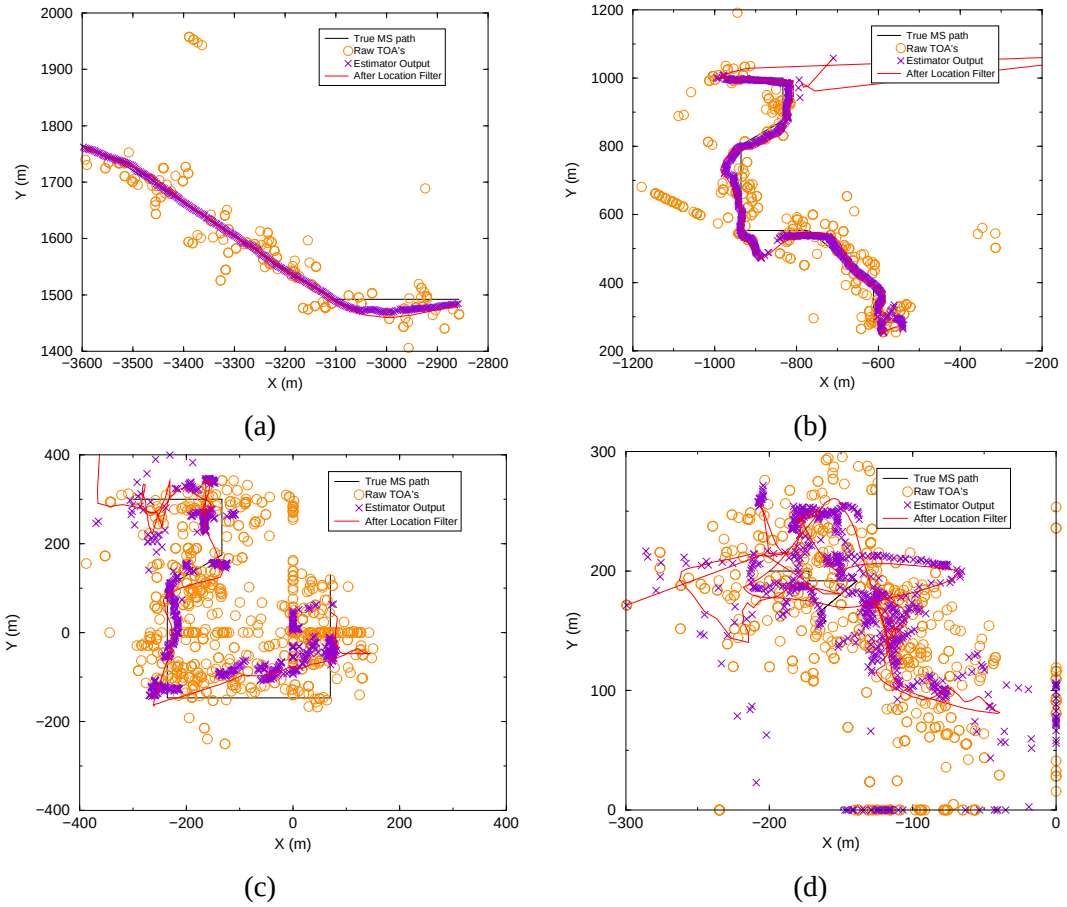

Figure 5.23: Example tracks using receiver R3A in the (a) rural, (b) suburban, (c) urban car, (d) urban pedestrian scenarios

The transmit power of the BS's is varied such that the mean received LOS SNR from the serving BS by an MS at the serving cell boundary (corner of hexagonal cell) varies in steps of 3dB from -18dB to 12dB. In this way hearability is varied. The hearability value is used in the results graphs as it is approximately independent of IPDL technique, thus the results are valid for all IPDL methods discussed. Figures 5.25(a), (b), (c), (d) show $E_{c\acute{e}}^{67}$ and $E_{c\acute{e}}^{95}$ against mean hearability in the rural, suburban, urban car and urban pedestrian scenarios respectively utilising receiver R3A. The location accuracy of the final output of receiver R3A, $\tilde{\mathbf{Z}}$, and the

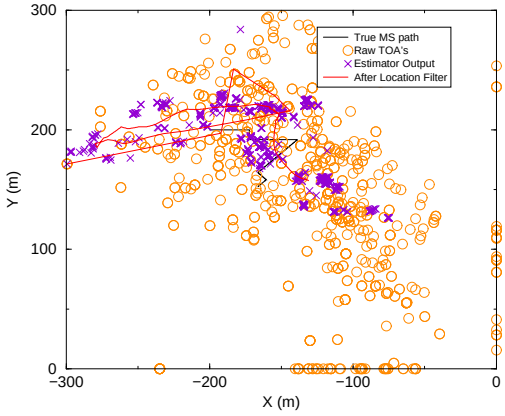

Figure 5.24: Example track using receiver R3B in the urban pedestrian scenarios

location estimator output, $\hat{\mathbf{Z}}$, are shown. For comparison the performance if no spatial filtering were carried out on the data, i.e. receiver R2, is shown. This location estimate is based on the measurements taken in a one second interval (which in the urban car scenario does give some spatial diversity). (These results are not the same as in Section 5.1.6 since the MS path does not cover the whole area of the cell.) Each point on the graphs represents a 3dB increase in pilot SNR.

In the rural scenario the location accuracy improves significantly with spatial filtering from $E_{ce}^{67} = 30$m to $E_{ce}^{67} < 10$m and $E_{ce}^{95} = 50$m to $E_{ce}^{95} = 20$m. Additionally utilising the spatial filtering allows good performance at low instantaneous hearability (<3 BS's) since data can be extrapolated from previous measurements. Increasing the hearability beyond 4 BS's per second did not improve the location accuracy since all BS's are LLOS. In the suburban scenario the improvement is more dramatic since the spatial diversity is used to discriminate NLLOS BS's. Location accuracy of $E_{ce}^{67} = 20$m and $E_{ce}^{95} = 50$m is achieved. Increasing the hearability beyond 3 BS's per second did not improve the location accuracy greatly. In both these scenarios the performance of $\tilde{\mathbf{Z}}$ is worse than $\hat{\mathbf{Z}}$. This is simply a manifestation of the instantaneous manoeuvres and in a more realistic track $\tilde{\mathbf{Z}}$ would have better accuracy than $\hat{\mathbf{Z}}$. In the urban car scenario location accuracy of $E_{ce}^{67} = 45$m and $E_{ce}^{95} = 80$m is achieved, compared to $E_{ce}^{67} = 60$m and $E_{ce}^{95} = 120$m without filtering. This improvement is not great but critically brings performance below the FCC regulations. Again the accuracy of $\tilde{\mathbf{Z}}$ is pessimistic due to the instantaneous manoeuvres. Location accuracy increases slowly with increasing hearability. The performance in the urban pedestrian scenario is not as good as the urban car scenario since less spatial diversity is available. The location accuracy is still below FCC requirements.

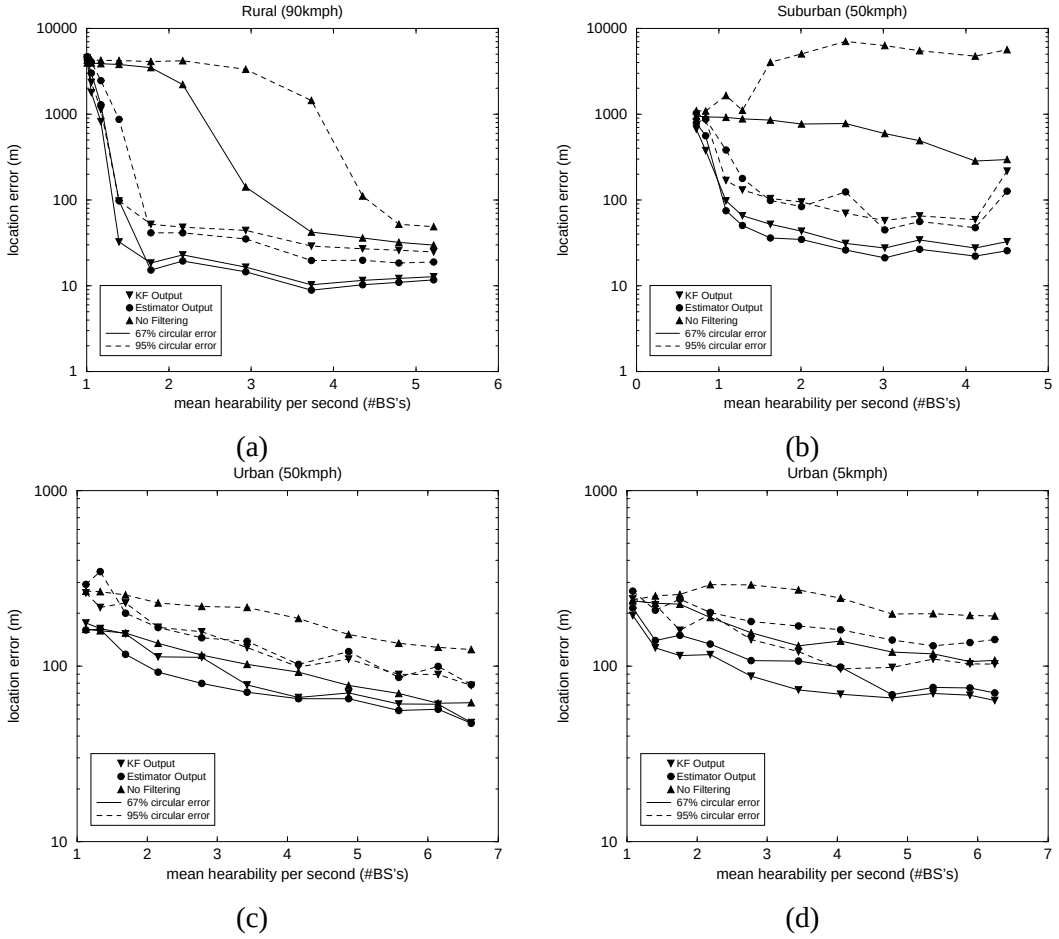

Figure 5.25: Location error against hearability using receiver R3A in the (a) rural, (b) suburban, (c) urban car, (d) urban pedestrian scenarios

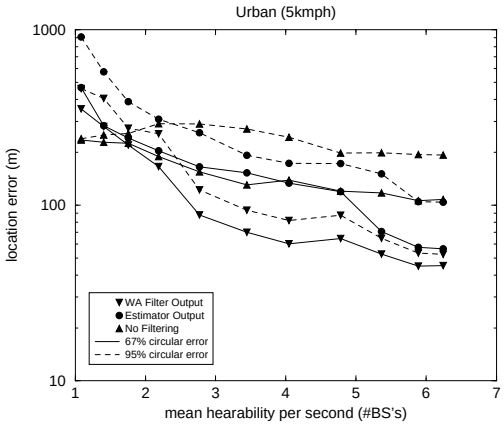

Figure 5.26: Location error against hearability using receiver R3B in the urban pedestrian scenario

In Figure 5.26 the location accuracy is shown for the urban pedestrian scenario using receiver R3B. At high hearability this receiver outperforms R3A. The best achieved location accuracy is $E_{ce}^{67} = 45$m and $E_{ce}^{95} = 53$m. This accuracy appears slightly better than can be achieved in the urban car scenario with receiver R3A, however it should be noted that the instantaneous manoeuvres will not worsen these results as they do in the urban car scenario.

Figures 5.27 (a), (b), (c) show the effect of varying P_{LLOS} in the suburban, urban car and urban pedestrian scenarios respectively for mid–level hearability (3–4BS's) with receiver R3A. In the suburban scenario performance stays constant down to $P_{LLOS} = 0.7$ since NLLOS BS's are rejected successfully. In the urban car scenario E_{ce}^{67} improves by about 25% between $P_{LLOS} = 0.2$ and $P_{LLOS} = 1.0$. In the urban pedestrian scenario the accuracy increase is about 50% over the same P_{LLOS} change.

Figure 5.28 shows the effect of varying P_{LLOS} with receiver R3B. At $P_{LLOS} = 1.0$ the performance is no longer better than receiver R3A in the same scenario.

The performance of the spatial filtering depends on the spatial correlation of the LLOS, CLOS and multipath surroundings. The parameters L_{LLOS}, L_{CLOS} and L_s and L_{dcorr} define the degree of spatial correlation. A geometry multiplier, K_g, is applied to the base values of these parameters (shown in Tables 5.1, 3.1, 3.2) to examine the effect on the performance of the receivers. In the case of receiver R3B this is identical to slowing down the MS by a factor K_g, but not for receiver R3A due to the velocity driving noise term. Figures 5.29(a), (b), (c) show the location accuracy against K_g for the rural, suburban and urban car scenarios respectively with receiver R3A at a medium hearability level (3-4 BS's).

The location accuracy in suburban and urban car scenarios deteriorates with increasing K_g. The effect is greatest in the suburban scenario since there are few multipaths. The NLLOS states last for longer and any multipath detected will last for longer, thus resembling an LLOS state. Therefore the NLLOS rejection (via the variance estimation) breaks down. In the urban scenario there are more multipaths present so, even though the geometry factor increases, multipaths still appear and disappear with regularity giving some spatial diversity. In the rural scenario location accuracy is fairly constant. L_{CLOS} and L_{dcorr} have little effect on location accuracy. Figure 5.30 shows the results for the urban pedestrian scenario with receiver R3B at a high hearability level (6 BS's). The performance tails off quicker in this scenario since the MS experiences no spatial diversity during L_{fTOA} seconds. The problem is experienced identically

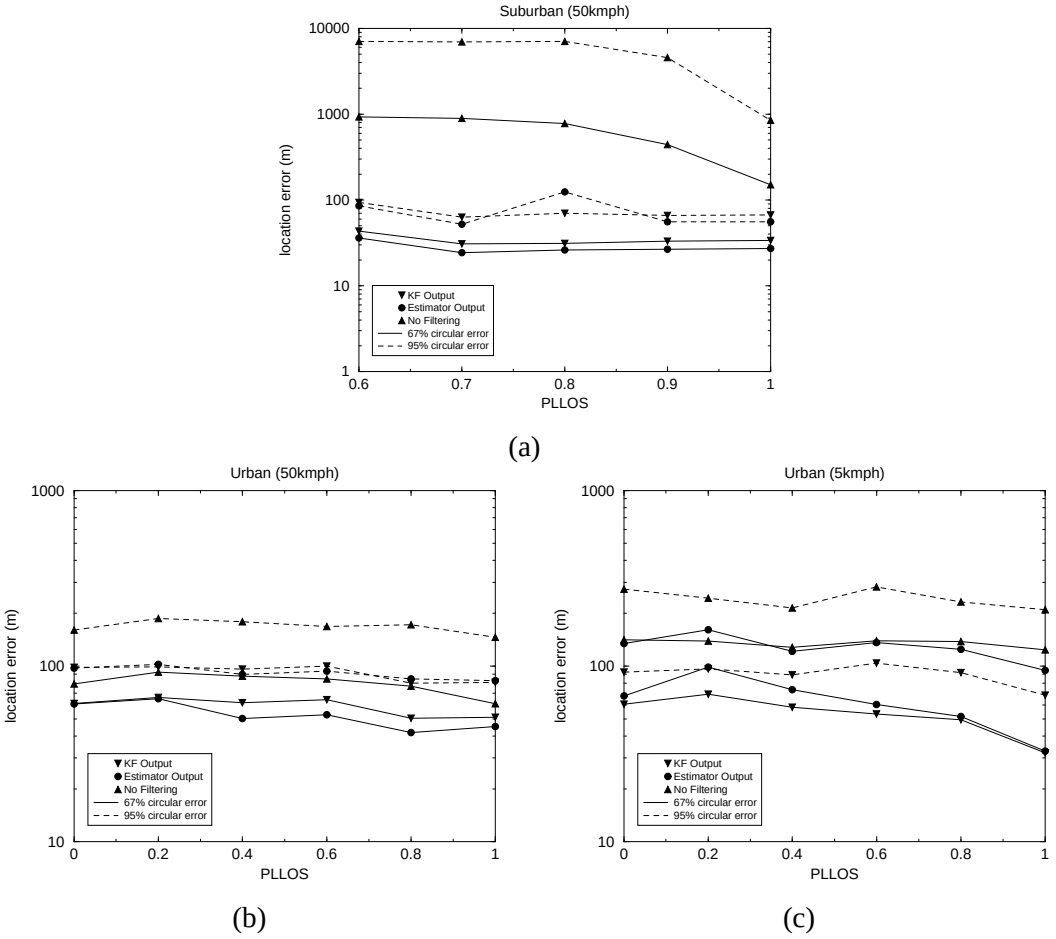

Figure 5.27: Location error against P_{LLOS} using receiver R3A in the (a) suburban, (b) urban car, (c) urban pedestrian scenarios

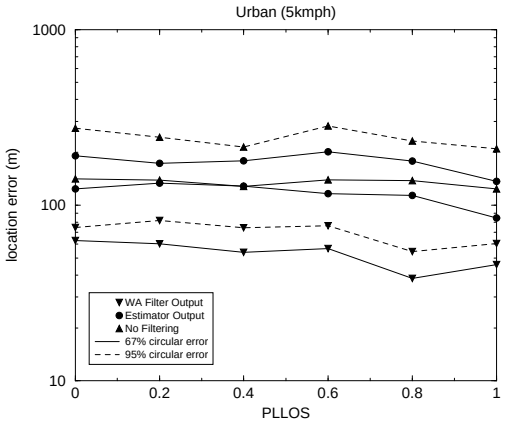

Figure 5.28: Location error against P_{LLOS} using receiver R3B in the urban pedestrian scenario

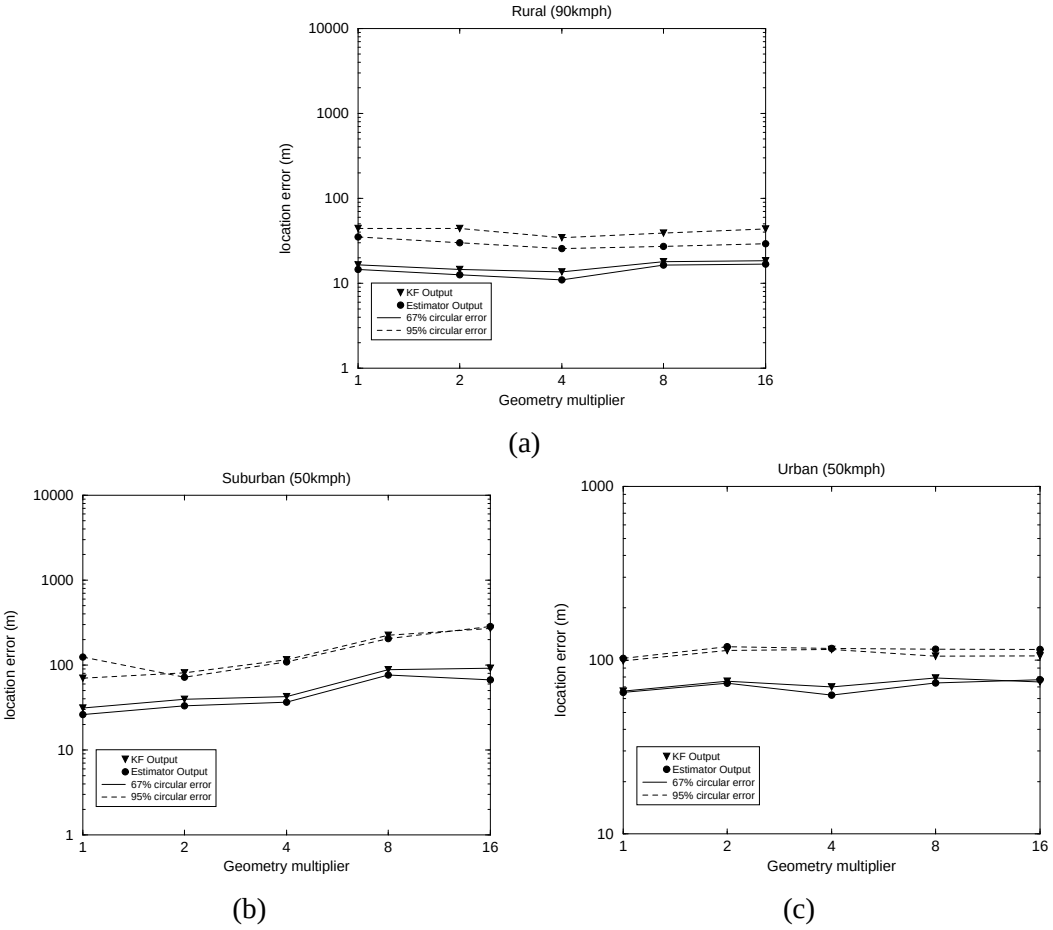

Figure 5.29: Location error against K_g using receiver R3A in the (a) rural, (b) suburban, (c) urban car scenarios

in slow moving MS's. In Section 5.3.8 a method to overcome this is described.

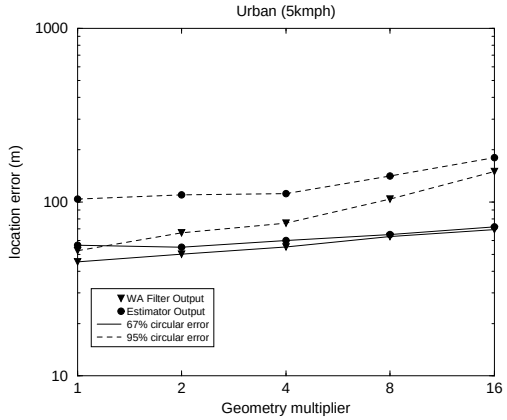

Figure 5.30: Location error against K_g using receiver R3B in the urban pedestrian scenario

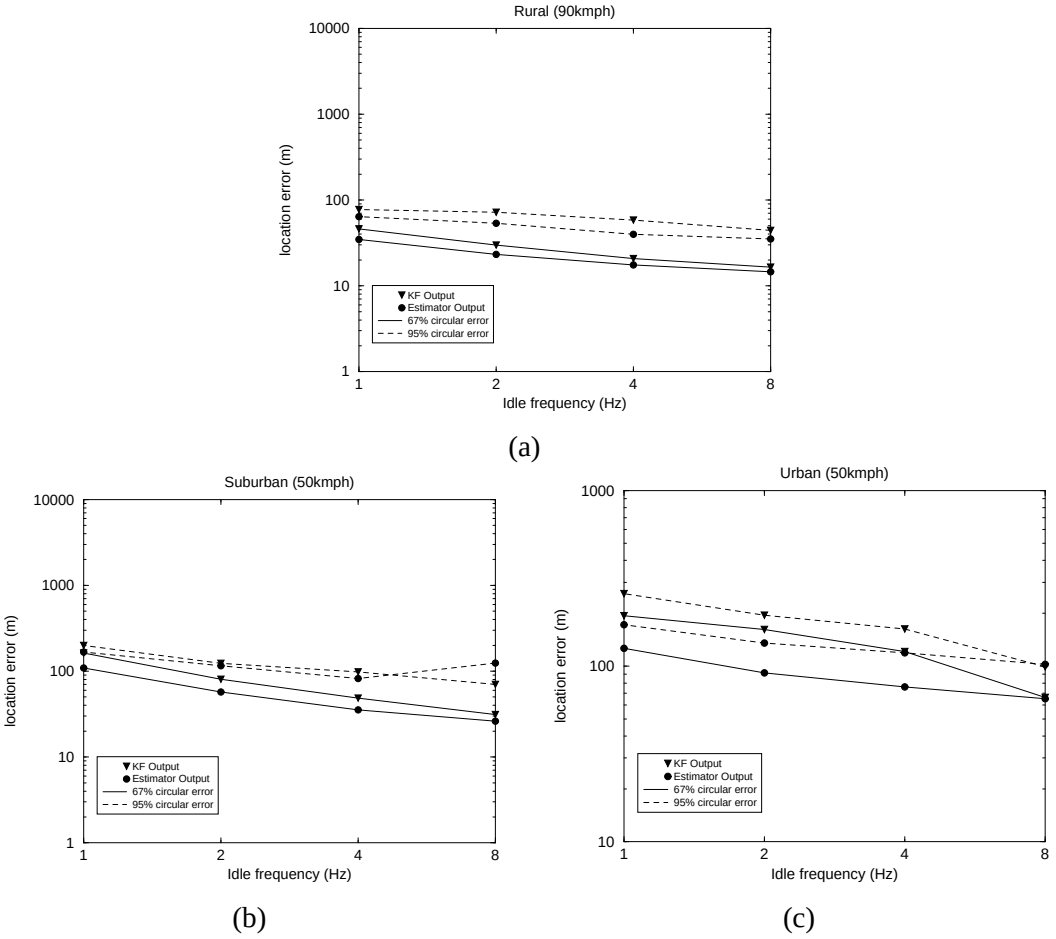

Figure 5.31: Location error against F_{idle} using receiver R3A in the (a) rural, (b) suburban, (c) urban car scenarios

Figures 5.31 (a), (b), (c) show the effect of varying F_{idle} in the rural, suburban, and urban car scenarios respectively for a medium hearability level (3–4 BS's) with receiver R3A. Generally decreasing F_{idle} has a negative effect on the location accuracy, more so in the urban and suburban scenarios where NLLOS situations can occur. The main effect of decreasing the idle frequency is that track acquisition takes significantly longer. Furthermore, after the cornering points (especially in the urban car scenario), re–acquisition of the track takes longer. This is the reason why the accuracy of $\tilde{\mathbf{Z}}$ appears especially poor. Figure 5.32 shows the effect for receiver R3B in the urban pedestrian scenario at high hearability (6 BS's).

To summarise using receiver R3A in fast moving environments improves E_{ce}^{67} and E_{ce}^{95} significantly. Furthermore it allows the hearability level to drop below 3 BS's by extrapolating old data. In the pedestrian scenario receiver R3B gives significantly better location accuracy than receiver

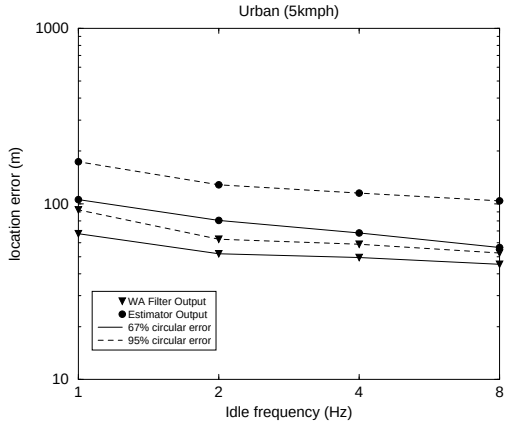

Figure 5.32: Location error against F_{idle} using receiver R3B in the urban pedestrian scenario

R3A when the hearability level is high. However if P_{LLOS} is high receiver R3A gives better accuracy than receiver R3B for all speeds. The LLOS geometry parameters have a significant effect on the performance. However with $K_g < 4$ the location accuracy is still a significant improvement over receiver R2. Reducing F_{idle} diminishes location accuracy though less so with receiver R3B. Table 5.3 summarises the location accuracy gain of receiver R3A/R3B over receiver R2 at a high hearability level.

		R3A	R3B	R2	% improvement
Rural	E_{ce}^{67}	10		33	70
	E_{ce}^{95}	20		$>$250	$>$92
Suburban	E_{ce}^{67}	20		200	90
	E_{ce}^{95}	40		$>$250	$>$84
Urban Car	E_{ce}^{67}	45		65	30
	E_{ce}^{95}	75		130	42
Urban Pedestrian	E_{ce}^{67}		45	65	30
	E_{ce}^{95}		55	130	58

Table 5.3: Summary of location accuracy improvement of receiver R3A/B over receiver R2

5.3.7 Velocity Feedback

Speed feedback is required to set γ_1 and γ_2 and switch between receiver R3A and receiver R3B in a real scenario. Figure 5.33 shows an example of the magnitude of the velocity component of $\tilde{\mathbf{Z}}$ for all scenarios. The dashed lines show a 10 second smoothed average. Note that the true speeds 90kmph, 50kmph and 5kmph correspond to 25ms^{-1}, 14.7ms^{-1} and 1.47ms^{-1}

respectively. At faster speeds the speed estimate is more accurate especially with smoothing. The urban pedestrian speed is over estimated. Both receivers could be implemented in parallel and a speed threshold around 7ms^{-1} could be used to decide which receiver to take the current location estimate from.

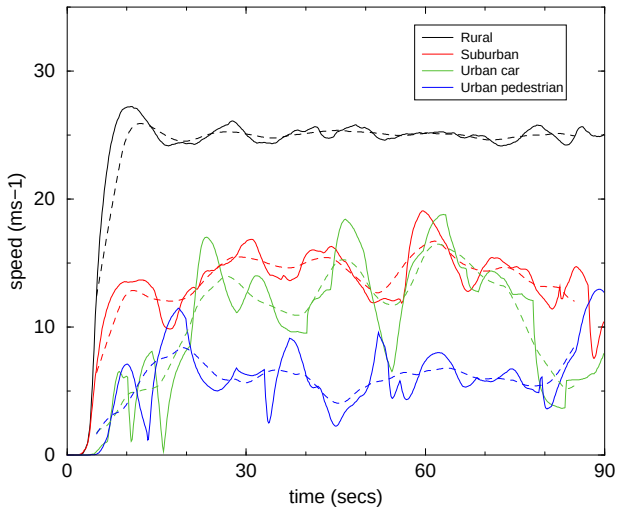

Figure 5.33: Examples of speed estimates in all scenarios

5.3.8 Stationary MS Problem

Naturally if the MS is stationary little or no spatial diversity will be experienced. In this case the location estimates of either receiver would converge in time to a location with the same accuracy as receiver R2. This is undesirable since the performance of this receiver is below the FCC regulations in urban and suburban scenarios.

Once receiver R3A has converged the smoothed speed estimate will drop very close to zero. This can trigger a further speed threshold which can then hold a previous location estimate as the current estimate (conveniently the last L_{WA} location estimates are stored in receiver R3B). Updated location estimates would not occur again till the speed threshold is once more exceeded (possibly with hysteresis).

5.3.9 Further Modifications to KF Implementation

In Section 2.10.1 several KF implementations with manoeuvre tracking or detection were introduced. These provide greater track stability in the case when manoeuvres are known to occur

infrequently and with spatial correlation, i.e. typically in manned manoeuvring objects. In this case the MS can be considered a manned manoeuvring object. The manoeuvre detectors utilise the residual between measured and predicted parameters to detect the start of a manoeuvre. Before the manoeuvre a constant velocity filter is employed. At the manoeuvre detection point the velocity driving noise is increased, thus allowing the manoeuvre to take place. After several seconds the velocity driving noise is reset to zero and the filter reverts to constant velocity.

Unfortunately NLLOS errors have precisely the same characteristics as a manoeuvre in that they cause long term bias in the tracked parameter, thus triggering the manoeuvre detector. The KF implementations were not found to be suitable for the sort of TOA noise or location estimate noise present in the system.

Since the manoeuvre detection strategies do not work another method is proposed. The velocity of the MS is known from the KF with a certain uncertainty. Since the manoeuvring capabilities of the MS are approximately known as a function of speed, a velocity based manoeuvre inhibition (VMI) technique is proposed.

Figure 5.34 shows a possible surface defining the acceleration capability of an MS. V is the ratio of current speed to maximum speed, V_{max}, and u_x^2 and u_y^2 represent the velocity driving noise power σ_u^2 in the direction of motion and perpendicular to motion respectively (in the figure these are normalised to σ_u^2). At low speeds a manoeuvre can take place in any direction with equal maximum power. At speeds greater than V_2 sideways manoeuvres are inhibited. At speeds greater than V_1 forward acceleration is also reduced and a deceleration bias, μ_u, exists.

For the example surface u_x, u_y and μ_u are defined as

$$\mu_u = -\frac{\Delta t \sigma_u}{2}\left(\frac{V+1-V_1}{2-V_1}\right)^{S_1} \tag{5.15}$$

$$u_x^2 = \Delta t^2 \sigma_u^2 (1 - \frac{1}{2}\left(\frac{V+1-V_1}{2-V_1}\right)^{S_1})^2 \tag{5.16}$$

$$u_y^2 = \Delta t^2 \sigma_u^2 \left[\frac{1-(1-u_{min})\left(-V_2^{\frac{1}{S_3}} - (V-V_2)^{\frac{1}{S_3}}\right)}{\left(-V_2^{\frac{1}{S_3}} - (1-V_2)^{\frac{1}{S_3}}\right)}\right]^2 \tag{5.17}$$

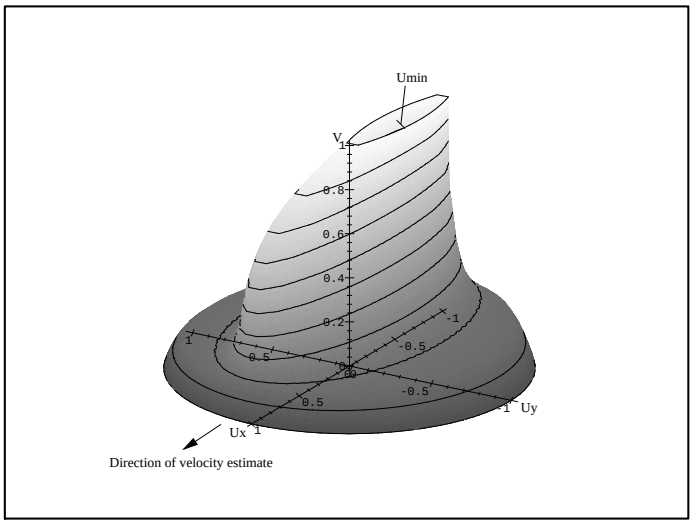

Figure 5.34: Acceleration capability of MS as a function of speed

where $S_1 = 10$, $S_2 = 4$, $S_3 = 3$ control the slope of the surface with these values for the example shown and u^2_{min} is the minimum sideways velocity driving noise expressed as a fraction of σ^u.

To apply VMI to the KF the coordinate space must be rotated in the direction of the velocity estimate for each measurement. $\theta_{n,0}$ represents the rotation from the normal (x,y) coordinate axes at sample n. The following extra steps at the start of the KF procedure described in Section 2.10 are required.

$$\theta_{n,n-1} = \tan^{-1}\left(\frac{x_{3/1}}{x_{4/1}}\right) \tag{5.18}$$

where $x_{a/b}$ represents the ath row, bth column entry in $\hat{\mathbf{X}}_{n-1,n-1}$.

$$\theta_{n,0} = \theta_{n-1,0} + \theta_{n,n-1} \tag{5.19}$$

Y_n, $\hat{\mathbf{X}}_{n-1,n-1}$, $\mathbf{R}_n$, $\hat{\mathbf{S}}_{n-1,n-1}$ must all be rotated. The transformation of the coordinate axes in Y_n, $\hat{\mathbf{X}}_{n-1,n-1}$ is achieved by

$$\mathbf{Y}_n = \mathbf{T}_1\mathbf{Y}_n \tag{5.20}$$

where

$$\mathbf{T}_1 = \begin{bmatrix} \cos\theta_{n,0} & -\sin\theta_{n,0} \\ \sin\theta_{n,0} & \cos\theta_{n,0} \end{bmatrix}$$

and

$$\hat{\mathbf{X}}_{n-1,n-1} = \mathbf{T}_2 \hat{\mathbf{X}}_{n-1,n-1} \tag{5.21}$$

where

$$\mathbf{T}_2 = \begin{bmatrix} \cos\theta_{n,n-1} & -\sin\theta_{n,n-1} & 0 & 0 \\ \sin\theta_{n,n-1} & \cos\theta_{n,n-1} & 0 & 0 \\ 0 & 0 & \cos\theta_{n,n-1} & -\sin\theta_{n,n-1} \\ 0 & 0 & \sin\theta_{n,n-1} & \cos\theta_{n,n-1} \end{bmatrix}$$

If errors are assumed Gaussian in 2D, the transformation is a linear combination of two Gaussian processes, thus the covariance matrices $\mathbf{R}_n$, $\hat{\mathbf{S}}_{n-1,n-1}$ can be rotated by applying

$$\mathbf{R}_n = \mathbf{T}_1 \mathbf{R}_n \mathbf{T}_1^T \tag{5.22}$$

and

$$\hat{\mathbf{S}}_{n-1,n-1} = \mathbf{T}_2 \hat{\mathbf{S}}_{n-1,n-1} \mathbf{T}_2^T \tag{5.23}$$

The noise covariance matrix is then updated to

$$\mathbf{Q}_u = \begin{bmatrix} 0 & 0 & 0 & 0 \\ 0 & 0 & 0 & 0 \\ 0 & 0 & u_x^2 & 0 \\ 0 & 0 & 0 & u_y^2 \end{bmatrix} \tag{5.24}$$

before the normal KF equations are carried out. The predictor equation is adjusted, to take into

account the bias term μ_u, to

$$\hat{\mathbf{X}}_{n,n-1} = \phi\hat{\mathbf{X}}_{n-1,n-1} + \begin{bmatrix} 0 \\ 0 \\ \mu_u \\ 0 \end{bmatrix} \tag{5.25}$$

The final location calculation $\hat{\mathbf{X}}_{n,n}$ and variance estimate $\hat{\mathbf{S}}_{n,n}$ are now defined in a coordinate axes rotated by $\theta_n, 0$. These outputs should therefore be rotated back when required.

The VMI KF was tested on the rural scenario results and yielded a further 12% increase in $E_{c\acute{e}}^{67}$ location accuracy. In this scenario the speed estimate is fairly accurate. In other scenarios the estimate will be less accurate. To avoid overestimating the speed V could be calculated based on a -3 sigma estimate of speed.

5.4 Conclusions and Further Ideas

In this chapter the performance of a TDOA location receiver with and without filtering to exploit spatial diversity has been presented under several scenarios. It has been shown that without filtering in NLOS conditions poor location accuracy results below the FCC regulations. The receivers with filtering showed location accuracy improvement of minimum 30% and 42% at the 67%ile and 95%ile respectively. These improvements are sufficient to reduce the location error below FCC regulations in all cases for the channel model scenarios presented. The filtering process also allows the hearability and hence transmit power to be reduced significantly since previous data can be extrapolated. Spatial filtering at high speed is possible using KF's. At low (pedestrian) speeds averaging techniques work better.

The detection stage of the receiver has also been analysed in detail. Suppression of autocorrelation and pulse shaping noise requires some extra consideration. The solutions presented are straightforward to implement and are robust, however do desensitise the receiver to true peaks. Once these sources of noise have been accounted for MPR can be solved satisfactorily with a simple first peak detection algorithm.

Finally it should be noted that the parameters γ_1 and γ_2 have been matched to the specific scenarios. It is well known that under the Gaussian measurement noise assumption, if the input

measurement noise covariance matrix, $\mathbf{Q}$, is known to a multiplicative constant, this constant (effectively γ_1) can be estimated directly from location estimate $\mathbf{b}_{ML}$ [23]. This method of setting γ_1 needs to be investigated further. A similar method based on the final KF output may also be possible to set γ_2.

Chapter 6
Performance of a AOA/TDOA Hybrid Location Estimator

In this chapter the performance of a hybrid location estimator, utilising TDOA measurements (similar to the previous chapter) and an AOA arrival measurement of the MS signal at the serving BS, is presented. Simulation results are presented which show that location accuracy improvement over the TDOA only system is possible even in highly NLOS conditions. Furthermore location estimation is now possible when only two BS's are detectable, rather than the three BS's required in the TDOA only system, thus reducing the hearability problem.

6.1 Introduction

A TDOA technique has been proposed for providing location services in future UMTS networks. The performance of such a system, evaluated in the previous chapter, is limited by errors in the TD measurements primarily caused by NLOS propagation conditions.

In future systems AOA measurements at the serving BS may be available, primarily as a requirement to increase downlink capacity via beamforming. In this case the MS's AOA will be known at the serving BS (and possibly adjacent BS's if the MS is in a soft handover region). The AOA measurements will be subject to NLOS errors correlated to the errors in the TD's involving the serving BS, but should still be useful to the location estimator.

In this study the AOA is only measured at the serving BS. There are several reasons for this restriction. Firstly and most importantly the AOA at the serving BS will be very useful to the network to allow beamforming and thus improve the cell capacity by lowering the interference power and allowing further multiple access reuse (code reuse in CDMA). Thus the measurement will be 'free' in that no additional processing would be required for the location service. Secondly, as previously discussed, except in the soft handover region the MS will only be detectable at non–serving BS's during idle periods. Thus non–serving BS's have a limited set of

data from which to derive AOA measurements. It could be expected that they would therefore be susceptible to a higher measurement noise. Finally if AOA measurements are taken at other BS's they will have to be transmitted to the location calculation point thus increasing network traffic, whereas in the serving BS only scenario, measurements are made only at the MS and serving BS.

To simplify the simulations in this chapter it is assumed that the serving BS is always detectable and that the AOA of the first arriving path can be measured without interference from the other paths (though Gaussian measurement noise is present). This AOA is used as the estimate of the LOS AOA. Another method would be to use the mean AOA if sufficient scatterers are present in the environment.

In the next section the performance of a hybrid AOA/TDOA receiver which does not exploit spatial diversity, is briefly presented.

6.2 Simple AOA/TDOA Hybrid Location Estimator Architecture

The hybrid receiver, R4, is identical to receiver R2 from the previous chapter except that AOA measurements are introduced to the estimator. The method for measuring the AOA is beyond the scope of this work, but the effect of the AOA measurement error is considered. In the following subsections the new location estimator is described and location accuracy performance evaluated by simulation.

6.2.1 AOA–TDOA Location Estimator

Identically to the previous chapter a TD vector, $\Delta\hat{\tau}(n)$ can be formed from $\hat{\tau}(n)$, defined as

$$\Delta\hat{\tau}(n) = \begin{bmatrix} \hat{\tau}_1(n) - \hat{\tau}_2(n) - s_{1,2} \\ .. \\ \hat{\tau}_1(n) - \hat{\tau}_N(n) - s_{1,N} \end{bmatrix} \tag{6.1}$$

where $s_{i,j}$ represents the measured synchronisation offset between BS$_i$ and BS$_j$.

The most likely MS location, $\hat{\mathbf{Z}}(n)$, can be found from the $N-1$ TD hyperbolae defined by

$$\begin{aligned} r_2 - r_1 &= c\hat{\tau}_{2,1}(n) \\ &.. \\ r_N - r_1 &= c\hat{\tau}_{N,1}(n) \end{aligned} \tag{6.2}$$

where r_i is the distance between the MS at (x_M, y_M) and BS$_i$ at (x_i, y_i); and the AOA such that

$$\tan\alpha_1 = \frac{x - x_1}{y - y_1} \tag{6.3}$$

Again the ML solution derived by Chan [29] is used, see Section 2.3.3. The equations for calculating the location are not affected by the addition of the AOA term. However the matrix definitions in Section 2.3.3 must be adjusted to include the AOA equation to

$$\mathbf{X} = -\begin{bmatrix} x_2 - x_1 & y_2 - y_1 & c\Delta\hat{\tau}_{2,1} \\ .. & .. & .. \\ x_N - x_1 & y_N - y_1 & c\Delta\hat{\tau}_{N,1} \\ -1 & \tan\alpha_1 & 0 \end{bmatrix}, \tag{6.4}$$

$$\mathbf{Y} = \frac{1}{2}\begin{bmatrix} (c\Delta\hat{\tau}_{2,1})^2 + x_1^2 + y_1^2 - x_2^2 - y_2^2 \\ .. \\ (c\Delta\hat{\tau}_{N,1})^2 + x_1^2 + y_1^2 - x_N^2 - y_N^2 \\ 2x_1 - 2y_1\tan\alpha_1 \end{bmatrix} \tag{6.5}$$

A sensible weighting must be applied between the measurements of α_1 and $\tau_{1..N}$ since they are a measure of different parameters, range and angle, in the estimator. The measurement weighting matrix ω is defined

$$\omega^{-1} = \begin{bmatrix} & & & 0 \\ & \omega_\tau^{-1} & & .. \\ & & & 0 \\ 0 & .. & 0 & \sigma_\alpha^2 \end{bmatrix} \tag{6.6}$$

where ω_τ^{-1} is the N by N matrix,

$$\omega_\tau^{-1} = \begin{cases} 2c^2\sigma_\tau^2 & i = j, \\ c^2\sigma_\tau^2 & i = 1 || j = 1, \\ 0 & \text{otherwise} \end{cases} \tag{6.7}$$

Note $||$ represents the exclusive–or operation The variances σ_τ^2 and σ_α^2 must be estimated through some *a priori* knowledge.

In the event of only 2 BS's being detected a unique solution is determined from the intersection of the AOA line and TD hyperbola. This is given by

$$x = \frac{x_1^2 - x_2^2 + (c\Delta\hat{\tau}_{2,1})^2 - (y_2 - y_1)^2 + \frac{2x_1}{\tan\alpha_1}(y_1 - y_2) + 2\Delta\hat{\tau}_{2,1}x_1\sqrt{1 + \frac{1}{(\tan\alpha_1)^2}}}{2\left(x_1 - x_2 + \frac{y_1 - y_2}{\tan\alpha_1} + \Delta\hat{\tau}_{2,1}\sqrt{1 + \frac{1}{(\tan\alpha_1)^2}}\right)} \tag{6.8}$$

$$y = \frac{x - x_1}{\tan\alpha_1} + y_1 \tag{6.9}$$

If only 1 BS is detected the AOA can be used to predict a location at a distance d_{1BS} from the BS.

$$\begin{bmatrix} x \\ y \end{bmatrix} = \begin{bmatrix} x_1 \\ y_1 \end{bmatrix} + d_{1BS}\begin{bmatrix} \sin\alpha_1 \\ \cos\alpha_1 \end{bmatrix} \tag{6.10}$$

6.2.2 Location Estimation Accuracy Performance

The simulation environment is identical to Section 5.1.6. $P_{FA} = 2.6 \cdot 10^{-5}$ for all simulations.

AOA measurements are corrupted by Gaussian measurement noise of varying power, $\sigma_{\alpha LOS}^2$, in addition to any NLOS errors that may be present. In ω^{-1} estimated LOS measurement

variances are used. This is necessary since the AOA and TDOA must be correctly weighted in the estimator. $c^2\sigma_\tau^2 = 100\text{m}^2$ is used. $\sigma_\alpha^2 = \sigma_{\alpha LOS}^2$ is assumed to be known precisely. $d_{1BS} = 50\text{m}$ is used.

Figure 6.1 shows the cumulative probability function for circular location error in the rural scenario for varying AOA measurement noise $\sigma_{\alpha LOS}^2$ with LOS SNR at the cell boundary equal to 0dB. The performance of the TDOA only estimator is also shown.

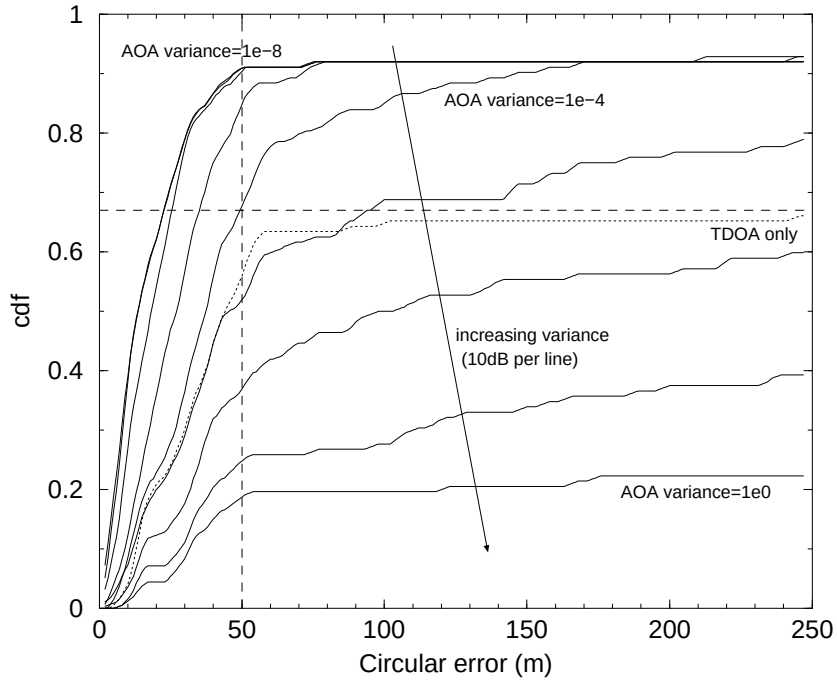

Figure 6.1: CDF of circular location error with varying $\sigma_{\alpha LOS}^2$ in the rural scenario

If $\sigma_{\alpha LOS}^2 < 10^{-3}\text{rad}^2$ a significant location accuracy improvement over the TDOA system is achieved. This can be put down to two factors. When the hearability is below 3 BS's the location can still be calculated precisely and when the hearability is $\geq$3 BS's the location estimator is improved. With $\sigma_{\alpha LOS}^2 > 10^{-3}\text{rad}^2$ the location accuracy becomes significantly worse. In the following simulations $\sigma_{\alpha LOS}^2 = 10^{-5}\text{rad}^2$.

Figures 6.2(a), (b), (c) show the effect on location accuracy of varying the pilot SNR at the cell boundary from -12dB to 12dB for the rural, suburban and urban scenarios respectively. In the rural scenario there is a great improvement over the TDOA only results of the previous chapter. This is due to the possibility of locating the MS precisely with only 2 BS's hearable. At higher SNR's there is a slight improvement in location accuracy. In the suburban scenario again lower SNR's are improved over the TDOA only results due to 2 BS location being

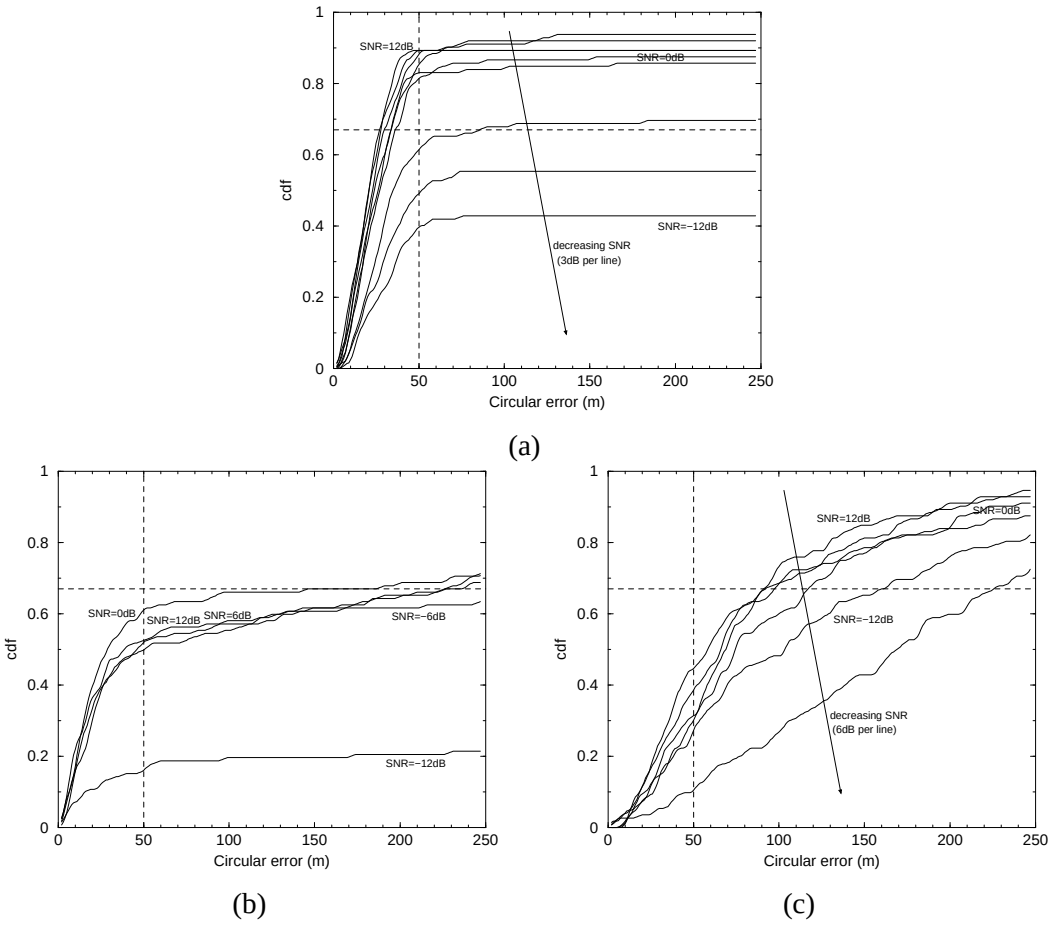

Figure 6.2: CDF of circular location error with varying pilot SNR in the (a) rural, (b) suburban, (c) urban scenarios

possible. However at higher SNR's (and hence higher hearability) there was no improvement since NLLOS corruption of any one TD or AOA will lead to a large location error. The 2 BS location method is then most robust to NLLOS errors and hence the mid SNR=0dB results are better than higher SNR's. The urban scenario shows similar trends. At high SNR's the location accuracy deteriorates compared to the TDOA only results of the previous chapter.

Figures 6.3(a), (b) show the effect on location accuracy of varying P_{LLOS} for the suburban and urban scenarios respectively for a fixed pilot SNR=0dB. These results reaffirm that for high P_{LLOS} values the AOA/TDOA estimator is significantly better than the TDOA only estimator.

The results of this section show AOA measurements could improve location accuracy. However in NLLOS environments or if the AOA measurement noise is high using the AOA measurements can have the opposite effect. Spatial diversity is required to attempt to recreate LLOS

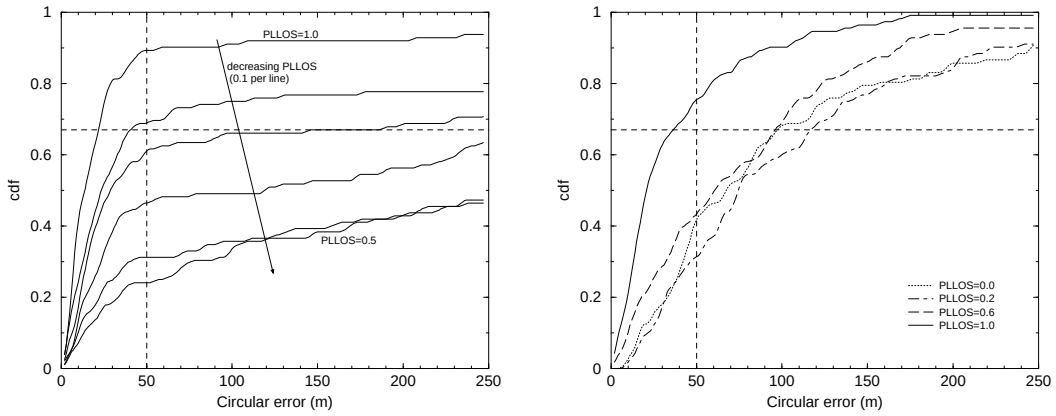

(a) (b)

Figure 6.3: CDF of circular location error with varying P_{LLOS} in the (a) suburban, (b) urban scenarios

measurements in NLLOS conditions and provide real time variance estimates $\hat{\sigma}_{\tau}^{2}$ and $\hat{\sigma}_{\alpha}^{2}$. In the next section a performance comparison between several methods of AOA filtering to exploit spatial diversity are presented.

6.3 Filtering of AOA Measurements to Exploit Spatial Diversity

The distribution of NLOS errors in AOA measurements was described in Section 2.7. In Figure 3.11 the first arriving NLLOS AOA PDF is shown. The NLLOS noise power of such measurements is quite large. This noise is multiplied by the MS–BS separation so that location accuracy of an AOA system is cell size dependent and potentially very large. Measurement noise, which is usually considered to be Gaussian distributed, is also present. Figure 6.4 shows the convolution of the measurement and NLLOS noises for the elliptical scatterer model.

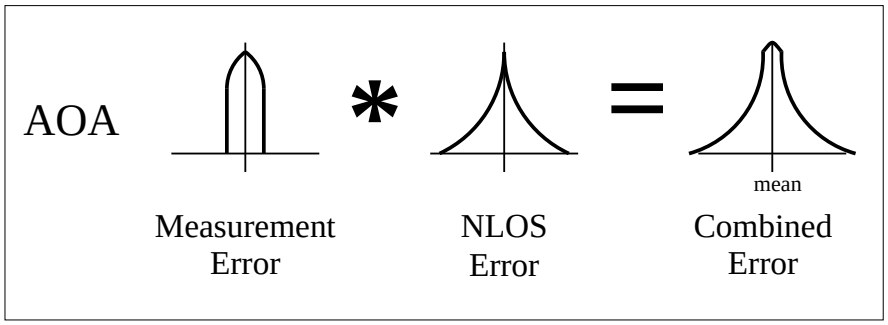

Figure 6.4: PDF of AOA in NLOS with measurement noise

The AOA measurements require to be filtered to exploit the fact that the NLOS long term mean is the true LOS AOA. Assuming some spatial diversity in multipath make–up is experienced a fair estimate for the true LOS AOA may be obtained.

Similarly to the last chapter the LS technique is compared to the ieKF, LOS–KF and NLOS–KF as a prefilter for the AOA measurements in order to exploit spatial diversity. In this section the performance of a smoothed average (SA) filter is also analysed.

6.3.1 AOA ieKF Implementation

The AOA ieKF implementation is similar to the timing measurement KF introduced in the previous chapter. However in AOA filtering, the NLOS error PDF is symmetric about the true PDF thus the early biasing technique is omitted in the implementation. The KF should naturally converge to the true LOS direction given enough uncorrelated NLOS measurements. Simulation shows that convergence can be slow if the initial measurements have large NLOS errors. In such cases resetting the ieKF greatly improved performance.

Since an MS travelling close to the BS has a much larger angular acceleration capability the velocity driving noise, σ_u^2, should be a function of MS–BS separation. This separation can be estimated by feedback of the MS location estimate and then used to update σ_u^2.

6.3.2 LS and SA Implementation

The AOA distribution is symmetrical about the mean so no adjustment is required to the LS technique (as in previous chapter). The smoothed average is simply

$$\mu = \frac{1}{L_{SA}F_{idle}} \sum_{i=0}^{L_{SA}F_{idle}} \alpha_{BS1}[n-i] \tag{6.11}$$

where L_{SA} is the filter length in seconds and n represents the current time in samples. The SA filter can also have a delay. For a delay of $L/2$ the SA and $N = 1$ LS techniques are mathematically the same.

Since the measurement space wraps around at 2π a preliminary estimate of the mean μ, via a smoothed average, is obtained first then this mean is used to recompute the measurements in the interval $\mu - \pi$ to $\mu + \pi$ by the addition or subtraction of 2π, before recalculating the AOA

output (for both SA and LS techniques).

6.3.3 Performance Comparison

The performance of ieKF, KF, LS and SA filters were compared for the central 30 second segment of a 90 second track in the urban environment with MS moving at 50kmph and 5kmph. The results reported are RMS performance over 10 data sets. The SA filter with delay $L_{SA}/2$ and LS $N_{LS} = 1$ filter with delay $L_{LS}/2$ are mathematically equivalent. For simplicity $\sigma_u^2 = 6.4 \cdot 10^{-5}$rad s^{-2} is fixed regardless of MS–BS separation.

The hearability fraction for the data sets is 1 (since only the serving BS is considered). Noise of power $\sigma^2_{\alpha LOS} = 10^{-5}$rad^2 corrupts the measurements as well as the NLLOS noise of the first arriving path.

The KF is implemented with both $\sigma_Y^2 = \sigma^2_{\alpha LOS}$ and with $\sigma_Y^2 = \sigma^2_{\alpha NLOS}$. These KF's are termed LOS–KF and NLOS–KF respectively. The LOS power is supposed to be known precisely while the NLOS noise power is estimated to be $\sigma^2_{\alpha NLOS} = 0.5$ rad^2.

Figures 6.5(a), (b) show example tracks for the LS, SA, ieKF and NLOS–KF techniques in the urban car and urban pedestrian scenarios respectively (the LOS–KF is not shown since it followed the data very closely). In the urban 50kmph scenario the SA with delay clearly performs poorly since the AOA is changing quickly. The ieKF diverges at a manoeuvre point since the velocity driving noise does not allow it to track the sudden velocity shift. This would not happen if manoeuvres were modelled more realistically. At 5kmph the spatial correlation can clearly be seen.

Tables 6.1(a), (b), (c) show the mean RMS error between the track and the true LOS AOA for the LS, SA and KF techniques respectively in the urban 50kmph scenario. The raw AOA data has an RMS error of 43.5 degrees. The ieKF outperforms all the other techniques, including the LS technique with delay. This can be explained by the large angular spread in measurements experienced. In the LS technique $N_{LS} = 1$ outperforms $N_{LS} = 2$ partly because of the linearity of the MS path, and secondly as higher orders will allow curve fitting to accommodate NLOS data, since there is no gradient constraint on the curve.

Tables 6.2(a), (b), (c) show the mean RMS error between the track and the true LOS AOA for the LS, SA and KF techniques respectively in the urban 5kmph scenario. The raw AOA data

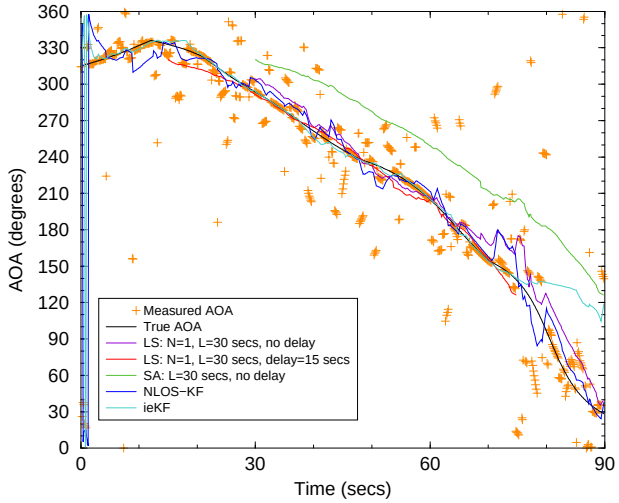

(a)

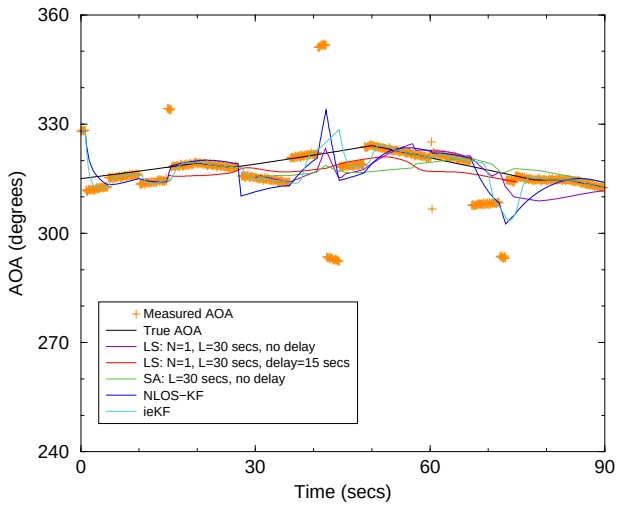

(b)

Figure 6.5: Example AOA tracks for (a) urban 50kmph (b) urban 5kmph scenarios

has an RMS error of 77.8 degrees. Again the ieKF outperforms all the other techniques. Since far less spatial diversity is obtained the performance of all systems is much worse than in the moving scenario.

To conclude at higher speeds the filtering of AOA is quite successful. The ieKF performs best though $N_{LS} = 1$ LS should also be considered. In fact LS methods might be improved by an iterative procedure to generate weights for the data based on goodness of fit to the previous fit. At 5kmph the performance of all techniques is very poor since little spatial diversity is gained. Furthermore unlike the tracking of TOA's (when early TOA's can be favoured) there is no way

	RMS error (deg)	
	$N = 1$	$N = 2$
$L = 10$	8.45 / 15.3	11.8 / 22.0
$L = 20$	6.73 / 11.3	8.86 / 15.9
$L = 30$	6.52 / 12.2	7.61 / 13.3

(a)

	RMS error (deg)
$L = 10$	18.7
$L = 20$	33.3
$L = 30$	46.7

(b)

	RMS error (deg)
LOS–KF	38.5
NLOS–KF	12.1
ieKF	5.16

(c)

Table 6.1: RMS error performance for (a) LS filter (with delay / no delay), (b) SA filter (no delay), (c) KF techniques in urban 50kmph scenario

	RMS error (deg)	
	$N = 1$	$N = 2$
$L = 10$	58.8 / 74.4	66.0 / 75.7
$L = 20$	26.2 / 34.7	37.0 / 43.9
$L = 30$	17.5 / 25.5	24.0 / 36.9

(a)

	RMS error (deg)
$L = 10$	52.7
$L = 20$	18.4
$L = 30$	17.0

(b)

	RMS error (deg)
LOS–KF	78.5
NLOS–KF	75.8
ieKF	12.7

(c)

Table 6.2: RMS error performance for (a) LS filter (with delay / no delay), (b) SA filter (no delay), (c) KF techniques in urban 5kmph scenario

of determining between two AOA samples which data is more likely to be LLOS.

6.4 AOA/TDOA Hybrid Location Estimator Architecture Utilising Spatial Diversity

Figure 6.6 shows the receiver R5. The architecture is identical to the TDOA implementation, receiver R3, discussed in the previous chapter except that an AOA measurement is also included. Similarly this measurement is prefiltered to suppress NLOS errors for which an ieKF is used for high speeds and an SA filter for low (pedestrian speeds). At high speeds the location is tracked by KF and at low speeds by a WA filter. The high speed receiver and low speed receiver are termed receiver R5A and receiver R5B respectively. The decision over which receiver to use is made by feedback of MS speed from the final KF tracking filter, though in simulation the feedback is not implemented. The receiver R5 is discussed in more detail in the following subsections.

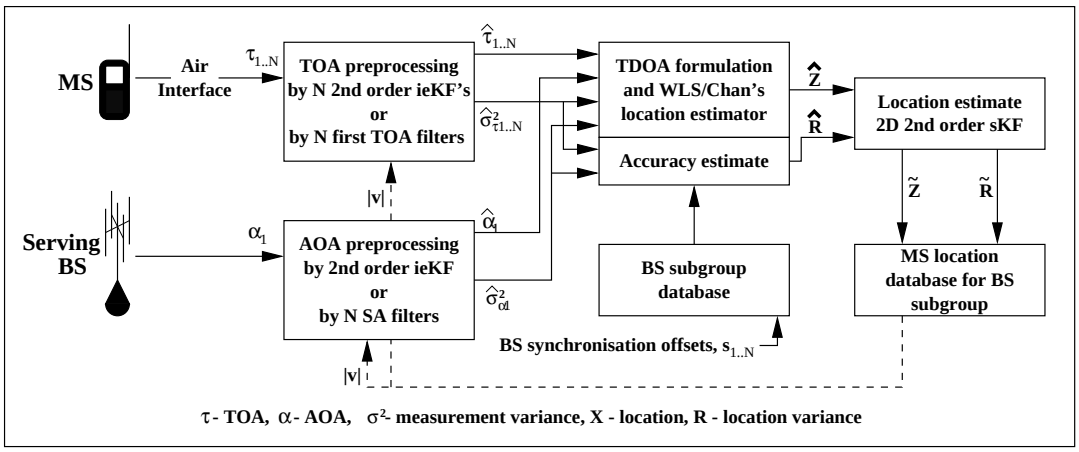

Figure 6.6: Receiver architecture with TOA and AOA data streams.

6.4.1 Preprocessor Stage

The variance calculation for the SA filter is made according to the standard variance definition for the filter length.

6.4.2 Dataset Reduction

This stage is identical to receiver R3, see Section 5.3.2

6.4.3 AOA–TDOA Location and Location Variance Estimator

The location calculation is performed similarly to Section 6.2.1. Variance estimates for the input TDOA streams and AOA stream now exist (from the preprocessing stage). The measurement covariance matrix ω^{-1} is redefined as

$$\omega^{-1} = \begin{bmatrix} & & & 0 \\ & \omega_\tau^{-1} & & .. \\ & & & 0 \\ 0 & .. & 0 & \hat{\sigma}_\alpha^2 \end{bmatrix} \tag{6.12}$$

where ω_τ^{-1} is the N by N matrix,

$$\omega_\tau^{-1} = \begin{cases} c^2(\hat{\sigma}_{\tau 1}^2 + \hat{\sigma}_{\tau j}^2) & i = j, \\ c^2\hat{\sigma}_{\tau 1}^2 & i = 1 || j = 1, \\ 0 & \text{otherwise} \end{cases} \tag{6.13}$$

In the definition of $\hat{\mathbf{Q}} = \omega^{-1}$ the covariance terms between τ_1 and α_1 are taken as zero for simplicity. In reality these covariances will lie in the range 0 to $\sigma_{\tau 1}\sigma_{\alpha 1}$.

The estimated accuracy of the location estimate $\hat{\mathbf{Z}}$ is determined by evaluating its covariance matrix, $\hat{\mathbf{R}}$. This is calculated by (2.37).

In the case where the solution is precisely determined, i.e. one TD and one AOA, the CRLB is used as an estimate of $\hat{\mathbf{R}}$. The CRLB, Φ^0, for the AOA–TDOA estimator can be derived as

$$\Phi^o = (\mathbf{G}^T\hat{\mathbf{Q}}^{-1}\mathbf{G})^{-1} \tag{6.14}$$

where

$$\mathbf{G} = \begin{bmatrix} \frac{(x_1-x)}{r_1} - \frac{(x_2-x)}{r_2} & \frac{(y_1-y)}{r_1} - \frac{(y_2-x)}{y_2} \\ .. & .. \\ \frac{(x_1-x)}{r_1} - \frac{(x_N-x)}{r_N} & \frac{(y_1-y)}{r_1} - \frac{(y_N-x)}{y_N} \\ \frac{1}{(y-y_1)\left(1+\frac{(x-x_1)^2}{(y-y_1)^2}\right)} & \frac{(x-x1)}{(y-y_1)^2\left(1+\frac{(x-x_1)^2}{(y-y_1)^2}\right)} \end{bmatrix}$$

The derivation is shown in Appendix A.

6.4.4 Location KF

This stage is identical to receiver R3, Section 5.3.4

6.4.5 Weighted Average Location Filter

This stage is identical to receiver R3, Section 5.3.5

6.4.6 Location Estimation Accuracy Performance

An identical simulation environment to Section 5.3.6 is used. AOA measurements are corrupted by Gaussian measurement noise of varying power, $\sigma^2_{\alpha LOS}$, in addition to any NLOS errors that may be present.

Figure 6.7 shows E^{67}_{ce} and E^{95}_{ce} for the rural scenario with varying Gaussian noise power on the AOA measurements. The mean hearability is approximately 3 BS's per second. The TDOA only performance (at $\hat{\mathbf{Z}}$ since this gives better performance than $\tilde{\mathbf{Z}}$ in this scenario) is shown for comparison purposes. Using the AOA measurements gives a substantial improvement, up to 60% for E^{67}_{ce} and up to up 70% for E^{95}_{ce} if the measurement noise power, $\sigma^2_{\alpha LOS}$, is less than 10^{-4} rad^2. By similar triangles it is reasonable to assume a smaller cell radius would further desensitise the location error to $\sigma^2_{\alpha LOS}$. Subsequent simulations use $\sigma^2_{\alpha LOS} = 10^{-5}$ rad^2. With $\sigma^2_{\alpha LOS} < 10^{-5}$ the location accuracy does not improve since the location error is now dominated by timing errors. With $\sigma^2_{\alpha LOS} > 10^{-3}$ the AOA/TDOA receiver performs slightly worse than the TDOA only receiver since the AOA noise is much larger than the timing measurement noise. Ideally the AOA would then have no effect on the performance but since the covariance weighting can never be perfect the location accuracy can decrease.

Figures 6.8(a), (b), (c), (d) show the location accuracy with varying received pilot SNR and hence varying hearability for the rural, suburban, urban car and urban pedestrian scenarios respectively with receiver R5A. With increasing hearability each point on the graph corresponds to a 3dB increase in SNR. Best location accuracy for the TDOA only receiver R3A is also shown. Due to the KF prefilters the location accuracy remains good even when the mean number of BS's detected per second is very small (i.e. < 3). The performance of the hybrid systems tails off slightly slower than TDOA only systems with lowering hearability as only a hearability of 2 BS's is required for a location estimate. The CRLB analysis in Figure 2.11

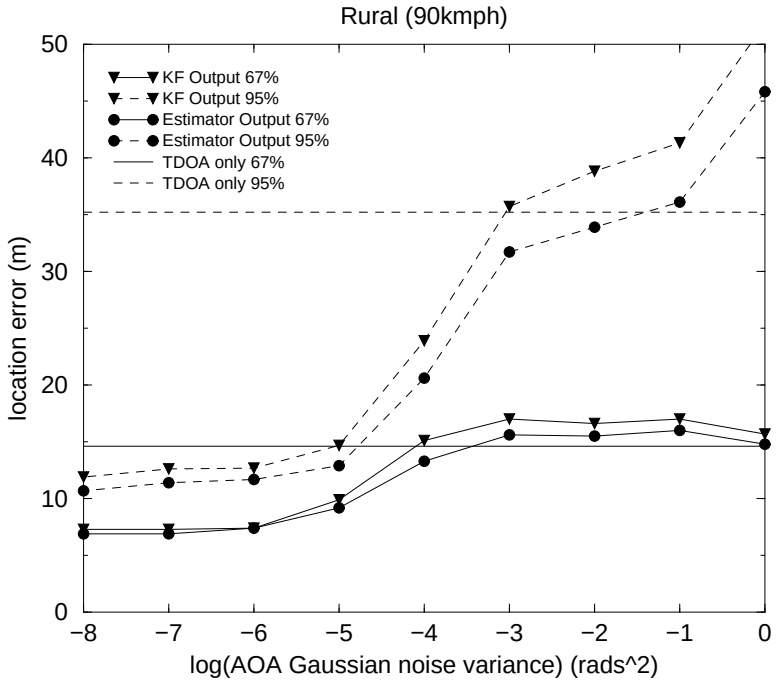

Figure 6.7: Location error against $\sigma^2_{\alpha LOS}$ using receiver R5A in the rural scenario

shows the noise sensitivity can be larger for the 1 TD, 1 AOA location compared with any 2 TD location method, thus the improvement is not as much as might be hoped. In the urban pedestrian scenario the performance of the hybrid estimator is worse than the TDOA only estimator if the hearability ≥ 3 BS's per second. At low speed it becomes increasingly difficult to differentiate between LLOS and NLLOS states since little spatial diversity is experienced. Figure 6.9 shows the performance with receiver R5B in the urban pedestrian scenario. This receiver performs much worse than receiver R3B.

Figures 6.10(a), (b), (c) show the location accuracy with varying P_{LLOS} for the suburban, urban car and urban pedestrian scenarios respectively with receiver R5A. Generally as P_{LLOS} increases the improvement of the AOA/TDOA estimator over the TDOA only estimator increases. This improvement is most significant in the urban scenarios. Figure 6.11 shows the performance with receiver R5B in the urban pedestrian scenario. The TDOA only estimator performs better for all P_{LLOS}.

To conclude utilising the AOA at the serving BS can improve the location accuracy of a TDOA only location estimator. This improvement is only possible with $\sigma^2_{\alpha LOS} \leq 10^{-4}\text{rad}^2$ for $R_C = 10\text{km}$. With a smaller cell radius the tolerable noise power could be proportionately larger. In low P_{LLOS} scenarios location accuracy only improves in the high speed scenario (urban car)

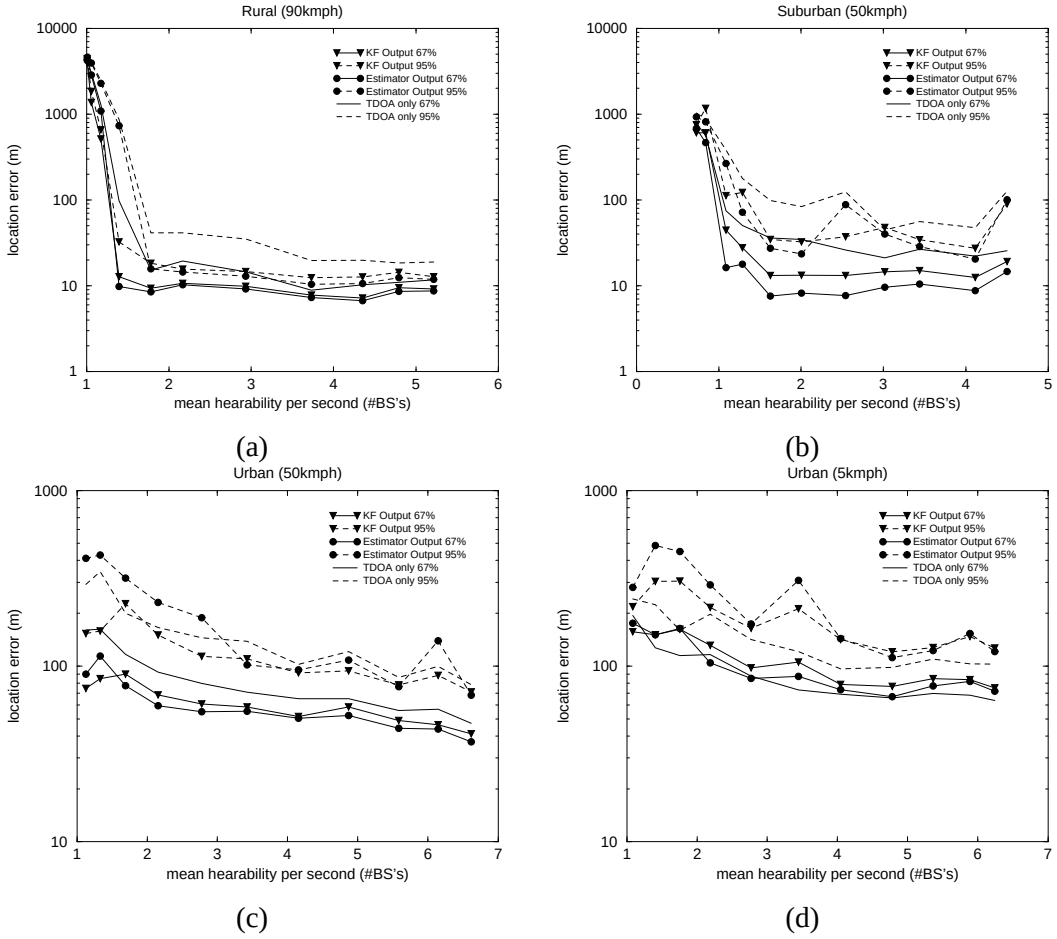

Figure 6.8: Location error against hearability using receiver R5A in the (a) rural, (b) suburban, (c) urban car, (d) urban pedestrian scenarios

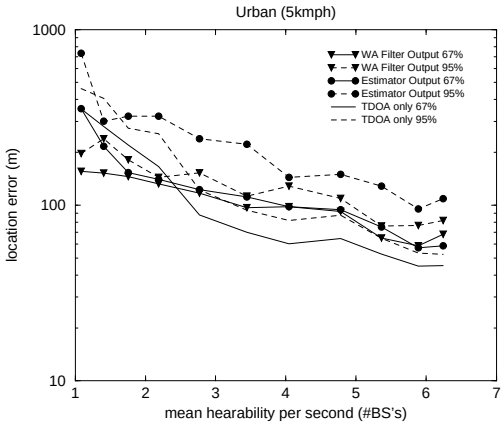

Figure 6.9: Location error against hearability using receiver R5B in the urban pedestrian scenario

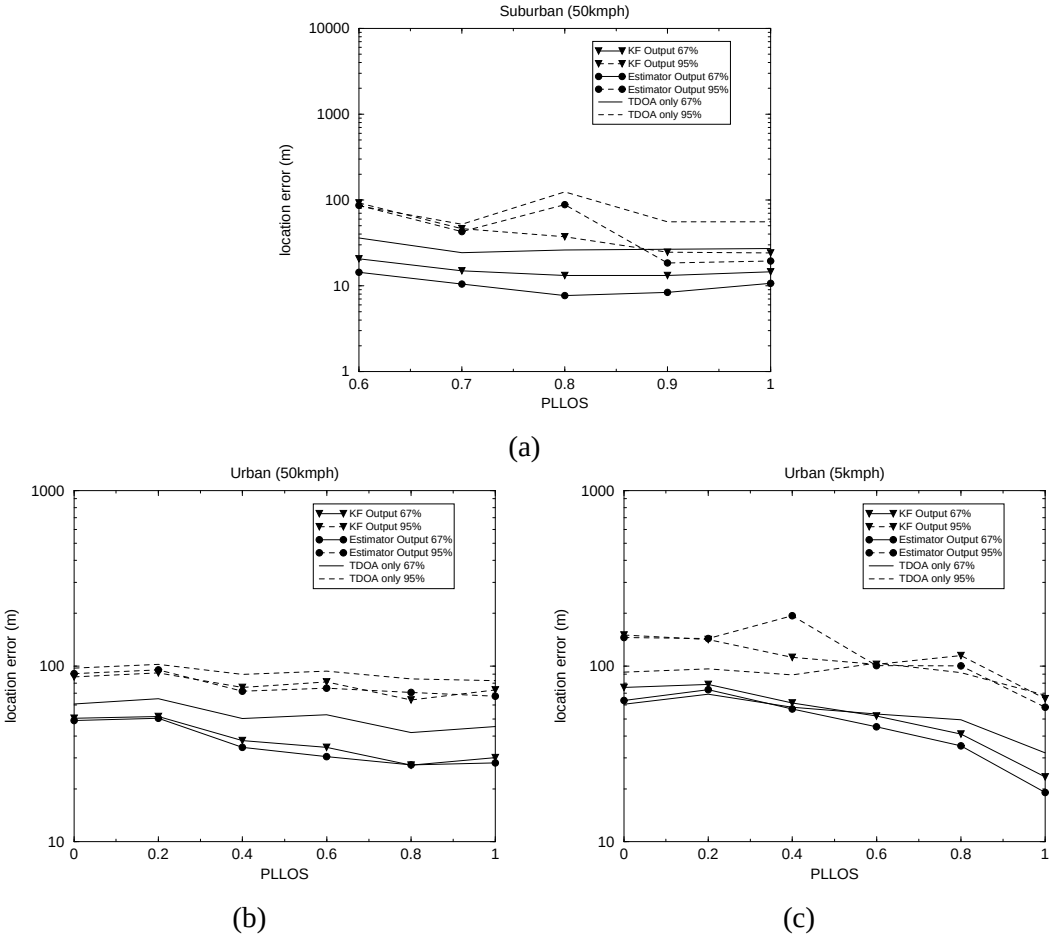

Figure 6.10: Location error against P_{LLOS} using receiver R5A in the (a) suburban, (b) urban car, (c) urban pedestrian scenarios

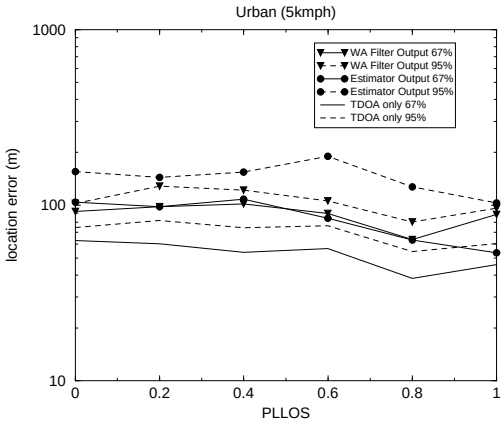

Figure 6.11: Location error against P_{LLOS} using receiver R5B in the urban pedestrian scenario

since at low speeds (urban pedestrian) the prefiltering process is unable to differentiate between LLOS and NLLOS AOA's. Receiver R5B did not perform well at all in the urban pedestrian scenario, thus for low speeds and low P_{LLOS} the AOA should not be used in the estimator. Table 6.3 summarises the location accuracy improvement of receiver R5A/B over receiver R3A/B at a high hearability level with $\sigma^2_{\alpha LOS} = 10^{-5}\text{rad}^2$.

		R5A	R5B	R3A	R5B	% improvement
Rural	E_{ce}^{67}	8		10		20
	E_{ce}^{95}	11		20		45
Suburban	E_{ce}^{67}	9		20		55
	E_{ce}^{95}	22		40		45
Urban Car	E_{ce}^{67}	37		45		18
	E_{ce}^{95}	66		75		12
Urban Pedestrian	E_{ce}^{67}		55		45	-22
	E_{ce}^{95}		77		55	-40

Table 6.3: Summary of location accuracy improvement of receiver R5A/B over receiver R3A/B

6.5 Conclusions

In this chapter the performance of a hybrid AOA/TDOA location receiver with and without spatial diversity has been presented under several scenarios. Without spatial diversity the performance of such a receiver is worse than the TDOA unless $P_{LLOS} = 1.0$. It could be advantageous if hearability is less than 3 BS's. The spatial filtering algorithms do not work as well for AOA measurements as for TOA measurements. However a significant improvement in location accuracy was achieved over the TDOA only receiver if the MS is moving fast or if P_{LLOS} is large. Unfortunately the location accuracy improvement is greatest in precisely those scenario's in which location accuracy is already very good (and below the FCC requirements). At 5kmph with low P_{LLOS} the performance deteriorates below TDOA only performance. Simulated performance might be improved if a circular scatterer model is used. This would reduce the angular spread of the AOA's compared to the elliptical scatterer model used and perhaps would be a more representative model.

Chapter 7
Source Location by Scatterer Back Tracing

In this chapter a novel Scatterer Back Tracing (SBT) approach to MS location estimation in multipath environments which is not degraded by NLOS conditions is described. The AOA, TOA relative to the first arriving ray, and Doppler shifts for individual rays are measured at the serving BS. Using the information from 6 arriving rays the MS location can be precisely calculated.

Location accuracy performance of the technique is assessed with the addition of Gaussian distributed noise to the measurements. Further simulations of an enhanced estimator augmenting the original estimator with signal strength measurements and utilising a Kalman filter (KF) to track a moving MS are presented. These show promising location accuracy results, significantly better than results obtained using conventional triangulation techniques discussed in previous chapters.

7.1 Problem Formulation

NLOS conditions can dramatically reduce the performance of conventional triangulation based mobile location techniques. However even in NLOS when sufficient resolvable multipaths are present the MS may be precisely located by back tracing the arriving rays under a single reflection assumption. Even in a multiple reflection scenario the technique may work if the reflection points are spatially close, which should be true for early arriving multipaths.

Figure 7.1 shows a possible geometry for a single reflection scatterer, S_n. The scatterer and BS are assumed fixed; the MS has speed v in direction ϕ_m with respect to line of sight to the BS. In a typical urban environment a number of such scatterers will be present, e.g. in the CoDiT urban model 20 scatterers are defined.

In the following section equations are formulated based on this single reflection geometry which

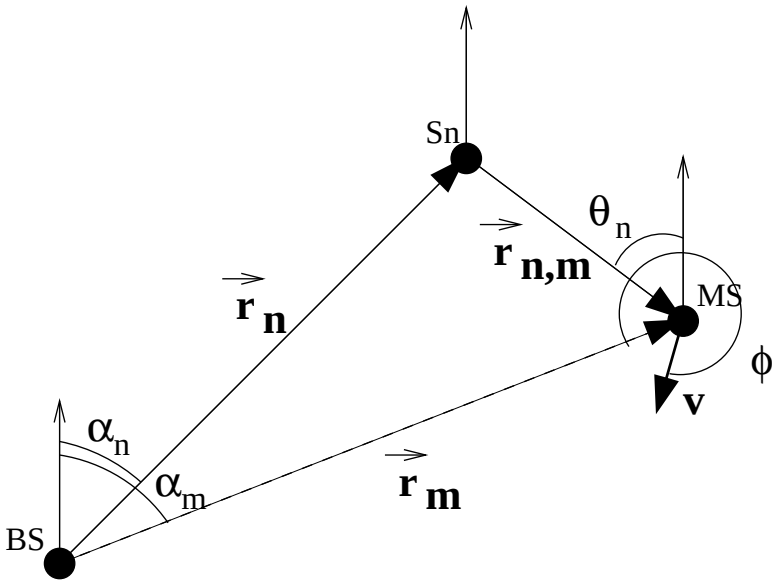

Figure 7.1: Single reflection scatterer geometry

use AOA, α_n; time of arrival with respect to first arriving ray, $\tau_{n,1}$; and Doppler shift, f_{dn}, measurements for each arriving ray. For the purpose of this work it is assumed that the required measurements could be found by using an antenna array and suitable processing on the received signals. These measurements, (α_n, f_{dn}) for $n = 1..N$ and $\tau_{n,1}$ for $n = 2..N$, will be subject to uncorrelated additive noise which again for simplicity is assumed to be Gaussian distributed. This assumption ignores the problem of resolving closely spaced scatterers, when the noise distribution could be non–Gaussian and correlated in time.

There are 5 unknowns, the MS polar coordinates, (r_m, α_m), velocity (v, ϕ_m) and time delay of the first arriving ray relative to the true LOS arriving time, $\tau_{1,0}$.

Using the temporal knowledge of the channel for each scatterer, see Figure 7.1

$$r_n + r_{n,m} - r_m = c\tau_{n,1} + c\tau_{1,0} \tag{7.1}$$

Using the cosine rule gives

$$r_{n,m} = \sqrt{r_n^2 + r_m^2 - 2r_n r_m \cos(\alpha_m - \alpha_n)} \tag{7.2}$$

Rearranging (7.1) and substituting in 7.2 gives

$$\begin{aligned} r_{n,m} &= r_n - r_m - c\tau_{n,1} - c\tau_{1,0} \\ r_{n,m}^2 &= (r_n - r_m - c\tau_{n,1} - c\tau_{1,0})^2 \\ -2r_n r_m \cos(\alpha_m - \alpha_n) &= (c\tau_{n,1} - c\tau_{1,0})^2 + 2(r_m - r_n)(c\tau_{n,1} - c\tau_{1,0}) - 2r_m r_n \\ r_n &= \frac{(c\tau_{n,1} + c\tau_{1,0})^2 + 2(c\tau_{n,1} + c\tau_{1,0})r_m}{2(r_m + c\tau_{n,1} + c\tau_{1,0} - r_m \cos(\alpha_m - \alpha_n))} \end{aligned} \tag{7.3}$$

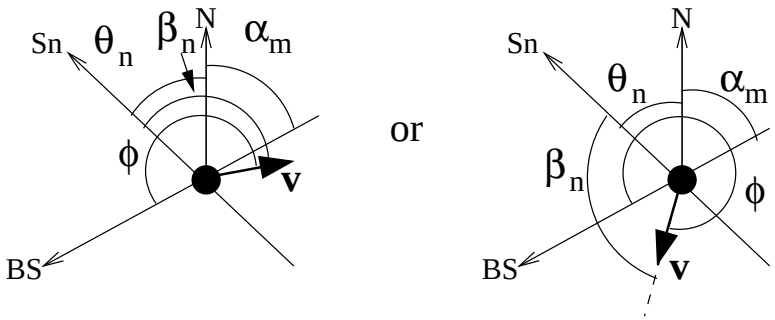

Figure 7.2: Possible geometry at MS

Using the geometrical knowledge of the channel for each scatterer

$$\vec{\mathbf{r}}_\mathbf{n} + \vec{\mathbf{r}}_{\mathbf{n,m}} - \vec{\mathbf{r}}_\mathbf{m} = \vec{\mathbf{0}} \tag{7.4}$$

Therefore for each scatterer (for convenience in the following equation complex notation is used to represent geometry with the real axis representing the x–axis and imaginary axis representing the y–axis)

$$\begin{aligned} E_n = r_n\,(j\sin(\alpha_n) + \cos(\alpha_n)) + \\ r_{n,m}\,(j\sin(\theta_n) - \cos(\theta_n)) - r_m\,(j\sin(\alpha_m) + \cos(\alpha_m)) = 0 \end{aligned} \tag{7.5}$$

where, (see Figure 7.2),

$$\theta_n = \pi - \alpha_m - \phi_m \pm \beta_n \tag{7.6}$$

and

$$\beta_n = \cos^{-1}\left(\frac{f_{dn}\lambda}{v}\right) \tag{7.7}$$

where λ is the carrier wavelength. If $\alpha_m > \pi$ the ϕ_m should be substituted with $\phi_m - \pi$ in all the prior analysis.

Substituting (7.2) and (7.3) into (7.5) gives a set of non–linear equations, E_n, in the 5 unknowns $(r_m, \alpha_m, v, \phi_m, \tau_{1,0})$ for each scatterer S_n. In the presence of measurement noise E_n may not equal zero, therefore a unique solution can be found by minimising the sum of $|E_n|^2$ for $n = 1..N$ with $N \geq 6$ scatterers ($N = 5$ is insufficient due to ambiguity in (7.6)). This leads to the simple estimator

$$\xi = \sum_{n=1}^{N} |E_n|^2 \tag{7.8}$$

The θ_n value in (7.6) that minimises the component of ξ from (7.5) is chosen. The final solution vector $(\hat{r}_m, \hat{\alpha}_m, \hat{v}, \hat{\phi_m}, \hat{\tau}_{1,0})$ is obtained by iteratively minimising (7.8).

Using a signal strength measurement an auxiliary estimate for r_m can be calculated. Assuming a lognormal distribution of signal strength, a conditional range PDF of the true range r_m about the estimate $\tilde{r}_m$ can be evaluated as

$$f_{R_m}(r_m|\tilde{r}_m) = \frac{\tilde{r}_m}{\sigma_s\sqrt{2\pi}} \exp\left[-\frac{P_L(r_m)^2}{2\sigma_s^2}\right] \tag{7.9}$$

where σ_s is the shadowing log standard deviation and $P_L(r_m)$ is the path loss equation. Figure 7.3 shows $f_{R_m}(r_m|\tilde{r}_m)$ (normalised to $\tilde{r}_m$) for the simple path loss model (2.3) with different σ_s values. The range spread encompassed by the PDF is quite wide for higher standard deviations. However most of the spread is in the region $r_m > \tilde{r}_m$, thus the PDF may still be helpful to eradicate false location estimates where the estimated range $\hat{r_m} < \tilde{r_m}$.

Utilising $f_{R_m}(r_m|\tilde{r}_m)$ leads to the enhanced scatterer back tracing (eSBT) estimator

$$\xi_e = f_{R_m}(r_m|\tilde{r}_m) \sum_{n=1}^{N} |E_n|^2 \tag{7.10}$$

7.1.1 Comments on Estimator Performance

As previously mentioned the mobile location, velocity and NLOS delay are the solution of a set of non–linear equations. The downhill simplex minimisation technique [24] is used to find a possible solution. Although there are five unknowns simulation shows that multiple roots occur

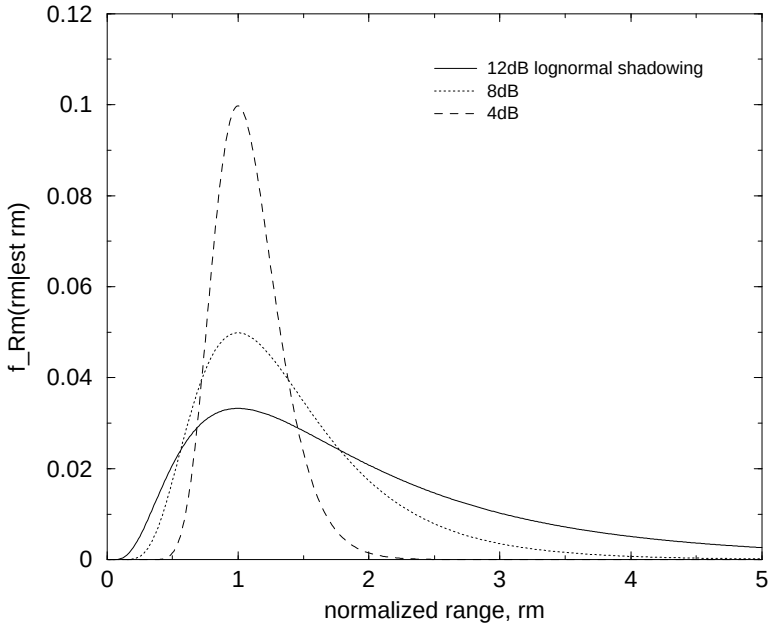

Figure 7.3: $f_{R_m}(r_m|\tilde{r}_m)$ against normalised r_m for different lognormal shadowing

when $N = 5$, i.e. when there are only five equations and thus five scatterer measurement sets are used in the sum ξ. Simulation shows using $N = 6$ never gives more than one root. In the presence of noise the minimised solution generally gives $\xi > 0$.

A great problem in minimising non–linear equations is that of converging on local minima. Figures 7.4(a), (b) demonstrate this problem for the minimisation of ξ for a particular MS location, $(-256m, -323m)$, and scatterer makeup (not shown). The serving BS is located at (0m,0m) for this and all subsequent examples. The graphs show the minimum ξ found at each location when the MS location (r_m, α_m) is artificially fixed in the estimator. Figure 7.4(a) shows the surface under low input noise ($\sigma_\alpha^2 = 10^{-7}$, $\sigma_{f_d}^2 = 10^{-5} f_{max}^2$, $\sigma_{c\tau}^2 = 10^{-1}$), and Figure 7.4(b) with higher noise power ($\sigma_\alpha^2 = 10^{-5}$, $\sigma_f^2 = 10^{-3} f_{max}^2$, $\sigma_{c\tau}^2 = 10$).

It can be seen under low noise, Figure 7.4(a), the minimum of the surface occurs very close to the true location. A number of other effects can be observed. Firstly the sensitivity of the estimator to range error (obtained from the Doppler information) is high. For this reason the enhanced estimator can perform significantly better. Secondly there are discontinuities in the surface where the estimator has failed to find the minimum. These can be eradicated by increasing the number of calculations of ξ in the estimator and thus the search time. Lastly several local minima are present. In the low noise case these are significantly shallower than the

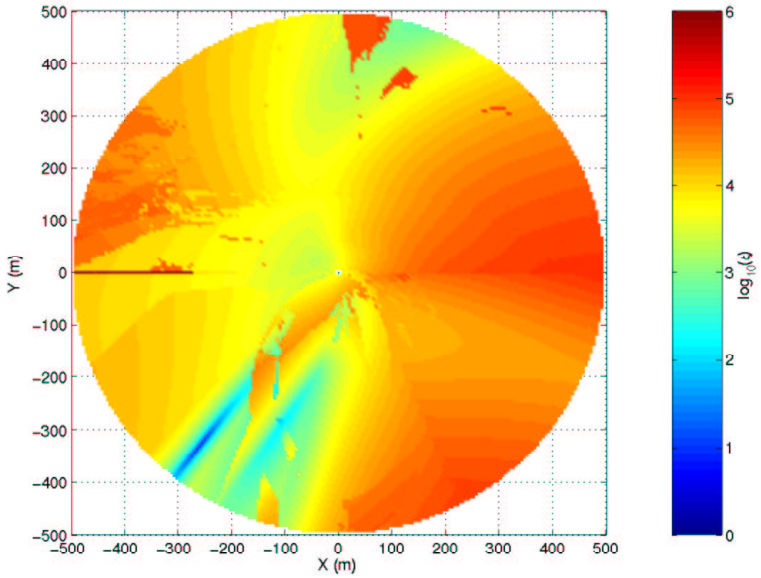

(a)

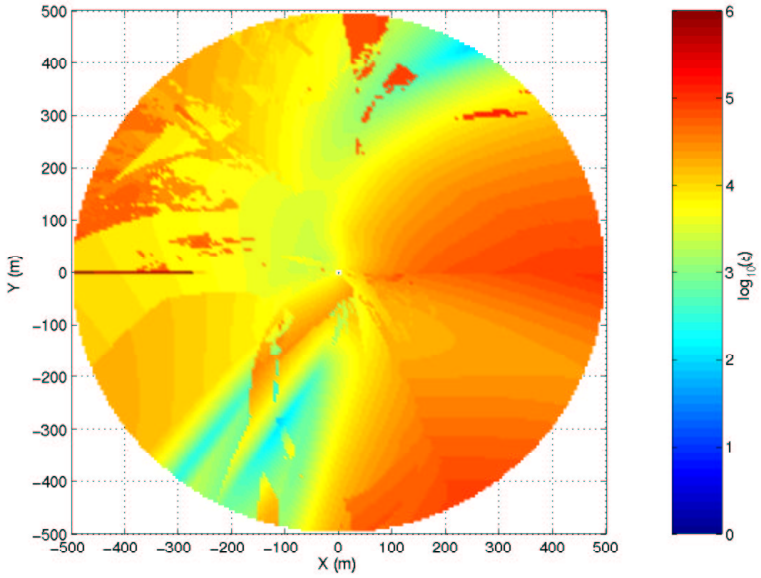

(b)

Figure 7.4: Minimised ξ against location for a (a) low noise, (b) high noise scenario

global minimum. In the high noise case, Figure 7.4(b), the minimum around the true location is less deep and deeper minima are now present at considerable distance from the true location. With high noise the noise performance can therefore not be derived from the partial derivatives or the desired parameters (location) with respect to the measured parameters.

7.2 Simulation Results and Discussion

The simulation uses the urban channel model scatterer definition (definition in Table B.1). The AOA at the MS is defined, therefore the transformation shown in Appendix B.2 is used to calculate the AOA at the BS. The estimator uses the $N = 6$ earliest arriving rays. A cell radius of 500m is used, with a path loss exponent of 3.76 and lognormal shadowing of 8dB. 1000 randomly dropped MS's are located within the cell, travelling at 50kmph ($f_c = 1.92$GHz, maximum Doppler shift ,$f_{dmax} = 92.7$Hz). The LLOS probability, P_{LLOS}, is set to 0.2. A tracking scenario is also simulated. A 2D 1st order KF identical to the implementation in Section 5.3.4, provides the tracking capability. For this scenario, again as in to Section 5.3.6, a spatially correlated LOS model is applied, where the shadowing decorrelation length and scatterer mean survival length are both 5m (see Table 3.2).

The estimator performance is simulated with varying measurement noise powers, with σ_α^2 varied from 10^{-7} to 10^{-3}rads^2; $\sigma_{c\tau}^2$ varied from 0.1 to 1000m^2; and $\sigma_{f_d}^2$ varied from $10^{-5} f_{dmax}^2$ to $10^{-3} f_{dmax}^2$Hz^2. The number of calculations of ξ required by the estimator depends greatly on the noise power corrupting the measurements. If the noise power is low a good solution is found with 5 thousand calculations of ξ. However for high noise even after 500 thousand calculations a good solution may still not be found.

Figures 7.5(a), (b) show the RMS location accuracy achieved for the SBT, eSBT and eSBT with KF post tracking estimators against Gaussian distributed noise power added to the measurements, $(\alpha_n, f_{dn}, \tau_{n,1})$. As a performance comparison to these estimators the performance of cell location only (CL), first arriving AOA and Signal Strength (AOA–SS); and first arriving AOA and TOA (AOA–TOA) estimators are shown. The performance of the latter is also shown with a KF tracking filter. Figure 7.5(a) shows results for low Doppler noise power, $\sigma_{f_d}^2 = 10^{-5} f_{dmax}^2$; and Figure 7.5(b) shows results for high Doppler noise power, $\sigma_{f_d}^2 = 10^{-3} f_{dmax}^2$. For the SBT, eSBT and First AOA–First TOA estimator the performance is shown with two different noise powers added to $c\tau_{n,1}$ of $0.1m^2$ (the lower solid line of the

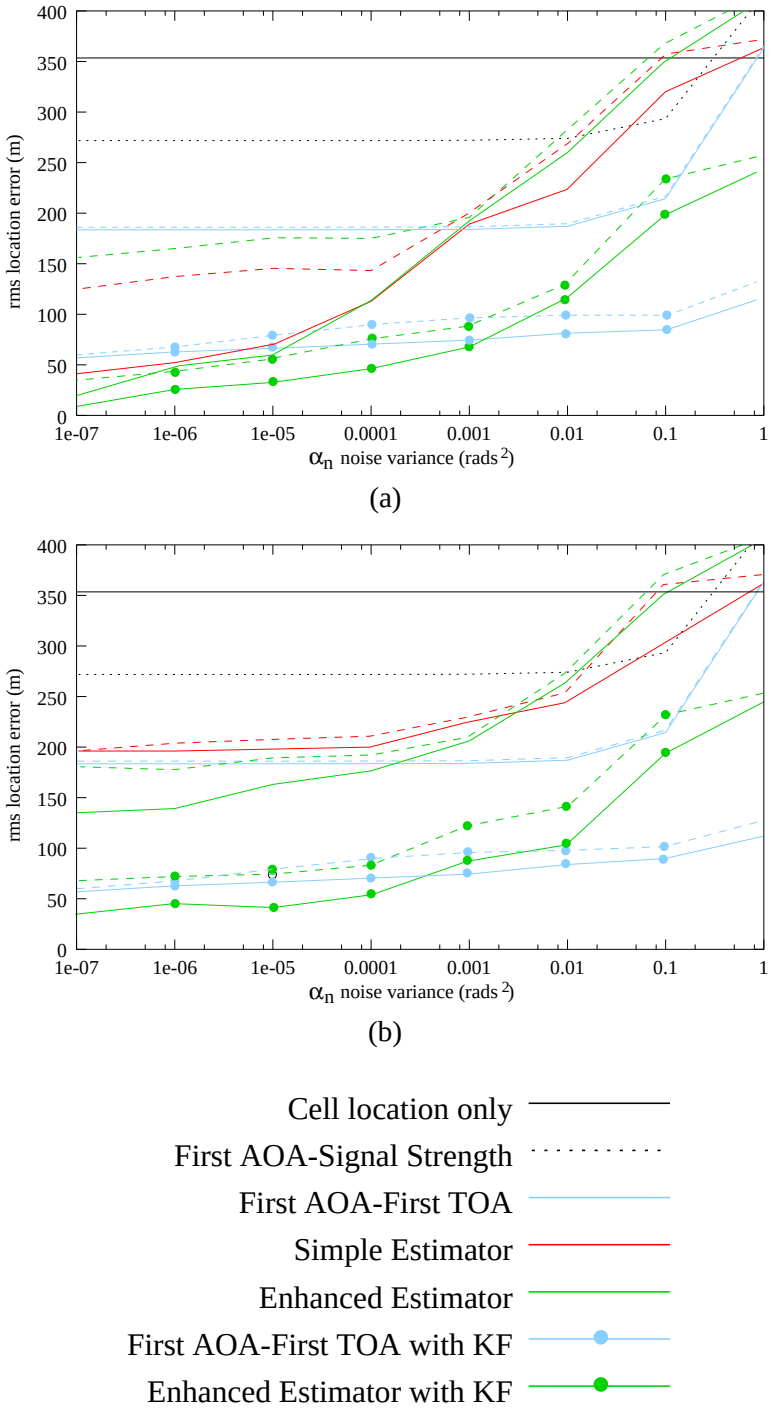

Figure 7.5: RMS location error performance for (a) low, (b) high Doppler noise

pair) and $1000m^2$ (the upper dashed line).

The results in Figures 7.5(a),(b) show that both SBT and eSBT techniques outperform the other location techniques (of which the AOA–TOA method is the best) in the low measurement noise region. In the lowest noise scenario location accuracy is an order of magnitude better (20m RMS to 200m RMS) than the other techniques and as noise levels are reduced further the location error is reduced to zero whereas performance of the other techniques is limited by NLOS errors. However performance deteriorates quite dramatically as the noise power of any one measurement type is increased. The eSBT estimator performs significantly better than the SBT estimator in the high Doppler noise, low AOA noise region. This can be attributed to the sensitivity of the location range estimate r_m to the Doppler measurements. In the presence of high AOA or TD noise the eSBT estimator generally performs slightly worse than the SBT estimator. This is due to the fact that with higher noise when the true solution is no longer in a global minimum the estimates tend to converge towards the BS with α_m uniformly distributed. Thus the range enhancement simply draws the location estimate away from the BS, but as the estimate of α_m bears no relation to the true value this on average increases the RMS error.

With KF tracking further improvement is possible in both SBT methods and conventional methods. Again in the low noise region the eSBT outperforms the AOA–TOA method though the RMS performance improvement is reduced to a factor of two. Figures 7.6(a), (b) show example tracks using the eSBT technique and AOA–TOA technique respectively with low measurement noise power. The measurement noise power in both cases was $\sigma_\alpha^2 = 10^{-4}$, $\sigma_{c\tau}^2 = 10^{-1}$ and additionally for the eSBT $\sigma_{f_d}^2 = 10^{-5}$. It is clear to see that the error distribution around the true path for the SBT technique is much more 2D Gaussian looking than the AOA–TOA technique. In the latter the radial error has a positive bias (away from the BS) due to NLOS positive bias on the TOA measurements. Figure 7.6(a) also highlights the KF overshoot caused by the unrealistic instantaneous direction change of the MS. Thus, especially for the eSBT technique, results may be pessimistic.

Figures 7.5(a),(b) show the performance of the eSBT technique with KF tracking deteriorates rapidly with increasing noise power whereas the AOA–TOA method is much more stable. Figures 7.7(a), (b) show example tracks using the eSBT technique and AOA–TOA technique respectively with high measurement noise power. The measurement noise power in both cases was $\sigma_\alpha^2 = 10^{-1}$, $\sigma_{c\tau}^2 = 10^{3}$ and additionally for the eSBT $\sigma_{f_d}^2 = 10^{-3} f_{dmax}^2$. Here it is clear to see the eSBT technique has broken down due to the high noise levels. The estimated loca-

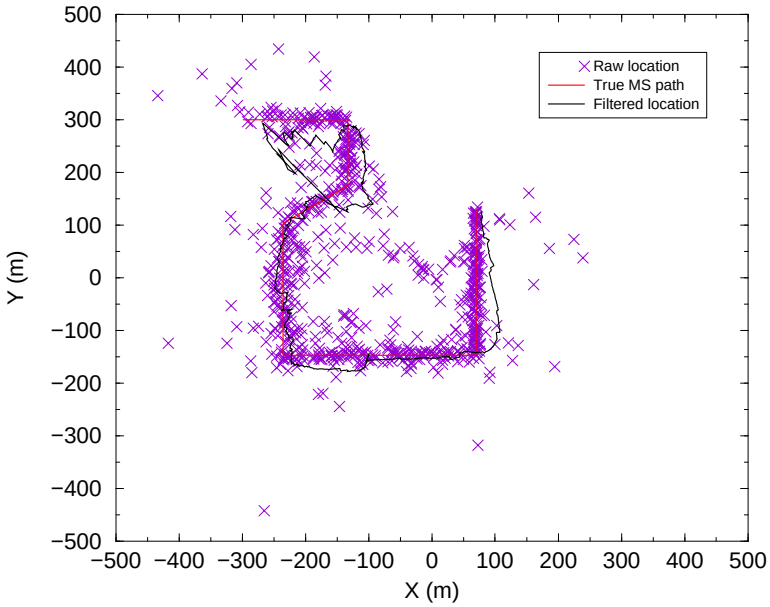

(a)

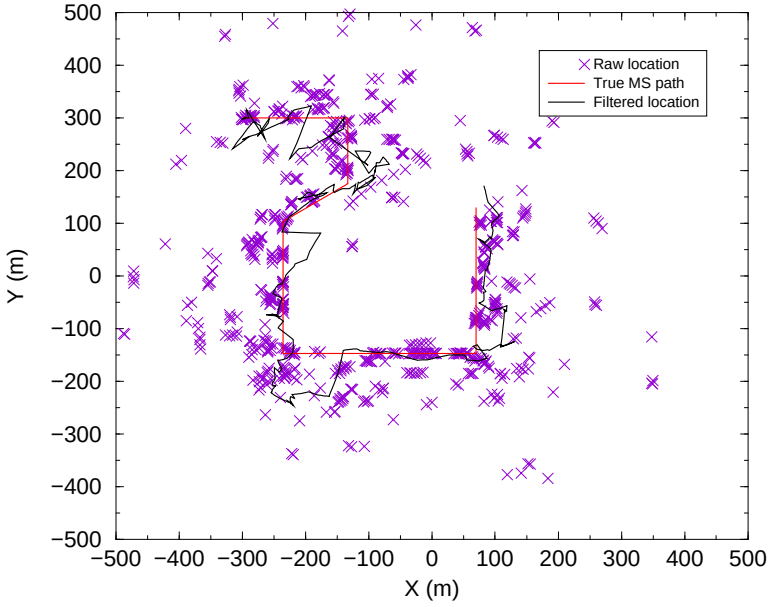

(b)

Figure 7.6: Example location tracks for the (a) eSBT, (b) AOA–TOA techniques with low measurement noise power

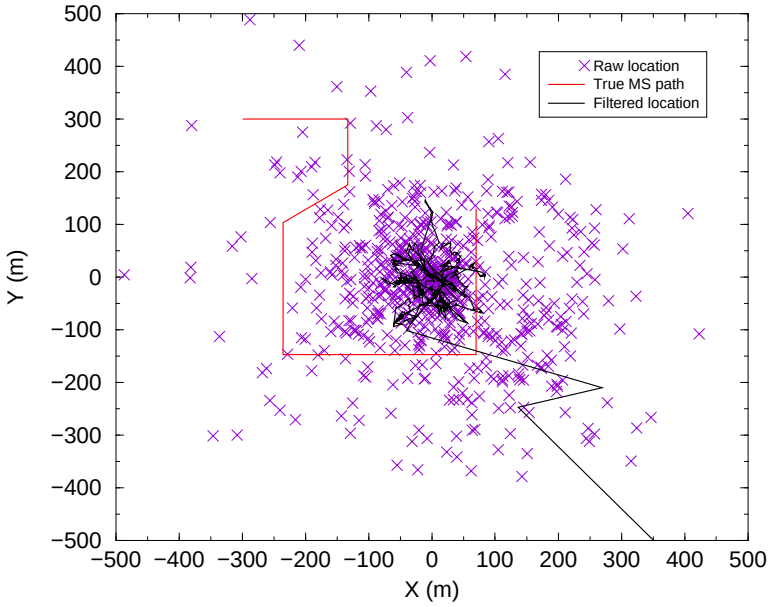

(a)

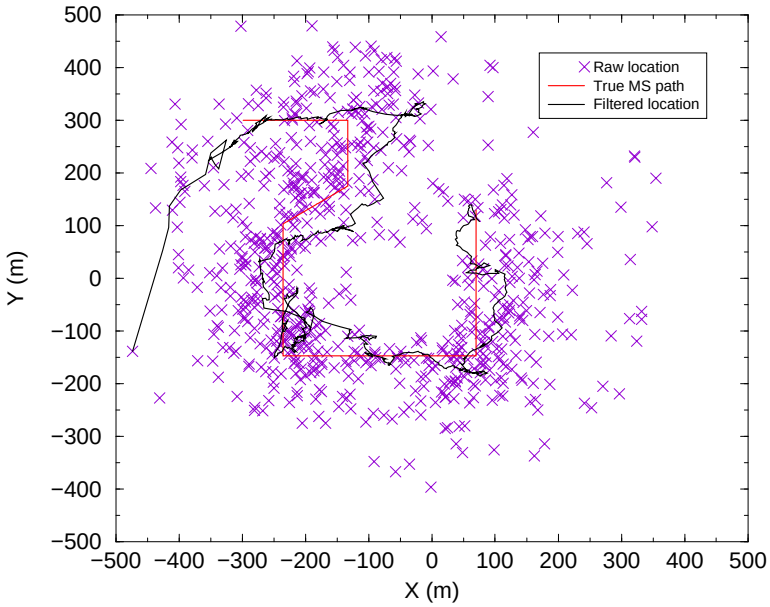

(b)

Figure 7.7: Example location tracks for the (a) eSBT, (b) AOA–TOA techniques with high measurement noise power

tions appear uniformly distributed in angle around the serving BS and bear no relationship to the true MS path. The AOA–TOA technique however is much more robust to the increased noise and a reasonable estimated path is still found. For the AOA–TOA technique the added Gaussian measurement noise has overpowered the NLOS noise and thus the location errors are approximately 2D Gaussian distributed about the true location.

7.3 Refinements to KF operation

There are some simple refinements that can be made to the KF tracker.

7.3.1 KF Tracking with Input Estimation

The noise on individual location estimates is distinctly heavy tailed (i.e. large location errors occur with comparative high frequency). In Figure 7.8 the measured CDF of circular location error (using the previously described simulation environment) is shown for the eSBT estimator with different noise powers.

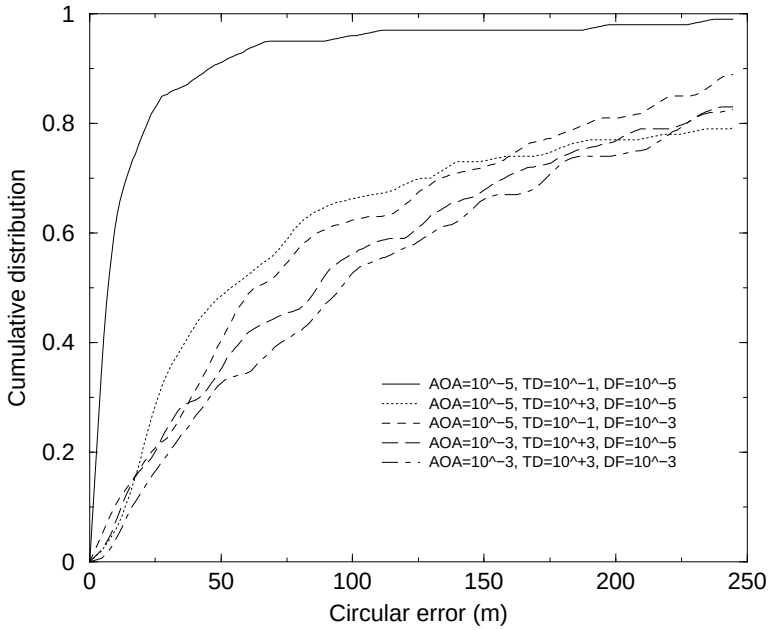

Figure 7.8: The CDF of circular location errors for a selection of measurement noise variances

It can be seen that a heavy tail in the distribution occurs when any one of the noise terms is

high. The reason for this heavy tail is the non–linearity of the estimator. As shown in Figure 7.4 when noise corrupts the measurements the global minimum may no longer be centred near the true solution, in which case the estimated locations are more evenly distributed across the cell. It is impossible to tell from the estimator whether a location is good, i.e. a location that is found in the same minimum as the true solution or bad, i.e. a location that is found in a different minimum. Therefore an input estimator is employed, similar to Section 5.2.1, to try to differentiate between good and bad data by utilising the KF predictor equation to form a likelihood function for the measured data. The measurement noise estimate for the individual location estimates, $\mathbf{R}_n$, then contains diagonal terms

$$\hat{\sigma}_x^2 = \max\left(\sigma_{min}^2, \frac{s_{1/1}}{\exp\left[-\frac{r_x^2}{2s_{1/1}}\right]}\right) \tag{7.11}$$

$$\hat{\sigma}_y^2 = \max\left(\sigma_{min}^2, \frac{s_{2/2}}{\exp\left[-\frac{r_y^2}{2s_{2/2}}\right]}\right) \tag{7.12}$$

where $s_{i,j}$ indicates the element on the ith row and jth column of $S_{n,n-1}$ and r is the residual between the measured parameter Y_n and the filter prediction $X_{n,n-1}$. σ_{min}^2 is the measurement variance including just good measurements, which can be estimated from the data.

7.3.2 Utilising Auxiliary Velocity Information in the KF Tracking

The location estimator produces an estimate for the MS's instantaneous velocity. It is possible to adjust the KF formulation to incorporate this new data.

Figure 7.9 shows the cumulative distribution of the Euclidean velocity estimate error for several values of measurement noise power. It is clear from the curves that the velocity estimate is quite accurate, within 5ms^{-1}, to the 60th percentile even at high noise powers. These velocity estimates may be useful to the KF and can be incorporated by changing the definition of the KF measurement matrices to

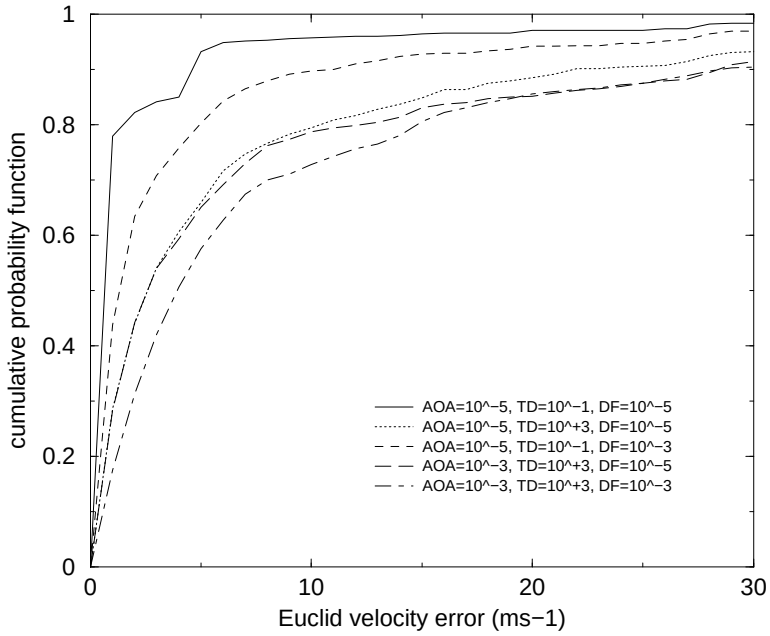

Figure 7.9: The CDF of Euclidean velocity errors for a selection of measurement noise variances

$$\mathbf{Y}_n = \begin{bmatrix} x \\ y \\ \dot{x} \\ \dot{y} \end{bmatrix}, \quad \mathbf{R}_n = \begin{bmatrix} \sigma_x^2 & 0 & 0 & 0 \\ 0 & \sigma_y^2 & 0 & 0 \\ 0 & 0 & \sigma_{\dot{x}}^2 & 0 \\ 0 & 0 & 0 & \sigma_{\dot{y}}^2 \end{bmatrix}, \quad \mathbf{K} = \begin{bmatrix} 1 & 0 & 0 & 0 \\ 0 & 1 & 0 & 0 \\ 0 & 0 & 1 & 0 \\ 0 & 0 & 0 & 1 \end{bmatrix} \tag{7.13}$$

Also apparent from Figure 7.9 is that for a small cumulative probability (10–20%) large velocity errors occur. These errors cause poor tracking performance unless the velocity measurement noise estimates, $\sigma_{\dot{x}}^2$ and $\sigma_{\dot{y}}^2$, are set high, in which case the performance improvement achieved using velocity information is negligible. For this reason an input estimation technique is applied to the velocity estimate again using the predicted velocity to form a measurement likelihood

function. The velocity measurement noise variance can then be calculated as

$$\hat{\sigma}^2_{\dot{x}} = \max\left(\sigma^2_{vmin}, \frac{s_{3/3}}{\exp\left[-\frac{r^2_{\dot{x}}}{2s_{3/3}}\right]}\right) \tag{7.14}$$

$$\hat{\sigma}^2_{\dot{y}} = \max\left(\sigma^2_{vmin}, \frac{s_{4/4}}{\exp\left[-\frac{r^2_{\dot{y}}}{2s_{4/4}}\right]}\right) \tag{7.15}$$

where $r_{\dot{x}}$, $r_{\dot{y}}$ are the differences in the x–axis direction and y–axis direction velocity estimates between the filter prediction $\mathbf{X}_{n,n-1}$ and the measurement $\mathbf{Y}_n$. These terms can be used in the lower diagonal terms of the measurement noise matrix H_n.

7.3.3 Simulation of KF Variants

Three alternative KF tracking implementations were applied to the simulation scenario from Section 7.2: a KF with input estimation (ieKF), a KF utilising auxiliary velocity information (vKF), and a KF with both methods (ie–vKF). (Note that both the vKF and ie–vKF have input estimation on velocity estimates.) Values of $\sigma^2_{min} = 2500$ and $\sigma^2_{vmin} = 25$ were used.

Simulation results show the performance of the KF variants was limited by the error caused by overshoot at the cornering points of the MS path. Thus the actual RMS error performance for the methods is similar. Figures 7.10(a), (b) show examples of the tracking performance with low ($\sigma^2_{f_d} = 10^{-5} f^2_{max}$) and high ($\sigma^2_{f_d} = 10^{-3} f^2_{max}$) Doppler noise respectively. The other noise powers were $\sigma^2_{\alpha} = 10^{-5}$ and $\sigma^2_{c\tau} = 10^{-1}$. In both scenarios the vKF implementation is an improvement over the simple KF in that it is smoother and more accurately captures the shape of the MS path though the RMS location errors are similar. The ieKF and ie–vKF offer further improvement over the simple KF and vKF in the low noise scenario. However in the higher noise scenario the ieKF and ie–vKF tracks tend to diverge from the good locations for some or all of the track. In the case of the ie–vKF the velocity estimates are still accurate thus it keeps a similar but shifted shape to the true MS path.

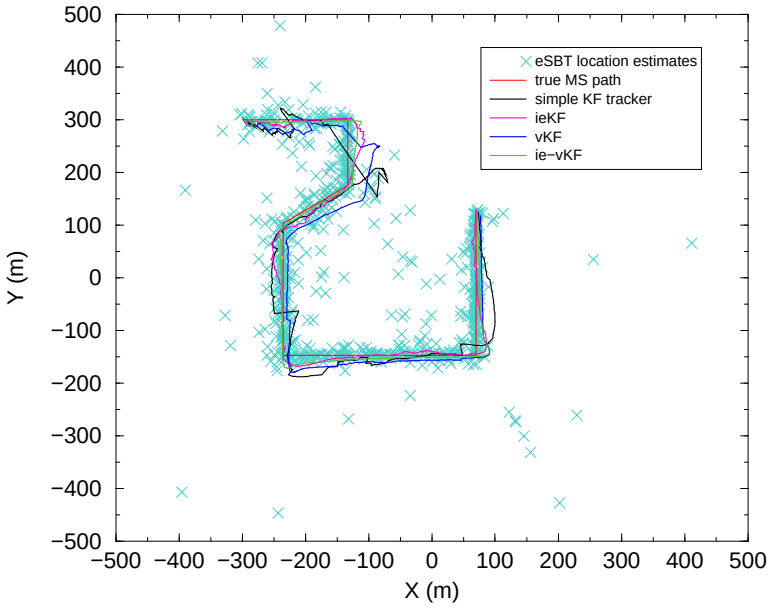

(a)

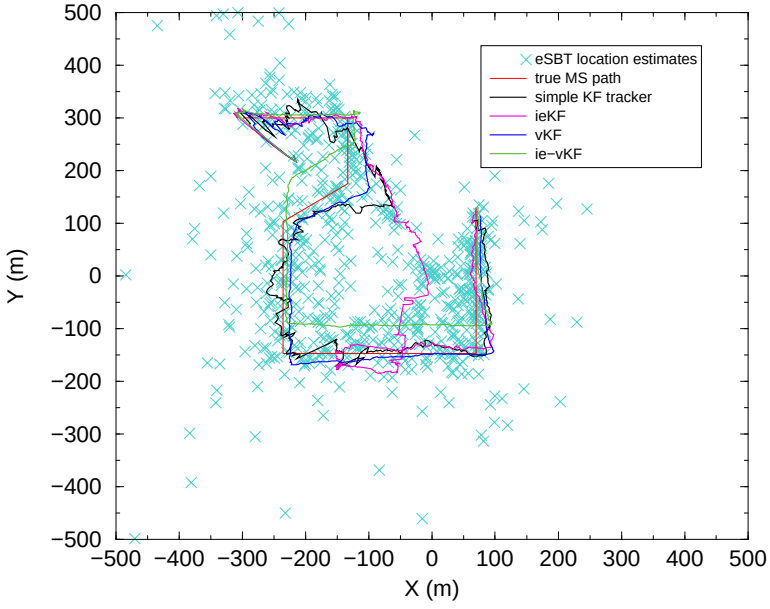

(b)

Figure 7.10: Example location tracks for (a) low, (b) high Doppler noise scenarios with different KF configurations

7.4 Conclusions and Further Considerations

In this chapter a new method for source location in a multipath environment has been presented. The SBT method utilises AOA, TDOA and Doppler shift measurements of individual scatterers and requires measurements from only one BS. Simulation results have shown that the method has the potential to give location accuracy to less than 50m RMS in the presence of low measurement noise power. The performance is significantly better than the performance of other single BS systems that were also presented in this chapter as well as the multiple BS (TDOA/AOA) methods considered in previous chapters. The best performance from the other single BS methods was the First AOA–First TOA with about 50–60m RMS with KF tracking.

In the tracking scenario utilising a KF further improves performance in all methods. Results also seem to suggest that utilising the auxiliary velocity information from the estimator in the KF further improves location accuracy. Additionally the performance of the SBT technique in the tracking scenario is not affected by the P_{LLOS} and spatial correlation properties of the environment in the same way as the conventional triangulation methods which require spatial diversity in measurements to mitigate NLOS errors.

However with increasing noise power the performance of the SBT techniques is much reduced. With $\sigma^2_{f_d} = 10^{-5} f^2_{dmax}\text{Hz}^2$ if $\sigma^2_{\alpha_n} > 10^{-3}\text{rad}^2$ or $\sigma^2_{c\tau_n} > 10^3\text{m}^2$ the performance is worse than the AOA–TOA method. With $\sigma^2_{f_d} = 10^{-3} f^2_{dmax}\text{Hz}^2$, this drops to $\sigma^2_{\alpha_n} > 10^{-4}\text{rad}^2$ or $\sigma^2_{c\tau_n} \geq 10^3\text{m}^2$.

Whether the noise levels simulated are realisable is unclear. It is envisaged that the measured parameters could be tracked using a KF before the estimation stage which would lower the noise variance. Probably the Doppler shift measurement noise would be the most critical. $\sigma^2_{f_d} = 10^{-3} f^2_{dmax}$ corresponds to a standard measurement noise of $0.032 f_{dmax}$. An FFT based method could be used to extract the Doppler frequencies from a large number of samples. Given that in UMTS a minimum of four times oversampling has been proposed, the time resolution will be about 20m. This implies noise variances well below 10^3m^2 could be achieved with a KF. $\sigma^2_{\alpha_n} = 10^{-4}\text{rad}^2$ gives a measurement standard deviation of 0.572^o. Even in conventional triangulation methods this level of accuracy is required to make AOA measurements useful.

There are several further problems to be considered with the SBT method. The simulation model assumed stationary scatterers. Non–stationarity of scatterers can lead to changing Doppler shifts and thus the calculated angle β_n being incorrect. The interaction between scatterers

with paths arriving at the BS temporally and spatially close has not been considered. At best this will skew the measurement noise distribution. At worst the two paths would be unresolvable and this would lead to a falsely identified scatterer. Simulation also omitted the possibility of multiple reflection scatterers. There is no way to account for the multiple reflections in the estimator. However multiple reflection paths would tend to have higher attenuation so initially in choosing scatterers for the estimator scatterers with a low power delay product should be ignored. Finally the carrier frequencies of the BS and MS in practice will not be matched. Generally the MS carrier will be phase locked to the frequency with largest received power. The Doppler shift measurements may therefore include an offset term, f_{do}. This term can be added into the definition of β_n in (7.7) to give

$$\beta_n = \cos^{-1}\left(\frac{(f_{dn} - f_{do})\lambda}{v}\right) \tag{7.16}$$

f_{do} can be either be solved by increasing the number of unknowns in the estimator which is undesirable as more scatterers will be required in the estimator. Alternatively f_{do} can be measured by analysing the Doppler spectrum of the channel and estimating the long term mid point. This technique might also provide an initial estimate for v from the frequency width of the spectrum which could be used to aid the SBT estimator.

Finally the SBT estimator could be aided by the location of known fixed scatterers, e.g. tall buildings in an urban environment. These could be identified by α_n measurements at the BS and the appropriate value of r_n inserted into the equations from a database.

Chapter 8
Conclusions

This thesis has been concerned with the performance of an MS location estimator in a UMTS system. Firstly a channel model suitable for testing location service performance has been implemented with specific attention to the spatial characteristics of the channel. Analysis of hearability with various IPDL techniques has been presented, with suggestions to improve these methods. Location accuracy performance for the TDOA system has been presented with and without spatial filtering, under various different channel scenarios. Further results have been presented for an AOA/TDOA hybrid system. A different method in which incoming rays are backtraced to pinpoint the MS has also been formulated and shown to be a viable alternative in urban scenarios. This chapter draws together the main conclusions of the work. Some suggestions for further work in this field are also presented.

8.1 Summary of the Work

In Chapter 3 a method for modelling spatial variations in LOS and NLOS was developed, based on some reasonable interpretations of the geometry of obstructions likely to present in urban, suburban and rural scenarios. The CoDiT model was used as the basis of this model which provided ratification for the some of the parameters developed. Where available other sources were used to substantiate parameter value choice. The critical statistics of excess delay and AOA of the first arriving path were evaluated and shown to be similar to theoretical models.

In Chapter 4 it was shown that in UMTS the hearability performance will limit the location accuracy of a TDOA based location estimation techniques. Upwards of 20% of MS's would not be able to detect the required 3 BS's. Using IPDL techniques improves matters significantly. A comparison of several such techniques has shown merits for each method. Based purely on hearability TA–IPDL is the best choice, however PR–IPDL has a relaxed synchronisation constraint. The author's own vTA–IPDL proposal also performs well and requires only one pilot code.

Further hearability improvement is possible by increasing the idle period length. However this is not desirable since QoS of real time services would be affected. Therefore the possibility to coherently and non–coherently combine measurements from successive idle periods was investigated. To provide coherent gain the separation of idle periods should be small. Again the minimum separation is limited by QoS considerations. Non–coherent integration is not effected by channel correlation, however selection diversity gain is possible with large shadowing if spatial diversity exists. To gain spatial diversity in shadowing increased separation is desirable. There is a trade off between providing closely spaced idle periods to allow coherent combining for slowly moving MS's and having widely spaced idle periods to increase selection diversity gain for fast moving MS's. Clustered idle periods can be created to take advantage of both situations with an adaptive receiver, giving several dB's gain over selection diversity and non–coherent integration only receivers.

In Chapter 5 the performance of a TDOA location receiver was investigated. Since MPR is employed the signal detection stage requires special consideration of autocorrelation and pulse shaping sidelobes. Iterative subtraction methods proved too sensitive to noise, thus simple thresholding methods were proposed. Location accuracy is very sensitive to P_{LLOS}, decreasing significantly at low P_{LLOS} values, and to a certain extent sensitive to hearability when P_{LLOS} is high. Location accuracy in the urban scenario was found to be worse than required by FCC regulations with reasonable channel parameters. Using spatial filtering the receivers showed location accuracy improvement of minimum 30% and 42% at the 67%ile and 95%ile respectively, sufficient to meet the FCC regulations. The receiver could also operate at much lower instantaneous hearability levels. The KF and LS implementations both seem reasonable candidates for filtering when the MS is moving fast. However at slower speeds averaging works better. As the MS speed is reduced it is necessary to hold the location updating otherwise spatial diversity gains will be lost.

In Chapter 6 the performance of a hybrid AOA/TDOA location receiver was presented under several scenarios. Without spatial diversity to help estimate the LLOS state the performance of such a receiver can be worse than a TDOA only receiver, though it does allow location to be calculated with only 2 BS's hearable. Significant improvement of a minimum 18% and 12% at the 67%ile and 95%ile respectively was achieved with spatial filtering at high speeds. At low speeds distinguishing LOS and NLOS conditions using the AOA time series alone becomes impossible.

In Chapter 7 the SBT method for locating the MS by using the multipath nature of the environment was investigated. Simulation results have shown that SBT has potential to give location accuracy to less than 50m RMS (with a 2D Gaussian noise assumption of the final tracked path this RMS value is approximately 50m at the 67%ile), but is very sensitive to measurement noise. Input estimation as a way of removing outliers is important as location error is a mixture of a low powered 2D Gaussian distribution and a uniform distribution across the cell. Using the auxiliary velocity estimate from the location estimator in the tracking process provides a more accurate track. Most importantly the performance of the SBT technique does not deteriorate with low P_{LLOS} or with large spatial correlation in the environment as the conventional triangulation methods do.

8.2 Suggestions for Further work

There are several areas in which further work could be carried out.

Channel Model A framework for the channel model has been developed, however several parameters values had to be estimated due to the lack of real characterisation of these parameters through real measurements. In particular the probability and length of LOS and NLOS states in urban and suburban areas and the associated NLOS error distributions in timing and bearing require qualification by actual measurement. The next stage after this would be to develop angular correlation models for the various parameters.

LOS/NLOS Detection In this thesis only spatial variation in measurements were used to detect and weight LOS and NLOS measurements. Performance could be enhanced by assisting the prefiltering process with collateral information. In particular the instantaneous shape of delay and azimuth power profiles could be used to determine whether a LOS component is present. Furthermore NLOS correction can never be completely accurate, similarly the weighting process, especially at low speeds when spatial diversity is much reduced. An appealing enhancement would be to generate further weights based on residual rank analysis as proposed in [40], [64].

Measurement Noise In this work genuine detection of signals was used to generate timing measurement noise distribution. However the AOA and Doppler measurement noise was assumed to have a Gaussian distribution with varying power. It would be desirable to

assess the performance of detection algorithms for these measurement types too. This is especially important in the back tracing technique which is highly sensitive to noise.

Statistical Location Methods for NLOS In Chapter 7 one method for robust estimation of the MS location in NLOS using only one BS was presented. This method uses precise geometry to calculate the location and thus is sensitive to noise. However other statistical methods may exist which are also robust to NLOS. Using the circular scatterer model as a basis for the multipath statistics it might be possible to exploit the relationship between angular spread and MS–BS separation. Another idea is to use the fact that the expectation of scatterer to BS separation is the same as the MS–BS separation.

Appendix A
Cramér–Rao Lower Bound Derivations

A.1 Cramér–Rao Lower Bound Calculations

The Cramér–Rao Lower Bound (CRLB), Φ^o, on the accuracy of an estimator for $\mathbf{z}$ is defined as [23]

$$\Phi^o = E\left[\left(\frac{\delta}{\delta \mathbf{z}} \ln p(\mathbf{u}|\mathbf{v})\right)\left(\frac{\delta}{\delta \mathbf{z}} \ln p(\mathbf{u}|\mathbf{v})\right)^T\right]^{-1} \tag{A.1}$$

where $\mathbf{u}$ is the true value of the vector of variables and $\mathbf{v}$ is the measured vector of variables.

Assuming $\mathbf{u}$ is assymptotically Gaussian with respect to $\mathbf{v}$ then

$$p(\mathbf{u}|\mathbf{v}) = \frac{1}{\sqrt{2\pi \mathbf{Q}}} \exp\left(-\frac{(\mathbf{u}-\mathbf{v})^2}{2\mathbf{Q}}\right) \tag{A.2}$$

$$\ln p(\mathbf{u}|\mathbf{v}) = \ln\left(\frac{1}{\sqrt{2\pi \mathbf{Q}}}\right) - \frac{(\mathbf{u}-\mathbf{v})^2}{2\mathbf{Q}} \tag{A.3}$$

where $\mathbf{Q}$ is the covariance matrix of $\mathbf{v}$. Therefore

$$\frac{\delta}{\delta \mathbf{z}} \ln p(\mathbf{u}|\mathbf{v}) = 0 - \frac{\delta}{\delta \mathbf{z}} \frac{\mathbf{u}^2 - \mathbf{u}\mathbf{v} + \mathbf{v}^2}{2\mathbf{Q}} \tag{A.4}$$

$$= -\frac{\delta \mathbf{v}^T}{\delta \mathbf{z}} \frac{-2\mathbf{u} + 2\mathbf{v}}{2\mathbf{Q}} \tag{A.5}$$

$$= \frac{\delta \mathbf{v}^T}{\delta \mathbf{z}} \mathbf{Q}^{-1}(\mathbf{u} - \mathbf{v}) \tag{A.6}$$

Noting that for an RV $\mathbf{z} = \mathbf{G}\varepsilon$, where $\mathbf{G}$ is a non–random matrix and ε is a random error matrix,

$$E[\mathbf{z}\mathbf{z}^T] = \mathbf{G}\mathbf{Q}\mathbf{G}^T \tag{A.7}$$

Therefore, as $(\mathbf{u} - \mathbf{v}) = \varepsilon$,

$$\Phi^o = \left(\frac{\delta \mathbf{v}^T}{\delta \mathbf{z}} \mathbf{Q}^{-1} \mathbf{Q} \mathbf{Q}^{-1} \frac{\delta \mathbf{v}}{\delta \mathbf{z}}\right)^{-1} \quad (A.8)$$

$$= \left(\frac{\delta \mathbf{v}^T}{\delta \mathbf{z}} \mathbf{Q}^{-1} \frac{\delta \mathbf{v}}{\delta \mathbf{z}}\right)^{-1} \quad (A.9)$$

$$= \left(\mathbf{G}^T \mathbf{Q}^{-1} \mathbf{G}\right)^{-1} \quad (A.10)$$

where $\mathbf{G}$ is a matrix containing the partial derivatives of the measured variables with respect to the unknown parameters.

A.1.1 Range Equation

The range equation is

$$r_1^2 = (x - x_1)^2 + (y - y_1)^2$$

$$r_1 = \sqrt{(x - x_1)^2 + (y - y_1)^2} \quad (A.11)$$

Therefore

$$\frac{\delta r_1}{\delta x} = \frac{x - x_1}{\sqrt{(x - x_1)^2 + (y - y_1)^2}}$$

$$= \frac{x - x_1}{r_1} \quad (A.12)$$

Similarly

$$\frac{\delta r_1}{\delta y} = \frac{y - y_1}{r_1} \quad (A.13)$$

A.1.2 Range Difference Equation

The range difference equation is

$$r_{2,1} = r_2 - r_1$$

$$= \sqrt{(x - x_2)^2 + (y - y_2)^2} - \sqrt{(x - x_1)^2 + (y - y_1)^2} \quad (A.14)$$

Therefore

$$\begin{aligned}\frac{\delta r_{2,1}}{\delta x} &= \frac{x-x_2}{\sqrt{(x-x_2)^2+(y-y_2)^2}} - \frac{x-x_1}{\sqrt{(x-x_1)^2+(y-y_1)^2}} \\ &= \frac{x-x_2}{r_2} - \frac{x-x_1}{r_1}\end{aligned} \tag{A.15}$$

Similarly

$$\frac{\delta r_{2,1}}{\delta y} = \frac{y-y_2}{r_2} - \frac{y-y_1}{r_1} \tag{A.16}$$

A.1.3 Bearing Equation

The bearing equation is

$$\alpha_1 = \tan^{-1}\left(\frac{x-x_1}{y-y1}\right) \tag{A.17}$$

Therefore

$$\frac{\delta \alpha_1}{\delta x} = \frac{1}{(y-y_1)\left(1+\frac{(x-x_1)^2}{(y-y_1)^2}\right)} \tag{A.18}$$

and

$$\frac{\delta \alpha_1}{\delta y} = \frac{(x-x1)}{(y-y_1)^2\left(1+\frac{(x-x_1)^2}{(y-y_1)^2}\right)} \tag{A.19}$$

Appendix B
Channel Model Definitions and Derivations

The following general formula [105] applies when determining the joint PDF of two RV's from that of another two RV's,

$$f_{w,z}(w,z) = \frac{f_{p,q}(p,q)}{|J(p,q)|} \tag{B.1}$$

where $|J(p,q)|$ is the determinant of the Jacobian matrix, i.e.

$$\begin{vmatrix} \frac{\delta w}{\delta p} & \frac{\delta w}{\delta q} \\ \frac{\delta z}{\delta p} & \frac{\delta z}{\delta q} \end{vmatrix} = \begin{vmatrix} \frac{\delta p}{\delta w} & \frac{\delta q}{\delta w} \\ \frac{\delta p}{\delta z} & \frac{\delta q}{\delta z} \end{vmatrix}^{-1}$$

B.1 Calculation of Joint (x,y) PDF for CoDiT Model

α_{MS} and $c\tau$ (c is the speed of light) can be expressed in terms of the cartesian coordinates x, y, where d is the MS–BS separation in metres, as

$$\alpha_{MS} = \tan^{-1}\left(\frac{y}{d-x}\right) \tag{B.2}$$

$$c\tau = \sqrt{x^2+y^2} + \sqrt{(d-x)^2+y^2} - d \tag{B.3}$$

The Jacobian matrix elements can be evaluated as

$$\begin{array}{llll} \frac{\delta \alpha_{MS}}{\delta x} & = \frac{y}{(d-x)^2+y^2}, & \frac{\delta \alpha_{MS}}{\delta y} & = \frac{(d-x)}{(d-x)^2+y^2} \\ \frac{\delta c\tau}{\delta x} & = \frac{x}{\sqrt{x^2+y^2}} - \frac{(d-x)}{\sqrt{(d-x)^2+y^2}}, & \frac{\delta c\tau}{\delta y} & = \frac{y}{\sqrt{x^2+y^2}} + \frac{y}{\sqrt{(d-x)^2+y^2}} \end{array} \tag{B.4}$$

For the transformation of $(\alpha_{MS}, c\tau)$ into (x, y) (B.1) can be rewritten as

$$f_{x,y}(x,y) = \frac{f_{\alpha_{MS},c\tau}(\alpha_{MS}, c\tau)}{|J(\alpha_{MS}, c\tau)|} \tag{B.5}$$

$$= \frac{f_{\alpha_{MS}}(\alpha_{MS}) f_{c\tau}(c\tau)}{|J(\alpha_{MS}, c\tau)|} \tag{B.6}$$

$$= \frac{1}{2\pi c(\tau_{max} - \tau_{min})} \left| \frac{\delta \alpha_{MS}}{\delta x} \frac{\delta c\tau}{\delta y} - \frac{\delta \alpha_{MS}}{\delta y} \frac{\delta c\tau}{\delta x} \right| \tag{B.7}$$

noting that in the CoDiT definition α_{MS} and $c\tau$ are independent and uniformly distributed RV's. After some manipulation this gives

$$f_{x,y}(x,y) = \frac{1}{2\pi c(\tau_{max} - \tau_{min})} \left| \frac{y^2 - (d-x)x}{(y^2 + (d-x)^2)\sqrt{x^2 + y^2}} + \frac{1}{\sqrt{(d-x)^2 + y^2}} \right| \tag{B.8}$$

B.2 Calculation of Joint $(\alpha_{BS}, c\tau)$ PDF for the CoDiT Model

To calculate $f_{\alpha_{BS},c\tau}(\alpha_{BS}, c\tau)$ an expression for α_{MS} in terms of α_{BS} is required. This is done by a transformation through the intermediary cartesian coordinates.

Expressions for x and y can be found by solving the intersection of the ellipse with delay $c\tau$, given by

$$\frac{(x - \frac{d}{2})^2}{a^2} + \frac{y^2}{b^2} = 1 \tag{B.9}$$

where

$$a = \frac{d + c\tau}{2}, \quad b = \frac{1}{2}\sqrt{(c\tau)^2 + 2c\tau d}$$

and the equation of the line with AOA α_{BS} at the BS, given by

$$x = \frac{y}{\tan \alpha_{BS}} \tag{B.10}$$

Substituting (B.10) in (B.9) and solving for the +ve root of y, after some manipulation, yields

$$y = \frac{b^2 d \tan \alpha_{BS} + ab \tan^2 \alpha_{BS} \sqrt{\frac{4b^2}{\tan^2 \alpha_{BS}} + 4a^2 - d^2}}{2(b^2 + a^2 \tan^2 \alpha_{BS})}, \quad 0 \leq \alpha_{BS} \leq \pi \tag{B.11}$$

From (B.10) x can be expressed as

$$x = \frac{b^2 d + ab \tan\alpha_{BS} \sqrt{\frac{4b^2}{\tan^2 \alpha_{BS}} + 4a^2 - d^2}}{2(b^2 + a^2 \tan^2 \alpha_{BS})}, \quad 0 \leq \alpha_{BS} \leq \pi \tag{B.12}$$

From (B.2) therefore α_{MS}, after some manipulation, is given by

$$\alpha_{MS} = \frac{\pi}{2} - \tan^{-1}\left(\frac{2d(b^2 + a^2 \tan^2 \alpha_{BS})}{b^2 d \tan\alpha_{BS} + ab \tan\alpha_{BS} \sqrt{\frac{4b^2}{\tan^2 \alpha_{BS}} + 4a^2 - d^2}} - \frac{1}{\tan\alpha_{BS}}\right) \tag{B.13}$$

Noting (B.1), $f_{\alpha_{BS},c\tau}(\alpha_{BS}, c\tau)$ can be expressed as

$$\begin{aligned} f_{\alpha_{BS},c\tau}(\alpha_{BS}, c\tau) &= \frac{f_{\alpha_{MS},c\tau}(\alpha_{MS}, c\tau)}{|J(\alpha_{MS}, c\tau)|} \\ &= f_{\alpha_{MS}}(\alpha_{MS}) f_{c\tau}(c\tau) \left| \frac{\delta\alpha_{MS}}{\delta\alpha_{BS}} \frac{\delta c\tau}{\delta c\tau} - \frac{\delta\alpha_{MS}}{\delta c\tau} \frac{\delta c\tau}{\delta\alpha_{BS}} \right| \\ &= \frac{1}{2\pi c(\tau_{max} - \tau_{min})} \cdot \left| \frac{\delta\alpha_{MS}}{\delta\alpha_{BS}} \right| \end{aligned} \tag{B.14}$$

where

$$\begin{aligned} \frac{\delta\alpha_{MS}}{\delta\alpha_{BS}} = {} & (1 + \tan^2 \alpha_{BS}) \left[\frac{4a^2 d \tan\alpha_{BS}}{g} - \frac{h}{g^2} \left(b^2 d + 2ab \tan\alpha_{BS} \sqrt{e} - \frac{4ab^3}{\tan\alpha_{BS}\sqrt{e}} \right) \right. \\ & \left. + \frac{1}{\tan^2 \alpha_{BS}} \right] / \left[1 + \left(\frac{h}{g} - \frac{1}{\tan\alpha_{BS}} \right) \right] \end{aligned}$$

and

$$\begin{aligned} e &= \frac{4b^2}{\tan^2 \alpha_{BS}} + 4a^2 - d^2 \\ g &= b^2 d \tan\alpha_{BS} + ab \tan\alpha_{BS} \sqrt{e} \\ h &= 2d(b^2 + a^2 \tan^2 \alpha_{BS}) \end{aligned}$$

It is noted that $1 + \tan^2 \alpha_{BS} = \sec^2 \alpha_{BS}$, however this substitution does not lead to any great simplification.

B.3 Calculation of the PDF of α_{BS} for the First Arriving Path in the CoDiT Model

In a similar way to (B.14)

$$\begin{aligned} f^{first}_{\alpha_{BS},c\tau}(\alpha_{BS}, c\tau) &= \frac{f_{\alpha_{MS}}(\alpha_{MS}) f_{ed}(\tau)}{|J(\alpha_{MS}, c\tau)|} \\ &= \frac{1}{2\pi} f_{ed}(\tau) \cdot \left| \frac{\delta \alpha_{MS}}{\delta \alpha_{BS}} \right| \end{aligned} \tag{B.15}$$

Integrating the above over all possible delays leads to

$$f^{first}_{\alpha_{BS}}(\alpha_{BS}) = \frac{1}{2\pi} \int_{\tau_{min}}^{\tau_{max}} f_{ed}(\tau) \cdot \left| \frac{\delta \alpha_{MS}}{\delta \alpha_{BS}} \right| d\tau \tag{B.16}$$

which cannot be derived explicitly.

B.4 CoDiT Model Scenario Definitions

Scatterer	Ω	m_i	α_i	$T_{bi}(\mu s)$	A_i	$q_{ai}q_{bi}$	$\Delta T_i(ns)$
1*	1	15	0*	0	[0,0.7]	[1000,2000]	0
2–20	[0.1,0.6]	1	[0,2π*]	[0,2]	[0,0.9]	[500,1000]	[0,200]

Table B.1: CODIT urban model with added LOS path

Scatterer	Ω	m_i	α_i	$T_{bi}(\mu s)$	A_i	$q_{ai}q_{bi}$	$\Delta T_i(ns)$
1	1	15	0*	0	[0,0.7]	[1000,2000]	0
2–6	[0.1,0.4]	[1,5]	[0,2π*]	[0.1,15]	[0.1,0.1]	[500,1000]	[0,400]

Table B.2: CODIT suburban model

Scatterer	Ω	m_i	α_i	$T_{bi}(\mu s)$	A_i	$q_{ai}q_{bi}$	$\Delta T_i(ns)$
1	1	25	0*	0	[0,0.5]	[1000,2000]	0

Table B.3: CODIT rural model

* changes made to original CoDiT model.

Appendix C
Original Publications

The following papers are included in this Appendix:

Channel Model Implementation for Evaluation of Location Services
presented at the 3G2000 conference in London, UK, March 2000.

A Robust Location Estimator Architecture with Biased Kalman Filtering of TOA Data for Wireless Systems
presented at the ISSSTA2000 conference in New Jersey, USA, September 2000.

Performance of a TDOA–AOA Hybrid Mobile Location System
presented at the 3G2001 conference in London, UK, March 2001.

Analysis of IPDL Patterns for Increased Signal Detection Probability in UMTS
presented at the VTC conference in Rhodes, Greece, May 2001.

Calculation of Mobile Location using Scatterer Information
accepted for publication in IEE Electronics Letters.

CHANNEL MODEL IMPLEMENTATION FOR EVALUATION OF LOCATION SERVICES

N. J. Thomas, D. G. M. Cruickshank, D. I. Laurenson

University of Edinburgh, UK

ABSTRACT

Simulation and evaluation of location services presents a number of new problems in the area of stochastic channel modelling which conventional models do not account for. Such problems are modelling of line of sight (LOS) probabilities, LOS to non–line of sight (NLOS) power ratios, NLOS excess propagation time delay, out of cell radio propagation/coverage, and spatial correlation factors.

A two level channel model which addresses these problems is introduced. Local level effects, based on the CODIT propagation model, and cell level effects are incorporated. LOS probabilities and shadowing effects are treated independently at each level. Several scenarios are developed to model different levels of radiowave propagation between cells, corresponding to flat and hilly terrain.

Simulation results for the two proposed Idle Period Downlink (IDPL) Time Difference of Arrival (TDOA) techniques for UMTS are presented.

INTRODUCTION

Traditional stochastic channel and propagation models were designed to provide typical scenarios for testing mobile communication systems. However realistic simulation of location services requires special consideration of a number of factors.

- Line of sight (LOS) path and corresponding probability of LOS. Non–line of sight (NLOS) conditions will seriously degrade the performance of all types of location techniques (e.g. TDOA, TOA, AOA systems).
- Time of arrival of multipaths with reference to a true LOS path. NLOS timing offsets will cause errors in location estimation using time based systems (e.g. TDOA, TOA systems).
- Dynamic delay and angular profile. NLOS timing errors and NLOS angular errors will not be constant due to dynamic propagation environment.
- Realistic out of cell path loss model and shadowing. Transmission from several sources must be compared at one receiver (or vica versa).
- Spatial correlation factors. The communication channel is correlated over distance.

A simple LOS model and path loss model to address these points, which can be incorporated into the CODIT propagation model [1], are introduced and then simulated. Although the simulation is a downlink TDOA system, the model can be applied to the uplink for both timing and angular measurement based location techniques.

CODIT MODEL

The CODIT model defines the scatterer make up of the terrain. Individual scatterers are characterized by mean power (Ω_i), coherence (Nakagami distribution, m_i), mean incidence angle (α_i) and mean time delay (τ_i). The model can generate a realistic time–varying channel impulse response and angular profile if the scatterers are regenerated after the MS moves a certain distance. This distance can be defined by a normal process (restricted to three standard deviations), N[L_S,$L_S/3$], where L_S is the mean scatterer length. However the LOS 'scatterer' (defined at zero delay) will have different statistics to the other scatterers. For this reason a LOS model is defined.

It is necessary to make some slight adjustments to the CODIT model. Firstly α_i should be defined relative to the LOS direction (i.e. $\alpha_{LOS} = 0$) to facilitate doppler shift and/or arrival angle calculation. Secondly, the urban model does not include a LOS scatterer. Therefore it is redefined according to Table 1 (for parameter definitions see the CODIT report).

PATH LOSS MODEL

Conventionally path loss is modelled by a lognormal distribution around a mean path loss provided by empirical formulae. A single slope path loss with a standard deviation of 8–12dB is usually chosen to cover a wide range of conditions. However if a LOS model is used only the variation of LOS path loss uncertainty should be modelled. A two slope model is employed which models the out of cell propagation more realistically than a single slope model [2]. The breakpoint, R_b, is calculated from:

$$R_b = min(\frac{4h_{BS}h_{MS}}{\lambda}, R_C) \quad (1)$$

Scatterer	Ω	m_i	α_i	$T_{bi}(\mu s)$	A_i	$q_{ai}q_{bi}$	$\Delta T_i(ns)$
1	1	15	0	0	[0,0.7]	[1000,2000]	0
2–20	[0.1,0.6]	1	[0,π]	[0,2]	[0,0.9]	[500,1000]	[0,200]

Table 1: *CODIT urban model with LOS path*

where h_{BS} is the BS height, h_{MS} is the mobile height, R_C is the cell radius, and λ is the carrier wavelength. Here it is assumed that for small cells the transmitters are tilted down to set the breakpoint at the cell radius. This will limit the out of cell propagation for improved capacity but may be detrimental to the performance of the location service.

The required parameters are the two slope indexes, s_1 (before the breakpoint) and s_2 (after the breakpoint) and their corresponding standard deviations, σ_1 and σ_2. The simulation values in Table 3 are derived from measured data reported in [2].

Spatial correlation of the path loss variation is required as the MS moves through the cell. This is modelled by a decreasing exponential autocorrelation function [3] defined by:

$$R_{xx}(\Delta x) = e^{-\frac{|\Delta x|}{L_{PL}} ln\, 2} \tag{2}$$

where L_{PL} is the decorrelation length where $R_{xx}(L_{PL}) = 0.5$. The method for generating this form of correlated Gaussian random variables is well known and defined by a 1st order IIR filter (3).

$$y[i] = y[i-1]p + x[i]\sqrt{1-p^2} \tag{3}$$

where $x[i]$ is a Gaussian distributed random variable, $y[i]$ is the autocorrelated output fed back into the filter, and p is the correlation factor, a function of L_{PL} and the sample frequency.

LOS MODEL

It is important in the simulation of location services to model the LOS/NLOS state of the channel. A LOS signal will tend to be of higher power and accurate for timing and/or angular measurements, thus improving the location estimator accuracy.

Considering Figure 1 it can be seen that the characteristics of the NLOS path(s) (power, absolute delay, arrival angle) change considerably when the location and size of the obstructor, relative to the MS, is changed. Two independent processes are modelled, either (or both) of which can be experienced by an MS at any one instance.

Local LOS (LLOS) model

Scenario 1 (Figure 1) shows an obstructor close to the MS (typically a large building). In this case, non–LLOS (NLLOS), the mechanisms for propagation between MS and BS will be reflections off local scatterers, as defined by the CODIT model, outwith the shadow region of the obstructor. Traversing regions of NLLOS and LLOS can be simulated by the disappearance and appearance of the LOS tap (defined at zero delay) in the CODIT model.

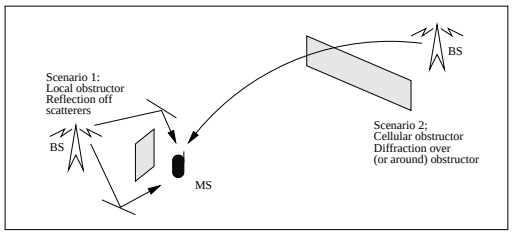

Figure 1: *Local and cellular obstructors.*

To generate the LLOS/NLLOS state sequence the LLOS probability, P_{LLOS}, mean LLOS run length, L_{LLOS}, and associated pdf are defined. In the following simulations the LLOS sequence is generated by re–evaluating the LLOS state (according to P_{LLOS}) and current run length (defined by a normal process (restricted to three standard deviations) N[L_{LLOS},$L_{LLOS}/3$]) each time the MS has travelled the previous run length.

Clearly P_{LLOS} is a quantity defined by the nature of the terrain. As no actual P_{LLOS} measurements have been found it is necessary to estimate the value. For simplicity P_{LLOS} is considered constant with MS–BS separation. L_{LLOS} will depend on the typical width of buildings and roads in urban and suburban areas.

In practice it may be possible to distinguish between LLOS and NLLOS regions by analysing the variance of the timing data [4]. Timing errors caused by NLLOS and multipath conditions can be corrected given enough *a priori* location diversity. [5] use an adjusted least squares fit of the timing data to estimate an unbiased timing.

Cellular LOS (CLOS) model

Scenario 2 (Figure 1) shows an obstructor at distance from the MS (typically a hill ridge). In this case, non–CLOS (NCLOS), it is assumed that a single path diffraction over (or round) the obstructor is the dominant propagation mechanism. Associated with this diffraction will be a change in coherence, attenuation, additional time delay and possible angular deflection which will affect all the local scatterers in

scenario 1 (it is assumed that the shadow of the obstructor is large enough to encompass all the local scatterers). It is important to note that with good cell planning a CLOS obstructor would not exist centrally within a cell, rather at or near the cell boundary and so would typically affect radiowave propagation between cells. A serving BS would be unlikely to be shadowed by such an obstructor.

Again to generate the CLOS/NCLOS state sequence the CLOS probability, P_{CLOS}, mean CLOS run length, L_{CLOS} and associated pdf are defined. The sequence is generated in the same way as the LLOS state sequence.

Three CLOS scenarios have been considered to simulate different radiowave propagation between cells.

Unobstructed – $P_{CLOS} = 1$ for all BS's, i.e. no obstructions between cells.

Partially obstructed – P_{CLOS} is defined by (4) for non–serving BS, $P_{CLOS} = 1$ for serving BS, i.e. flat terrain with some large features.

$$P_{CLOS}(r) = \begin{array}{ll} 1 & r < 1; \\ 1 - \frac{(r-1)}{4} & 1 \leq r \leq 5; \\ 0 & r > 5; \end{array} \quad (4)$$

where r is the MS–BS separation in cell radii.

Obstructed – $P_{CLOS} = 0$ for all but serving BS, $P_{CLOS} = 1$ for serving BS, i.e. all surrounding BS's are obstructed (e.g. by hills).

The value for L_{CLOS} depends on the terrain. In urban areas it might be expected to be the width of the shadow of a large building, in rural the width of the shadow of a hill.

The shadow regions caused by NCLOS conditions have four effects on the channel (all scatterers) experienced by the MS.

Loss of coherence (m_{NCLOS}) The diffracted path can be assumed to contain a summation of diffuse parts caused by the irregularity of the diffraction edge. This has an effect of decreasing the coherence of the path. Within the CODIT model this can be modelled by decreasing the Nakagami–m value of the paths in the CODIT model (towards Rayleigh fading, $m = 1$).

Power attenuation (Ω_{NCLOS}) All paths to the MS will be attenuated. Diffraction theory and measured data suggest the typical range for this attenuation is 0–30dB ([6] p55). In the following simulations a uniform distribution across subsections of this range is used.

Time delay (τ_{NCLOS}) The additional distance travelled round the obstructor causes a delay in the signal arriving at the MS. Typically this will be a small delay (0–1μs). In the following simulations a uniform distribution across subsections of this range is used.

Angular deflection (α_{NCLOS}) There is a possibility of a small angular deflection caused by the obstructor which can be modelled by a Gaussian distribution with a mean of zero degrees.

Ω_{NCLOS} and τ_{NCLOS} will clearly be correlated across their specified ranges. A correlation factor, $C_{\Omega-\tau}$, is used in the following simulations. Each time the MS enters an NCLOS region the four parameters are generated as defined by their pdfs. Transition from CLOS to NCLOS regions are smoothed over the first tenth of the actual CLOS run length.

IPDL SIMULATION

The fundamental problem with all location techniques in CDMA systems is that of hearability (i.e. the ability to 'hear' distant BS's which transmit on the same frequency). One suggestion for UMTS is to insert idle periods in the downlink of the BS. In these periods timing measurements can be made for more distant BS's.

Two slightly different proposals have been made. In pseudo random IPDL (PR–IPDL) each BS goes idle in one of 16 different slots, chosen randomly, in the idle frame [7]. In time aligned IPDL (TA–IPDL) each BS goes idle at the same time in the idle frame [8]. However in TA–IPDL the pilot code or broadcast channel is still transmitted in the idle slot with a certain probability. Both methods require known BS synchronisation offsets.

In following UMTS simulations the pilot codes (transmitted over 1/10 of the slot) are used for the timing measurements. This provides a lower processing gain than using the broadcast channel (continuous), but is much simpler as the pilot code is the same for all BS's. All the BS's are frame aligned at 1/16th slot offsets which allows the source of the received pilot symbols to be identified.

The TA–IPDL system simulated uses idle periods of length two slots and the pilot code transmit probability set to one. In that way at least one totally idle slot length is available to take measurements. In the PR–IPDL system the idle period length is one slot at double the frequency.

Parameter	TA–IPDL	PR–IPDL
Idle frame frequency (Hz)	5	10
Idle period length (slots)	2	1
Pilot transmit probability	1	NA
Idle guard length (slots)	0.1	0.1
System capacity loss (%)[1]	0.6875	0.75

Table 2: *IPDL parameters*

Receiver architecture and parameter settings

A simple receiver structure is implemented, consisting of a

[1] not including additional signalling required.

matched filter, square law envelope detector, and threshold detector. Trailing multipaths are removed from the output of the threshold detector and the remaining leading edges assigned to the most likely BS. Timing data is collected each idle slot over the one second run time and the earliest arriving path for each BS used as the final timing data for the location estimator. This assumes that the MS is approximately stationary over the one second, but provides some multipath and LLOS diversity as the channel will not be stationary. No knowledge of the timing error process variance is assumed in the location estimator and no *a priori* location data is available for Kalman filtering.

The simulation uses a hexagonal array of 16 cells for urban and suburban areas and 7 cells for rural areas. The MS is randomly placed in the area of the central BS cell with a random bearing. After one second the location is evaluated. This is simulated 50 times per terrain/scenario. It should be noted that in this short run time little spatial diversity of LLOS and CLOS effects will occur. The SNR value is the ratio of the average LOS power of the pilot channel at the cell boundary to the noise floor (considered constant over the cell).

TA–IPDL simulation results for different values of P_{LLOS} for the partially obstructed urban and suburban scenarios are also presented (the CODIT model does not allow for NLLOS in the rural setting).

Tables 3, 4, 5 shows the system, terrain specific and scenario specific parameters.

Results and Discussion

The results (Figure 2) show that for both the unobstructed and partially obstructed scenarios the IPDL method can probably perform at or above the original FCC E911 mandate [9] of $<$125m 67% of the time (these accuracy requirements have since been tightened). The hearability of BS's in the obstructed scenario drops to below that required for the TDOA location estimate. In the case of the urban scenario the cell scale is small enough that the location error may still be tolerable (just below the FCC E911 mandate level).

The TA–IPDL results are much better than the PR–IDPL results. The main reason for this is that the mean number of BS's hearable was below 3 for PR–IPDL. In this method clearly the probability of 'hearing' three BS's is affected by the probability of the two closest BS's going idle at the same time. In this case this probability is $1/16$, which gives the probability of this event happening at least once in the simulation as $1-(15/16)^{10}=0.476$. Simulating a longer run time would improve the PR–IPDL results, however there will always be an inherent problem of low measurement availability. For this reason TA-IPDL should be prefered as more timing data measurements will be possible because BS interference is not a (major) factor.

It can be seen that increasing hearability beyond a certain

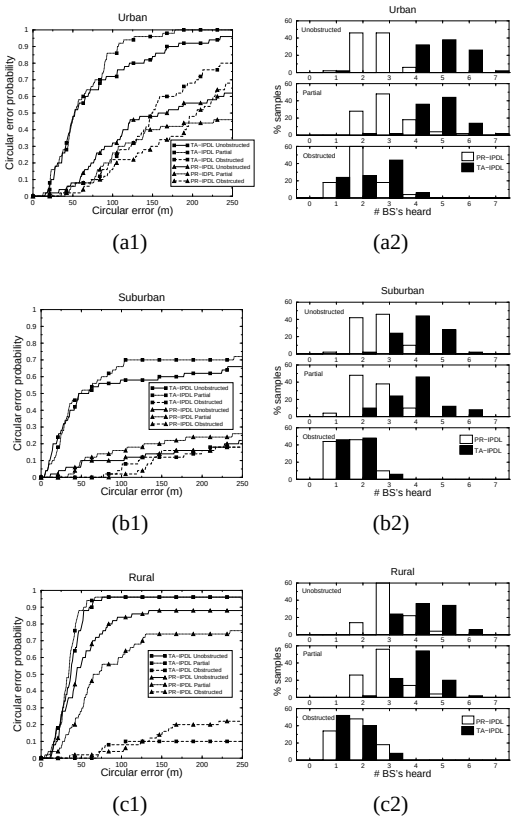

Figure 2: *Circular error and hearability results for different scenarios*

level (3–5 BS's) reduces the accuracy of the estimator (notice the partially obstructed scenario outperforms the unobstructed scenario for TA–IPDL, Figure 2 (a1,b1,c1)). This is due to an increased probability of using measurements corrupted by NLLOS/NCLOS errors. This suggests that reducing the set of data at the input to the location estimator based on an LLOS state estimate will be beneficial.

The results in Figure 3 show the high sensitivity of location error to the P_{LLOS} parameter for the suburban model which has a higher delay spread than the urban. In the urban model there are so many scatterers that usually the first detected path occurs quite close to zero delay. Hearability is also affected slightly in the suburban environment due to the loss of the LLOS path.

CONCLUSION

A channel model implementation suitable for evaluation of location services has been demonstrated. As the statistics of the LOS states and their properties are not known it is necessary to make intuitive estimates or carry out simulation over a wide range of values.

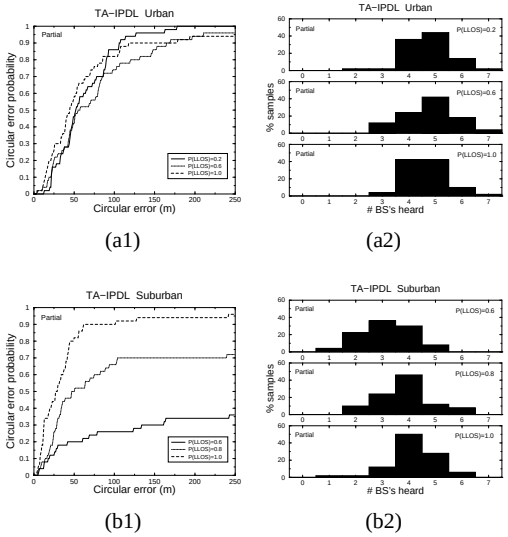

Figure 3: P_{LLOS} *sensitivity results*

It is clear from the simulation results that the LLOS and CLOS states have a great effect on the performance of the location estimator and therefore should be considered carefully. The results suggest that hearability in hilly rural and suburban areas may be a problem. The location accuracy figures provide a lower bound on location accuracy performance. To improve on the performance the receiver must be adapted to take advantage of the spatial diversity of the multipath, LLOS and CLOS states. With suitable LLOS state estimation, NLLOS mitigation and Kalman filtering this should be be possible.

An improvement to the model would be to include angular correlation of path loss variation and LOS states. Parameter sensitivities, development of a more robust receiver architecture, and doppler tracking techniques are areas of future research.

References

[1] Perez and Jimenez (editors). CODIT Final Propagation Model. Technical report, Telefonica, 1994.

[2] Seungwook Min and Henry L. Bertoni, "Effect of Path Loss Model on CDMA System Design for Highway Microcells", presented at *VTC*, pages 1009–1013, 1998.

[3] M. Gudmundson, "Correlation Model for Shadow Fading in Mobile Radio Systems", *Electronic Letters*, vol. 27, no. 23, pp. 2145–2146, November 1991.

[4] Joan Borras, Paul Hatrack, and Narayan B. Mandayan, "Decision Theoretic Framework for NLOS Identification", presented at *VTC*, vol. 2, pages 1583–1587, 1998.

[5] M. Wylie and J. Holtzmann, "The Non–Line of Sight Problem in Mobile Location Estimation", presented at *Proc. IEEE ICUPC*, pages 827–831, 1996.

[6] Lars Ahlin and Jens Zander, *Principles of Wireless Communications*. Studentlitteratur, 1998.

[7] Ericsson. Recapitulation of the IPDL positioning method, TSGR1#4(99)346. Technical report, 3GPP, 1999.

[8] Motorola. Time Aligned IPDL positioning technique, TSGR1#7(99)b79. Technical report, 3GPP, 1999.

[9] FCC. Report WT 97–43 E911 Calls. Technical report, FCC, 1997. http://www.fcc.gov/Bureaus/Wireless/News_Release/1997/nrw17048.txt.

Parameter	Value
Carrier frequency	1.92GHz
Chip rate	3.86Mchips/s
Over sampling rate	4
Modulation scheme	QPSK
Slot frequency	1600Hz
Pilot length	256 chips
Pilot transmit power (% of total)	20%
Pilot SNR	0dB
Time resolution	1/64 chip
Max. frame desynchronisation	0 chips
Pulse shaping roll off rate (α)	0.22
h_{MS}	2m
s_1,σ_1	3.0, 2.6
s_2,σ_2	6.0, 5.8
$C_{\Omega-\tau}$	0.8
m_{NCLOS}	5

Table 3: *System parameters*

Parameter	Rural	Suburban	Urban
CODIT model	rural	suburban	urban
R_C (km)	10.0	2.0	0.5
h_{BS} (m)	50.0	30.0	30.0
L_S (m)	NA	20	5
L_{PL} (m)	20	20	5
P_{LLOS}	1.0	0.8	0.2
L_{LLOS} (m)	NA	30	15
L_{CLOS} (m)	1000	200	50
MS speed (kmph)	150	50	5

Table 4: *Terrain specific parameters*

Parameter	Unobst.	Partial	Obstructed
P_{CLOS} (serving BS)	1	1	1
P_{CLOS} (other BS's)	1	see (4)	0
NCLOS shadow (dB)	NA	U[0,10]	U[10,20]
NCLOS delay (μs)	NA	U[0.0,0.4]	U[0.2,0.8]

Table 5: *Scenario specific parameters*

IEEE 6th Int. Sypm. on Spread-Spectrum Tech. & Appli., NJIT, New Jersey, USA, Sept. 6-8, 2000

A Robust Location Estimator Architecture with Biased Kalman Filtering of TOA Data for Wireless Systems

N. J. Thomas, D. G. M. Cruickshank and
D. I. Laurenson
Department of Electronics & Electrical Engineering,
University of Edinburgh, UK
e-mail: njt@ee.ed.ac.uk

Abstract — **This paper presents a robust location estimator architecture for a time difference of arrival (TDOA) system, which mitigates non–line of sight (NLOS) and multipath errors, using biased Kalman filtering of time of arrival (TOA) estimates. With additional Kalman filtering of location estimates a high degree of location accuracy is demonstrated. Simulations of an idle period downlink (IPDL) UMTS system give accuracy to within 50m at the 67th percentile for most scenarios.**

I. Introduction

In wireless systems the need for accurate location estimation has been motivated by the US FCC's E911 mandate for emergency services [1], as well as customer services (e.g. fleet navigation, location billing), and network aspects (e.g. improved traffic management).

Recent location estimation proposals incorporate either angle of arrival (AOA), signal strength, and timing (TOA or TDOA) measurements or a combination of the three to solve the location function.

Whichever methods are used it is clear that the mobile communication air interface does not provide an ideal environment for making such measurements, to provide the required location accuracy (e.g. FCC require <100m 67% and <300m 95% of the time for network based solutions). The main problem is that of NLOS scenarios. In these conditions communication is maintained via multipaths. However multipaths will have a different trajectory and path length to the line of sight (LOS) path, which will cause errors in the final location accuracy. These errors will be spatially correlated, potentially over large distances, and often biased in nature. A further problem is lack of data in systems which require measurements from more than one base station (BS).

Clearly these considerations need to be addressed when designing a receiver architecture. A generalised location estimator architecture is shown in Figure 1. The measurement data is fed into a preprocessor which attempts to unbias and/or smooth it[1]. The corrected data is then used to calculate the location estimate by the location function. A tracking filter is then used on the location estimates to provide a final time continuous motion.

In this paper a robust location estimator architecture for TDOA measurements, based on the general architecture previously described, is introduced. Simulation results for measurements from a time aligned idle period downlink (TA–IPDL) [2] UMTS system are presented.

[1]Timing and signal strengths measurements will always have a positive bias in NLOS conditions. Angular measurements will have an unbiased mean and so probably need only be smoothed.

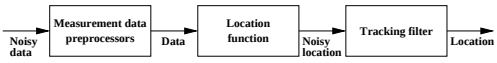

Figure 1: *Generalised location estimator architecture.*

II. Overview of Kalman filter operation

A Kalman filter is a tracking filter that allows for an uncertainty in the target motion by adding a random acceleration component, $\mathbf{u}_n$, between measurement samples [3]. In matrix notation

$$\mathbf{X}_n = \mathbf{\Phi}\mathbf{X}_{n-1} + \mathbf{U}_n \tag{1}$$

where $\mathbf{X}_n = [\ \mathbf{x}_n \quad \dot{\mathbf{x}}_n\ ]^T$ is the state vector and $\mathbf{\Phi} = \begin{bmatrix} \mathbf{I} & \Delta t\mathbf{I} \\ \mathbf{0} & \mathbf{I} \end{bmatrix}$ is the state transition matrix, where Δt is the sample time, and $\mathbf{U}_n = [\ \mathbf{0} \quad \mathbf{u}_n\ ]^T$ is the dynamic model driving noise vector.

Equations (2–6) define the recursive operation of the filter.

$$\hat{\mathbf{X}}_{n,n-1} = \mathbf{\Phi}\hat{\mathbf{X}}_{n-1,n-1} \tag{2}$$

$$\hat{\mathbf{S}}_{n,n-1} = \mathbf{\Phi}\hat{\mathbf{S}}_{n-1,n-1}\mathbf{\Phi}^T + \mathbf{Q}_u \tag{3}$$

$$\mathbf{H}_n = \hat{\mathbf{S}}_{n,n-1}\mathbf{K}^T[\mathbf{R}_n + \mathbf{K}\hat{\mathbf{S}}_{n,n-1}\mathbf{K}^T]^{-1} \tag{4}$$

$$\hat{\mathbf{X}}_{n,n} = \hat{\mathbf{X}}_{n,n-1} + \mathbf{H}_n[\mathbf{Y}_n - \mathbf{K}\hat{\mathbf{X}}_{n,n-1}) \tag{5}$$

$$\hat{\mathbf{S}}_{n,n} = \hat{\mathbf{S}}_{n,n-1} - \mathbf{H}_n\mathbf{K}\hat{\mathbf{S}}_{n,n-1} \tag{6}$$

where $\mathbf{Y}_n$ is the measured data vector, $\hat{\mathbf{S}}_{n,n}$ is the covariance matrix of $\hat{\mathbf{X}}_{n,n}$, $\mathbf{K} = [\ \mathbf{I} \quad \mathbf{0}\ ]$, $\mathbf{R}_n = [\sigma_x^2\mathbf{I}]$, is the covariance matrix of the measurement noise vector, $\mathbf{n}_x$, $\mathbf{Q}_u = \begin{bmatrix} \mathbf{0} & \mathbf{0} \\ \mathbf{0} & \sigma_u^2\mathbf{I} \end{bmatrix}$, is the covariance matrix of $\mathbf{U}_n$.

The output state vector, $\hat{\mathbf{X}}_{n,n}$, is calculated from a variance weighted sum, set by the Kalman gain, $\mathbf{H}_n$, of the filter prediction, $\hat{\mathbf{X}}_{n,n-1}$, based on the previous state vector output and the current measured data, $\mathbf{Y}_n$.

In practice the variance of $\mathbf{u}_n$, σ_u^2, and the variance of $\mathbf{n}_x$, σ_x^2, may not be known so should be estimated.

III. Overview of proposed location estimator architecture

Figure 2 shows the proposed location estimator architecture. The measured TOA data streams[2], $\tau_{1..N}$, for

[2]Note that these TOA's may be relative to an arbitrary reference which need not reflect the true MS–BS separation.

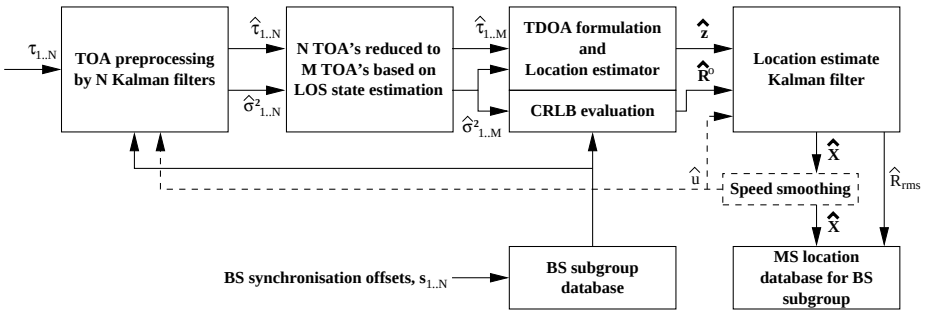

Figure 2: *Location estimator architecture.*

each of N BS's, including corrupting noise, are each fed into an biased Kalman filter which estimates the true uncorrupted TOA, $\hat{\tau}_{1..N}$, and provides the estimated variance of $\hat{\tau}_{1..N}$, $\hat{\sigma}^2_{1..N}$. The set of N TOA estimates is reduced to M by selecting only the data from those BS's estimated to be LOS. The reduced data set is then converted to TDOA's (incorporating any measured synchronisation offsets between BS's) and fed into the minimum variance location estimator. The location estimate, $\mathbf{z}^0$, can be used to determine the Cramér-Rao lower bound (CRLB), $\mathbf{R}^0$, the estimated accuracy of the estimate with the given input variances $\hat{\sigma}^2_{1..M}$. $\mathbf{z}^0$ and $\mathbf{R}^0$ are fed into one last Kalman filter to give the final smoothed location estimate, $\hat{\mathbf{X}}^{final}$, and estimated rms error, $\hat{R}^{final}_{rms}$. Feedback of the smoothed velocity estimator is required to optimally set some of the Kalman filter parameters.

IV. Biased Kalman filtering of measured TOA data

Measured TOA data may be corrupted by several stochastic independent processes: NLOS errors, τ_{NLOS}, sampling quantisation errors, τ_n, and noise caused by a false alarm in the TOA measuring device. Neglecting the false alarm errors for the meantime, the expectation of the error in the measured TOA can be expressed as

$$\begin{aligned} E[\tau(n) - \tau_{true}(n)] &= E[\tau_n] + E[\tau_{NLOS}] + E[\tau_g] \\ &= 0 + \mu_{NLOS} + \mu_g \end{aligned} \tag{7}$$

where $\tau_{true}(n)$ is the expected arrival time according to the LOS mobile (MS) to base station (BS) separation at time $n\Delta t$ and μ_{NLOS} is the non–stationary *positive* mean NLOS error. τ_g is an additional positive mean error term which includes errors due to lack of z-dimension in calculation, atmospheric effects, highly reflective environments, etc... where $\mu_g \ll \mu_{NLOS}$. The variance of the error in the measured data can be expressed as

$$\sigma^2_\tau = \sigma^2_n + \sigma^2_{NLOS} + \sigma^2_g \tag{8}$$

where the sampling noise is uniform over ± 0.5 samples, giving $\sigma^2_n = \frac{1}{12}$. Ideally the μ_{NLOS} term should be eliminated from $\tau(n)$. [4] use an adjust least squares fit of $\tau(n)$ to estimate μ_{NLOS}. However simulations using this method were found to be unstable unless a significant delay was introduced into the estimator and the estimated unbiased $\hat{\tau}(n)$ series was interpolated rather than extrapolated from the data. A Kalman filter is advantageous because it provides a real time parameter estimate and parameter covariance matrix.

A Kalman filter is used to provide 2nd order of tracking of $\tau(n)$ (1D) giving $\mathbf{X}_n = [\ \tau(n) \quad \dot{\tau}(n)\ ]^T$.

Under normal operation a Kalman filter used to track the TOA's will tend towards the mean defined in (7) which is the minimum variance solution to the stochastic process. However using the knowledge that μ_{NLOS} is always positive it is possible to partially cancel the NLOS bias by biasing the filter towards early (low) TOA's. In terms of the Kalman filter formulation this is achieved by asymmetrical weighting of the measurement noise variance estimate $\hat{\sigma}^2_x$ on a sample by sample basis depending on whether $\tau(n)$ is earlier or later than the filter prediction $x_{n,n-1}$, or in equation form

$$\begin{aligned} \sigma^2_x &= \frac{s_{1/1}\sqrt{2\pi(s_{1/1}+\hat{\sigma}^2_g)}}{P(\mathbf{Y}_n|\hat{\mathbf{X}}_{n,n-1})} \quad \text{if } \hat{\tau}_{err}(n) \geq \sigma_s \\ &= s_{1/1} \quad \text{otherwise} \end{aligned} \tag{9}$$

where

$$P(\mathbf{Y}_n|\hat{\mathbf{X}}_{n,n-1}) = \frac{1}{\sqrt{2\pi(s_{1/1}+\hat{\sigma}^2_g))}} e^{-\frac{\hat{\tau}_{err}(n)^2}{2(s_{1/1}+\hat{\sigma}^2_g)}}$$

where $s_{1/1} = \mathbf{K}\hat{\mathbf{S}}_{n,n-1}\mathbf{K}^T$, $\hat{\tau}_{err}(n) = \mathbf{Y}_n - \mathbf{K}\hat{\mathbf{X}}_{n,n-1}$, $P(\mathbf{Y}_n|\hat{\mathbf{X}}_{n,n-1})$ is the probability that $\mathbf{Y}_n$ is the true LOS TOA given the estimate $\hat{\mathbf{X}}_{n,n-1}$ assuming that the true LOS TOA is Gaussian distributed, with variance $s_{1/1} + \hat{\sigma}^2_g$, around the filter prediction $\hat{\mathbf{X}}_{n,n-1}$. σ_s is the maximum expected deviation of the uniform sampling process. In this way the filter optimally disregards the

TOA data which is NLOS corrupted for as long the certainty in the prediction allows.

Additionally if $\hat{\tau}_{err}(n) < -\sigma_s$ the filter outputs are forced to reflect $\tau(n)$, i.e. $x_{n,n}$ is set to $\tau(n)$ (note the velocity estimate $\dot{x}_{n,n}$ is still valid). Furthermore if this difference is larger than a threshold, $\sigma_e rr$, the filter prediction must be so badly wrong that estimates of $\dot{x}_{n,n}$ and its variance will also be inaccurate so should be reinitialised.

Finally it should be noted that (9) means that the filter is extremely sensitive to noise generated by false alarms in the TOA measurement device causing $\hat{\tau}_{err}(n) < -0.5$. Discarding TOA data under the following condition works well at desensitising the filter to reasonable false alarm probabilities.

$$((|\tau(n) - \tau(n-1)| > \sigma_e) \&\& (\hat{\tau}_{err}(n) < -\sigma_e)) \qquad (10)$$

where σ_e is the maximum allowable deviation to noisy TOA's, which should account for the likely multipath delay spread and MS motion.

$\hat{\sigma}_g^2$ is added to the output variance estimate $\hat{\sigma}_\tau^2$.

V. LOS state estimation and dataset reduction

To improve the location estimation data reduction from N data sets to M data sets, based on the $\hat{\sigma}_\tau^2$ variance estimates may be useful, when the location function is over determined (e.g. for a TA–IPDL system typically 3–6 BS's can be heard at any one time ([2],[5]).

The strategy investigated requires to estimate the LOS state to each BS and reduce the data set to those only LOS (minimum 3 BS's). Assuming no a priori knowledge of the NLOS measurement error pdf the best strategy is a simple variance threshold test [6], of the form

$$\begin{array}{ll} H_0 \text{ :LOS condition} & \hat{\sigma}_\tau^2 \leq \gamma \hat{\sigma}_n^2 + \hat{\sigma}_g^2 \\ H_1 \text{ :NLOS condition} & \hat{\sigma}_\tau^2 > \gamma \hat{\sigma}_n^2 + \hat{\sigma}_g^2 \end{array} \qquad (11)$$

Clearly as $\gamma \to \infty$ there will be no reduction, and as $\gamma \to 0$ there will be reduction to the best 3 BS's.

VI. Location estimator and Cramér Rao lower bound (CRLB)

A time difference vector, $\mathbf{\Delta}\hat{\tau}(n)$, and covariance matrix, $\mathbf{Q}$, can be formed from $\hat{\tau}(n)$ and $\hat{\sigma}_\tau^2$, defined as

$$\mathbf{\Delta}\hat{\tau}(n) = \begin{bmatrix} \hat{\tau}_1(n) - \hat{\tau}_2(n) - s_{1,2} \\ .. \\ \hat{\tau}_1(n) - \hat{\tau}_M(n) - s_{1,M} \end{bmatrix},$$

$$\mathbf{Q} = \begin{bmatrix} \hat{\sigma}_{\tau 1}^2(n) + \hat{\sigma}_{\tau 2}^2(n) & .. & \hat{\sigma}_{\tau 1}^2(n) \\ .. & & .. \\ \hat{\sigma}_{\tau 1}^2(n) & .. & \hat{\sigma}_{\tau 1}^2(n) + \hat{\sigma}_{\tau M}^2(n) \end{bmatrix}$$

where $s_{i,j}$ represents the measured synchronisation offset between BS_i and BS_j.

The most likely MS location, $\mathbf{z}^0(n)$, can be found from the $M-1$ time difference hyperbolae defined by

$$\begin{array}{l} r_2 - r_1 = c\Delta\hat{\tau}_{2,1}(n) \\ .. \\ r_M - r_1 = c\Delta\hat{\tau}_{M,1}(n) \end{array} \qquad (12)$$

where r_i is the distance between the MS at (x, y) and BS_i at (x_i, y_i). Chan's method [7] is used which yields a solution close to the lower bound described below. This lower bound is used subsequently as a measure of confidence in the location estimate.

The Cramér Rao lower bound (CRLB), $\mathbf{R}^0$ is a lower bound on the accuracy of the estimate, $\mathbf{z}^0$, given the unbiased measurement vector, $\mathbf{d}$, and its associated covariance matrix, $\mathbf{Q}$, and is given by

$$\mathbf{R}^0 = \left(E\left[\left(\frac{\delta}{\delta \mathbf{z}} \ln p(\mathbf{d}|\mathbf{z}) \right) \left(\frac{\delta}{\delta \mathbf{z}} \ln p(\mathbf{d}|\mathbf{z}) \right)^T |_{\mathbf{z}=\mathbf{z}^0} \right] \right)^{-1} \qquad (13)$$

where $\mathbf{d} = \mathbf{\Delta}\hat{\tau}(n)$.

Under a Gaussian assumption[3] for the distribution of $\mathbf{\Delta}\tau(n)$ the conditional probability function can be evaluated and $\mathbf{R}^0$ is given by [7]

$$\mathbf{R}^0 = c^2 \left(\mathbf{G}\mathbf{Q}^{-1}\mathbf{G}^T \right)^{-1} \qquad (14)$$

where

$$\mathbf{G} = \begin{bmatrix} \frac{(x_1 - x^0)}{r_1^0} - \frac{(x_2 - x^0)}{r_2^0} & \frac{(y_1 - y^0)}{r_1^0} - \frac{(y_2 - y^0)}{r_2^0} \\ .. & .. \\ \frac{(x_1 - x^0)}{r_1^0} - \frac{(x_M - x^0)}{r_M^0} & \frac{(y_1 - y^0)}{r_1^0} - \frac{(y_M - y^0)}{r_M^0} \end{bmatrix}$$

VII. Location Kalman filter

An orthodox 2D 2nd order Kalman filter is used to track the location estimates. Successful use of such a filter has been reported in [8].

The observation inputs, $\mathbf{Y}$ and $\hat{\mathbf{R}}$, are equated to $\mathbf{z^0}$ and $\mathbf{R}^0$ (the outputs of the location and CRLB estimator) respectively. The output $\hat{\mathbf{X}}_{n,n}^{final}$ is the final location and velocity estimate which could then be stored in an MS location database. The final rms error confidence, $\hat{R}_{rms}^{final}$, is given by the square root of the sum of the first two diagonal terms of $\hat{\mathbf{S}}_{n,n}^{final}$.

VIII. Simulation

A UMTS system incorporating TA-IPDL was simulated. Cells were arranged in a hexagonal grid around the serving BS. A variation of the CODIT propagation model [9] incorporated a LOS model described in [5] was simulated. The closest (serving) BS was considered to have a reasonable link, only obstructed by objects local to the MS with probability $(1 - P_{LLOS})$. More distant BS have a probability, that increases with MS–BS separation, of being shadowed by a major obstructor as well as the same probability, $(1 - P_{LLOS})$, of being obstructed locally. Timing measurements are made from the pulsed pilot channel during idle periods when all BS's stop transmitting traffic channels. Table 3 shows the system parameters.

Four scenarios were simulated: fast car in rural terrain (150kmph, curve, 90 seconds), car travelling in suburban

[3] In fact the true pdf of $\mathbf{\Delta}\tau(n)$ has significant outliers.

terrain (50kmph, zig–zag, 90 seconds), car travelling in urban terrain (50kmph, zig–zag, 60 seconds), and pedestrian walking in urban terrain (5kmph, zig–zag, 140 seconds). Table 4 shows the scenario dependent parameters. Five statistically identical runs at each scenario were made.

$\mathbf{\Phi}$, $\mathbf{K}$ and an initial value, $\mathbf{S}_{0,0}$, for the biased Kalman filters are

$$\mathbf{\Phi} = \begin{bmatrix} 1 & \Delta t \\ 0 & 1 \end{bmatrix}, \mathbf{K} = \begin{bmatrix} 1 & 0 \end{bmatrix},$$

$$\mathbf{S}_{0,0} = \begin{bmatrix} 10000 & 0 \\ 0 & 0.77 \end{bmatrix}$$

where the variance (samples^2) in $\mathbf{S}_{0,0}$ is initially set high so the measurement data is initially favoured. σ_u^2 is set to $1.5^2(ms^{-2})^2$, as $0.09(samp_{\Delta t} ms^{-2})^2$ where the sample period $\Delta t = 0.2s$.

Similarly for the location Kalman filter

$$\mathbf{\Phi} = \begin{bmatrix} 1 & 0 & \Delta t & 0 \\ 0 & 1 & 0 & \Delta t \\ 0 & 0 & 1 & 0 \\ 0 & 0 & 0 & 1 \end{bmatrix}, \mathbf{K} = \begin{bmatrix} 1 & 0 & 0 & 0 \\ 0 & 1 & 0 & 0 \end{bmatrix},$$

$$\mathbf{S}_{0,0} = \begin{bmatrix} \hat{\mathbf{R}}_0 & \mathbf{0} \\ \mathbf{0} & 15^2\mathbf{I} \end{bmatrix}$$

where $\hat{\mathbf{R}}_0$ is the initial uncertainty of the first location estimate given by the calculate CRLB, $\mathbf{R}_0^0$.

$\sigma_s = 4$ samples was found to be necessary due to some uncertainty in the detection of the centre of the pulse shaping function. $\sigma_e = 10$ samples (~200m) was arbitrarily chosen, and σ_{max} was set to 3 standard deviations. Optimum values for γ and σ_g^2 to minimise rms location error were determined experimentally.

IX. Results and Discussion

Table 1 shows the optimum values for γ and σ_g^2 ($samples^2$) for each scenario. The optimal σ_g^2 seemed dependent on MS speed probably because at low MS speeds multipaths can often survive long enough to exhibit similar low variances to true LOS paths. The Kalman filter therefore becomes over–confident in the TOA estimates it is producing. In these cases σ_g^2 is increased to artificially reduce the confidence in such estimates. γ was not found to be critical to the estimator performance if chosen above a certain value. It must be presumed that the TOA variance estimates are causing NLOS data to be optimally ignored in the location estimator.

	Rural (150kmph)	Suburban (50kmph)	Urban (50kmph)	Urban (5kmph)
σ_g^2	0	2	7	64
γ	$\geq$40	$\geq$20	$\geq$20	$\geq$10

Table 1: *Optimum parameter values*

Table 2 shows a comparison between the mean 67%, 95% location errors if the TOA measurements are used raw and with the receiver architecture described. The results show that in all cases a reasonable location error accuracy can be obtained. In practice the rural location accuracy might be expected to be worse than simulated because the CODIT rural model is extremely unchallenging (always LOS, no multipaths). However the performance is still reasonable for the suburban and urban models, which both contain challenging NLOS conditions.

	Raw data		Filtered data	
error (m)	67%	95%	67%	95%
Rural	48.0	855	24.2	54.6
Suburban	495	1650	32.5	71.3
Urban (car)	177	393	47.6	76.8
Urban (ped)	167	350	63.4	108.8

Table 2: *Mean location errors*

Figures 3–5 show an example of the receiver performance for the suburban scenario. In Figure 3 the output of a TOA Kalman filter for one BS is shown. The two functions of the Kalman filter are shown clearly. Firstly the ability to discard obvious multipath data and extrapolate TOA estimates in NLOS conditions and secondly the ability to produce real time variance estimates. Figure 4 shows the true MS path and the estimated path, $\mathbf{X}^{final}$. The raw location estimates are those that would be obtained with no prefiltering of the TOA measurements. It is noticeable that the estimated path tends to overshoot at the cornering points, due to an unrealistic instantaneous velocity jump at these points. In practice it would be expected that this effect would be less pronounced. Figure 5 shows the estimate speed and estimated location error compared to their true values. After initial acquisition a smoothed speed estimate would be quite accurate and could be fedback to set an optimal value of σ_g^2. The location error, $\hat{R}_{rms}^{final}$, is always underestimated and is much smoother than the actual error (other scenarios showed closer correlation), although the main differences occur at the cornering points. For all scenarios the acquisition time (i.e. the time taken for the location error to fall below rms level and speed estimate to converge to its true value) is less than 15 seconds.

Although the final location tracking Kalman filter has been found to work well for high MS speeds, for the pedestrian case the individual estimates, whilst being close to the true position, are impossible to track (even by eye). Reducing the magnitude of σ_u^2 has a smoothing effect, but this is a trade off against an acceptable response under heavy acceleration.

X. Conclusion

A robust location estimator architecture has been presented that demonstrates a good location accuracy performance (typically to within 50m at the 67th percentile) in the presence of timing measurements corrup-

ted with correlated NLOS noise. Biased Kalman prefiltering of the timing measurements is a crucial stage which provides real time TOA variance estimates and can extrapolate TOA's if the LOS path is lost. Final speed estimates are also accurate enough (with smoothing) to provide feedback to optimise the parameter settings.

Without such a receiver architecture it is doubtful if the FCC regulations can be met.

References

[1] FCC, Enhanced Wireless 911 Services, 1999, http://www.fcc.gov/Bureaus/Wireless/News_Releases/1999/nrwl9040.html.

[2] Motorola, "Time Aligned IPDL positioning technique", TSGR1#7(99)b79, 3GPP, 1999.

[3] E. Brookner, "Tracking and Kalman Filtering Made Easy", Ch. 2, Wiley, 1998.

[4] M. Wylie and J. Holtzmann, "The Non–Line of Sight Problem in Mobile Location Estimation", *Proc. IEEE ICUPC*, pp. 827–831, 1996.

[5] N. J. Thomas, D. G. M. Cruickshank and D. I. Laurenson, "Channel Model Implementation for Evaluation of Location Services", *Proc. 3G2000*, March 2000.

[6] Joan Borras, Paul Hatrack and Narayan B. Mandayan, "Decision Theoretic Framework for NLOS Identification", *Proc. Vehicular Technology Conference*, Vol. 2, pp. 1583–1587, 1998.

[7] Y. T. Chan, "A Simple And Efficient Estimator for Hyperbolic Location ", *IEEE Transactions on Signal Processing*, Vol. 42, No. 8, August 1994, pp. 1905–1915.

[8] M. Hellebrandt and R. Mathar, "Location Tracking of Mobiles in Cellular Radio Networks", *IEEE transactions on Vehicular Technology*, Vol. 48, pp. 1558–1562, September 1999.

[9] Perez and Jimenez (editors), CODIT Final Propagation Model, Telefonica, 1994.

Parameter	Value
Carrier frequency	1.92GHz
Chip rate	3.86Mchips/s
Over sampling rate	4
Sample distance @c=3e8ms^{-1}	19.5m
Modulation scheme	QPSK
Pilot length	256 chips
Pilot transmit power (% of total)	20%
Pilot SNR[4]	-10dB
Max. frame desynchronisation	0 chips
Pulse shaping roll off rate (α)	0.22
Idle period frequency	5Hz
Idle period length	5120 chips

Table 3: *System parameters*

Parameter	Rural	Suburban	Urban
CODIT model	rural	suburban	urban
Cell radius (km)	10.0	2.0	0.5
P_{LLOS}	1.0	0.8	0.2

Table 4: *Scenario specific parameters*

[4]The SNR value is the ratio of the average LOS power of the pilot channel at the cell boundary to the noise floor (considered constant over the cell).

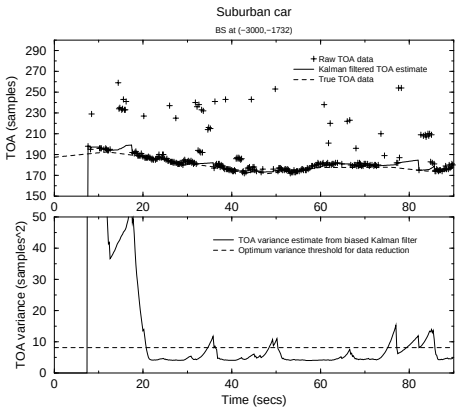

Figure 3: *Biased Kalman filter performance for suburban scenario.*

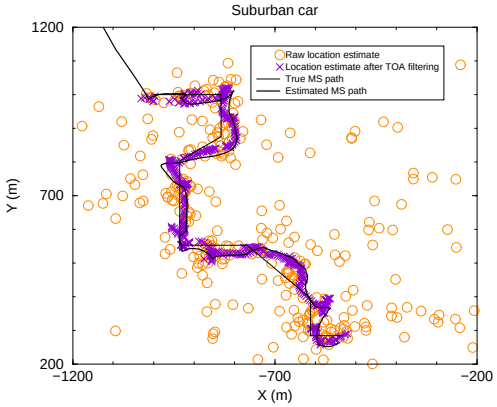

Figure 4: *Location tracking performance for suburban scenario.*

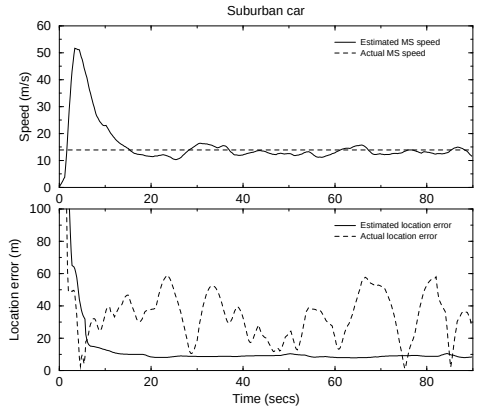

Figure 5: *Speed and location error estimate performance for suburban scenario.*

PERFORMANCE OF A TDOA–AOA HYBRID MOBILE LOCATION SYSTEM

N. J. Thomas, D. G. M. Cruickshank and D. I. Laurenson

University of Edinburgh, UK
email: njt@ee.ed.ac.uk

ABSTRACT

A time difference of arrival (TDOA) technique has been proposed for providing location services in future UMTS networks. The performance of such a system is limited by errors in the time difference (TD) measurements primarily cause by non–line of sight (NLOS) propagation conditions. In future systems angle of arrival (AOA) measurements at the serving base station (BS) may be available, primarily as a requirement to increase downlink capacity via beamforming. These measurements may also be useful for location purposes, though they will also be subject to errors caused by NLOS propagation conditions between the mobile (MS) and the serving BS. In this paper the performance improvement of a TDOA location system utilising the AOA measurement from the serving BS, over a TDOA only system is evaluated. Simulation results are presented which show that location accuracy improvement is possible even in highly NLOS conditions. Furthermore location estimation is now possible when only two BS's are detectable, rather than the three BS's required in the TDOA only system, thus increasing the coverage of the system.

1. INTRODUCTION

In wireless systems the need for accurate location estimation has been motivated by the US FCC's E911 mandate for emergency services [1], as well as customer services (e.g. fleet navigation, location billing), and network aspects (e.g. improved traffic management).

In UMTS a TDOA based location estimation technique has been proposed utilising idle period downlink (IDPL) to allow time differences (TD's) to be calculated between the serving BS's and more distant BS's.

Naturally in line of sight (LOS) conditions the performance of such a system can be very accurate. However if any of the TD's are measured when a BS is non–LOS (NLOS) then sizeable location errors may be generated. In [2] it is noted that NLOS propagation lengths may be typically 400m greater than LOS.

Increasing the number of measurements can increase the location accuracy, but care must be taken not to utilise NLOS measurements where possible. In [3] a robust receiver architecture was introduced in which timing measurements were tracked via a Kalman filter (KF) with a simple LOS state input estimator. The KF variance estimates generated are used as a weighting matrix in the location estimator. The receiver performs well even in a largely NLOS environment.

In future mobile systems antenna arrays may become standard. In this case the MS's angle of arrival (AOA) will be known at the serving BS (and possibly adjacent BS's if the MS is in a soft handover region). The AOA measurements will be subject to NLOS errors correlated to the errors in TD's involving the serving BS, but should still be useful to the location estimator.

In this paper the performance improvement of a TDOA location system utilising the AOA measurement from the serving BS, over a TDOA only system is evaluated. The NLOS problem is first discussed in more detail then the proposed location receiver architecture is described. Simulation results for measurements from a time aligned idle period downlink (TA–IPDL) [4] UMTS system are then presented.

2. NON–LINE OF SGHT PROBLEM

Timing and AOA measurements in NLOS conditions will be subject to large errors. The received signal in NLOS conditions is made up of a superposition of arriving rays from local and distant scatterers. As the MS moves through the environment, scatterers appear and disappear, thus there is a high degree of spatial correlation in measurements. This correlation is inversely proportional to the MS speed, and also dependent on the environment type.

The NLOS error in timing measurements (or excess delay) is positive only, with a distribution usually considered to be exponentially decaying [5]. In AOA measurements at the BS there is an angular spread around the true LOS AOA. In [6] an angular spread with standard deviation 17.6 degrees in an urban environment is measured.

2.1. LOS model

In modelling the LOS/NLOS characteristics of the environment a LOS model based on the CoDiT model[7] is used. N scatterers exist in each environment, defined in terms of delay (uniformly distributed within a range) and AOA at the MS (uniformly distributed over 2π). Scatterers appear and exist for a length normally distributed around L_S. A LOS path is present with probability P_{LOS}. The LOS path exists for a length normally distributed around L_{LOS}, before the LOS state is re–evaluated. L_{LOS} is dependent on the

geometry of, for example, surrounding buildings and streets and thus conceptually the L_{LOS} might be expected to have a value of the order 10–100 metres.

The probability density function of the NLOS excess delay, τ_{ed}, in the model or identically the pdf of the arrival time of the first of N paths in the uniformly distributed delay range can be derived as (space does not permit the derivation)

$$\begin{aligned} f(\tau_{ed}) &= \frac{P_{det}N}{\tau_{max}-\tau_{min}}\left[1-P_{det}\left(\frac{\tau_{ed}-\tau_{min}}{\tau_{max}-\tau_{min}}\right)\right]^{(N-1)} \\ &\qquad \tau_{min} \geq \tau_{ed} \geq \tau_{max}, \\ &= 0 \qquad otherwise. \end{aligned} \tag{1}$$

where P_{det} is the identical detection probability of each scatterer and τ_{min} to τ_{max} is the range of scatterer delays. $f(\tau_{ed})$ has a shape similar to the exponential pdf but over a finite range, and does not always integrate to one. In such cases P_{det} is too low and there is a probability that the signal is not detected.

The pdf of the AOA of the first received path at the BS in NLOS conditions is complicated to derive in closed form. However Monte–Carlo simulation have shown that as the MS–BS separation increases the angular spread around the true AOA decreases and, even in NLOS conditions, a fair estimate for the AOA may be obtained if there is some spatial diversity.

3. RECEIVER ARCHITECTURE

Figure 1 shows the receiver architecture implementation. The architecture can be thought of in three stages: prefiltering of measurement data to correct/remove as far as possible NLOS data as well as smooth sampling measurement noise; the variance weighted location calculation; and a final KF tracking stage to provide a time continuous smoothed motion.

3.1. Prefilter stage

The received timing measurements, $\tau_{1..M}$, and AOA measurement, α_1, may be heavily corrupted with NLOS errors, which ideally would be discarded. However the environment may be such that no good data is available for considerable periods of time, so the function of the prefilter stage should be to make the best use of the available data. Also, in tracking the measured parameters, the manoeuvring capability of the MS must be taken into account.

KFs are used to track $\tau_{1..M}$ and α_1 to their first derivative. If the true parameter value is known the pdf of the parameter's new value after a time interval can be predicted. For example if the MS has manoeuvred and its velocity is considered uniform in speed (to a maximum speed) and direction, a pdf of the new parameter, $f(P)$ can be derived as

$$\begin{aligned} f(P) &= \int_0^{\cos^{-1}(P/P_{max})} \frac{1}{\pi P_{max}\cos\phi}d\phi \\ &= \frac{\ln\left[\left(P_{max}+P_{max}\sqrt{1-\frac{P^2}{P_{max}^2}}\right)/|P|\right]}{\pi P_{max}} \end{aligned} \tag{2}$$

where P_{max} is the maximum change in parameter in the time interval. (2) is of similar shape to the Gaussian pdf with equal variance; the major difference being that the Gaussian pdf is over an infinite range whereas (2) is limited to 2.5σ.

This pdf leads to a simple input estimator which discards data that is definitely NLOS and cannot be due to a manoeuvre. A weighting is applied to the measurement noise variance estimate, σ_Y^2, as follows

$$\hat{\sigma}_Y^2 = \max\left(\sigma_{LOS}^2, \frac{s_{1/1}}{W(r)}\right) \tag{3}$$

where $s_{1/1}$ is the parameter variance estimated by the KF, σ_{LOS}^2 is the minimum parameter measurement variance in LOS conditions, and $W(r)$ is a weighting function, a function of the residual r between the measured parameter and the KF prediction. In the following the weighting function is defined as a Gaussian curve normalised to one at its maximum,

$$W(r) = \frac{e^{-\frac{r^2}{2s_{1/1}}}}{\gamma_1}$$

where γ_1 allows for some magnitude adjustment in the KF output variance estimates, $\sigma_{\tau 1..N}^2$ and $\sigma_{\alpha 1}^2$, which were found by simulation to be smaller than anticipated due primarily to correlated NLOS data.

In TOA filtering, the NLOS error pdf is not symmetric about the true LOS TOA. If a TOA is measured that is earlier than the predicted TOA LOS measurement noise region the filter outputs are forced to take the measured value on the assumption that a manoeuvre has occurred (the parameter velocity estimate should also be adjusted). In this way the filter attempts to track to the LOS edge of the data.

In AOA filtering, the NLOS error pdf is symmetric about the true pdf. The KF should naturally converge to the true LOS direction given enough uncorrelated NLOS measurements. Simulation shows that convergence can be slow if the initial measurements have large NLOS errors. In such cases resetting the KF greatly improved performance.

3.2. AOA–TDOA estimator

A time difference vector, $\mathbf{\Delta}\hat{\tau}(n)$, and covariance matrix, $\mathbf{Q}_\tau$, can be formed from $\hat{\tau}(n)$ and $\hat{\sigma}_\tau^2$, defined as

$$\mathbf{\Delta}\hat{\tau}(n) = \begin{bmatrix} \hat{\tau}_1(n) - \hat{\tau}_2(n) - s_{1,2} \\ .. \\ \hat{\tau}_1(n) - \hat{\tau}_N(n) - s_{1,N} \end{bmatrix},$$

$$\mathbf{Q}_\tau = \begin{cases} \hat{\sigma}_{\tau 1}^2(n) + \hat{\sigma}_{\tau j}^2(n) & i = j, \\ \hat{\sigma}_{\tau 1}^2(n) & i = 1 \| j = 1, \\ 0 & otherwise \end{cases}$$

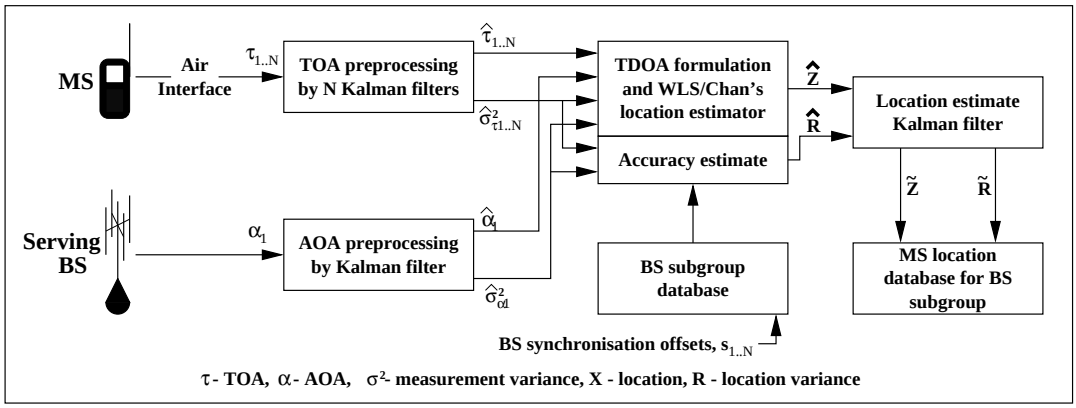

Figure 1: *Receiver architecture with TOA and AOA data streams.*

where $s_{i,j}$ represents the measured synchronisation offset between BS$_i$ and BS$_j$, and $\mathbf{Q}_\tau$ is an N by N matrix with terms as defined.

The most likely MS location, $\mathbf{z}^0(n)$, can be found from the $N-1$ time difference hyperbolae defined by

$$\begin{aligned} r_2 - r_1 &= c\Delta\hat{\tau}_{2,1}(n) \\ &\cdots \\ r_N - r_1 &= c\Delta\hat{\tau}_{N,1}(n) \end{aligned} \tag{4}$$

where r_i is the distance between the MS at (x, y) and BS$_i$ at (x_i, y_i); and the AOA such that

$$\tan\alpha_1 = \frac{x - x_1}{y - y_1} \tag{5}$$

In [8] a linearization of (4) in terms of dependent variables (x, y, r_1) is demonstrated which yields a standard weighted least squares (WLS) solution. The further constraint from equation (5) is added to yield the WLS solution of the form

$$\hat{\mathbf{Z}} = \left(\mathbf{X}^T\mathbf{Q}^{-1}\mathbf{X}\right)^{-1}\mathbf{X}^T\mathbf{Q}^{-1}\mathbf{Y} \tag{6}$$

where

$$\mathbf{X} = -\begin{bmatrix} x_2 - x_1 & y_2 - y_1 & c\Delta\hat{\tau}_{2,1} \\ \cdots & \cdots & \cdots \\ x_N - x_1 & y_N - y_1 & c\Delta\hat{\tau}_{N,1} \\ -1 & \tan\alpha_1 & 0 \end{bmatrix},$$

$$\mathbf{Y} = \frac{1}{2}\begin{bmatrix} (c\Delta\hat{\tau}_{2,1})^2 + x_1^2 + y_1^2 - x_2^2 - y_2^2 \\ \cdots \\ (c\Delta\hat{\tau}_{N,1})^2 + x_1^2 + y_1^2 - x_N^2 - y_N^2 \\ 2x_1 - 2y_1\tan\alpha_1 \end{bmatrix}$$

and

$$\mathbf{Q} = \begin{bmatrix} & & & 0 \\ & \mathbf{Q}_\tau & & \cdots \\ & & & 0 \\ 0 & \cdots & 0 & \sigma^2_{\alpha 1} \end{bmatrix}$$

In the definition of $\mathbf{Q}$ the covariance terms between τ_1 and α_1 are taken as zero for simplicity. In reality these covariances will lie in the range 0 to $\sigma_{\tau 1}\sigma_{\alpha 1}$.

This WLS solution implies independence between the variables (x, y, r_1) which is not the case. Chan [8] suggests a further calculation which imposes the true dependencies on the variables which is shown in [8] to be a more efficient estimator. In this paper both WLS and Chan's method are assessed.

The accuracy of $\hat{\mathbf{Z}}$ is determined by evaluating its covariance matrix, $\hat{\mathbf{R}}$. In the case where the solution is precisely determined, i.e. one TD and one AOA, the Cramér Rao lower bound (CRLB) is used as an estimate of $\hat{\mathbf{R}}$. The CRLB, $\mathbf{\Phi}^0$, for the AOA–TDOA estimator can be derived as

$$\mathbf{\Phi}^0 = (\mathbf{G}^T\mathbf{Q}^{-1}\mathbf{G})^{-1} \tag{7}$$

where

$$\mathbf{G} = \begin{bmatrix} \frac{(x_1-x)}{r_1} - \frac{(x_2-x)}{r_2} & \frac{(y_1-y)}{r_1} - \frac{(y_2-x)}{y_2} \\ \cdots & \cdots \\ \frac{(x_1-x)}{r_1} - \frac{(x_N-x)}{r_N} & \frac{(y_1-y)}{r_1} - \frac{(y_N-x)}{y_N} \\ \frac{1}{(y-y_1)\left(1+\frac{(x-x_1)^2}{(y-y_1)^2}\right)} & \frac{(x-x1)}{(y-y_1)^2\left(1+\frac{(x-x_1)^2}{(y-y_1)^2}\right)} \end{bmatrix}$$

Simulation shows that trace$\{\hat{\mathbf{R}}\}$ is often smaller than the true mean squared error. The variance calculation assumes no bias in the measured TD's. Clearly the prefilters can never correct perfectly the NLOS bias, thus a multiplicative factor, γ_2, is applied to $\hat{\mathbf{R}}$ before the final KF tracking stage to give a more realistic error measure.

4. SIMULATION AND RESULTS

A UMTS system incorporating TA-IPDL was simulated. Cells were arranged in a hexagonal grid around the serving BS. Timing measurements are made from the pulsed pilot

channel during idle periods when all BS's stop transmitting traffic channels. Table 1 shows the system parameters. Four 90 second scenarios were simulated: fast car in rural terrain (150kmph, curve), car travelling in suburban terrain (50kmph, zig–zag), car travelling in urban terrain (50kmph, zig–zag), and pedestrian walking in urban terrain (5kmph, zig–zag). Table 2 shows the scenario dependent parameters. Table 3 shows reasonable values for γ_1 and γ_2. Ten statistically identical runs at each scenario were made. The receiver architecture is simulated with and without AOA information and with both WLS and Chan's estimator to calculate the location.

Figure 2 shows the simulated measured AOA data from the serving BS and KF outputs of a typical track in the urban car scenario. Figure 3 shows the simulated measured TOA data from a non–serving BS and KF outputs of a typical track in the urban car scenario.

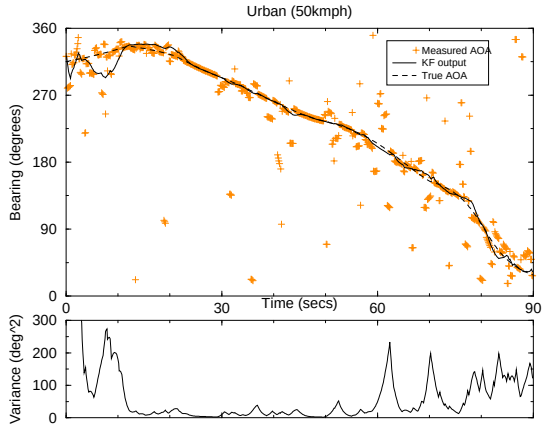

Figure 2: *A typical AOA track in urban car scenario.*

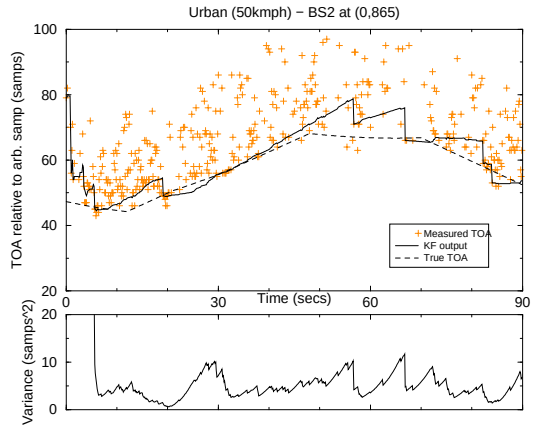

Figure 3: *A typical TOA track in urban car scenario.*

Figure 4(a1) shows the results of simulations for the rural scenario with varying Gaussian noise power on the AOA measurements. The mean number of BS's detectable (or hearability) in each idle period was approximately 2.5. It is clear that Chan's algorithm outperforms the WLS algorithm, and it is noted that the gain achieved by using the AOA can easily lost by using an inefficient estimator. Using the AOA measurements gives a substantial improvement (up to 60%) in 67% location accuracy if the measurement noise power, $\sigma^2_{\alpha LOS}$, is less than 10^{-4} rads^2. By similar triangles it is reasonable to assume a smaller cell radius would further desensitise the location error to $\sigma^2_{\alpha LOS}$. Subsequent simulations use 10^{-5} rads^2 as an attainable value for $\sigma^2_{\alpha LOS}$.

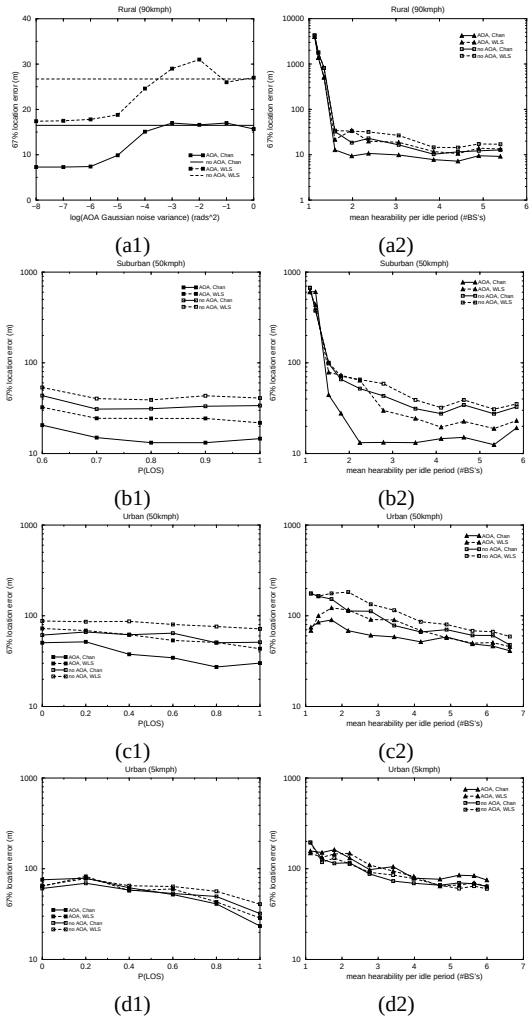

Figure 4: *67% circular location error against (a1) AOA noise power, for the rural scenario; (b1)–(d1) P_{LOS}, for the suburban, urban car, urban pedestrian scenarios; (a2)–(d2) hearability, for all scenarios*

In Figure 4(a2) the hearability is varied. In TA–IPDL this is possible by increasing the pilot channel power; in interference limited systems the processing gain would require to be increased. Each point on the graph corresponds to a 3dB change in SNR (after processing). It can be seen that the receiver performance does not improve greatly as the number of BS's detectable increases. Due to the KF prefilters the location accuracy remains good even when the mean number of BS's detected per idle period is very small (i.e. < 3).

Figures 4(b2), 4(c2), 4(d2) show the effect of varying the hearability in the suburban, urban car and urban pedestrian scenarios respectively. As in the rural case a practical limit is reached above which increasing hearability does not improve performance. Utilising the AOA data improves location accuracy in the suburban and urban car scenarios. This improvement is not as great as in the rural (simple LOS) scenario, but is upwards of 20%. In the urban pedestrian scenario the performance is worse using the AOA data. In this case the KF operation is poor due to the high level of correlation between AOA samples.

Figures 4(b1), 4(c1), 4(d1) show the effect of varying P_{LOS} in the suburban, urban car and urban pedestrian scenarios respectively. The suburban model is only realistic for high values of P_{LOS}. As would be expected performance improves with increasing P_{LOS}. This is most noticeable in the pedestrian example where at low P_{LOS} due to low spatial diversity performance is poor.

It should be noted that during the urban car and suburban scenarios the MS underwent unrealistic instantaneous direction changes so the actual location errors predicted are probably quite pessimistic as they include errors as the filters adapted to the manoeuvre.

5. CONCLUSIONS

The simulation results show that utilising potentially available AOA information at the serving BS in the location function can lead to a significant improvement in location error performance (20%-60%) in most scenarios.

In the pedestrian environment no improvement was possible as the KF implementation fails to cope with the high level of correlation in the NLOS AOA errors. In such a scenario long term averaging of the filtered AOA may be a sensible strategy and this is the subject of ongoing work.

A further advantage of using the AOA measurement is in coverage. The system can operate with reduced detection of surrounding BS's that might, for instance, occur at the edge of a cell network or in rural areas where BS's are distantly spaced.

REFERENCES

[1] FCC. Enhanced Wireless 911 Services. Technical report, FCC, 1999. http://www.fcc.gov/Bureaus/Wireless/News_Releases/1999/nrwl9040.html.

[2] M. Wylie and J. Holtzmann, "The Non–Line of Sight Problem in Mobile Location Estimation", presented at *Proc. IEEE ICUPC*, pages 827–831, 1996.

[3] N. J. Thomas, D. G. M. Cruickshank, and D. I. Laurenson, "A Robust Location Estimator Architecture with Biased Kalman Filtering of TOA Data for Wireless Systems". ISSSTA 2000, New Jersey, September 2000.

[4] Motorola. Time Aligned IPDL positioning technique, TSGR1#7(99)b79. Technical report, 3GPP, 1999.

[5] William C. Y. Lee. *Mobile Communciations Engineering*, chapter 9. McGraw-Hill, 1988.

[6] R. H. Owen, "An Analysis of Adaptive Antenna Frequency Division Duplex Operation in a Highly Scattered Environment", presented at *Workshop on Smart Antenna Design and Technology*, pages 2.18–2.27, Dubrovnik, Croatia, December 1997. COST Action 260.

[7] Perez and Jimenez (editors). CODIT Final Propagation Model. Technical report, Telefonica, 1994.

[8] Y. T. Chan, "A Simple And Efficient Estimator for Hyperbolic Location", *IEEE Transactions on Signal Processing*, vol. 42, no. 8, pp. 1905–1915, Aug 1994.

Parameter	Value
Carrier frequency	1.92GHz
Chip rate	3.86Mchips/s
Over sampling rate	4
Sample distance @c=3e8ms^{-1}	19.5m
Modulation scheme	QPSK
Pilot length	256 chips
Max. frame desynchronisation	0 chips
Pulse shaping roll off rate (α)	0.22
Idle period frequency	5Hz
Idle period length	2560 chips

Table 1: *System parameters*

Parameter	Rural	Suburban	Urban
CoDiT model	rural	suburban	urban
Cell radius (km)	10.0	2.0	0.5
P_{LOS}	1.0	0.8	0.2
L_{LOS} (m)	N/A	30	15
L_S (m)	N/A	20	5

Table 2: *Scenario specific parameters*

Scenario	γ_1	γ_2
Rural	1	1–16
Suburban	1	16
Urban car	4	25
Urban ped	4	40

Table 3: *Values for variance correction factors*

Analysis of IPDL Patterns for Increased Signal Detection Probability in UMTS

N. J. Thomas, D. G. M. Cruickshank, D. I. Laurenson

Department of Electronics and Electrical Engineering,
University of Edinburgh, UK
email:njt@ee.ed.ac.uk

ABSTRACT

To support mobile location services in UMTS systems, idle period downlink (IPDL) techniques have been proposed to avoid the near–far effect in CDMA systems and thus to facilitate the measurement of time difference of arrivals. In this paper the effects of the idle period pattern and variable coherent and non–coherent integration lengths on the detection of signals from distant base stations are evaluated theoretically under some simplifying assumptions and by simulation. The proposed clustered idle period patterns are assessed and shown to outperform regular patterns in certain conditions.

1. INTRODUCTION

In wireless systems the need for accurate mobile station (MS) location estimation has been motivated by the US FCC's E911 mandate for emergency services [1], as well as customer services (e.g. fleet navigation, location based billing), and network aspects (e.g. improved traffic management).

Currently favoured for UMTS, the 3rd generation CDMA system, is to use a time difference of arrival (TDOA) method which utilises timing measurements from a pilot channel (PC), either the primary synchronisation channel (pSCH) or primary common pilot channel (pCPICH), obtained from at least 3 base stations (BS's). The primary problem in such a scheme is that all BS's transmit on the same broadband frequency. Therefore obtaining the required timing measurements from distant BS's becomes impossible when close to the serving BS. In these situations the interference power from the serving BS can be more than 40dB above the power of the distant BS. To reduce this interference effect IPDL techniques have been proposed ([2],[3]) whereby the serving BS ceases transmission during idle periods, allowing distant BS's to be detected. Such systems introduce a capacity loss to the downlink which should not cause an unacceptable loss in quality of service (QoS) in real time communication, such as speech and video services. Therefore choice of an efficient idle period pattern is important.

In this paper the effects on the detection probability of distant BS's of varying the idle period pattern are presented. The performance of a matched filter (MF) receiver with variable coherent and non–coherent integration lengths is presented. The effect of Rician and Rayleigh fading, shadowing and different MS speeds are investigated. Specifically it is of interest to evaluate any trade off in idle period spacing between decreased spacing, to allow longer coherent integration time, and increased spacing, to allow greater fading and shadowing diversity. In the following section the IPDL and PC structures are discussed in more detail. The receiver architecture is then introduced and some theoretical performance calculations made under some simplifying assumptions. Simulation results are then presented.

2. IDLE PERIOD DOWNLINK AND PILOT CHANNEL

The pSCH is a pulsed pilot symbol of length $L_{code} = 256$ chips transmitted once per 2560 chip slot (slot period, $T_{slot} = 0.667ms$). Each BS uses one of sixteen different code alignments in the slot at 160 chip intervals. pSCH symbols from different BS's therefore overlap fractionally in time at the transmission instance. At the MS there can be further overlapping of pilot codes due to varying propagation times between BS's and MS. The pCPICH is a continuous transmission of the scrambling code with no data modulation, its primary function being scrambling code acquisition and a phase reference for other channels [4].

In the pseudo random IPDL (PR–IPDL) proposal [2] idle UMTS frames are transmitted at regular intervals, see Figure 1. In each frame of period $T_{frame} = 16T_{slot}$, a random idle period position (IPP) is chosen in which the serving BS switches off, allowing the MS to take timing measurements from the PC of other transmitting BS's. As interference will be present during the idle period using the continuous pCPICH ($L_{code} = L_{idle}$) for timing measurements is preferable due to the increased processing gain available.

The length of the idle period, L_{idle} and the separation between idle frames, L_{sep} are key parameters. Practical values of $L_{idle} = 0.5T_{slot}$ or T_{slot} and $F_{idle} = 2 - 10Hz$ to avoid QoS degradation have been proposed in [5]. If the idle periods are regularly spaced then the idle period frequency, L_{sep} is simply the reciprocal of F_{idle}. In this paper clustered idle period patterns, implying $L_{sep} < 1/F_{idle}$, are also investigated. Idle period clusters are only considered regularly spaced with frequency, $F_{cluster}$. Figure 2 defines the parameters more clearly. Note that when $L_{sep} = L_{idle}$ the idle periods become consecutive and that between each cluster there is a spacing larger than L_{sep}.

In PR–IPDL the probability that any non–serving BS will be transmitting during the serving BS idle period, P_{trans}, can be evaluated as

$$P_{trans} = 1 - \frac{L_{idle}}{T_{frame}} \quad (1)$$

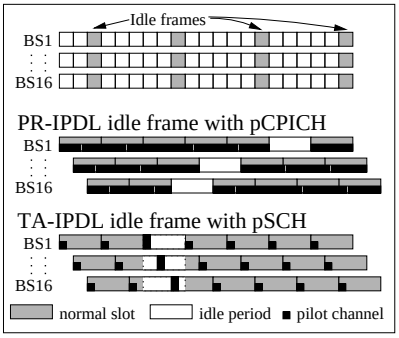

Figure 1: *IPDL frame structures*

[3] proposed a time aligned scheme (TA–IPDL) whereby all BS's cease all transmission, except their PC with probability P_{trans}, at the same time (see Figure 1). If the pSCH is used then $P_{trans} = 1$ since the arriving codes will be almost non–overlapping in time and measurements will be noise limited during idle periods. If the pCPICH is used $P_{trans} = 0.3$ has been proposed in [5]. An advantage of TA–IPDL is that the PC power can be boosted to 100% of the transmit power during the idle period.

Continuous and burst mode operation [6] may also be supported. In burst mode the idle periods are transmitted only in regular bursts with enough idle periods present in each burst to make the timing measurements. Burst mode can reduce capacity loss if MS location updates are required infrequently.

In this paper a TA–IPDL system utilising the pSCH for timing measurements is analysed. However with consideration of P_{trans} the conclusions apply to other methods.

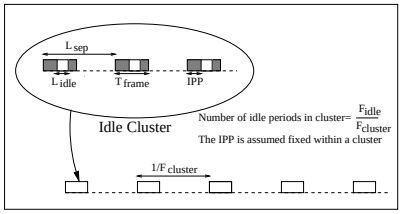

Figure 2: *IPDL parameter definitions*

3. RECEIVER ARCHITECTURE

The receiver architecture, R1, (see Figure 3) is based on a conventional matched filter (MF) synchronisation circuit. It is supposed that the receiver can adapt the coherent and non–coherent integration lengths to maximise the power of the output signal, $I(i)$.

The coherent integration length is described as a multiple, N_c, of the UMTS slot length ($L_{idle} = T_{slot}$). The Doppler frequencies are low enough that the channel can be assumed constant over the slot length. The non–coherent integration length is described as a multiple, N_n, of coherent parts. For simplicity N_c and N_n are always whole powers of two, and $N_{max} = N_c N_n$ is the number of stored idle periods.

3.1. COHERENT INTEGRATION

The MF output is stored slotwise, M(i,s) (i is the sample in slot index and s is the idle slot index), and integrated over N_c idle slots. In R1 it should be noted that due to the variable gain factor, N_c, the MF output power must be normalised by a factor $1/N_c$ to allow power levels to be compared. The output of the coherent integration stage, $C(i,p)$ (p is the coherent segment index), is the signal power envelope.

The normalised power gain of the matched filter depends on the Doppler shift of the channel and, for a simple single phasor channel, can be expressed as

$$G_{fgMF} = \frac{1}{L_{code}^2} \frac{\sin^2(\pi f_d T_c L_{code})}{\sin^2(\pi f_d T_c)} \quad (2)$$

where T_c is the chip duration and f_d is the Doppler shift. For variable coherent integration length with a pulsed pilot code the gain is defined with $N_c \epsilon \{2^K, K = 0..\log_2(N_{max})\}$ to maximise

$$G_{vgMF} = \frac{N_c \sin^2(\pi f_d T_c (L_{code} + L_{sep}(N_c - 1)))}{(L_{code} + L_{sep}(N_c - 1))^2 \sin^2(\pi f_d T_c)} \quad (3)$$

where L_{sep} is measured in chips. For computational simplicity only $N_c = 2^K$, $K \in I$ values are used.

C(i,p) with no signal and complex Gaussian noise present has chi squared pdf with 2 degrees of freedom of the form

$$f_{Cns}(y) = \frac{1}{2\sigma_n^2} e^{-\frac{y}{2\sigma_n^2}} \quad (4)$$

where $2\sigma_n^2$ is the total noise power (identical in $M(i,s)$ and $C(i,p)$), assumed constant, which must first be estimated, for which there are several strategies. C(i,p) with signal present has a non–central chi squared pdf with 2 degrees of freedom of the form

$$f_{Cs}(y) = \frac{1}{2\sigma_n^2} e^{\frac{(S^2+y)}{2\sigma_n^2}} I_0\left(\sqrt{y}\frac{S}{2\sigma_n^2}\right) \quad (5)$$

where $I_\alpha(x)$ is the αth order modified Bessel function of the first kind, and S^2 is the signal power in $C(i,p)$, assumed constant over N_c idle periods, and N_c times that the signal power in $M(i,s)$. In Rayleigh fading S^2 has a chi squared distribution about the short term mean signal power $\bar{S}^2$. In Rician fading a non–central chi squared distribution applies.

3.1.1. THRESHOLD CALCULATION

A Neyman–Pearson decision threshold, T_h, can be calculated based on an acceptable false alarm probability, P_{FA},

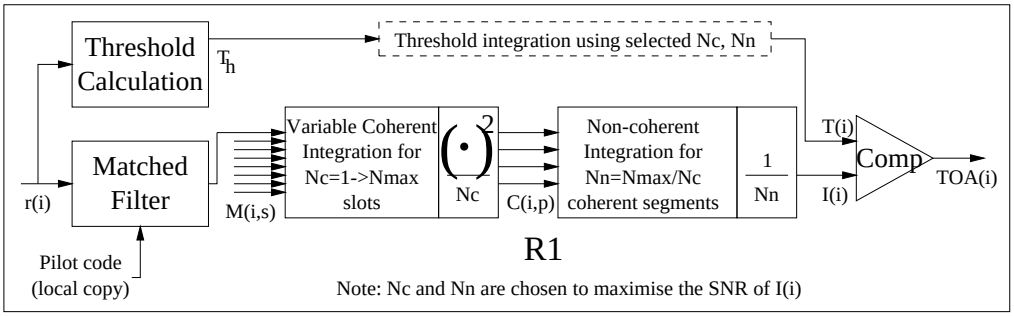

Figure 3: *Receiver architecture R1*

of the noise process. T_h (expressed in power) can be calculated from (4) as

$$T_h = 2\sigma_n^2 \ln\left(\frac{1}{P_{FA}}\right) \tag{6}$$

In practice the autocorrelation sidelobes of the pilot code may be greater than T_h in high SNR conditions. So a further additive threshold is required to ensure that the autocorrelation sidelobes do not exceed the threshold. In this paper low SNR's are assumed so the effect of the autocorrelation threshold is not considered.

The probability of detecting a signal, P_{det}, can be calculated from (5) as

$$P_{det} = Q_1\left(\frac{\sqrt{C(i)}}{\sigma_n}, \frac{\sqrt{T_h}}{\sigma_n}\right) \tag{7}$$

where $Q_m(a,b)$ is Marcum's Q function of order m.

3.2. NON–COHERENT INTEGRATION

$C(i,p)$ for the last N_n idle periods are summed non–coherently to give $I(i)$. Values of $I(i)$ larger than $T(i)$ are selected as arrival peaks. Again a normalisation factor, $1/N_n$, is applied to allow power levels to be compared when selecting an optimum N_n value. Assuming $2\sigma_n^2$ is constant over N_n idle periods $T(i) = T_h$.

$I(i)$ with no signal present has a chi squared pdf with $2N_n$ degrees of freedom of the form

$$f_{Ins}(y) = \frac{N_n}{\sigma_n^{2N_n} 2^{N_n} \Gamma(N_n)} (N_n y)^{N_n - 1} e^{-\frac{N_n y}{2\sigma_n^2}} \tag{8}$$

With signal present $I(i)$ has a non–central chi squared pdf with $2N_n$ degrees of freedom of the form

$$f_{Is}(y) = N_n \left(\frac{N_n y}{P^2}\right)^{\frac{N_n-1}{2}} e^{\frac{(P^2+N_n y)}{2\sigma_n^2}} I_{N_n-1}\left(\sqrt{N_n y}\frac{P}{2\sigma_n^2}\right) \tag{9}$$

where P^2 is the sum of N_n partially correlated S^2 values.

The false alarm probability after the non-coherent detection stage, $P_{FA(out)}$, assuming constant noise power, can be evaluated as

$$P_{FA(out)} = e^{-\frac{N_n T_h}{2\sigma_n^2}} \sum_{k=0}^{N_n-1} \frac{1}{k!}\left(\frac{N_n T_h}{2\sigma_n^2}\right)^k \tag{10}$$

Figure 4(a) shows $P_{FA(out)}$ against P_{FA} for various values of N_n. Clearly the effect of increasing N_n is to reduce $P_{FA(out)}$ for the same P_{FA}.

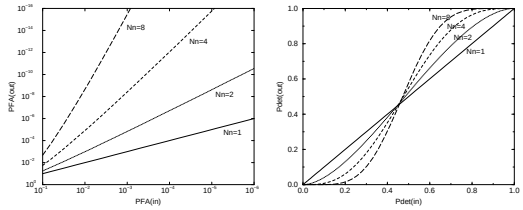

(a) (b)

Figure 4: *(a)* $P_{FA(out)}$ *against* P_{FA}*, (b)* $P_{det(out)}$ *against* P_{det}*, for various* N_n *values*

Similarly $I(i)$ with signal present has a non–central chi squared distribution with $2N_n$ degrees of freedom. The detection probability after the non-coherent detection stage, $P_{det(out)}$ can be evaluated as

$$P_{det(out)} = Q_{N_n}\left(\frac{\sqrt{P}}{\sigma_n}, \frac{\sqrt{N_n T_h}}{\sigma_n}\right) \tag{11}$$

Figure 4(b) shows $P_{det(out)}$ against P_{det} for various values of N_n. For $P_{det} > 0.45$ $P_{det(out)}$ is increased and for $P_{det} < 0.45$ $P_{det(out)}$ is decreased.

If $P_{FA(out)}$ is fixed then (from Figure 4) as N_n is increased P_{FA} can be increased and subsequently T_h lowered. This allows signals at lower SNR's to have increased $P_{det(out)}$ values. Figure 5 shows the effective SNR gain from threshold reduction against N_n and for various values of $P_{det(out)}$ and $P_{FA(out)}$. For small $P_{FA(out)}$ values the gain available is close to 3dB/octave. For more useful values of $P_{FA(out)}$ the

gain is close to 2dB/octave. As the P_{det} value drops the SNR gain possible from non–coherent integration decreases. For signals well below the noise power non–coherent integration can produce little gain.

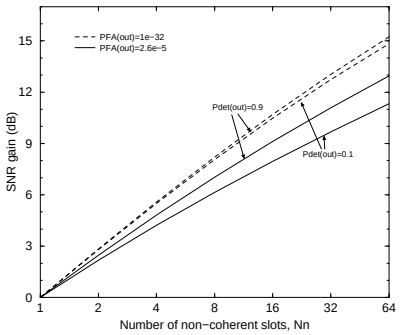

Figure 5: *SNR gain against N_n for fixed $P_{FA(out)}$*

3.3. Fading and Shadowing Effects

Assuming a fixed coherent gain over N_n $C(i,p)$ idle periods and uncorrelated Rayleigh fading between idle periods, P^2 has a chi squared distribution with pdf of the form

$$f_{P^2}(y) = \frac{N_n}{\left(\frac{\bar{S}^2}{2}\right)^{2N_n} 2^{N_n}\Gamma(N_n)} (N_n y)^{N_n - 1} e^{-\frac{N_n y}{\bar{S}^2}} \quad (12)$$

In Rician fading a non–central chi squared distribution will apply.

The pdf for the lognormal shadowing term after the non–coherent integration can be derived as

$$f_{sh}(y) = \frac{\sqrt{N_n}}{\sqrt{2\pi}\sigma_{sh}} e^{-\frac{(N_n y)^2}{2N_n \sigma_{sh}^2}} \quad (13)$$

where σ_{sh} is the standard deviation of shadowing in dB.

In both fading and shadowing cases it can be seen that increasing N_n averages the power. Therefore it is interesting to examine if using a low N_n value, to allow peaks on the fading/shadowing profile to be exploited, would be beneficial. Figures 6(a), (b) show the minimum fading and shadowing gain occurring with 50% probability (i.e. the median gain) against number of uncorrelated measurements for $N_n = 1, 4$.

Both shadowing and fading provide a potential gain. However the fading gain is quite low; typically the fading gain from using a low N_n is less than the threshold reduction gain from using a high N_n (see Figure 5). However the shadowing gain can far outweight the threshold reduction gain. Therefore an effective idle period pattern should be able to exploit any shadowing diversity. The figures also show the gain available by using continuous as opposed to burst mode. Of course in a real scenario measurements will

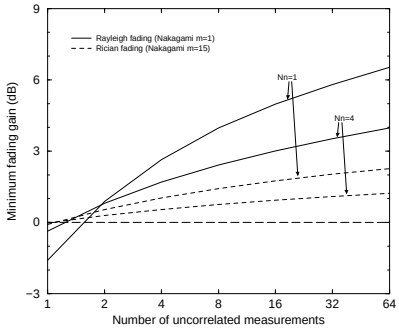

(a)

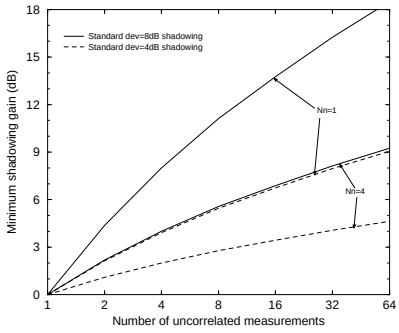

(b)

Figure 6: *(a) Minimum fading gain, (b) Minimum shadowing gain, against number of uncorrelated measurements*

be correlated, so the diversity gain available will decrease and will depend on the MS speed and environment.

In practice due to movement of the MS the position of MF peaks will stray or slip across the N_n idle periods. Thus the total integration time must be limited by the MS radial speed. For moving scenarios this might be less than 5 seconds.

4. Simulation Results

Simulations were carried out for Rayleigh and Rician (Nakagami $m = 15$) fading environments. In the Rician fading environment 4dB standard deviation lognormal shadowing is modelled, in the Rayleigh environment 8dB is used. An exponential decaying shadowing decorrelation length of 20m is used. A hexagonal cell geometry is modelled. For TDOA location purposes timing measurements from three BS's are required, therefore the BS's of most interest are the 2nd and 3rd closest BS's (the serving BS will always be detectable).

100k random placements of MS with random bearing were simulated. Two MS speeds were used: 5kmph, 50kmph, corresponding to maximum Doppler frequencies, with a 1.92GHz carrier frequency, of 8.90, 89.0Hz respectively.

Mean path loss variation was not modelled. An idle frequency, F_{idle}, of 8Hz was simulated, which allowed $F_{cluster}$ values of 1, 2, 4Hz. The maximum integration time was set at 1 second for simplicity and to limit the rms radial error to below the desired location accuracy in all cases. In practice it may of course be desirable to increase the integration time if the MS is stationary. The threshold power reduction for $P_{FA(out)} = 2.6 \cdot 10^{-5}$‡ and $P_{det(out)} = 0.1$ from Figure 5 was used. Burst and continuous mode were simulated. In burst mode one set of measurements were taken (1 second) in continuous mode measurements were taken for 5 seconds. The results reported are the maximum SNR gain possible in that time averaged over the all placements and the 2 BS's.

Figures 7(a), (b) show the results for Rician/LOS and Rayleigh/NLOS conditions respectively in burst mode. It should be noted that the minimum L_{sep} value (1 slot) implies that the idle periods are consecutive, effectively creating idle periods with $F_{idle} = 1Hz$, $L_{idle} = 8T_{slot}$. The maximum L_{sep} value ($1/F_{idle}$) implies idle periods regularly spaced and therefore no clustering is present (results for all $F_{cluster}$ values are identical). Also included is the performance of a fixed non–coherent gain receiver for comparison.

The results show that clustering idle periods together can increase the SNR gain available, and thus the detection probability of the signal. In the LOS case, with low shadowing variation, performance is defined by the coherency of the channel and $F_{cluster}$ =1Hz provides the greatest SNR gain. However in the NLOS case, with larger shadowing variation, performance is determined more by the shadowing diversity available. At $L_{sep} = 1$ UMTS frame, which might be a practical minimum due to QoS considerations, the SNR increase over the non clustered gain is about 1.5dB at 5kmph. In the NLOS case using $F_{cluster}$ =2Hz marginally improves the performance over $F_{cluster}$ =1Hz. At 50kmph clustering in the NLOS case can have a detrimental effect. With $F_{cluster} = 1Hz$ the SNR gain is down by 1dB over the unclustered case. A higher $F_{cluster}$ value is required to provide some shadowing diversity.

The unexpected peaks present occur when coincidental aliasing of the Doppler frequency to F_{idle} provide apparent coherency in the channel. In practice these peaks would be time varying as the MS's Doppler frequencies will also time vary.

Results for contiuous mode showed similar trends, but were about 2.5dB and 5dB improved in the LOS and NLOS environments respectively, a cause of the greater shadowing diversity available in the measurement window.

5. Conclusions and Further Comments

In this paper it has been shown that clustering idle periods together and utilising an adaptive receiver can increase the SNR of weak signals. The preformance of the receiver depends on the coherency of the channel and also the shadowing diversity available. Fading diversity is less significant.

The actual gain available depends on the number of measurements taken and the detection probability of the signals. In the simulations reported 8 measurements were utilised. Clustering to a realistic L_{sep} value gave a 1.5dB SNR improvement over the regularly spaced pattern. To avoid deteriorated performance at higher speeds $F_{cluster}$ >1Hz is essential.

‡This $P_{FA(out)}$ was found to give a good location accuracy performance, approximately 1 false peak in 15 measurements

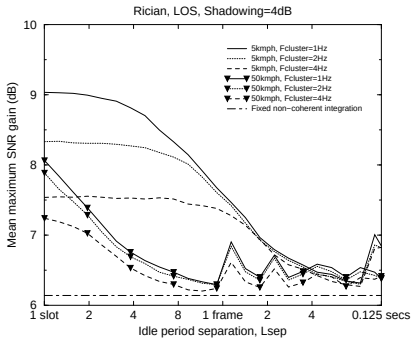

(a)

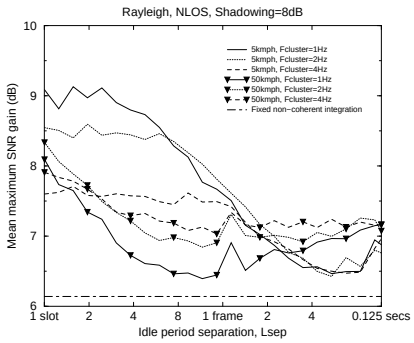

(b)

Figure 7: *Maximum SNR gain per second (dB) against L_{sep} in burst mode for (a) Rician/LOS, (b) Rayleigh/NLOS cells*

References

[1] FCC. Enhanced Wireless 911 Services. Technical report, FCC, 1999. http://www.fcc.gov/Bureaus/Wireless/News_Releases/1999/nrwl9040.html.

[2] Ericsson. Recapitulation of the IPDL positioning method, TSGR1#4(99)346. Technical report, 3GPP, 1999.

[3] Motorola. Time Aligned IPDL positioning technique, TSGR1#7(99)b79. Technical report, 3GPP, 1999.

[4] 3GPP. Physical channels and mapping of transport channels (FDD), 3G TS 25.211. Technical report, 3GPP, 2000.

[5] Ericsson. Proposal for Downlink Positioning, TSGR1#7(99)c61. Technical report, 3GPP, 1999.

[6] 3GPP. Idle periods for IPDL location method, TS 25.214. Technical report, 3GPP, 2000.

Calculation of mobile location using scatterer information

N. J. Thomas, D. G. M. Cruickshank, D. I. Laurenson

A technique using scatterer information and backwards ray tracing is proposed which can locate a target precisely in non–line of sight multipath conditions. The technique requires accurate measurement of angle of arrival, time of arrival (with reference to the first arriving ray) and Doppler shift for six arriving rays. Utilising auxiliary signal strength measurements can improve performance when measurement noise is present. Further improvement is demonstrated using a Kalman filter in a tracking scenario.

Introduction: Non–line of sight (NLOS) conditions can dramatically reduce the performance of conventional triangulation based mobile location techniques [1]. However even in NLOS when sufficient resolvable multipaths are present the MS may be precisely located by back tracing the arriving rays under a single reflection assumption. Even in a multiple reflection scenario the technique may work if the reflection points are spatially close.

In this Letter location is calculated based on a single reflection assumption using angle of arrival (AOA), time of arrival (TOA) with respect to first arriving ray, and Doppler shift measurements from each arriving ray. The equations derived solve simultaneously the MS location, MS velocity and excess time delay of the first arriving ray. The equations are non–linear thus a simple minimisation based estimator is used to solve them. In simulation the CoDiT urban geometrically based single reflection radio channel model is used [2]. As the power of the Gaussian distributed noise corrupting the measurements is increased, performance deteriorates quickly, so an enhancement is proposed using signal strength measurements to give an approximate range estimate. Finally a further improvement is presented by utilising a 1st order 2D Kalman filter (KF) on the estimator output in a tracking scenario using a similar method to [3].

Formulation of Equations: Figure 1 shows a possible geometry for a single reflection scatterer, S_n. The scatterer and base station (BS) are assumed fixed; the MS has speed v in direction ϕ with respect to line of sight to the BS.

The measured parameters are the angle of arrival, α_1, and Doppler shift, f_1, for the first arriving scatterer. For subsequent arriving scatterers ($n = 2..N$) relative time delay $\tau_{n,1}$ is also measured to give $(\alpha_n, f_n, \tau_{n,1})$.

There are 5 unknowns, the MS polar coordinates, (r_m, α_m), velocity magnitude and bearing, (v, ϕ), and time delay of the first arriving ray relative to the true LOS arriving time, $\tau_{1,0}$.

Using the temporal knowledge of the channel for each scatterer

$$r_n + r_{n,m} - r_m = c\tau_{n,1} + c\tau_{1,0} \tag{1}$$

where c is the speed of light and the distances r are the magnitude of the corresponding vectors shown in Figure 1. Using the cosine rule gives

$$r_{n,m} = \sqrt{r_n^2 + r_m^2 - 2r_n r_m \cos(\alpha_m - \alpha_n)} \tag{2}$$

Substituting this into (1) and rearranging gives

$$r_n = \frac{(c\tau_{n,1} + c\tau_{1,0})^2 + 2(c\tau_{n,1} + c\tau_{1,0})r_m}{2(r_m + c\tau_{n,1} + c\tau_{1,0} - r_m \cos(\alpha_m - \alpha_n))} \tag{3}$$

Using the geometrical knowledge of the channel for each scatterer

$$\vec{\mathbf{r}}_\mathbf{n} + \vec{\mathbf{r}}_{\mathbf{n,m}} - \vec{\mathbf{r}}_\mathbf{m} = \vec{\mathbf{0}} \tag{4}$$

Therefore for each scatterer (for convenience in the following equation complex notation is used to represent geometry)

$$E_n = r_n\left(j\sin(\alpha_n)+\cos(\alpha_n)\right)+ r_{n,m}\left(j\sin(\theta_n)-\cos(\theta_n)\right)-r_m\left(j\sin(\alpha_m)+\cos(\alpha_m)\right)=0 \quad (5)$$

where,

$$\theta_n = \pi-\alpha_m-\phi\pm\cos^{-1}\left(\frac{f_n\lambda}{v}\right) \quad (6)$$

where λ is the carrier wavelength.

Substituting (2) and (3) into (5) gives a set of non–linear equations, E_n, in the 5 unknowns $(r_m, \alpha_m, v, \phi, \tau_{1,0})$ for each scatterer S_n. In the presence of measurement noise E_n may not equal zero, therefore a unique solution can be found by minimising the sum of $|E_n|^2$ for $n = 1..N$ with $N \geq 6$ scatterers ($N = 5$ is insufficient due to ambiguity of (6)). This leads to the simple estimator

$$\xi = \sum_{n=1}^{N}|E_n|^2 \quad (7)$$

Using a signal strength measure, assumed to have a lognormal distribution, a range pdf can be evaluated. Utilising the conditional probability density of r_m given the estimate $\hat{r}_m$, $f_{R_m}(r_m|\hat{r}_m)$, leads to the enhanced estimator

$$\xi_e = f_{R_m}(r_m|\hat{r}_m)\sum_{n=1}^{N}|E_n|^2 \quad (8)$$

Simulation: The simulation uses the CoDiT urban model scatterer definition. The $N = 6$ earliest arriving rays are used in the estimator. The simplex method [4] is used to minimise ξ and ξ_e. A cell radius of 500m is used, with a path loss exponent of 3.76 and lognormal shadowing of 8dB. 1000 randomly placed MS's are located within the cell, travelling at 50kmph ($f_{carrier} = 1.92$GHz, maximum Doppler shift $f_{max} = 92.7$Hz). The line of sight probability is set to 0.2. In the tracking scenario with KF a spatially correlated LOS model is applied [5] whose shadowing decorrelation length and scatterer mean survival length are 5m.

Figures 2(a), (b) show the rms location accuracy achieved for the simple, enhanced by signal strength, and enhanced by signal strength with KF post tracking receivers against Gaussian distributed noise power added to the measuremed parameters as follows: Figure 2(a) shows results for low Doppler noise power, $\sigma^2 = 10^{-5}f_{max}^2$; and Figure 2(b) shows results for high Doppler noise power, $\sigma^2 = 10^{-3}f_{max}^2$; for each estimator the performance is shown with two different noise powers added to $c\tau_{n,1}$ of $0.1m^2$ (the lower line of the pair) and $1000m^2$ (the upper line); noise power added to α_n is shown on the x–axis. The performance of locating the MS by cell location; first received AOA and signal strength; and first received AOA and TOA are shown for comparison. The performance of the latter is also shown with a KF tracking filter.

Discussion and Conclusions: At low noise the location performance is almost perfect. At more practical noise levels the performance tails off severely and becomes worse than the AOA–TOA combination receiver. The enhanced estimator performs significantly better than the simple estimator in the high Doppler noise case, Figure 2(b). Utilising a KF a fourfold increase in location accuracy is observed. Results are pessimistic as manoeuvres during the track are instantaneous, thus the KF loses track

momentarily. Individual KF tracking of $(\alpha_n, f_n, \tau_{n,1})$ could be used to further reduce the input noise variance [6].

The technique gives simulated performance of below 50m rms for a MS moving at 50kmph, a significant improvement over conventional methods. Non–stationary scatterers and multiple scatterer reflections are potentially problematic to the technique.

References

[1] T. S. Rappaport, J. H. Reed, and B. D. Woerner, "Position Location Using Wireless Communications on Highways of the Future", *IEEE Communications Magazine*, pp. 33–41, October 1996.

[2] Perez and Jimenez (editors). CODIT Final Propagation Model. Technical report, Telefonica, 1994.

[3] M. Hellebrandt and R. Mathar, "Location Tracking of Mobiles in Cellular Radio Networks", *IEEE transactions on Vehicular Technology*, vol. 48, pp. 1558–1562, September 1999.

[4] William H. Press, Saul A. Teukolsky, William T. Vetterling, and Brian P. Flannery, *Numerical Recipies in C*. Cambridge University Press, 1996.

[5] N. J. Thomas, D. G. M. Cruickshank, and D. I. Laurenson, "Channel Model Implementation for Evaluation of Location Services", presented at *3G2000 Conference*. IEE, London, March 2000.

[6] N. J. Thomas, D. G. M. Cruickshank, and D. I. Laurenson, "Performance of a TDOA–AOA Hybrid Mobile Location System", presented at *3G2001 Conference*. IEE, London, March 2001.

Authors' affiliations:

N. J. Thomas, D. G. M. Cruickshank and D. I. Laurenson (Department of Electronics and Electrical Engineering, University of Edinburgh, King's Buildings, Edinburgh, EH9 3JL, UK. email: njt@ee.ed.ac.uk)

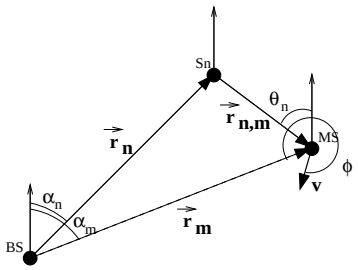

Figure 1: *Single reflection scatterer geometry*

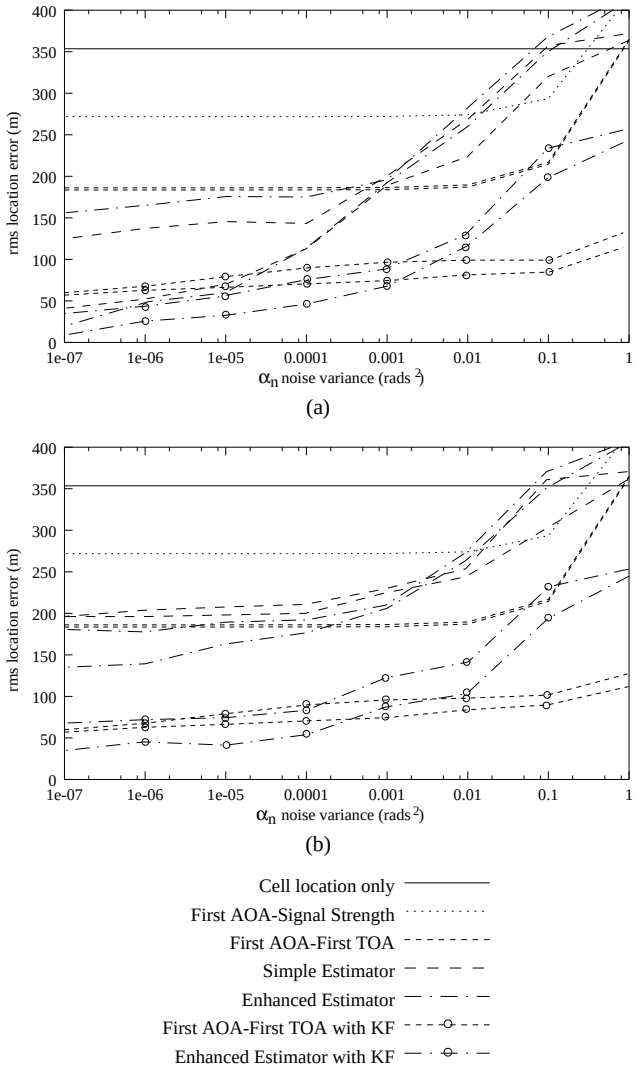

Figure 2: *RMS location error performance for (a) low, (b) high Doppler noise*

References

[1] FCC, "Enhanced wireless 911 services," tech. rep., FCC, 1999. http://www.fcc.gov/Bureaus/Wireless/ News_Releases/1999/nrwl9040.html.

[2] ETSI, "UMTS terrestrial radio access (UTRA) ITU–R RTT candidate submission," tech. rep., ETSI, June 1998. UTRA Concept evaluation – updated version of UMTS 30.06 version 3.0.0.

[3] R. B. Ertel, P. Cardieri, K. W. Sowerby, T. S. Rappaport, and J. H. Reed, "Overview of spatial channel models for antenna array communication systems," *IEEE Personal Communications*, pp. 10–22, February 1998.

[4] J. G. Proakis, *Digital Communications*. McGraw Hill, 2001.

[5] K. R. Schaubach, N. J. Davis, and T. S. Rappaport, "A ray tracing method for predicting path loss and delay spread in microcellular environment," in *IEEE VTC*, pp. 932–935, 1992.

[6] J. Rossi and A. Levi, "A ray model for decimetric radiowave propagation in an urban area," *Radio Science*, vol. 27, no. 6, pp. 971–979, 1993.

[7] D. I. Laurenson, S. McLaughlin, and A. U. H. Sheikh, "A ray tracing approach to channel modelling for the indoor environment," in *IEEE VTC*, pp. 246–249, May 1993.

[8] Y. Okumura, "Field stength and its variability in UHF and VHF land–mobile radio services," *Elec. Communications Lab.*, vol. 16, 1968.

[9] M. Hata, "Empirical formula for propagation loss in land mobile radio services," *IEEE Transactions on Vehicular Technology*, vol. 29, pp. 317–325, August 1980.

[10] M. Toeltsch, J. Laurila, A. Molisch, K. Kalliola, P. Vainikainen, and E. Bonek, "Spatial characterization of urban mobile radio channels," in *Vehicular Technology Conference*, pp. 399–403, May 2001.

[11] S. Min and H. L. Bertoni, "Effect of path loss model on CDMA system design for highway microcells," in *VTC*, pp. 1009–1013, 1998.

[12] M. Gudmundson, "Correlation model for shadow fading in mobile radio systems," *Electronic Letters*, vol. 27, pp. 2145–2146, November 1991.

[13] E. Perahia, D. Cox, and S. Ho, "Shadow fading cross correlation between basestations," in *Vehicular Technology Conference*, pp. 313–317, May 2001.

[14] G. L. Turin *et al.*, "A statistical model of urban multipath propagation," *IEEE Transactions on Vehicular Technology*, February 1972.

[15] A. A. M. Saleh and R. A. Valenzuela, "A statistical model for indoor multipath propagation," *IEEE Journal on Selected Areas of Communications*, February 1987.

[16] CEC, "Digital land mobile radio communications – COST 207," tech. rep., CEC, 1988.

[17] D. I. Laurenson, D. G. M. Cruickshank, and G. J. R. Povey, "A computationally efficient multipath channel simulator for the cost 207 models," in *IEE Colloquium on Computer Modelling of Communication Systems*, May 1994.

[18] Q. Spencer, M. Rice, B. Jeffs, and M. Jensen, "A statistical model for angle of arrival in indoor multipath propagation," in *VTC*, vol. 3, pp. 1415–1419, 1997.

[19] J. W. C. Jakes, *Microwave Mobile Communications*. John Wiley & Sons, 1974.

[20] R. J. Piechocki, G. V. Tsoulos, and J. P. McGeehan, "Simple general formula for PDF of angle of arrival in large cell operational environments," *Electronics Letters*, vol. 34, pp. 1784–1785, Sep 1998.

[21] J. C. Liberti and T. S. Rappaport, "A geometrically based model for line–of–sight multipath radio channels," in *IEEE VTC*, pp. 844–848, 1996.

[22] Perez and J. (editors), "CODIT final propagation model," tech. rep., Telefonica, 1994.

[23] J. V. Beck and K. J. Arnold, *Parameter Estimation in Engineering and Science*. Wiley, 1977.

[24] W. H. Press, S. A. Teukolsky, W. T. Vetterling, and B. P. Flannery, *Numerical Recipies in C*. Cambridge University Press, 1996.

[25] H. L. Song, "Automatic vehicle location in cellular systems," *IEEE Transactions on Vehicular Technology*, vol. 43, pp. 902–908, November 1994.

[26] K. A. Stroud, *Further Engineering Mathematics*. MacMillan Press, 1990.

[27] J. S. Abel, "A divide and conquer approach to least squares estimation," *IEEE Transactions on Aerospace and Electronic Systems*, pp. 423–427, March 1990.

[28] B. T. Fang, "Simple solutions for hyperbolic and related position fixes," *IEEE Transactions on Aerospace and Electronic Systems*, vol. 26, pp. 748–753, September 1990.

[29] Y. T. Chan, "A simple and efficient estimator for hyperbolic location," *IEEE Transactions on Signal Processing*, vol. 42, pp. 1905–1915, Aug 1994.

[30] R. Schmidt, "Least squares range difference location," *IEEE Transactions on Aerospace and Electronic Systems*, vol. 32, pp. 234–242, Jan 1996.

[31] T. S. Rappaport, J. H. Reed, and B. D. Woerner, "Position location using wireless communications on highways of the future," *IEEE Communications Magazine*, pp. 33–41, October 1996.

[32] J. J. Caffery and G. L. Stuber, "Overview of radiolocation in CDMA cellular systems," *IEEE Communications Magazine*, pp. 38–45, April 1998.

[33] W. G. Figel, N. H. Shepherd, and W. F. Trammell, "Vehicle location by a signal attenuation method," *IEEE Transactions on Vehicular Technology*, vol. 18, pp. 105–109, November 1969.

[34] M. Hata and T. Nagatsu, "Mobile location using signal strength measurements in a cellular system," *IEEE Transactions on Vehicular Technology*, vol. 29, pp. 245–251, May 1980.

[35] M. Hellebrandt, R. Mathar, and M. Schiebenbogen, "Estimating position and velocity of mobiles in a cellular radio network," *IEEE Transactions on Vehicular Technology*, vol. 46, pp. 65–71, February 1997.

[36] M. Hellebrandt and R. Mathar, "Location tracking of mobiles in cellular radio networks," *IEEE transactions on Vehicular Technology*, vol. 48, pp. 1558–1562, September 1999.

[37] Z. Salcic, "AGPCS – an automatic GSM–based positioning and communication system," in *GeoComputation97*, 1997.

[38] J. Scourias, "Overview of the global system for mobile communications," tech. rep., University of Waterloo, Canada, 1995. http://ccnga.uwaterloo.ca/ jscouria/GSM/gsmreport.html.

[39] M. Silventoinen and T. Rantalainen, "Mobile station locating in GSM," in *WCSS'95*, 1995.

[40] M. Silventoinen and T. Rantalainen, "Mobile station emergency locationing in GSM," in *Proc. IEEE ICPWC*, pp. 232–238, 1996.

[41] S. Fischer, H. Koorapaty, and A. Kangas, "System performance evaluation of mobile positioning methods," tech. rep., Ericsson, 1999.

[42] M. Pent, M. A. Spirito, and E. Turco, "Method for positioning GSM mobile stations using absolute time delay measurements," *Electronics Letters*, vol. 33, pp. 2019–2020, Nov 1997.

[43] L. Dumont, M. Fattouche, and G. Morrison, "Super–resolution of multipath channels in a spread spectrum location system," *Electronics Letters*, vol. 30, September 1994.

[44] R. O. Schmidt, "Multiple emitter location and signal parameter estimation," *IEEE Transactions*, pp. 276–280, 1986.

[45] P.-C. Chen, "A cellular based mobile location tracking system," in *VTC 1999*, vol. 3, pp. 1979–1983, 1999.

[46] G. D. Morley and W. Glover, "Improving location estimation with pulse–ranging in presence of shadowing and multipath excess–delay effects," *Electronics Letters*, vol. 31, pp. 1609–1610, Aug 1995.

[47] C. H. Knapp and G. C. Carter, "The generalized correlation method of estimation of time delay," *IEEE Transactions on Accoustics, Speech and Signal Processing*, vol. 24, pp. 320–327, Aug 1976.

[48] C.-K. Chen and W. A. Gardner, "Signal–selective time–difference–of–arrival estimation for passive location of man–made signal sources in highly corruptive environments, part II: Algorithms and performance," *IEEE Transactions on Signal Processing*, vol. 40, pp. 1185–1197, May 1992.

[49] L. Izzo, A. Napolitano, and L. Paura, "Modified cyclic methods for signal selective TDOA estimation," *IEEE Transactions on Signal Processing*, vol. 42, pp. 3294–3298, November 1994.

[50] M. Aatique, "Evaluation of TDOA techniques for position location in CDMA systems," Master's thesis, Virginia Polytechnic Institute, USA, 1997.

[51] CPS, "CURSOR." (http://www.cursor–system.com).

[52] D. Porcini, "Performance of a OTDOA–IPDL positioning receiver for 3G–FDD mode," in *3G2001 Conference*, IEE, London, March 2001.

[53] N. J. Thomas, D. G. M. Cruickshank, and D. I. Laurenson, "Channel model implementation for evaluation of location services," in *3G2000 Conference*, IEE, London, March 2000.

[54] B. Ludden and L. Lopes, "Cellular based location technologies for UMTS: A comparison between IDPL and TA–IPDL," in *Vehicular Technology Conference*, Motorola, Spring 2000.

[55] J. J. Caffrey and G. L. Stuber, "Radio location in urban CDMA microcells," in *IEEE International Symposium on Personal, Indoor and Mobile Radio Communications, PIMRC*, vol. 2, pp. 858–862, 1995.

[56] N. Tyler, "CDMA mobile station location," in *Novel Methods of Location and Tracking of Cellular Mobiles and their System Applications*, IEE, May 1999.

[57] R. Roy and T. Kailath, "ESPRIT – estimation of signal parameters via rotational invariance techniques," *IEEE Transactions on Acoustics, Speech and Signal Processing*, vol. 29, July 1989.

[58] I. Ziskind and M. Wax, "Maximum likelihood localization of multiple sources by alternating projection," *IEEE Transactions on Acoustics, Speech and Signal Processing*, vol. 36, October 1988.

[59] KSI, "Telesentinel." (http://www.telesentinel.com).

[60] S. C. Swales, J. E. Maloney, and J. O. Stevenson, "Locating mobile phones and the US wireless E–911 mandate," in *Novel Methods of Location and Tracking of Cellular Mobiles and their System Applications*, IEE, May 1999.

[61] P. T. Thompson and D. Brooks, "Results of the TSUNAMI field trials: Position location in macro and micro cell environments," in *Novel Methods of Location and Tracking of Cellular Mobiles and their System Applications*, IEE, May 1999.

[62] M. A. Spirito, "Further results on GSM mobile station location," *Electronics Letters*, vol. 35, May 1999.

[63] D. Kothris, M. Beach, B. Allen, and P. Karlsson, "Performance assessment of terrestrial and satellite based position location systems," in *3G2001 Conference*, IEE, London, March 2001.

[64] L. Cong and W. Zhuang, "Hybrid TDOA/AOA mobile user location in wideband CDMA systems," in *Proc. IEEE International Conference on Third Generation Wireless Communications*, pp. 648–655, June 2000.

[65] N. J. Thomas, D. G. M. Cruickshank, and D. I. Laurenson, "Performance of a TDOA–AOA hybrid mobile location system," in *3G2001 Conference*, IEE, London, March 2001.

[66] D. Walsh, S. Capaccio, D. Lowe, P. Daly, P. Shardlow, and G. Johnston, "Real time differential GPS and GLONASS vehicle positioning in urban areas," in *ITSC*, (Boston, Massachusetts), Novemeber 1997.

[67] S. Soliman, P. Agashe, I. Fernandez, A. Vayanos, P. Gaal, and M. Oljaca, "gpsone^{tm}: A hybrid position location system," in *ISSSTA Conference*, September 2000.

[68] J. S. Thompson, *Bearing Estimation Techniques for Improved Performance Spread Spectrum Recievers*. PhD thesis, Uinversity of Edinburgh, Scotland, 1995. Chapter 6.

[69] N. J. Thomas, D. G. M. Cruickshank, and D. I. Laurenson, "Calculation of mobile location using scatterer information," *Electronic Letters*, vol. 37, pp. 1193–1194, September 2001.

[70] J. J. Caffrey and G. L. Stuber, "Overview of radiolocation in CDMA systems," *IEEE Communications Magazine*, pp. 38–45, April 1998.

[71] V. Erceg, D. G. Mickelson, S. S. Ghassemzadeh, L. J. Greenstein, A. J. Rustako, P. B. Guerlain, M. K. Dennison, R. S. Roman, D. J. Barnickel, S. C. Wang, and R. R. Miller, "A model for the multipath delay profile of fixed wireless channels," *IEEE Journal on Selected Areas in Communications*, vol. 17, pp. 399–410, March 1999.

[72] W. C. Y. Lee, *Mobile Communciations Engineering*, ch. 9. McGraw-Hill, 1988.

[73] A. Paulraj and C. Papadias, "Space–time processing for wireless communications," *IEEE Signal Processing Magazine*, pp. 49–83, November 1997.

[74] M. Wylie and J. Holtzmann, "The non–line of sight problem in mobile location estimation," in *IEEE ICUPC*, pp. 827–831, 1996.

[75] J. Borras, P. Hatrack, and N. B. Mandayan, "Decision theoretic framework for NLOS identification," in *VTC*, vol. 2, pp. 1583–1587, 1998.

[76] Y. Jeong, H. You, and C. Lee, "Calibration of NLOS error for positioning systems," in *Vehicular Technology Conference*, pp. 2605–2609, May 2001.

[77] 3GPP, "Physical channels and mapping of transport channels (FDD), 3G TS 25.211," tech. rep., 3GPP, 2000.

[78] Ericsson, "Recapitulation of the IPDL positioning method, TSGR1#4(99)346," tech. rep., 3GPP, 1999.

[79] Nortel Networks, "Pilot signal coverage for location services (LCS), TSGR1#7(99)c36," tech. rep., 3GPP, 1999.

[80] D. J. Torrieri, "Statistical theory of passive location systems," *IEEE Transactions on Aerospace and Electronics Systems*, March 1984.

[81] E. Brookner, *Tracking and Kalman Filtering Made Easy*, ch. 2. Wiley, 1998.

[82] R. E. Kalman and R. S. Bucy, "New results in linear filtering and prediction theory," *Journal of Basic Engineering*, vol. 83, pp. 95–107, March 1960.

[83] R. A. Singer, "Estimating optimal tracking filter performance for manned maneuvering targets," *IEEE Transactions on Aerospace and Electronic Systems*, vol. 6, pp. 473–483, July 1970.

[84] R. McAulay and E. Denlinger, "A decision–directed adaptive tracker," *IEEE Transactions on Aerospace and Electronics Systems*, March 1973.

[85] Y. T. Chan, J. B. Plant, and J. R. T. Bottomley, "A kalman tracker with a simple input estimator," *IEEE Transactions on Aerospace and Electronics Systems*, March 1982.

[86] T. Kawase, H. Tsurunosono, N. Ehara, and I. Sasase, "A kalman tracker with a turning acceleration estimator for maneuvering target tracking," in *Vehicular Technology Conference*, pp. 2057–2061, 1999.

[87] R. L. M. Norman H. Gholson, "Maneuvering target tracking using adaptive state estimation," *IEEE Transactions on Aerospace and Electronic Systems*, May 1977.

[88] G. G. Ricker and J. R. Williams, "Adaptive tracking filter fo maneuvering targets," *IEEE Transactions on Aerospace and Electronic Systems*, January 1978.

[89] T. Song and J. Speyer, "A stochastic analysis of a modified gain extended kalman filter with application to estimation with bearings-only measurements," *IEEE Transactions on Automatic Control*, vol. AC–30, no. 10, pp. 940–949, 1985.

[90] P. J. Galkowski and M. A. Islam, "An alternative derivation of the modified gain function of song and speyer," *IEEE Transactions on Automatic Control*, vol. 36, pp. 1323–1325, November 1991.

[91] L. Ahlin and J. Zander, *Principles of Wireless Communications*. Studentlitteratur, 1998.

[92] R. G. Kouyoumjian and P. H. Pathak, "A uniform geometrical theory of diffraction for an edge in a perfectly conducting surface," *Proceedings of the IEEE*, pp. 1448–1461, November 1974.

[93] P. M. Grant and I. A. Glover, *Digital Communications*. Prentice Hall, 1998.

[94] R. H. Owen, "An analysis of adaptive antenna frequency division duplex operation in a highly scattered environment," in *Workshop on Smart Antenna Design and Technology*, (Dubrovnik, Croatia), pp. 2.18–2.27, COST Action 260, December 1997.

[95] V. Graziano, "Propagation correlations at 900MHz," *IEEE Transactions on Vehicular Technology*, pp. 182–189, 1978.

[96] A. Mawira, "Models for the spatial correlation functions of the (log)-normal component of variability of VHF/UHF field strength in urban environment," in *PIMRC*, pp. 1503–1507, 1992.

[97] T. Sorenson, "Slow fading cross–correlation against azimuth separation of base stations," *Electronics Letters*, vol. 35, pp. 127–129, January 1999.

[98] T. Klingenbrunn and P. Mogensen, "Modelling cross–correlated shadowing in network simulations," in *VTC*, pp. 1407–1412, 1999.

[99] G. Bruckert, A. Ghosh, M. Panjwani, and B. Verbiscer, "Location power up function," tech. rep., ETSI TR45.5.2.3, 1997.

[100] Ericsson, "Proposal for downlink positioning, TSGR1#7(99)c61," tech. rep., 3GPP, 1999.

[101] 3GPP, "Idle periods for IPDL location method, TS 25.214," tech. rep., 3GPP, 2000.

[102] Motorola, "Time aligned IPDL positioning technique, TSGR1#7(99)b79," tech. rep., 3GPP, 1999.

[103] Samsung, "Pilot channel structure for location services, TS#8(99)f51," tech. rep., 3GPP, 1999.

[104] S. M. Spangenberg, I. Scott, S. McLaughlin, D. G. M. Cruickshank, G. J. R. Povey, and P. M. Grant, "An FFT–based approach for fast acquisition in spread spectrum communications systems," tech. rep., Mobile VCE, 1997.

[105] A. Papoulis, *Probability, Random Variables and Stochastic Processes*, ch. 6–3. McGraw–Hill, 1991.

[106] N. L. Johnson and S. Kotz, *Distributions in Statistics: Continuous Multivariate Distributions*, ch. 41. Wiley, 1972.